Design and Characterisation of Multifunctional Tools for the Elucidation of the Cu⁺ Chemistry in Alzheimer`s Disease

Dissertation

zur Erlangung des mathematisch-naturwissenschaftlichen Doktorgrades

"Doctor rerum naturalium"

der Georg-August-Universität Göttingen

im Promotionsprogramm Chemie

der Georg-August University School of Science (GAUSS)

vorgelegt von

Diplom Chemiker

Markus Rittmeier

aus Köln

Göttingen, 2013

Thesis Committee

Prof. Dr. Franc Meyer, Institute of Inorganic Chemistry

Prof. Dr. Ulf Diederichsen, Institute of Organic Chemistry

Member of the examination board

Referent: Prof. Dr. Franc Meyer, Institute of Inorganic Chemistry

Korreferent: Prof. Dr. Ulf Diederichsen, Institute of Organic Chemistry

Further members of the examination board

Jun.-Prof. Dr. Guido Clever, Institute of Inorganic Chemistry

Dr. Inke Siewert, Institute of Inorganic Chemistry

Prof. Dr. Sven Schneider, Institute of Inorganic Chemistry

Prof. Dr. Markus Hauck, Albrecht von Haller Institute of Plant Sciences

Day of the Disputation: 05.02.2013

Abstract

Alzheimer's disease is the most common neurodegenerative disease in the world. Alzheimer's disease is clinically characterised by decreased cognitive performance and pathologically characterised by formation of fibrillar amyloid plaques, so called Aβ-plaques and neurofibrillary tangles, which are aggregated tau proteins. It was first described by the German physician Alois Alzheimer in 1906. Even after 100 years, no therapies are available which can cure the disease or stop its progression. Current drugs only alleviate the symptoms and even this is strongly limited. Reason for the lack of effective drugs is that, to date, many questions remain unanswered. The exact biochemical processes which lead to the Aβ-plaques and to the cell death are not known. Since elevated levels of redox-active transition metals, primarily copper and iron, were found in the Aβ-plaques, evidence is provided that these processes are metal-mediated. Several biological markers indicate an increased oxidative stress in Alzheimer's disease afflicted brain tissues, which could be induced by the enrichment of metals. In contrast to iron, which is associated with ferritin, copper is directly incorporated in the Aβ-plaques. Thus, an involvement of copper is more likely than of iron. A redox cycle was thus proposed which focuses on copper as the cause of increased oxidative stress. However, without an analytical tool which can intercept the cycle through coordination of intermediary formed Cu^+, this and other hypotheses involving copper are yet to be unambiguously proven. The aim of this study is the synthesis and characterisation of such a tool. For the desired application a system is necessary which is not only selective for Cu^+ but also targets the Aβ-plaques. This was achieved by the synthesis of a multifunctional compound consisting of two subunits, a Cu^+-selective chelating moiety and one with a high affinity for Aβ-plaques. For the synthesis of the latter, dyes which can intercalate in the β-sheet structure of the Aβ-plaques were used as a basis. By combining modern drug design with inorganic aspects, a set of tripodal {NS$_2$} and tetradentate {N$_2$S$_2$} ligands were synthesised and evaluated with respect to their metal binding properties. The systems with the best results with respect to affinity, selectivity, and stability, were then introduced into the multifunctional tool. Three multifunctional systems could be synthesised and first studies indicate that the compounds can be used for *in vivo* studies.

Table of Contents

Chapter 1

Alzheimer's Disease

1907	Characterisation by Alois Alzheimer: plaques and neurofibrillary tangles
1910	Emil Kraepelin names the disease "Alzheimer's Disease" (AD)
1911	Enlightenment of the plaques as aggregated amyloid proteins
1920s	Discovery of Congo red and Thioflavin T as dyes for amyloid plaques
1967	Sequencing of the Amyloid Protein
1970s	First AD therapies with acetylcholinesterase (AChE) inhibitors
1993	Determination of the sequestration of the Amyloid Precursor Protein; the origin of the amyloid protein
1990s	Discovery of metal-enrichments in Aβ plaques and an alteration of the oxygen metabolism, leads to the hypothesis of metal induced oxidative stress as key event in AD

1.1 Alzheimer´s Disease - Some General Information

One of the most common neurodegenerative diseases in the world is Alzheimer's disease (AD).[1] One of six people aged 70-74 is afflicted by AD and this number increases with age, resulting in 2 % of the world population.[2] In Germany, as in many other industrialised nations, this number will greatly increase in future due to demographic changes and increasing life expectancy, so it is essential to elucidate the biochemical mechanisms of AD in order to develop therapeutic options.

In 1906, AD was first described by the German physician Alois Alzheimer, whom it was named after.[3–5] AD is a neurodegenerative disease of the brain, during which progressive loss of neurons in different cognitive domains occurs, in particular the entorhinal cortex, hippocampus, basal forebrain and the amygdale. The clinical course can be divided into seven stages, from no impairment (Stage 1) to severe AD (Stage 7), which describe the continuously on-going mental decline.[6] The diagnosis of AD is problematic since the clinical symptoms match with many other neurological defects, such as vascular dementia, which is caused by circulatory disturbances in the brain. It is true that imaging diagnoses provide reasonable assurance but a final confirmation of the diagnosis is only possible *post mortem*. Characteristic for AD is the accumulation of protein aggregates, which can be detected *via* pathological examination. These include β-amyloid plaques (Aβ plaques) and intracellular neurofibrillary tangles (NFTs).[4,7] Another pathological finding in Alzheimer's disease is the increased concentration of various transition metals, namely iron, copper and zinc.

1.2 The Origin of Aβ Peptide: Amyloid Hypothesis

AD is clinically characterised by decreased cognitive performance and pathologically characterised by formation of fibrillar Aβ and formation of NFTs, which consist of aggregated *tau* protein plaques.[8–11] The amyloid protein (Aβ), typically a 40/42 amino acid protein,[9][10] is produced through metabolism of the amyloid precursor protein (APP), which is a 695-770 residue ubiquitous transmembrane protein.[14,15] Physiological function of the APP has still to be elucidated but functions such as neurite outgrowth, synaptogenesis, cell adhesion, neuronal survival, apoptosis and axonal transport have been proposed.[16] *In vivo* two proteolytic metabolic pathways are known, the amyloidogenic and the non-amyloidogenic pathway (Scheme 1).[17,18] The non-amyloidogenic pathway leads first to the α-amyloid by cleavage of the 687-residue through α-secretase and then after further cleavage by γ-secretase[19,20] to the P3 peptide.[21] In contrast to this, in the amyloidogenic pathway, cleavage of the 671-residue of APP by ß-secretase[22–25] occurs first to yield the β-amyloid precursor protein. A second cleavage of the 711 or 713-residue with γ-secretase releases $Aβ_{1-40}$ or $Aβ_{1-42}$, respectively.[26] Both pathways are present under physiological conditions and are strongly dependent of the cell environment.[27] The amino acid sequences of the natural Aβ proteins as well as the most important truncated analogues $Aβ_{16}$ and $Aβ_{28}$ are shown in Figure 1.[10] $Aβ_{1-40}$ is the dominant Aβ species in neuronal cultures with an expression of 90 to 95 %, but in AD the more fibrillogenic $Aβ_{1-42}$ is the predominant species. [28–32] The Aβ proteins differ in many aspects, although structural differences are only minor.
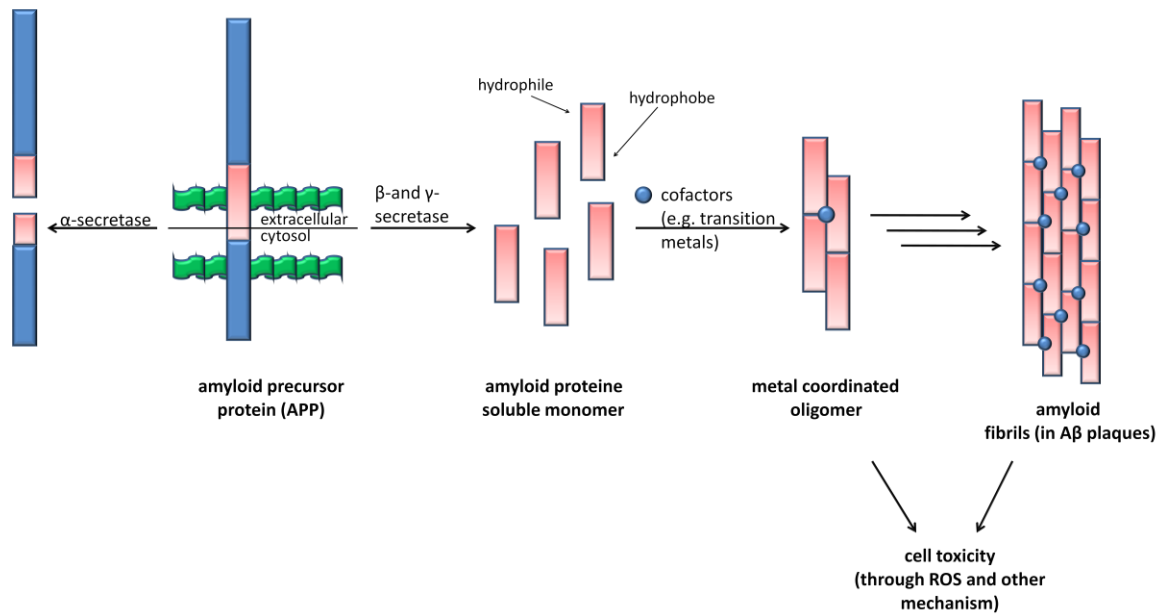
Scheme 1 Cleavage of the amyloid precursor protein (APP) resulting in Aβ$_{1-40}$ and Aβ$_{1-42}$

The truncated analogue Aβ$_{1-16}$ shows no tendency to aggregate and is therefore used in studies which require an unchanged protein structure, for example ROS (reactive oxygen species) or metal binding studies. For studies on the aggregated protein or direct studies on aggregation, Aβ$_{1-28}$ is often used, because the aggregation under moderate concentration and conditions is quite slow in comparison with Aβ$_{1-40/42}$. The Aβ´s consist of a large hydrophilic N-terminal domain (1-28) and a hydrophobic C-terminus domain (29-40/42). In the monomeric form Aβ is soluble and can also be found in the healthy brain, indicating that it is nontoxic.[33–35] Even the opposite seems to be the case. Studies with metal induced oxidative stress have shown a protective function of Aβ, leading to the hypothesis that Aβ normally functions as an antioxidant and regulator of free metal concentration in the brain.[36] When Aβ is bound to an appropriate amount of Cu^{2+} and Zn^{2+} it can catalyse the dismutation of superoxide to hydrogen peroxide. Thus, Aβ can operate as an antioxidant.
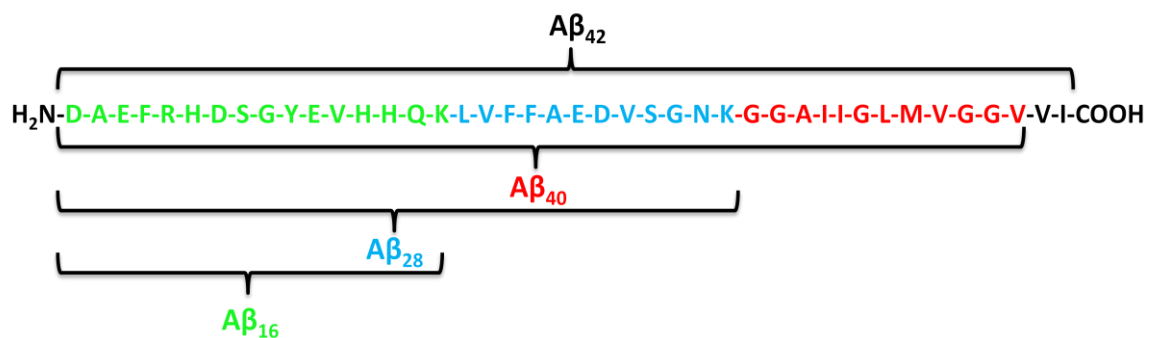
Figure 1 Amino acid sequence of natural and truncated Aβ proteins

Formation of Aβ-plagues is one of the hallmarks of AD and it seems that the aggregation process from Aβ to fibrils is the key event. According to the amyloid hypothesis, the self-assembly process of Aβ involves increased release of amyloid protein, which accumulates and then aggregates forming first small oligomers, and then protofibrils.[17,37] These small hydrophobic aggregates appear to be the most toxic species in the AD process, as they can insert into

neuronal lipid bilayers and increase levels of oxidised products through increased lipid peroxidation.[38–40] Further aggregation finally leads to the Aβ-plaque found in the AD brain. Under physiological conditions the amyloid protein is present in an α-helical structure, but in the aggregated fibrils only ß-sheet structures are found (Figure 2).[41]
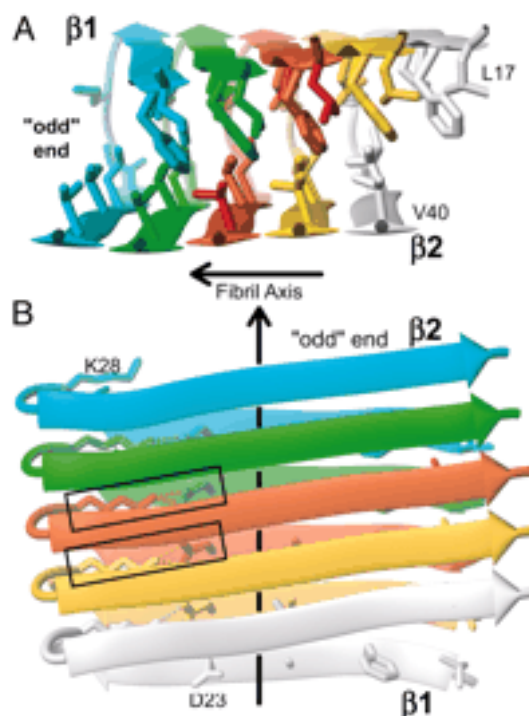
Figure 2 3D core structure of two stacked Aβ$_{1-42}$ protofilaments along the different axes (A and B). The figure illustrates the nature of the inter-β-strand interactions present in fibrils. K^{28} and D^{23} can interact via an intermolecular salt bridge, which is indicated by the dotted line in B. The picture was taken from the literature.[41]

This finding raises the question whether the change in the protein structure initiates the aggregation or if the transformation towards β-sheets occur *in situ*, when the fibrils are formed.[42,43] In the last few years evidence was found for a metal induced aggregation resulting in the metal enriched fibrils found in AD.[7] One hypothesis suggests that a conformational change is induced by metal coordination in the Aβ proteins, which then aggregate by pure peptide-peptide contacts (Scheme 2).[44]
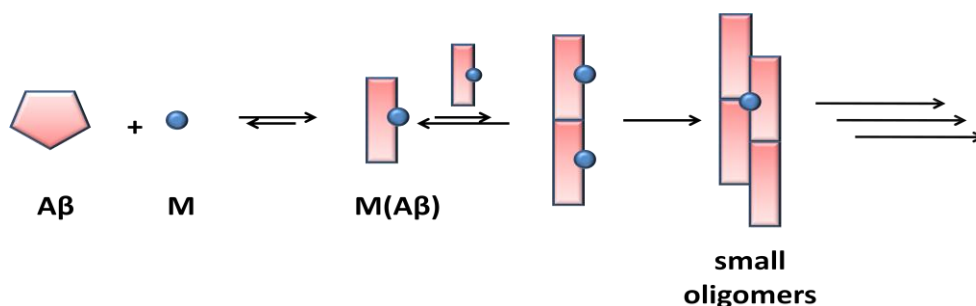
Scheme 2 Putative mechanism of the metal induced aggregation of Aβ to protofibrils.

It is worth mentioning that protein misfolding leading to amyloid-like fibrils is not only found in AD, but also in the normal homeostasis of some proteins.[45] Recently such plaques were also found in healthy brain tissues, where the person shows no clinical symptoms of AD.[46] One

hypothesis, which has been formed, is a protective mechanism against toxic misfolded intermediates through sequestration. Part of this theory is an equilibrium between the soluble monomer and the formed fibrils (Scheme 3).[47–50] Taking this into consideration, metal accumulation could be a trigger for promoting the pathway towards the toxic oligomers.
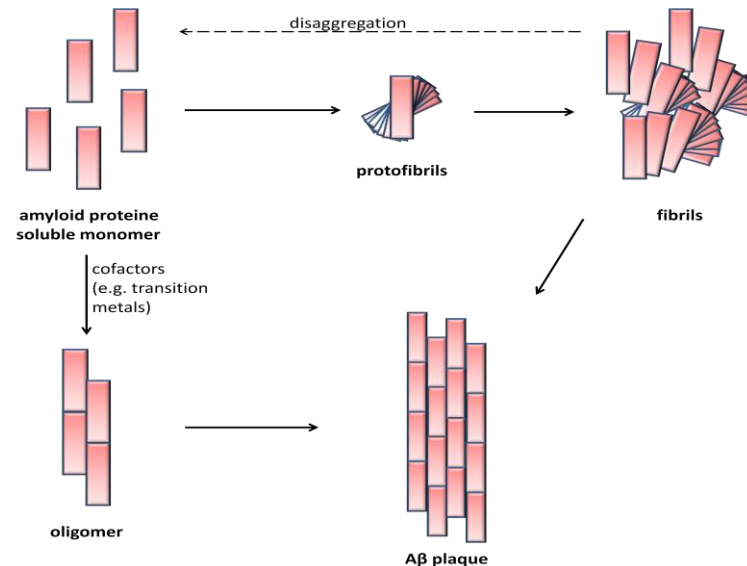
Scheme 3 Aggregation pathways to Aβ plaques

1.3 Detection of Aβ Plaques

From the pathological point of view Alzheimer's disease is relatively complex. The various hallmarks and their development over time allow a selective observation of the current state of AD and its progress. For *in vivo* visualisation of these pathological hallmarks non-invasive methods like magnetic resonance imaging (MRI) are necessary. MRI is a technique which can also visualise NFTs in AD.[51–55] The advantage in comparison with topographic techniques, such as positron emission tomography (PET)[56–59], which are also used in AD, is that with MRI no exposure to radiation occurs. Since Aβ plaques are predominantly β-pleated sheets, dyes can selectively intercalate the secondary structure. Thus, in order to image Aβ plaques, a series of dyes were synthesised with binding affinities in the low nanomolar region, the ability to cross the blood brain barrier (BBB), fast retention, and fast clearance from healthy brain tissues (Figure 3). Congo red was the first reported molecule known to function as a dye in AD, as it undergoes an absorption band shift upon interaction with Aβ.[60,61] Later it could be shown that Thioflavin T (ThT) and Thioflavin S (ThS) have not only similar affinities to Aβ, but also many advantages, for example, higher selectivity towards Aβ plaques and a unique change in the absorption and in the fluorescence spectra.[62,63] The reason or mechanism which causes the spectral alteration and induces the noteable 115 nm hypochromic spectral red shift of ThT is presently unknown. Thus, even today ThT is widely utilised in many studies to detect the formation of Aβ plaques *in vivo* and *in vitro*. The second generation of dyes for AD granted access to new imaging techniques, namely positron emission tomography (PET)[56–59], single photon emission computed tomography (SPECT)[64–66] and multiphoton imaging.[67,68]
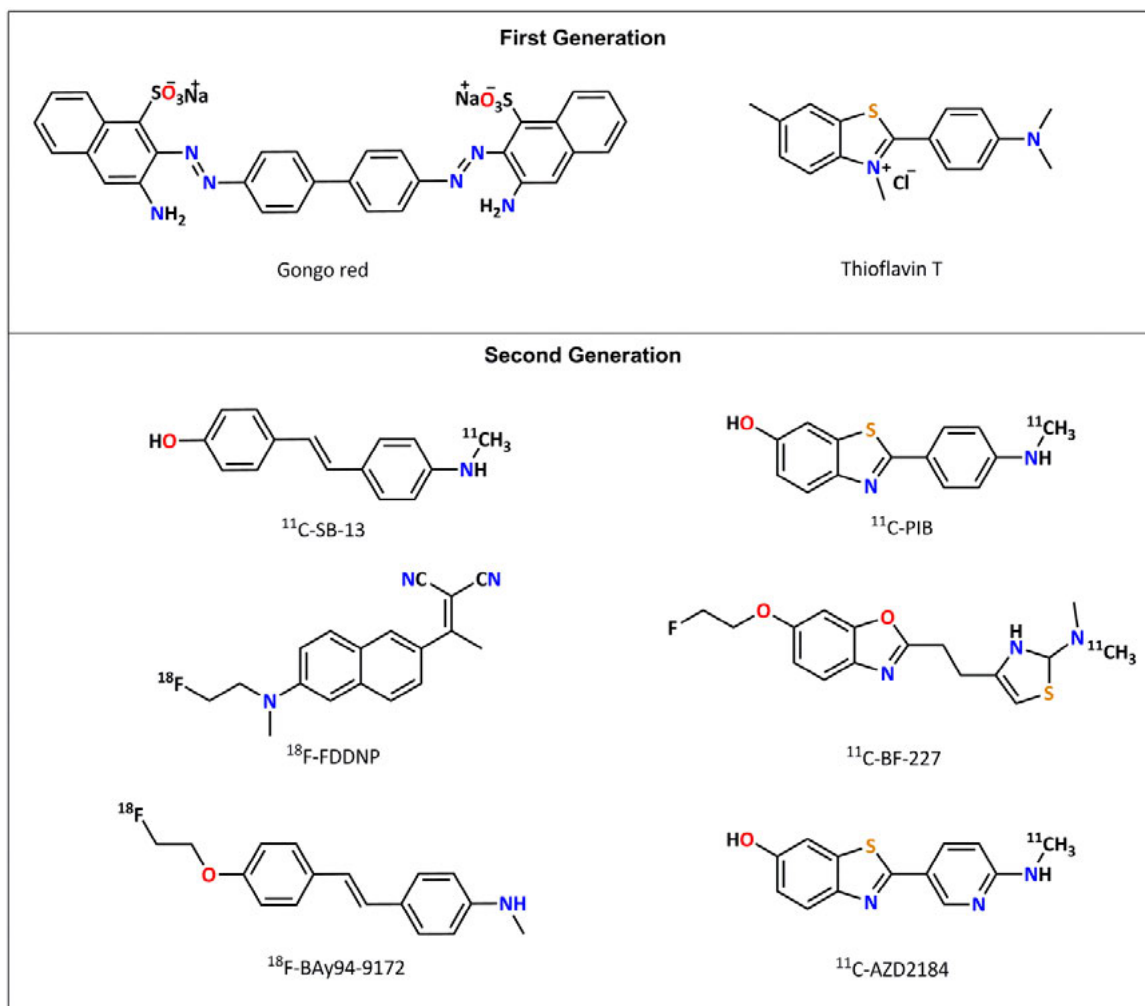
Figure 3 The first and second generation dyes used to visualise Aβ plaques in vivo. The second generation is also utilised for topographic methods through radiolabeling.

From the second generation compounds ^{11}C-BIP (Pittsburgh Compound B) and ^{18}F-FDDNP are of specific interest.Both compounds have passed several clinical trials. They show differences in the regional retention and also in their intercalation properties. The lower retention for ^{18}F-FDDNP could be explained by its lower binding affinity, but ^{18}F-FDDNP has the advantage of also imaging NFTs.[69] However, insufficient sensitivity and a lack of its specificity, as determined by immunohistochemistry, are still challenges which have to be overcome. For a clear diagnosis different methods are often combined to complete the picture.[51]

1.4 Transition Metals in AD

For a variety of specific processes of life, nature uses the special properties of transition metals. Proteins which include one or more metals as a cofactor are called metalloproteins. If these proteins also have catalytic activity they are called metalloenzymes. As well as for the rest of the human body, transition metals are also essential for natural metabolism in the brain. Iron, zinc and copper are especially necessary for neuronal activities. These three transition metals are

involved in neurotransmission, synaptogenesis, neurogenesis, neurite outgrowth, neuro-transmitter biosynthesis, oxidative phosphorylation, and oxygen transport.[70]

In the AD brain microparticle-induced X-ray emission (PIXE) and other techniques have shown up to 3-5 fold excesses of different trace metals in comparison with age matched control.[71–73] In the senile plaques high metal deposits could also be detected in the mM or µM range (zinc/iron ≈ 1 mM, copper ≈ 400 µM) (Table 1).[74] Under physiological conditions iron, copper and zinc can induce fast Aβ aggregation. The redox active iron and copper are especially of great interest and are in the main focus of research. There is evidence that cell damage and also neuronal loss could have their origin in oxidative stress, which makes these two metals good candidates to play an important role in the progression of AD.[74–77] Thus, dysregulation of brain metals has been implicated in the pathogeneses of AD.[34][78,79] In the following, the metals accumulated in AD will be discussed in more detail with respect to their binding affinities and influence on the aggregation.

Table 1 Copper, iron and zinc concentration in senile plaque, in AD and in controls subjects modified after Lovell et al.[80]

	Copper [µg/g]	Iron [µg/g]	Zinc [µg/g]
Senile Plaque	25.0 ± 7.8	52.4 ± 13.7	69.0 ± 18.4
AD neuropil	19.3 ± 6.3	38.8 ± 9.4	51.4 ± 11.0
Control neuropil	4.4 ± 1.5	18.9 ± 5.3	22.6 ± 2.8

1.4.1 Copper in AD

With around 70 mg/person (70 Kg) copper is the third most common essential transition metal in the human body.[81] Physiologically, it is mainly found in protein-bound form, where it can be present in both the oxidised (Cu^{2+}) and the reduced (Cu^+) form. The most important copper metalloproteins in the human body are Cu,Zn superoxide dismutase (Cu,Zn-SOD, antioxidant defence), cytochrome c oxidase (CCO, electron transport and oxidative phosphorylation), tyrosinase (pigmentation), ceruplasmin (copper transporter), albumin (copper transporter) and dopamine β-hydrolase (neurotransmission). Copper containing proteins can be divided into three classes according to their coordination geometry and ligand sphere. Type 1 copper proteins, also known as blue copper proteins, are characterised by a strongly distorted tetrahedral structure and an absorption of the oxidised species at 600 nm. The coordination sphere consists of two histidine residues, a hydrogen bond-forming cysteine residue and another amino acid (e.g. methionine). Type 2 copper proteins, which are not blue in colour, have a nearly planar geometry. In this case there are three histidine residues and one water molecule coordinated to the metal. The last class, the type 3 copper proteins, comprises two copper ions, in contrast to the type 1 and type 2 centres. The spatial arrangement of the ligands, six histidine residues and one or two bridging molecules results in a pyramidal geometry for each metal ion. Of all the copper in the human body 7.3 % is located in the brain, where it is released as a neurotransmitter in the glutamatergic synapses of the cortex and hippocampus.[82,83] Due to the high redox activity of copper and the relatively low antioxidant levels in the brain, tight regulation of copper transporters is necessary.[84] Age dependent dyshomeostasis can lead to copper enrichment in extracellular amyloid plaques.[85–88] Controversially, copper levels in cerebrospinal fluid and plasma of AD published so far differ in a broad range.[89–97] Furthermore,

the brain tissues of AD patients show a decrease of copper levels in comparison to aged match control.[72,97] Recently, together with an elevated Aβ level, an increased "labile copper pool" was reported in the AD affected human brain.[98] As a consequence, all previous assumptions of an enrichment of copper seem to be wrong. Treatment methods using metal chelating need to be reconsidered. The copper imbalance and missregulation needs to be re-equilibrated from the labile pool to the copper proteins.[99] Under physiological conditions (pH ≈ 6.6) Cu^{2+} can promote Aβ aggregation, but unlike Zn^{2+} and Fe^{3+}, without fibril formation.[100–102] Instead, highly toxic small oligomers are formed.[103] Furthermore, cultured neurons treated with Cu^{2+} result in hydrogen peroxide production by the $[AβCu]^{2+}$ complex.[104,105] The copper promoted aggregation, the generation of oxidative stress through the $[AβCu]^{2+}$ complex, the high copper levels found in senile plaques and the imbalance in the copper pool all point in one direction; copper is part of the AD progression, if not the key to the disease and its cure. To understand the many possible interactions in AD, structural features of the copper-APP and copper-Aβ complex firstly have to be evaluated.

Copper-Protein Complexes in AD

Under conditions of copper deficiency the amyloidogenic degradation pathway of APP is promoted, whereas elevation of intracellular copper levels enhances the non-amyloidogenic pathway and diminishes Aβ release.[106–112] The change in metabolism is likely due to structural changes in the APP.[113] Therefore, the copper binding sites of APP are of great interest. APP has two Cu^{2+} binding domains, one in the N-terminus and another in the later Aβ protein sequence. The first binding domain involves one methionine, one tyrosine and two histidine residues (His^{147}, His^{151}, Tyr^{168} and $Met1^{70}$) and binds Cu^{2+} relatively strong, with a dissociation constant K_d of approximately 10 nM.[113,114] The Aβ protein also shows two binding sites for Cu^{2+}, which can sequentially bind Cu^{2+}.[102,115,116] However, the relatively low binding constant of the second binding pocket (see Table 2) and the substoichiometric amount of copper found in Aβ indicates that the second binding domain is unoccupied. The apparent K_d values for $[AβCu]^{2+}$ vary with 0.1 to 47 μM in a large range, which is a result of the different conditions and also the sensitivity of the used methods.[117] A pH dependence of coordination could be determined. Under physiological conditions (pH ≈ 6.7) species I is predominant. However, at higher pH values (pH ≈ 8.9) a second species is formed.[36][56] Interconversion of the two species can be observed at pH 8 ± 1 (Figure 4).[42,88,116,118,127–129] It is noteworthy, that under mildly acidic conditions (pH ≈ 6.6), where species I is predominant, Cu^{2+} can promote Aβ aggregation.[100] Under physiological conditions species I appears to be the predominant species, where the metal is coordinated in {N_3O_1} environment similar to type II Cu proteins.[56][58][130–133]. The His residues which are most likely involved in Cu^{2+} coordination are His^6, His^{13} and His^{14}, but it is still unknown if these coordinate *in vivo*. Concerning the O-donor atom, the carboxylate groups of Asp^1 and Tyr^{10} are of great interest, since surveys indicate an interaction with Cu^{2+}.[42][131,134][135] UV/Vis experiments confirmed the unlikelihood of the Tyr^{10} binding to Cu^{2+}.[58][116,118] Instead the coordination *via* Asp^1 is much more likely, since EPR data with a mutant, Asn^1 instead of Asp^1, show drastic changes in the spectra.[128]

Table 2 Reported dissociation constants (K_d values) for the [AβCu]$^{2+}$ complex. a) numbers in brackets are according to the low affinity second binding domain.

Utilised Aβ	K_d/μM	Calculated K_d/μM	Buffer (pH)/ competing ligand	Experiment/lit.
1-16/28		0.21/0.024	(7.4)	Potentiometry[118]
1-40/42	1.6-2.0		10 mM TRIS (7.4)	Tyr fl.[119]
1-16/28		100	Gly (His, 7.8)	Tyr fl.[88]
1-16/28/40	11-47		100 mM TRIS (7.4)	Tyr fl.[120]
1-40	8		50 mM PO$_4^-$ (7.2)	Tyr fl.[121]
1-40	2.5		10 mM HEPES (7.2)	Tyr fl.[122]
	0.4		10 mM PO$_4^-$ (7.2)	Tyr fl.[122]
1-40	1.2/3.8/3.0		20/50/100 mM TRIS (7.4)	Tyr fl.[123]
	0.6/0.9/2.5		20/50/100 mM HEPES (7.4)	Tyr fl.[123]
1-16/28	0.1		50 mM HEPES (7.4)	ITC[116]
1-40	16		5 mM PO$_4^-$ at 4 °C (7.3)	NMR[124]
1-16/40		0.4	Gly (His, 7.4)	ITC[125]
1-40		13 (0.05)$^{a)}$	different chelator (7.4)	Chelator/Aβ separation[126]
1-42		5(6·10^{-9})$^{a)}$	different chelator (7.4)	Chelator/Aβ separation[126]
1-40/42	4/0.3		20 mM CH$_3$COO$^-$ (7.4)	Abs. at 214 nm[100]

A 3D structural model of species I at low pH is given in Figure 5. At pH values above 8, and with large reorganisation of the Cu^{2+} binding site, species II is formed. This structural change is most likely induced by deprotonation of an amide backbone or a lateral side chain. Thus, His^{13} and/or His^{14} are no longer within a distance suitable for coordination.[42] For the second binding pocket with lower affinity to Cu^{2+}, a {N$_3$O$_1$} as well as a {N$_2$O$_2$} coordination could be possible.[55][56] All coordination modes described so far concern only the soluble monomeric Aβ, but of much greater interest are the binding modes of Cu^{2+} in the small toxic aggregates and in the fibrils. Relatively few studies were done so far on Cu^{2+} loaded aggregates, which indicated also a {N$_3$O$_1$} coordination sphere in the oligomers.[115,120]

species I (low pH)   species II (high pH)
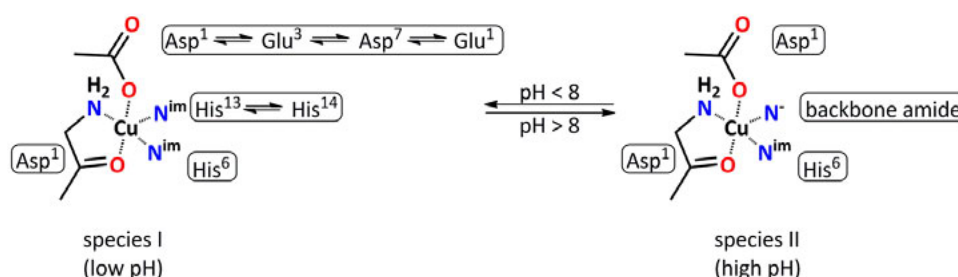
Figure 4 Species I and II of [CuAβ]$^{2+}$ complex. Interconversion occurs around pH 8.
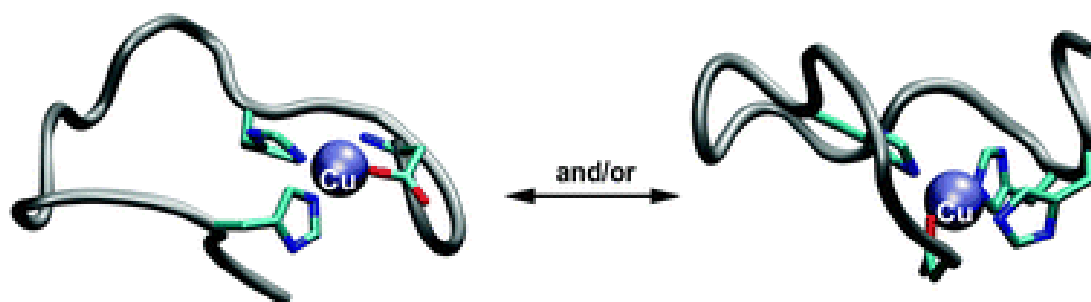
Figure 5 3D structural models of the possible coordination modes in species I at low pH. Left: The coordination by the N-terminus, His^6, His^{13} or His^{14}, Asp^1-COO$^-$ and, right: the coordination by three His and Asp^1-COO$^-$. The picture was taken from the literature.[117]

The brain has a rather reductive environment. The Intracellular potential is -300 mV vs. NHE and in the extracellular environment an ascorbate concentration of approximately several hundred micromolar is present.[136,137] Therefore, an involvement of Cu$^+$ in the progression of AD is possible. Binding studies on the protein are quite complicated, since the metal can easily be re-oxidised and many analysing methods (e.g. EPR and UV) do not detect Cu$^+$. However, through X-ray absorption studies the 3D structure of the [AβCu]$^+$ complex could be elucidated, revealing a linear coordination geometry.[138–140] Two nitrogen atoms from His^{13} and His^{14} coordinate Cu$^+$ in a linear fashion.[141–143] Furthermore, dissociation constants of the [AβCu]$^+$ complex could be determined, showing an affinity of Aβ in the micromolar region (Table 3). Recently, it could be demonstrated that, in contrast to Cu^{2+}, the Cu$^+$-fibril complex undergoes significant structural changes from the monomeric form.[144] Thus, XANES data have shown that even a tetrahedral coordination could be possible. However, further research is necessary for verification.

Table 3 Reported dissociation constants (K_d values) for the [AβCu]$^+$ complex

Utilised Aβ	Calculated K_d/μM	Buffer (pH)/ competing ligand	Experiment/lit.
1-16/40	7.5/19	different chelator (7.4)	chelator/Aβ separation[145]
1-40	6·10^7	different chelator (7.4)	chelator/Aβ separation[146]

After defining the distinct coordination pockets for Cu^{2+} and Cu$^+$, kinetics for the electrochemistry of copper loaded Aβ were investigated (Figure 6).[147] Three different mechanisms were suggested. The first is an electron transfer mechanism, where the coordination sphere changes from the distorted square planar {N$_3$O$_1$} coordination to the linear N-Cu-N structure. This mechanism requires a large rearrangement which, due to the high reorganisation energy, is relatively unlikely. The second mechanism is the so called square scheme mechanism. Pathway A and pathway B describe mechanisms already known for other copper complexes.[148–151] Pathway A progresses from Cu$^+$ to Cu^{2+} through a metastable complex which is similar to the final complex.[147] The same is proposed in pathway B, where a similar Cu^{2+} complex coordinated by only the two His residues is formed. Even with this structural "intermediate" the reorganisation energy is still too high, therefore the third proposed mechanism seems to be most likely. The third mechanism proceeds through reorganised complexes, where small fractions of the [AβCu]$^+$ and [AβCu]$^{2+}$ complexes adopt similar structures, and which therefore affords relatively low reorganisation energy of the electron-transfer. In this mechanism the pre-organised metastable [AβCu]$^+$ and [AβCu]$^{2+}$ complexes are in rapid equilibrium with the stable forms.

Simple Electron Transfer Mechanism

$E^0_{Cu^{II}/Cu^{I}} = 0.170$

$N_{/////} Cu^{II} \cdot_{\text{\tiny\textbackslash}} His_6$, O, $His_{13/14}$ $\underset{-e^-}{\overset{+e^-}{\rightleftharpoons}}$ $His_{13} — Cu^{I} — His_{14}$

$\lambda = 0.3$
$Z = 5 \times 10^{-3}$

Square Scheme Mechanism

Stepwise pathway A

$E^0_{Cu^{II}_{st}/Cu^{I}_{ms}} = 0.500$

$\underset{-e^-}{\overset{+e^-}{\rightleftharpoons}}$

$\lambda = 0.3$
$Z = 1$

$K^{II}_{ms \rightarrow st} = 10^5$ $K^{I}_{ms \rightarrow st} = 10^6$

$\lambda = 0.3$
$Z = 1$

$His_{13} — Cu^{II} — His_{14}$ $\underset{-e^-}{\overset{+e^-}{\rightleftharpoons}}$ $His_{13} — Cu^{I} — His_{14}$

$E^0_{Cu^{II}_{ms}/Cu^{I}_{st}} = -0.150$

Stepwise pathway B

Preorganization Mechanism

$N_{/////} Cu^{II} \cdot_{\text{\tiny\textbackslash}} His_6$, O, $His_{13/14}$ $His_{13} — Cu^{I} — His_{14}$

$K^{II}_{st \rightarrow ms} = 1.5 \times 10^{-4}$ $K^{I}_{st \rightarrow ms} = 1.5 \times 10^{-3}$

$\lambda = 0.3$
$Z = 1$

$His_6 _{/////} Cu^{II} \, His_{13}$, His_{14}, O $\underset{-e^-}{\overset{+e^-}{\rightleftharpoons}}$ $His_6 _{/////} Cu^{I} \, His_{13}$, His_{14}, O

$E^0_{Cu^{II}_{ms}/Cu^{I}_{ms}} = 0.300$

Figure 6 Different pathways possible for the redox [AβCu]²⁺/ [AβCu]⁺ system. The picture was taken from the literature.[147]

1.4.2 Zinc in AD

After iron, Zinc is the second-most abundant element in the human organism and is involved in many processes. With 0.12 to 0.15 mм zinc is one of the most abundant metals in the central nervous system.[152] In the hippocampus zinc functions as an endogenous neuromodulator in synaptic neurotransmission and is released together with glutamine.[153,154] In AD altered brains elevated zinc levels could be detected not only in the frontal cortex but also in the senile plaques.[74]

Zn-Aβ Interaction

In contrast to Cu^{2+}, there is only one binding site for Zn^{2+} in Aβ. The binding pocket lies in the N-terminus of the protein and allows formation of a 1 : 1 $[AβZn]^{2+}$ complex (Figure 7).[155,156] It is commonly assumed that three histidine residues (His^6, His^{13} and His^{14}) coordinate the metal, but the identity of further ligands is still unknown. Other amino acid residues such as Tyr^1 or Asp^{10}, as well as exogenous ligands are viable donors in order to complete a four to six ligand coordination sphere.[44,122,131,133,155,157]
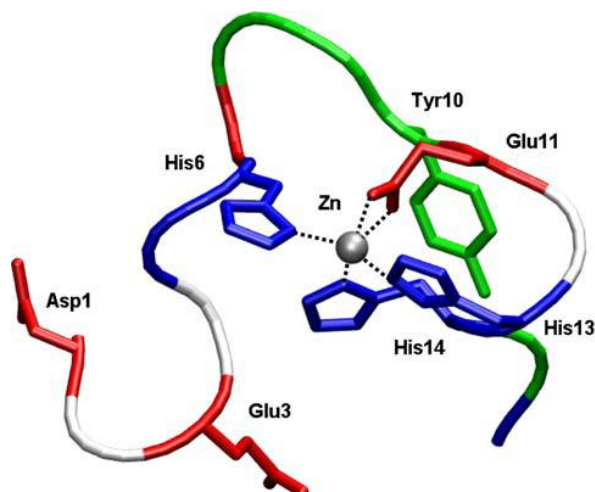
Figure 7 Structure of the [AβZn]²⁺complex determined by NMR studies. Further exogenous ligands cannot be excluded. The picture was taken from the literature.[156]

The K_d for Zn(Aβ) is in the range of 1-20 μM, although higher values have also been reported (Table 4).[117] Upon coordination of Zn^{2+}, fast aggregation of Aβ takes place and nontoxic fibrils are formed, similar to the natural ones.[44] Thus, at current, the zinc-induced fibril formation is being considered as a curative competition for the toxic pathway in AD.[49,103] In the Aβ aggregates all three histidine residues seem to provide the primary binding domain.[42] Intermolecular His-Zn-His bridges are supposed to be present in the aggregates, which could also explain the fast formation of the fibrils induced by Zn^{2+} coordination.[43,85] Besides the Aβ aggregation, altered Zn^{2+} levels also have a direct influence on APP metabolism. High zinc levels promote the amyloidogenic pathway, since zinc ions are directly involved in the modulation of α- and γ-secretase.[158–160] In contrast to iron and copper, zinc is redox silent with distinct chemical properties. Metal induced oxidative stress is therefore not possible. Thus, the role of the interaction between Zn^{2+} and Aβ is still unclear. A protective function of elevated Zn^{2+} levels is still a possibility but current knowledge is too limited to evaluate such a hypothesis.

Table 4 Reported dissociation constants (K_d values) for the [AβZn]$^{2+}$ complex

Utilised Aβ	K_d/μM	Calculated K_d/μM	Buffer (pH)/ competing ligand	Experiment
1-40/42	30/57		10 mM TRIS (7.4)	Tyr fl.[119]
1-16/28/40	22/10/7		HEPES ans TRIS (7.4)	ITC[161]
Soluble 1-16/28/40/42		14/12/7/7	HEPES	competition with Zincon[161]
Aggregated 1-40/42		3/3	HEPES	competition with Zincon[161]
1-40	1.1		10 mM PO$_4^-$ (7.2)	Tyr fl. of Zn/Cu competition NMR[122]
1-40	60/184 65		10/100 mM PO$_4^-$ (7.2) 20 mM HEPES (7.4)	Tyr fl.[123] Tyr fl.[123]
1-40/42		2	Zincon (7.4)	competition with Zincon after 30 min[123]
		>11	Zincon (7.4)	before incubation[123]
1-40	3.2		10 mM HEPES or TRIS (7.4)	displacement assay with cold and radioactive Zn^{2+}[162]
	5		20 mM TRIS (7.4)	displacement assay with cold and radioactive Zn^{2+}[163]
1-16/40742	1-10		100 mM TRIS (His, 7.4)	Tyr fl.[164]

1.4.3 Iron in AD

As the most abundant transition metal in the human body iron is found in a wide variety of proteins and enzymes.[81] Besides in proteins, iron is also found in the cellular tissue in the so-called "labile iron pool" (LIP).[165]. For normal functioning of the brain, and neural development a specific amount of iron (around 60 mg[166]) is needed.[167] Like copper, iron is also a redox active transition metal with Fe^{2+} and Fe^{3+} as the main oxidation states. Low iron levels can therefore cause deficiency symptoms, whereas increased iron levels can cause cellular damage through metal induced oxidative stress. Thus, strict regulation of iron levels is necessary. *Post mortem* brain tissue samples reveal increased Fe^{3+} levels in AD afflicted brains but, in contrast to Zn^{2+} and Cu^{2+}, Fe^{3+} cannot be co-purified with Aβ although *in vitro* studies indicate Fe^{3+}-Aβ interactions.[97,168–172] Instead Fe^{3+} is associated with ferritin, an iron storage protein, within the fibrils themselves.[173] This finding is accompanied by a change in the natural iron homeostasis. Increased level of ferritin and transferritin are present not only in the senile plaques, but also in other non-neuronal cells, indicating a dysfunction of the iron metabolism in AD.[174–176]

The Fe(Aβ)complex

The role of iron in AD is controversially discussed in literature. The strongest evidence for participation of iron in the amyloidosis of AD involves metal induced oxidative stress.[75,104,177,178] *In vivo* and *in vitro* studies have shown iron induced lipid peroxidation, which could be diminished by the addition of iron chelators or amplified by increasing intracellular iron levels.

As a consequence of elevated iron levels, even cell death could be observed. Metal reduction by Aβ and shuttling of the iron to the membrane is one proposed mechanism for the observed cell death.[179] Another indication for iron involvement in AD progression is Fe^{3+} induced aggregation, which takes place under mildly acidic conditions.[120][179,180] Very recently the coordination environment of the Fe^{2+}(Aβ) complex was partially revealed *in vitro*, indicating dynamic exchanges between various coordination modes.[166,181] Most likely three histidine residues (His[6], His[13] and His[14]) as well as the NH_2 group of the N-terminus are involved in coordination. Further ligands could be the COO^- groups of Asp[1] and Glu[3] (Scheme 4).
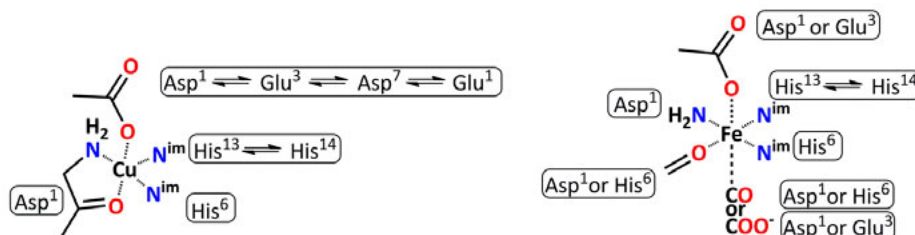
Scheme 4 Comparison of the possible coordination environments for the [AβCu]$^{2+}$ complex (left) and [AβFe]$^{2+}$ complex (right)

It is likely that dyshomeostasis of iron metabolism takes place in AD, but iron does not seem to play a key role in amyloidosis. Firstly, it cannot be co-purified with the Aβ plaques and, secondly, no direct correlation between iron accumulation and increased senile plaques could be detected.[170]

1.5 Oxidative Stress in Alzheimer´s Disease

Reactive oxygen species (ROS) are highly reactive forms of oxygen (hydrogen peroxide H_2O_2, superoxide anion radical $O_2^{\cdot-}$, hydroxyl radical $OH^\cdot$) which are harmful to an organism and are involved in various diseases like cancer[182], Parkinson's disease, Alzheimer's disease, heart failure[183], myocardial infarction[184], Bipolar disorder[185], fragile X syndrome[186], Sickle Cell Disease[187], and chronic fatigue syndrome[188]. In particular, they play an important pathophysiological role in aging, since progressing age leads to an increased dysregulation of protective or repair mechanisms of the body. This imbalance between the generation of ROS and the repair mechanisms is called oxidative stress and occurs when either the production of oxidising species increases or the effectiveness of the antioxidants decreases. The free radicals produced in oxidative stress can damage all parts of the cell through reaction with lipids, proteins or DNA. In the early phases this leads first to disturbance of normal cell function and later even to cell death. The natural origin of ROS often lies in the respiration chain, or to be more precise, in the oxidative phosphorylation in mitochondria.[189] Other sources are enzymes (Cytochrome P450 or NADPH oxidases) which produce ROS as a key intermediate to oxidise/metabolise substrates.[81] Thus, the production of ROS is essential for cell function, as signal transporter, not mentioned prior, or oxidative reagent, but has to be tightly regulated. The same also applies for redox active transition metals like iron or copper. These metal ions can produce ROS and therefore as "free" metals, not bound by enzymes or proteins, are highly toxic.

1.5.1 Indication for Oxidative Stress in AD

As there is a high accumulation of different transition metals in AD brain tissues (chapter 1.4) and the brain is the most aerobic organ in the body, it is likely that cell damage in AD could be the result of oxidative stress. Evidence for extensive oxidative stress in AD afflicted neocortex could be revealed by various biomarkers (lipid peroxidation[190–192], oxidised proteins[193–197], oxidised DNA and RNA[80,198–200]).[201,202] Further confirmation of altered oxygen metabolism is found in high concentrations of reactive electrophilic aldehydes (e.g. malondialdehyde), carbonyls and free 4-Hydroxy-2-nonenal (HNE)[203–206]. The high toxicity of these compounds is not due to an extremely high reactivity but rather because of their metastability. Their long half-lifes allow them to diffuse through the cell and damage it extensively, especially through reaction with biochemical nucleophiles, such as DNA, lipids and proteins. Further evidence is also the absence of poly unsaturated fatty acids, which are easy to oxidise. This is consistent with the increased levels of lipid peroxidation. Further indicators are increased activity of heme oxygenase and glucose-6-phosphate dehydrogenase, as well as a change of the normal antioxidant levels in the AD brain. One example for the latter is superoxide dismutase (SOD) expression. SOD´s are enzymes that catalyse the dismutation of superoxide into oxygen and hydrogen peroxide and therefore are important antioxidants. In comparison to healthy brain tissues higher expression levels of SOD were found in AD brains which, is known to be a biochemical response to increased oxidative stress. An analogous confirmation of this is found in red blood cells and lymphopblasts. Here the levels of antioxidants are also elevated leading to the same conclusion.[207]

1.5.2 Mechanisms of Metal Induces Oxidative Stress in AD

As mentioned previously, iron and copper are the main redox active transition metals which can cause oxidative stress in biological systems. Metal induced cytotoxicity with respect to AD was thus studied in many cases, but did not provide any valuable information about the role of the metal and the conditions responsible for oxidative damage. While Aβ tissues incubated with Zn^{2+} show rapid aggregation to fibrils, no direct cell damage occurs, and it is proposed that Zn^{2+} cooperation with Aβ may protect neuronal cells against ROS. In contrast, after incubation with Aβ, Cu^{2+} and Fe^{3+} show increased cell toxicity through the generation of ROS, especially H_2O_2.[104,177] Experiments with the H_2O_2 scavenging enzyme catalase have shown inhibition of Aβ toxicity, leading to the conclusion that the neurotoxicity in AD is mediated by ROS generation. In the case of Fe^{3+} the toxicity could also be decreased by adding desferrioxamine, a strong Fe^{3+} chelator.[178] Toxicity could then be restored by further addition of Fe^{3+}. Cu^{2+} has shown analogous behaviour to Fe^{3+}. On the basis of Haber-Weiß and Fenton chemistry, a catalytic mechanism of metal induced oxidative stress in AD was postulated (eq. 1.1-1.5).

$$A\beta + M^{(n+1)+} \rightarrow A\beta\cdot + M^{n+} \tag{1}$$
$$M^{n+} + O_2 \rightarrow M^{(n+1)+} + O_2^-\cdot \tag{2}$$

$$O_2^-\cdot + O_2^-\cdot + 2H^+ \rightarrow H_2O_2 + O_2 \tag{3}$$

$$M^{n+} + H_2O_2 \rightarrow M^{(n+1)+} + OH^- + OH\cdot \tag{4}$$

$$O_2^- + H_2O_2 \rightarrow O_2 + OH^- + OH\cdot \tag{5}$$
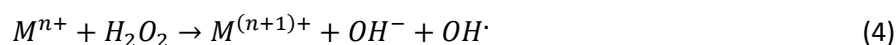
In AD, the metals in equation 1 and 2 are proposed to be Cu^{2+} and Fe^{3+}.[208] Aβ has a strong reduction potential and can rapidly reduce Cu^{2+} and Fe^{3+}.[208] In the second step, the reduced metal ion can be re-oxidised *via* oxygen to generate superoxide, which can then form hydrogen peroxide followed by the Fenton (equation 4) and Haber-Weiß reaction (equation 5). The end products are hydroxide and the highly reactive cytotoxic hydroxide radical.

The significance of iron in AD progression is still controversially discussed in the literature and indication is given that it plays only a minor role. Hence, the focus in the following section lies on Cu^{2+}. A proposed Cu^{2+} redox cycle of the cascade leading to ROS, cellular dysfunction and finally to cell death is shown in Scheme 5.[173] The cycle starts with the reduction of Cu^{2+} to Cu^+ through the uptake of one electron from Aβ. The Aβ radical can then further react with lipids and proteins to generate HNE or reactive carbonyls. On the other side the cycle is closed by the re-oxidation of Cu^+ to Cu^{2+} in which oxygen reacts to superoxide.
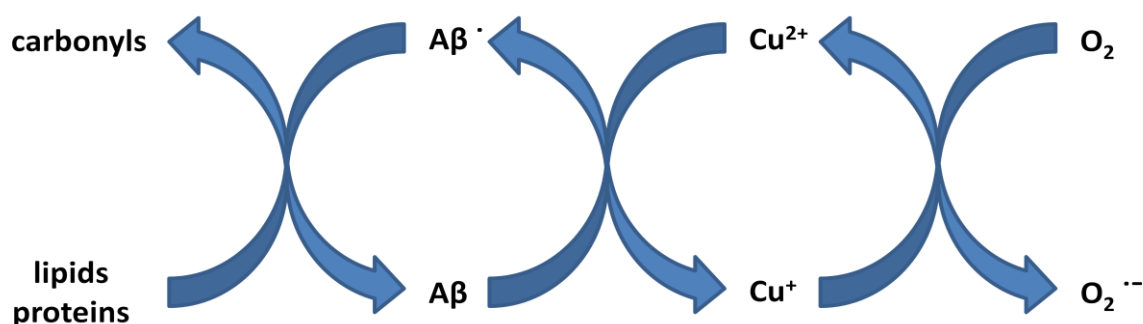
Scheme 5 Possible Cu⁺/Cu²⁺ controlled redox cycle in AD, generating Carbonyls (HNE) and superoxide[173]

One open question in this reaction cycle is the localisation of the radical on the Aβ protein. The Aβ protein sequence shows only two possible positions which could directly stabilise a radical, the Met^{35} or the Tyr^{10} residues DFT calculations indicate a reduction of Cu^{2+} *via* proton-coupled electron transfer (PCET) from ascorbate on the Tyr^{10} residue.[135] Inhibition of the redox process by substitution of the Tyr^{10} by alanine strongly supports this hypothesis. In contrast, there is also evidence given which indicates that the radical is more likely stabilised by the Met^{35} residue. Under relatively mild conditions, through a specific support of the Lys^{31}, Met^{35} can be reversibly oxidised to a diastereotopic pure methionine sulfoxide.[209–213] Of greater significance than the mere oxidation is the generation, stability and reactivity of the radical localised on the sulphur. Mechanistic studies revealed a fast radical oxidation to a sulfuramyl radical cation ($R\text{-}S^{\cdot+}\text{-}CH_3$).[209] In a subsequent step the radical is shifted to a carbon centred radical which immediately reacts with paramagnetic oxygen to a peroxylradical. The propagating radical process starts after reaction with other electrophilic biomolecules. Products of this process can be the above mentioned HNE and other lipid peroxidation products. In this mechanism the intermediate, $R\text{-}S^+H(CH_3)$, is generated, which has a pK_a value of -5[214] and therefore is directly deprotonated, reforming Met^{35}. Thus, the Aβ protein can function as a catalyst.

Through substitution of the Met^{35} to norleucine (S to CH_2) all oxidative and neurotoxic properties of $Aβ_{1-42}$ to cultured neurons were suppressed.[215] Even when methionine sulfoxide was used instead of the normal Met^{35} no protein oxidation could be observed.[216] These two results gave evidence that the Met^{35} can undergo a radical oxidation to the sulfuramyl radical cation without further reaction to the methionine sulfoxide, which would be inactive in ROS production.

Furthermore it could be proven that the Met[35] is crucial for Aβ induced oxidative stress in AD. Still, independent from the modification of the Met residue, norleucine or methionine sulfoxide, small aggregated fibrils were formed.[216]

1.6 Treatment of AD

Since the discovery of AD 100 years ago, a steady increase in afflicted persons has been recorded, not only through better diagnostic techniques but also due to the increase in life span. The consequence is exploding costs in the pharmaceutical sector and health care. The growing interest in developing new drugs and therapeutically strategies is therefore only natural. The first developed drugs for the treatment of AD were based on enhancing the acetylcholine level in the synaptic cleft by inhibiting the acetylcholinesterase (AChE).[217] These drugs were developed after the discovery of elevated release of acetylcholine in the mid 1970s. After further investigation it could be shown that this kind of treatment with, for example, tetrahydroaminoacridine, donepezil, huperzine A or galantamine simply reduces the symptoms but does not cure the disease.[26] The progressive development of isolation, analytic and structural determination techniques allowed the development of new therapeutical strategies. One approach is the suppression of Aβ aggregation.[48] Three different strategies which already reached phase II clinical trials should be mentioned in this context. The first is vaccination using Aβ-derived immunogens (Elan's Aβ vaccine).[218,219] The second strategy targets monomeric Aβ directly.[220] Small compounds can bind to the protein and create complexes which cannot aggregate. The third and last approach involves the cleavage of APP.[221] By inhibition of γ-secretase the amount of total Aβ can be reduced and with this the amount of aggregates.

With increasing evidence for metal accumulation combined with metal induced oxidative stress in AD, chelating therapies are favoured. The first ligand systems used for application in AD were "classical" ligands with strong binding affinities for most transition metals (Figure 8). Clioquinol (5-chloro-7-iodoquinolin-8-ol, CQ) is one of the ligands which has to be highlighted for several reasons. CQ is a lipophilic brain-permeating ligand with mid-nanomolar affinity, not only to zinc but also to copper. With the small doses used in AD treatment, the formed metal complex does not precipitate.[222–224] Therefore CQ and its derivatives were widely studied and even reached clinical trials. Although CQ and several other systems have the required coordination abilities and show good *in vitro* results, their application in AD research is limited. Most of the systems (DFO, TETA, etc.) cannot cross the blood brain barrier (BBB) and show no selectivity towards a specific metal. Nonetheless these ligands opened the door to chelating therapies in AD. A second generation of CQ, PBT2 (8-hydroxyquinoline), was developed. Due to impressive positive results, such as lowering the Aβ levels, reduced formation of phosphorylated tau, and better cognitive performance, a phase IIa clinical trial was started.[225–227] PBT2 is not only a chelating agent, in addition it fulfils the duty of a chaperon, functions as transport and regulation protein, and can redistribute Cu^{2+}.
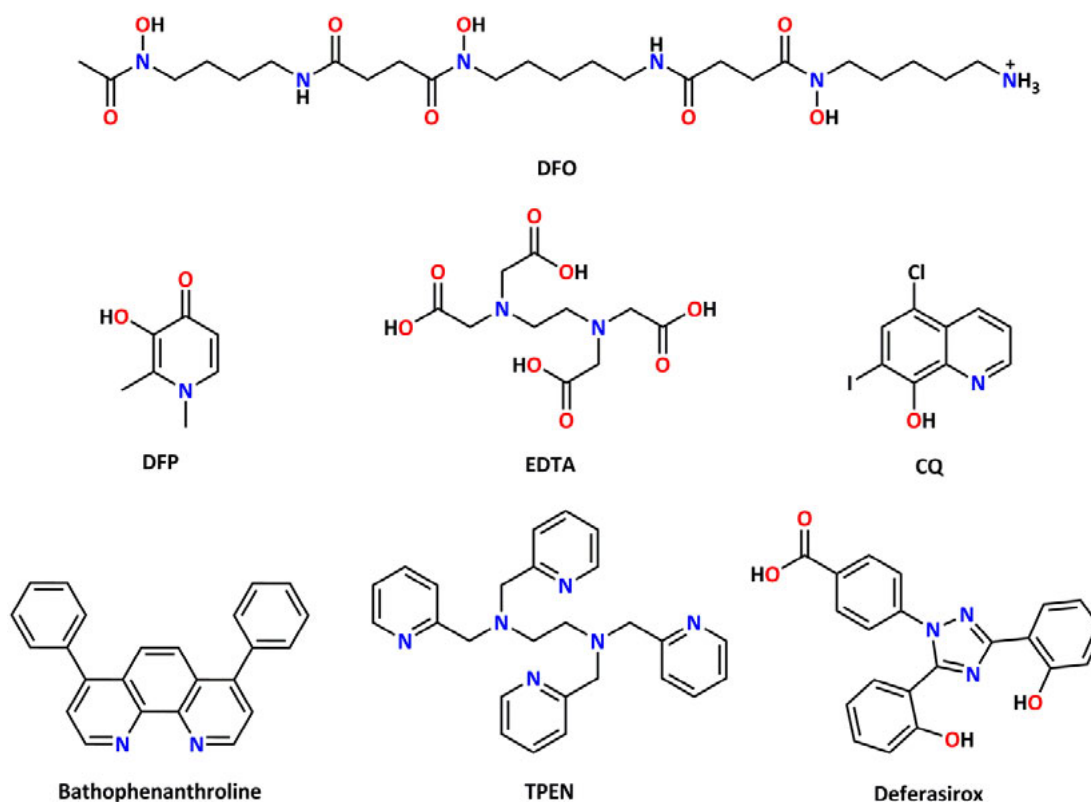
Figure 8 First generation of chelators used to remove metal ions from AD tissues.

As mentioned previously, a copper imbalance in AD leads to accumulation of Cu^{2+} in affected brain regions.[228] Therefore, a chaperon-like activity could be the key to restore the copper distribution.[99] At the moment PBT2 is still under research and has already shown promising results in clinical trials.[226] A relatively new approach is the combination of two or more functional building blocks to create multifunctional systems with high potential for applications in AD (Figure 9). Often one of these components is a metal-binding compound. The classical chelators or their derivatives were often used as a basis. These compounds were then linked to an amyloid binding-motif, antioxidant, or inhibitor of Aβ aggregation. Simple glycol-conjugated or peptide coupled systems are also known. Since this approach is quite new, and combination possibilities are more or less endless, the efficacy of drugs generated by this approach has to be proven. In conclusion many questions relating to AD are still unanswered. While some drugs and therapies with promising performance in clinical trials have been developed, so far these cannot cure the disease, nor stop its progression. They can only temporarily reduce the symptoms. Therefore a better understanding of AD progression is essential for the synthesis of new, more effective drugs.
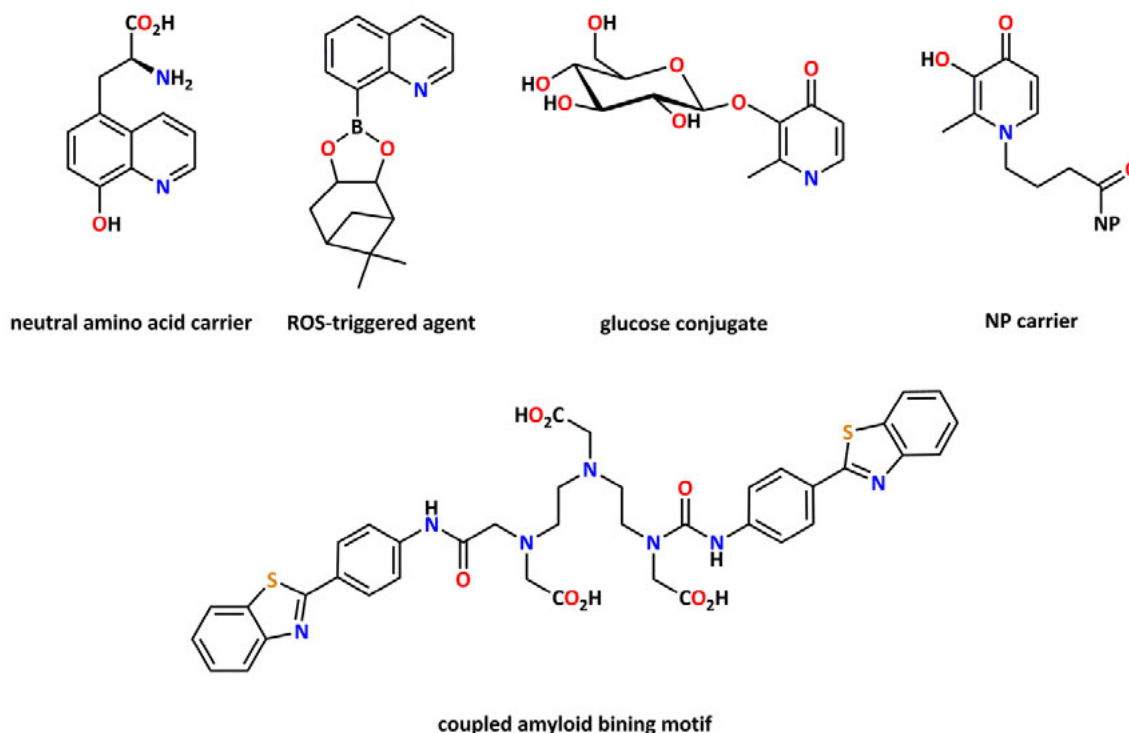
Figure 9 Multifunctional tools with applications in AD (NP = nanoparticle).

1.7 Modern Drug Design

Drug design is an important part of medical science. One approach is target-orientated drug design with consideration of the biological and chemical behaviour of the targeted molecule. Normally these molecules play an important role in physiological metabolism. An important and challenging task is that drugs have to bind to the target but should not affect other molecules similar to the target. Thus, prior to the synthesis, a model has to be created considering all chemical, biochemical and medical aspects. From an economic point of view drugs should fulfil several requirements like low manufacturing cost and appropriate stability for storage and transport. However the main issues arise from biological factors: absorption, distribution, metabolism, selectivity, excretion and toxicity (ADMET).[229,230] In the following, the ADMET concept will be shortly explained.

Absorption: Orally administrated medication is preferred over inhalation and injection. For an oral medication to take effect the drug must be well absorbed from the digestive tract. In general, drugs must be able to pass through cell membranes and to be transportable in the blood. For neuro-pharmaceutics, there is an additional requirement: The pharmaceutics have to cross the blood brain barrier (BBB). Since this is not always possible, precursors are frequently used which are able to cross the BBB and release the active molecule afterwards.

Distribution: The distribution and transport of the drug is the second important biological aspect. It has to be ensured that the distribution of the drug is selective for the diseased organs or regions. Otherwise an insufficient distribution would result in an ineffective treatment. Medications with severe side effects can even lead to serious damage in the case of wrong distribution in the body.

Metabolism: In some cases the metabolism of the pharmaceutical is desired, e. g. prodrugs. Generally it should not be too easily metabolised by the body because its effectiveness would be too low.

Excretion: Many drugs are only temporarily necessary and an accumulation would also lead to several problems. Most drugs are excreted after an extended time, whereas others are metabolised.

Toxicity: The non-toxicity of a drug is one of the most difficult challenges to be achieved. Drugs are designed to change or interrupt biological processes. Unfortunately the interaction of the drug with the body often results in side effects like headaches, allergic reactions or dizziness. Nowadays already during the design of new drugs, partial focus lies on reducing possible side effects but a complete prevention is not always possible e.g. in the case of anti-cancer drugs.

To sum up all the biological aspects and develop a chemical concept out of it is a difficult task. Fortunately a connection between the uptake, the distribution and the chemical properties of a drug was found empirically.[231] "Lipinski's Rule of Five" outlines the essential characteristics an orally administered drug should possess:

- Not more than 5 hydrogen bond donors (NH_2, NH, OH)
- Not more than 10 hydrogen acceptors (N, O)
- A molar mass of less than 500 daltons
- A partition coefficient log P (octanol-water) not greater than 5

The name "Rule of Five" originates from the fact that each rule includes a number which can be divided by five. It should also always be considered that it is only an empirical finding which indeed is valid in many applications, but there are also deviations from the norm, such as insulin.

Chapter 2

Motivation – Drawing the Blueprints for Multifunctional Tools with Applications in Alzheimer's Disease Research
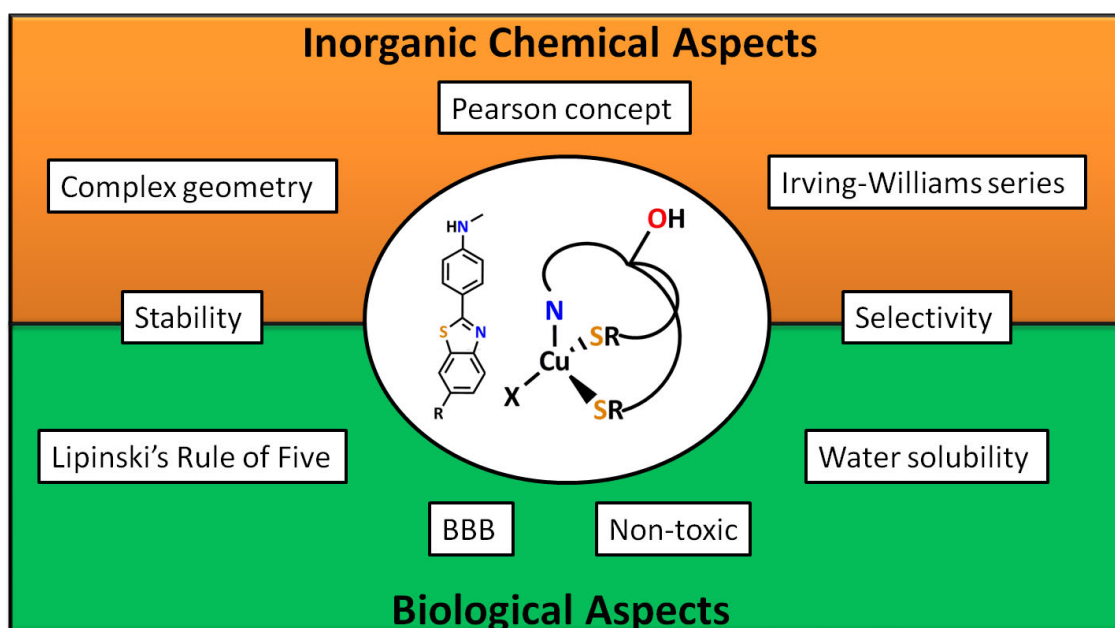
2.1 Motivation

Around 2 % of the population in the industrial countries is currently affected by Alzheimer disease (AD). This disease is of increasing importance especially under consideration of the demographic development from both financial and ethnic point of view. Since its discovery 100 years ago, no efficient therapies for AD have been found.[217] One reason for this is the limited knowledge about the exact formation of Aβ plaques and their specific neuro-toxic effects. Metal induced oxidative stress, which damages the cell and finally leads to neuronal loss in specific regions in the brain, is proposed to be the main event in AD progression. For the elucidation of the specific redox processes in the cell unfortunately only a small number of studies have been accomplished. Besides, most of the studies were performed *in vitro* and extrapolation of the data to the cells is not always possible. Therefore, the production of ROS in the AD afflicted brain remains a process that requires further investigation. Previous inhibition of ROS generation using metal chelators targeting Cu^{2+} and Fe^{3+} yields promising results. However in order to prove the proposed redox cycles (Scheme 5), the intermediates have to be captured. Therefore Cu^{+} or Fe^{2+} selective ligands are needed and their coordination properties toward the metals have to be evaluated. As discussed in the previous chapter, the involvement of Cu^{+} in the AD progression seems to be more likely than iron participation. The aim of this study is therefore not to develop new drugs for AD, but to provide a multifunctional tool for further investigation on the relatively unknown Cu^{+}-Aβ interaction. Nevertheless, ligand design was done on basis of modern drug design to keep the path open for advanced biological studies in mammals. In order to achieve the goals a five-stage plan for the gradual course of the study was developed (Scheme 6).

1. Synthesis and characterization of Cu^{+} selective ligands considering inorganic and biological aspects.

2. Exploring the complexation abilities of the designed ligands with respect to selectivity, stability and metal exchange properties.

3. Studies of the inhibition of ROS generation.

4. Synthesis of benzothiazole derivatives as Aβ-plaque markers and coupling with the evaluated ligands.

5. Binding studies of the final compounds with Aβ-plaques.

Scheme 6 Five-stage plan for the development of multifunctional tools for applications in AD.

2.2 The Chelator – Inorganic Aspects Combined with Modern Drug Design

Selectivity is an essential requirement for all drugs and biomarkers. Especially metal targeting drugs have to be selective, not only for the targeted metal, but also for the specific protein, since otherwise serious consequences are looming. Metals are not only used in the active centre of various proteins, but are also involved in many biological activities like signal transduction, electron transfer, structure factors and others. Dysregulation of the natural metal homeostasis, which is a tightly regulated process, can therefore lead to several disease patterns and also to cell death. Thus, for pharmaceutics and compounds with biological applications is selective coordination essential. The overriding aim of this study is to achieve a more profound understanding of the Cu^+ chemistry in AD. A multifunctional tool, which not only selectively binds Cu^+ with a defined stability constant, but comprises selectivity for Aβ plaques, should therefore be developed.

Coordination of a metal depends on the donor strength of the ligand, including the size of the binding pocket, the charge, electronegativity, bond lengths and angles in the ligand but also on the concentrations, of the reaction partners as well as of co-ligands. Especially the latter is an important factor for *in vivo* studies, complicating simple metal-ligands reactions. A better description of ligation reactions would therefore be the equilibrium between the aqueous $M(H_2O)_x^{n+}$ complexes and the chelated LM complexes. Thus, basic concepts like the principle of Pearson are of limited application.[232] More precise is the Irving-Williams series, which directly considers the aqueous milieu and compares equilibrium constants for most donor groups. The Irving-Williams series shows that the most stable Cu^{2+} complexes are formed with a mixed {NS$^-$} donor set.[233] Although, Cu^{2+} has different chemical behaviours than Cu^+, this empirical finding was used as starting point for the synthesis of Cu^+ selective ligands and was refined with the HSAB (hard and soft acids and basis) concept from Pearson.[232] After Pearson, Cu^+ has a softer character, since it is big, has a low charge and can easily be polarised. Cu^+ should therefore prefer soft donor atoms like sulphur. Thus, a {NS$_2$} and {N$_2$S$_2$} donor set was chosen in the ligands (Figure 10). Conversely, Lewis acids like Mg^{2+} or Ca^{2+} will not be coordinated and according to the Irving-Williams series also the chelation of Mn^{2+}, Fe^{2+}, Co^{2+} and Ni^{2+} is disfavoured in the presence of copper. The second aspect considered in the ligand design is the complex geometry. Cu^+ comprises due to its closed d^{10} electron shell no ligand field stabilisation energy (LFSE). The complex geometry is therefore defined by the steric demand of the ligands, which results for four donor atoms in a preferred tetrahedral geometry. In contrast to that, Cu^{2+} forms square planar complexes with four and square pyramidal or trigonal pyramidal complexes with five ligands. A tetrahedral complex formation can be achieved by a strong pre-organisation of the ligand. Complex formation with Cu^{2+} should therefore be disfavoured and selectivity towards Cu^+ should be given.

The increased copper levels involved in AD could have their origin in a dyshomeostasis forming a labile copper pool.[98] Taken this into account rather weak ligand systems are required, which do not remove the excessive copper, but can relocate it and thus restore normal copper levels. To be more precise, the chelator should have a higher affinity than the Aβ protein but low enough, that the Cu^+ can be released again to metal transport proteins. Under consideration of this, the first generation of ligands developed in this project features only a tridentate {NS$_2$} donor set. The corresponding Cu^+ complexes should therefore be thermodynamically metastable and be

able to release the metal again. In a second generation more stable tetradentate ligands with a $\{N_2S_2\}$ donor set, to ensure tight Cu^+ coordination, were synthesised. As nitrogen donors pyridine and imidazole groups were chosen. Both are good σ-donors and can tightly coordinate to copper. The sulphur donor groups are realised by thioether functionalities instead of thiolate groups. This offers various advantages to the ligand system: i) less hydrogen bond donors enhance the chance to cross the BBB and to permeate cell membranes due to the hydrophobic character, ii) thiolate groups have a high tendency to form thiolate bridges between two metal ions[234–236], iii) possible cell toxicity due to the formation of disulphide bridges and thus generation of ROS is reduced,[237–241] iv) lower binding affinities, since no charge is compensated. The latter increases the chance for a copper release and also weakens coordination of other transition metals besides Cu^+. Thus, the ligands should not be able to compete with the $M(H_2O)_x^{n+}$ complexes, except in the case of Cu^+. The ligands will be evaluated with regard to their coordination properties and the most suitable candidates will then be coupled to a compound, which is sensitive for Aβ-plaques. To give access to coupling reactions an alcohol function was introduced in the ligands. The alcohol should also allow the attachment of other functional groups or molecules to confer chemical and biochemical properties (e.g. water solubility by coupling with an alkyl sulfonate) to the chelators. Overall, the ligands were designed as plain as possible to follow "Lipinski's Rule of Five" and ensure their absorption and permeation of cell membranes.

One aspect in modern drug design is the distribution of the compound. In the previous chapter dyes like ThT and PIB were presented with the remarkable ability to selectively interact with Aβ plaques and with low clearance times from healthy tissues. By coupling of such a benzothiazole derivative with the evaluated ligands *via* a spacer a multifunctional compound can be created, which should be suitable for the desired application. This compound exhibits on one side a selective metal binding unit and on the other side a marker for Aβ plaques (Figure 10). Although, different pathways for the synthesis of benzothiazole derivatives are known, they lack flexibility in the variation of functional groups.[242,243] Herein, a synthetic route was created with *Suzuki Coupling* as the key step, which offers the possibility to combine various building blocks leading to new benzothiazoles.
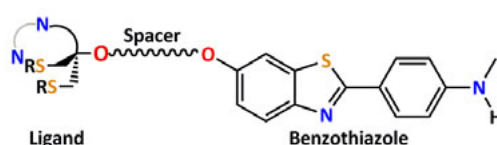
Figure 10 Design of multifunctional systems for application in AD research.

Tripodal pre-organised ligand systems, like tris(pyrazol)borate (tpb) or tris(pyrazol-1-yl)methane (tpm), have been used for many years in model complexes in bioinorganic chemistry. Their specific binding properties were also utilised with respect to CO releasing molecules (CORMs), with remarkable results.[244–246] The compounds synthesised in this study provide with their soft $\{NS_2\}$ binding moiety a unique type of tripodal pre-organised chelator with unknown reactivity. Thus, besides the applications in AD, the tripodal ligands were also used for the synthesis of a new class of CORMs.

Chapter 3

Synthesis and Characterisation of Tridentate Ligands for Applications in AD

flexible – pre-organised
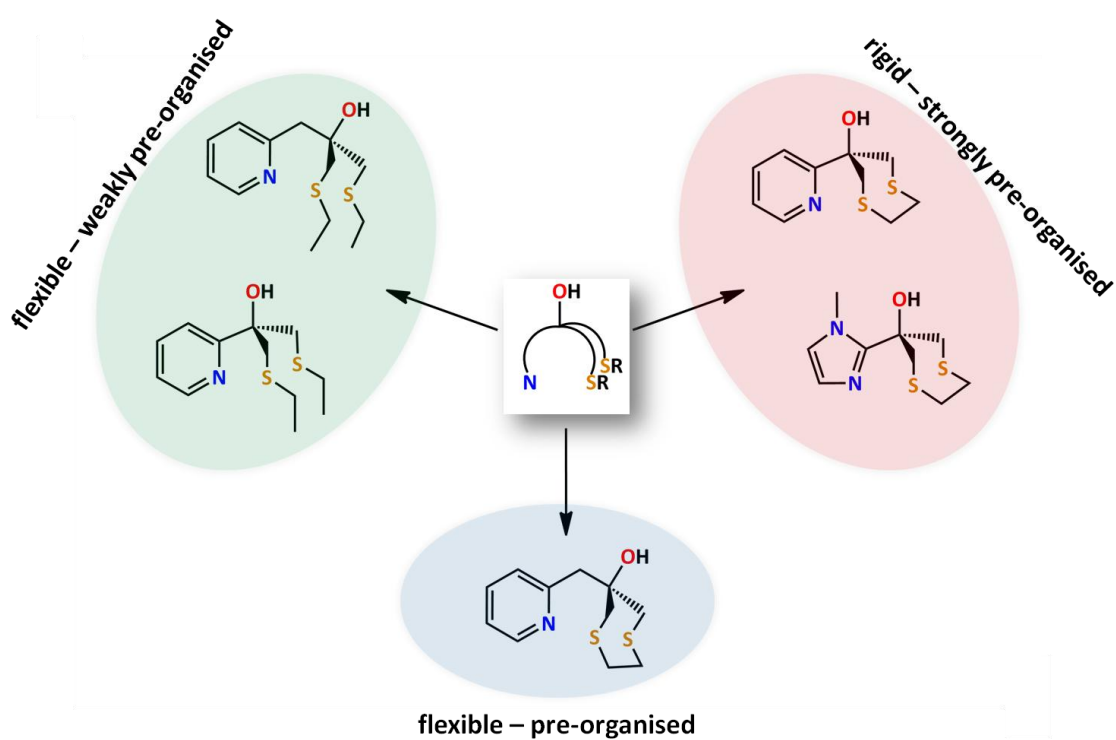
3.1 Introduction

In order to investigate the role of Cu$^+$ in AD, selective ligands have to be provided. Under consideration of the labile copper pool, the formed complexes should not be too stable allowing a redistribution of the copper and recovery of normal copper levels. Five tripodal ligands with a {NS$_2$} binding motive were synthesised, to fulfil this task. The ligand design was done according to the concept outlined in chapter 2.2. The synthesised ligands were evaluated with respect to their complexation properties towards Cu^{2+} and Cu$^+$ and to determine which systems are most suited for the desired application in AD research.

3.2 Ligand Synthesis

The ligand systems follow two different approaches which should lead to metastable Cu$^+$ complexes. The first approach comprises of two relatively flexible ethyl thioether sidearms. These should allow a rearrangement of the ligands upon coordination. The two ligands, **L^{1H}** and **L^{2H}**, belong to the first approach and are only slightly pre-organised (Scheme 7). In the second approach a cyclic thioether side chain was introduced in the ligands. The resulting ligands are more pre-organised and should enforce mononuclear Cu$^+$ complex formation with a tetrahedral geometry. Furthermore, cyclic thioethers have shown higher affinities towards Cu$^+$ than acyclic analogues.[247,248] Thus, the rigid ligands should comprise higher affinities. **L^{3H}**, **L^{4H}** and **L^{5H}** belong to these chelators.

The ligands **L^{1H}**-**L^{5H}** used in the present study were synthesised in a two-step synthesis (Scheme 7). Starting reagent for all five ligands was the commercially available 1,3-dichloroacetone, in which thioether groups were introduced *via Williamson ether synthesis* in the first step. The precursor **I** for the synthesis of **L^{1H}** and **L^{2H}** was synthesised by the reaction of 1,3-dichloroacetone with ethane thiole under basic conditions. In the second step, **I** was diluted in THF and the solution cooled to -78 °C. The reaction mixture was then treated with either lithium pyridin-2-yl or lithium methyl pyridine-2-yl, which was prepared prior, resulting in the formation of **L^{1H}** and **L^{2H}**, respectively. The mechanism of the reaction is a nucleophilic attack of the lithium-organyl on the electrophilic ketone function. The ketone functionality becomes *in situ* reduced, providing the alcohol functionality, which is desired for subsequent coupling reactions. For the second approach 1,2-ethanedithiole was coupled to 1,3-dichloroacetone, providing the cyclic ketone **II**. Analogous to the synthesis of **L^{1H}** and **L^{2H}**, lithium-organyl solutions were prepared and added to **II** at -78 °C. After aqueous workup the ligands could be obtained in moderate to good yields of 52 to 82 %. It should be mentioned that **L^{1H}** is literature known.[249] However, optimisation of the reaction conditions led to higher yields in both steps.
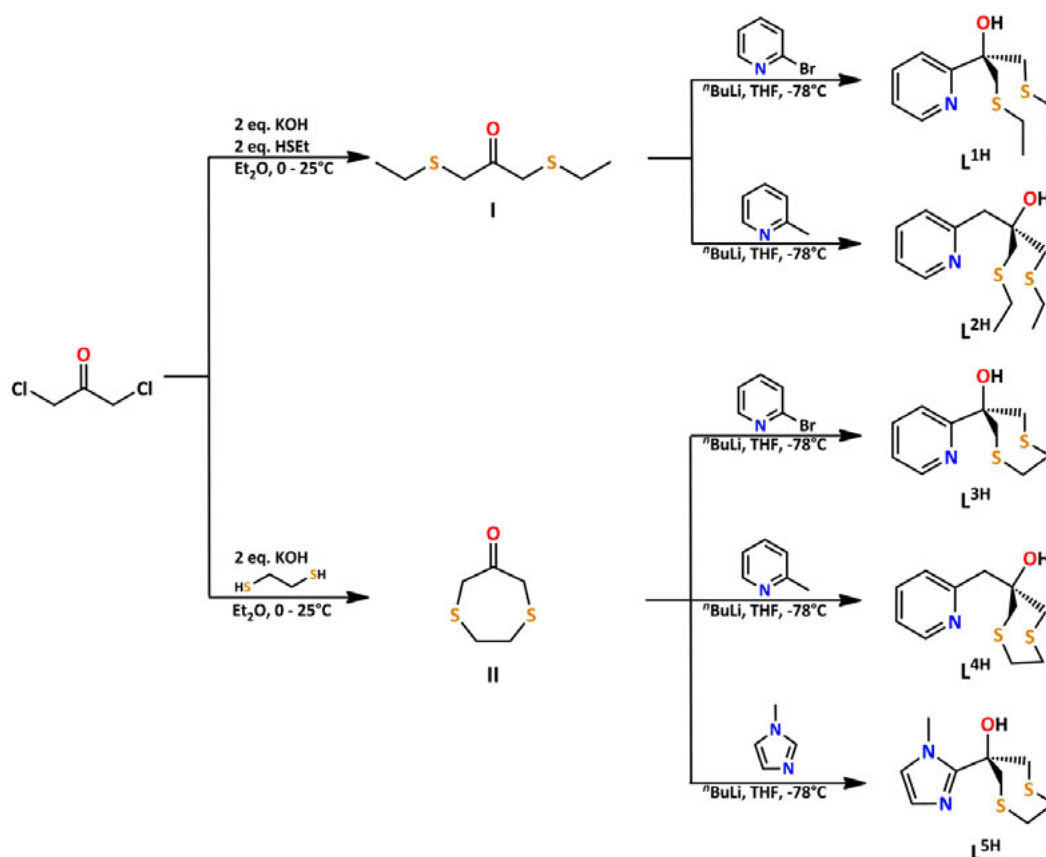
Scheme 7 Synthetic route for the tridentate ligands L¹ᴴ-L⁵ᴴ.

In addition to the mixed {NS$_2$} ligands, the literature known system **L⁶ᴴ** was synthesised to compare the affinity of the thioether donor atoms of **L¹ᴴ** - **L⁵ᴴ** to stronger σ-donors, such as pyridine. The ligand **L⁶ᴴ** is also a tripodal pre-organised system and should therefore form analogous complexes to the {NS$_2$} ligands. **L⁶ᴴ** was synthesised according to literature starting from the commercially available 2-(aminometyl)pyridine and 2-(chloromethyl)pyridine and could be provided in good yields of 87 % (Scheme 8).[250,251] Although, various complexes with **L⁶ᴴ** are literature-known, its coordination properties towards Cu⁺ have not been investigated so far. However, complexes with Cu²⁺ and Zn²⁺ have already been widely studied and show that the ligand is not selective.
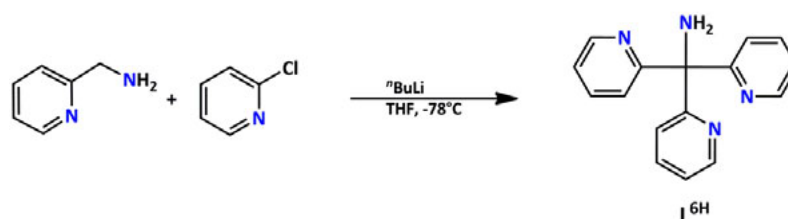
Scheme 8 Synthesis of L⁶ᴴ.

Complexation and affinity studies require analytic purity of the used compounds. Thus, all compounds were purified by column chromatography on silica and purity was determined by NMR, MS and EA (for details see experimental section).

3.3 Synthesis of Cu$^+$ Complexes

Cu$^+$ complexes were synthesised by treating either [Cu(MeCN)$_4$]PF$_6$ or [Cu(MeCN)$_4$]OTf in MeCN with equimolar amounts of the ligands (Scheme 9) under inert atmosphere. Table 5 summarises the obtained complexes with their yield. The complexes **1**-**6** were then precipitated by addition of diethyl ether to the reaction solution or layering a saturated complex solution in MeCN with diethyl ether. All compounds were analysed by ^{1}H- and ^{13}C-NMR spectroscopy and ESI-MS spectrometry. The utilised ligands are tridentate and leave a vacant coordination site on the metal. In the presence of MeCN, this site will be saturated by one MeCN molecule, which is a good donor for Cu$^+$.[252]
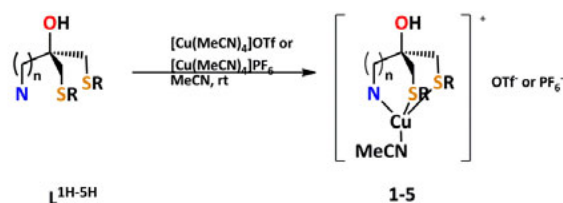
Scheme 9 General procedure for the synthesis of Cu$^+$ complexes.

In ESI-MS spectra the peaks of the highest mass/charge ratio could be assigned to either the [**L**Cu]$^+$ or [**L**Cu(MeCN)]$^+$ species, whereas peaks of the highest intensity belonged to a [**L**H]$^+$ species, indicating a rather weak coordination. Applying ^{1}H- and ^{13}C-NMR spectroscopy the complex spectra could be detected, except for **L^{4H}** were a paramagnetic spectrum was recorded. Both experiments indicate, that in solution complexes of the structure [**L^x**Cu(MeCN)]$^+$ could be present. Thus all five ligands should be suitable for the desired applications in AD.

Table 5 Yields of synthesised Cu$^+$ complexes.

	Complex	Yield [%]
1	[**L^{1H}**Cu(MeCN)]OTf	85
2	[**L^{2H}**Cu(MeCN)]OTf	78
3	[**L^{3H}**Cu(MeCN)]PF$_6$	76
4	[**L^4**$_2$ Cu^{2+}Cu$^+$$_2$(MeCN)$_3$](PF$_6$)$_2$	30
5	[**L^{5H}**Cu(MeCN)]PF$_6$	65
6	[**L^{6H}**Cu(MeCN)]PF$_6$	93

In order to select the most promising ligand and to explore the unexpected complexation behaviours of **L^{4H}**, complex formation was studied in solid state. With exception of **4**, crystals useable for X-ray crystallography could be obtained by slow diffusion of diethyl ether in saturated complex solutions in MeCN. The most flexible ligand **L^{2H}** forms a complex which crystallises in a chain structure (Figure 11). The tetrahedral complex is constituted by the pyridine, a thioether group of the same ligand and a thioether sidearm of a second ligand. The vacant coordination site is saturated with one MeCN molecule. The alcohol group forms a hydrogen bonding to one fluorine atom of the triflate counterion (2.0790 Å). It is possible that also **L^{1H}** forms a chain structure in solid state due to the similar ligand structure. However, since no crystalline material suitable for X-ray crystallography could be obtained no evidence is given for this hypothesis. In contrast to the molecular structure of **2**, **3** crystallises in the desired mononuclear complex structure. The metal ion is coordinated by the {NS$_2$} moiety and one

MeCN molecule. The hydrogen of the alcohol forms a hydrogen bond (2.0094 Å) to one of the fluorine atoms of the hexafluorophosphate counterion. For **5** was a similar structure expected as for **3**. However, a chain structure was instead obtained, although **L^{5H}** is structurally more related to **L^{3H}** than to **L^{2H}**. This leads to the suggestion that the solid state structure strongly depends on crystallisation conditions. In the structure of **5**, the thioether sidearm bridges two Cu⁺ ions. With a distance of 2.2332 Å a hydrogen bond is formed between the free alcohol and one fluorine atom of the hexafluorophosphate.

*Figure 11 Molecular structure of **2** (top left), **3** (top right) and **5** (bottom). **2** and **5** crystallise in a chain structure, whereas **3** crystallises in a mononuclear structure. Hydrogen atoms and the triflate counterion of **2** were omitted for a better overview.*

Crystals could also be obtained from an attempt to crystallise [**L^{4H}**Cu(MeCN)]PF$_6$, but instead of a mononuclear or a chain structure a trinuclear [(**L^{4H}**)$_2$Cu(II)Cu(I)$_2$](PF$_6$)$_2$ complex crystallised under inert conditions. Hence it was possible to explain the paramagnetic behaviour of **4** in the NMR experiments. *In situ* the Cu⁺ is partially oxidised, and since the oxidation takes place only in the presence of **L^{4H}**, it is likely that **L^{4H}** is a non-innocent ligand. One possible mechanism includes the reduction of the proton of the alcohol and formation of H$_2$. Disproportionation of Cu⁺ could be excluded due to the fact, that no formation of elemental copper could be observed. To ensure

that the oxidation of the Cu$^+$ is caused by the ligand and not by trace amounts of oxygen, the reaction was repeated several times and also in a clove box. Furthermore, reaction was carried out utilising [Cu(MeCN)$_4$]OTf instead of [Cu(MeCN)$_4$]PF$_6$. Crystalline material could be obtained directly from the saturated solution, but could not be successfully refined. Thus only a picture could be obtained after solving the data, but this picture strongly resembles **4**.

*Figure 12 Molecular structure of **4** (left) and picture of [**L^4**Cu^{2+}Cu$^+_2$(MeCN)$_2$]OTf$_2$ (right). Hydrogen atoms and counterions were omitted for a better overview.*

Complex **6** crystallises in the space group *P-1* and reveals a mononuclear complex structure (Figure 13). The Cu$^+$ is distorted tetrahedrally coordinated by the three pyridine sidearms and one MeCN molecule. Although the amino functionality could also coordinate to Cu$^+$, the formation of three six-membered rings is preferred by the strong σ-donor and π-acceptor character of the pyridines. The amino functionality forms a hydrogen bond to one fluorine atom of the counterion hexafluorophosphate.

*Figure 13 Molecular structure of **6**. Hydrogen atoms were omitted for a better overview.*

In all five crystal structures Cu$^+$ is coordinated in a distorted tetrahedral fashion by a {NS$_2$}, a {NOS$_2$} or a {N$_3$} donor set and by one MeCN molecule. Prominent structural parameters of the Cu$^+$ complexes are summarised in Table 6 and Table 7. With 2.2843 Å to 2.3919 Å the Cu–S distances are in or just slightly above the literature known range for thioether-Cu$^+$ bond lengths (2.26 Å to 2.36 Å).[253,254] The same applies also for the pyridine groups with distances of 2.0063 Å to 2.0806 Å and the MeCN molecule with 1.8793 Å to 1.9891 Å.[255,256] Comparison of the bond angles shows, that in **2**, with 5 to 6 °, the smallest deviation from the ideal tetrahedral coordination is present. This was anticipated since **L^{2H}** has the highest flexibility. The Cu$^+$ centres

in the other complexes are with up to 20 ° deviation much greater distorted. The largest angles are in all complexes found toward the MeCN molecule. Since there is no steric hindrance from the ligand also bigger molecules, like buffer, counterions ore small proteins should be able to coordinate and even formation of ternary complexes is possible. This reactivity has to be considered, for all further experiments and data interpretation.

*Table 6 Selected bond lengths of **2**-**6**.*

	Cu–S [Å]	Cu–N$_{MeCN}$ [Å]	Cu–N$_{Py/Im}$ or O [Å]
2	2.2843(5)	1.9891(21)	2.0472(16)
	2.3182(5)	-	-
3	2.3514(11)	1.9025(33)	2.0063(32)
	2.3021(10)	-	-
4	2.3787(4)	1.8879(19)	2.0786(15)
	2.3499(5)	1.8857(19)	2.0806(15)
	2.3611(4)	-	-
	2.3595(6)	-	-
5	2.3016(16)	1.9259(29)	2.0164(25)
	2.3919(8)	-	-
6	-	1.8793(15)	2.0640(21)
	-	-	2.0658(18)
	-	-	2.0313(15)

*Table 7 Selected bond angles of **2**-**6**.*

	S1–Cu–S2 [°]	N–Cu–N/O[°]	S1–Cu–N1/O [°]
2	110.50(2)	111.16(7)	105.80(5)
3	87.38(4)	120.13(13)	96.81(9)
4	86.055(16)	120.06(6)	88.47(3)
	86.212(16)	119.47(6)	89.11(3)
5	105-63(3)	127.64(11)	99.66(8)
6	-	87.53(7)	-
	-	131.47(8)	-
	-	122.64(8)	-

From the structural characterisation in solution and also in solid state, **L³ᴴ** seems to have the highest potential for further applications. **L³ᴴ** was the only tridentate {NS₂} ligand which showed mononuclear complex formation not only in solution but also in solid state. Second in order would then be ligand **L⁵ᴴ**, because of its structural similarity with **L³ᴴ**. **L¹ᴴ** and **L²ᴴ** have shown in the characterisation in solid state, that their flexibility could be disadvantageous.

3.4 Synthesis of Cu²⁺ Complexes

In the previous chapter, it could be demonstrated that the synthesised ligands can coordinate Cu⁺ in organic solvents. However, the desired ligands should be selective for Cu⁺. Thus, their complexation properties towards Cu²⁺ have to be evaluated. Since complexation properties of

L^{6H} with Cu^{2+} have already been reported in the literature, no Cu^{2+} complexes were synthesised utilising L^{6H}. The complexation properties of L^{6H} strongly depend on the used reaction condition. Mononuclear complexes of the structure $[L^{6H}CuX_2]^+$ can be formed in the presence of coordinating counterions like acetate. Otherwise octahedral complex species with two ligands are formed. The metal centre in these complexes is coordinated by two pyridine and the amine function of each ligand.[250] L^{1H} and L^{5H} were also not considered for Cu^{2+} complexation experiments due to the structural similarity to L^{2H} and L^{3H}. Thus, only L^{2H}, L^{3H} and L^{4H} were used for the synthesis of Cu^{2+} complexes.

Cu^{2+} complexes were synthesised by either stirring acetonitrile solutions of the corresponding Cu^+ complexes in air over night or in a direct pathway using $CuCl_2$. After stirring the Cu^+ complexes for 1 to 2 h oxidation takes place and the reaction solution started to turn green. Precipitation by addition of diethyl ether did not provide the pure complexes. The crude products were therefore recrystallised from $MeCN/Et_2O$. With this procedure $[L^2_2Cu_2Cl_2]$ (**7**), $[L^4_2Cu_2(MeCN)_2]OTf_2$ (**8**) and $[L^3_4Cu_4]OTf_4$ (**9**) could be synthesised. It is worth mentioning that in all three complexes the alcohol is deprotonated *in situ* by the acidifying effect of the metal. Thus, in the absence of any base an acidic complex solution is formed, from which crystals of the complexes, but no crystals of the protonated ligands could be obtained. Molecular structures obtained *via* X-ray crystallography are pictured in Figure 14. Reaction of L^{2H} with $CuCl_2$, results in the neutral $[L^2_2Cu_2Cl_2]$ complex (**7**), which crystallises in the space group $P2_1/c$. The two metal ions are bridged by the deprotonated alcohol function of the ligand, a behaviour that could also be observed in the molecular structure of the trinuclear complex **4**. Besides the alcohol, each metal is further coordinated by one pyridine, one chlorine ion and one a thioether sidearm. With the sulphur atoms in the axial positions, the metal ions are coordinated in a distorted square pyramidal coordination geometry. To define the distortion in more detail the parameter τ can be determined.[257] The τ value for an ideal trigonal bipyramid ($\beta = 180\,°$ and $\alpha = 120\,°$) is $\tau = 1$ and $\tau = 0$ for an ideal square pyramid ($\beta = \alpha = 180\,°$). For the complex **7** a τ value of 0.16 could be determined.

By stirring L^{4H} with equimolar amounts of $[Cu(MeCN)_4]OTf$ in MeCN over night in an open vessel, the complex $[L^4_2Cu_2(MeCN)_2]OTf_2$ (**8**) could be synthesised. Crystallisation succeeded by overlayering the reaction solution with diethyl ether and storage at 4 °C. The obtained complex geometry of **8** is similar to **7**. Two Cu^{2+} ions are constituted by the nitrogen of a pyridine, one sulphur atom of a thioether group and the two bridging alkoxide groups in the square plane. In the axial position one MeCN molecule is coordinated, completing the square pyramidal geometry ($\tau = 0.08$). The second thioether group is in a distance of 2.9922(5) Å where interactions cannot be excluded and therefore the complex geometry could also be regarded as a very strongly distorted octahedron (N_{MeCN}–Cu–S2 angle = 148.81 °).

*Figure 14 Molecular structures of **7** (left top), **8** (right top) and **9** (left bottom). Picture of the possible molecular structure of [**L^1**$_3$Cu$_3$PF$_6$](PF$_6$)$_2$ is on the right bottom. Hydrogen atoms and counterions were omitted for a better overview.*

Following the same procedure crystalline material could also be obtained for **9**. A dinuclear divalent molecule structure was expected, similar to **7** and **8**. However, instead the tetranuclear complex **9** was formed. The reason for the different solid state structures is the short distance between the alcohol and the pyridine sidearm. Thus, upon coordination a five-membered chelation ring is formed. In **7** and **8,** picoline sidearms are present, which can enclose the metal more easily. Thus, the formation of dinuclear complexes is due to the rigid ligand structure not possible and instead a tetranuclear complex is generated. In the molecular structure of **9,** each metal centre is coordinated in a distorted square pyramid (τ = 0.19). The plane of the pyramid is constituted by one sulphur atom of a thioether, one nitrogen atom of a pyridine and two bridging alkoxide groups. In the axial position the metal is saturated by another sulphur atom. To gain further evidence, that the ligands with smaller biting angles are not capable to form dinuclear complexes, attempts were carried out to crystallise a Cu^{2+} complex with **L^{1H}**. Unfortunately, refinement was not possible. Thus, only a picture of a possible molecular structure could be provided (Figure 14).

Structural features of the three complexes **7** - **9** are summarised in Table 8 and Table 9. With 2.3256 Å to 2.8075 Å for the S-Cu^{2+} bond lengths and with 1.9588 Å to 2.0031 Å for the $N_{Py/Im}$–Cu^{2+} bond lengths, the synthesised complexes have shown similar structural features to analogous systems reported in the literature.[258–261]

*Table 8 Selected bond lengths of **7**-**9**.*

	Cu–S [Å]	Cu–O [Å]	Cu–$N_{Py/Im}$ [Å]	Cu–N_{MeCN}/Cl [Å]	Cu–Cu [Å]
7	2.8075(11)	1.9891(17)	2.0031(20)	2.3073(8)	3.1902(9)
	-	2.0242(20)	-	-	-
8	2.3451(5)	1.9228(14)	1.9895(16)	2.8654(22)	2.9659(4)
	-	1.9186(14)	-	-	-
9	2.3256(5)	1.9334(12)	1.9620(17)	-	3.3835(3)
	2.7636(5)	1.9295(12)	1.9588(17)	-	3.3644(3)
	2.3384(4)	1.9378(13)	-	-	-
	2.7820(5)	1.9337(14)	-	-	-

*Table 9 Selected bond angles of **7**-**9**.*

	O–Cu–O [°]	N1–Cu–O [°]	S1–Cu–O [°]	Cu–O–Cu [°]
7	105.28(7)	93.51(8)	72.42(6)	74.72(7)
8	78.92(6)	92.99(6)	84.14(4)	78.92(6)
9	121.83(7)	82.93(6)	86.19(4)	121.14(7)
	121.14(7)	82.87(6)	80.13(4)	121.83(7)
	-	-	87.19(4)	-
	-	-	80.21(4)	-

Structural characterisation of the complexes **7** and **8** showed that both Cu^{2+} ions and both bridging alkoxides are constituted in one plane. These systems should therefore be predestinated for magnetic superexchange. Thus, SQUID measurements performed (Figure 15) for 7 - 9. Due to an antiferromagnetic superexchange interaction, all three complexes have the diamagnetic S_T = 0 ground state. Coupling constants for the magnetic exchange were determined by using a fitting procedure to the appropriate Heisenberg-Dirac-van-Vleck (HDvV) spin Hamiltonian for isotropic exchange coupling and Zeeman splitting (for **7** and **8** was equation 6 used and for **9** equation 7 was used). Temperature-independent paramagnetism (*TIP*) and a paramagnetic impurity (*PI*) with spin *S* = 1/2 and *Curie* behaviour were included according to equation 8.[262] The determined coupling constants and magnetic parameters are summarized in XXXX.

$$\hat{H} = -2JS_1S_2 + g\mu_B\vec{B}(\vec{S}_1 + \vec{S}_2) \tag{6}$$

$$\hat{H} = -2J(S_1S_2 + S_2S_3 + S_3S_4 + S_1S_4) + \sum_i g\mu_B\vec{B}\vec{S}_i \tag{7}$$

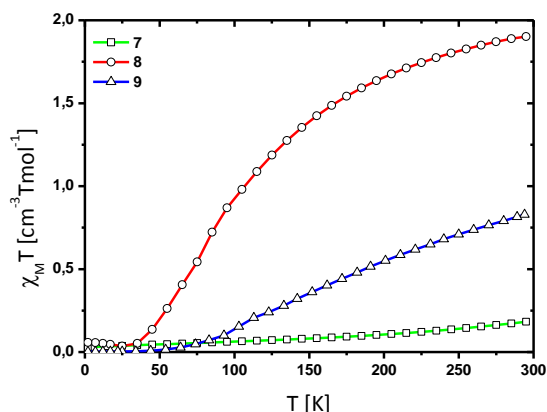$$\chi_{calc} = (1 - PI)\cdot\chi + PI\cdot\chi_{mono} + TIP \tag{8}$$

*Figure 15 χMT versus temperature for **7**, **8** and **9** at 0.5 T.*

The *J* values for di-μ-alkoxo Cu_2O_2 complexes depend linearly on the Cu–O–Cu angle ⬚ as − 2 *J* = 82.1 ⬚-7857. Thus, the expected *J* values for **7** and **8** are -291 cm⁻¹ (⬚ = 102.8°) and -222 cm⁻¹ (⬚ = 101.1 °). With *J* = -108, just a half so large coupling constant could be observed in the experiment. However, this finding can be well explained be the large angle ⬚ between Cu_2O_2 plan and C–O axis (35.7 °), which also strongly influences the coupling strength.[263] The experimental *J* value determined for **7** is with *J* = -421 however larger than expected and cannot be explained alone by the small ⬚ angle (25.0°). Also other structural parameters such as the dihedral angle formed by the two coordination planes can influence the coupling constant.[264] However, the influence is too minor and the other structural parameters are similar to **8** and cannot explain the large *J* value for **7**.

*Table 10 Magnetic parameters of **7**, **8** and **9**.*

	Cu-O-Cu [°]	*J* [cm⁻¹]	*g*	*TIP* [cm³/mol]	*PI* [%]
7	102.8	−421	2.18	$3.5 \cdot 10^{-4}$	7.5
8	101.1	-108	1.88	0.0	0.0
9	121.1	-111	2.05	$0.9 \cdot 10^{-4}$	0.5
	121.9				

For complex 9 a very strong antiferromagnetic interaction of ca. 1000 cm⁻¹ was expected due to the correlation between *J* and ⬚⬚⬚121.1 or 121.9 °). However, only a relative weak magnetic coupling could be observed (*J* = -111). This difference can be mainly explained by the single ⬚-alkoxide bridge and other structural reasons. As mentioned before, the dihedral angle formed by the two coordination planes has significant influence on the strength of the magnetic coupling. In case of 9 the torsion amounts 75.3 ° and causes a poor overlap of the magnetic orbitals.

Complexes were further characterised by UV/Vis spectroscopy. In MeCN four absorption bands could be recorded (Figure 16). Assignment of the transitions were done according to the literature.[248,265]The most intensive band at around 265 nm could be assigned to the π → π* transition of the pyridine sidearms.
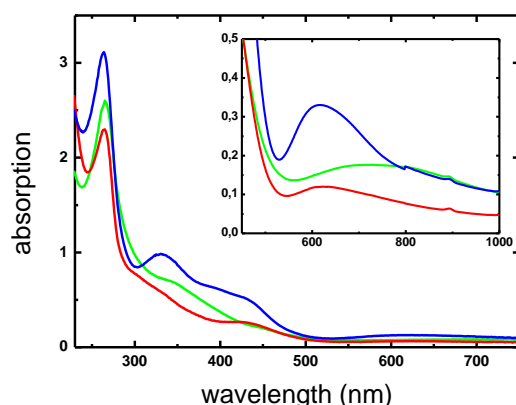
*Figure 16 UV/Vis-spectra of the Cu²⁺ complexes **7** (green), **8** (red) and **9** (blue) in MeCN (0.16 mM). The small graph shows the d-d metal transition at higher concentrations (5 M).*

The absorption bands at 335 nm and 420 nm (440 nm) are most likely ligand to metal charge transfers (LMCT's), but differentiation between oxygen and sulphur induced transfer is not easy to assign. Since sulphur atoms have lone pairs relatively high in energy the more intense absorption band is likely induced by the sulphur. Thus, the less intense band at lower wavelength was assigned to LMCT from the bridging oxygen. In the red region of the electromagnetic spectrum a relatively weak absorption could be monitored and assigned to a d-d metal transition. The possibility of an enhancement of the transition, due to a π(S)-d(Cu) charge transfer, cannot completely be eliminated. Prominent spectroscopic parameters of the complexes are summarised in Table 11.

*Table 11 UV/Vis-parameter of the Cu²⁺ complexes **7**, **8** and **9** in MeCN.*

	λ [nm]	ε [$M^{-1}cm^{-1}$]	assignment
7	265	16263	$\pi \rightarrow \pi^*$ (pyridine)
	366	4719	$\sigma(S) \rightarrow dx^2\text{-}y^2$ LMCT
	444	1438	$\sigma(O) \rightarrow dx^2\text{-}y^2$ LMCT
	729	353	d-d metal transition
8	264	14752	$\pi \rightarrow \pi^*$ (pyridine)
	335	3761	$\sigma(S) \rightarrow dx^2\text{-}y^2$ LMCT
	421	1952	$\sigma(O) \rightarrow dx^2\text{-}y^2$ LMCT
	609	239	d-d metal transition
9	263	19477	$\pi \rightarrow \pi^*$ (pyridine)
	331	6369	$\sigma(S) \rightarrow dx^2\text{-}y^2$ LMCT
	420	3633	$\sigma(O) \rightarrow dx^2\text{-}y^2$ LMCT
	624	682	d-d metal transition

3.5 Conclusion

Six tripodal pre-organised, tridentate ligands have been synthesised and were investigated with respect to their complexation behaviour towards Cu⁺ and Cu²⁺. The synthesised ligands were therefore treated with Cu⁺ salts providing the corresponding complexes, which were studied in solution as well as in solid state. The MS and NMR experiments indicate mononuclear complex formation with all ligands except for ligand **L⁴ᴴ**, where a paramagnetic NMR spectrum was recorded. By X-ray crystallography it could be elucidated that, in case of **L⁴ᴴ**, the Cu⁺ becomes

partially oxidised and forms the trinuclear $[\mathbf{L^4}_2Cu^{2+}Cu^+_2(MeCN)_2]OTf_2$ complex. Furthermore, the molecular structures revealed, that the flexibility of $\mathbf{L^{1H}}$ and $\mathbf{L^{2H}}$ can lead to chain structures. Surprisingly, also complex **5** crystallised in a chain structure. The ligand $\mathbf{L^{3H}}$ was the only ligand, which forms mononuclear Cu^+ complex in solution as well as in solid state. Thus, $\mathbf{L^{3H}}$ and the structurally similar $\mathbf{L^{5H}}$ were chosen for further investigation. Besides the Cu^+ complexes, Cu^{2+} complexes were synthesised with the new ligands to get a first impression of their reactivity towards Cu^{2+}. The characterisation shows that in organic solvents the tripodal ligands lack the desired selectivity for Cu^+. However, the affinity to Cu^{2+} is most likely based on the coordination by an *in situ* generated alkoxide. The aim of this study is the synthesis and characterisation of a multifunctional tool, were the ligands will be integrated *via* coupling at their alcohol function. Thus, deprotonation and coordination of the alcohol should no more possible. To prove this hypothesis, model systems have to be synthesised, were the alcohol function is protected and evaluated with respect to their metal affinities.

Chapter 4

Synthesis and Characterisation of Tetradentate Ligands for Applications in AD

substitution   expansion

flexible – pre-organised   rigid – strongly pre-organised
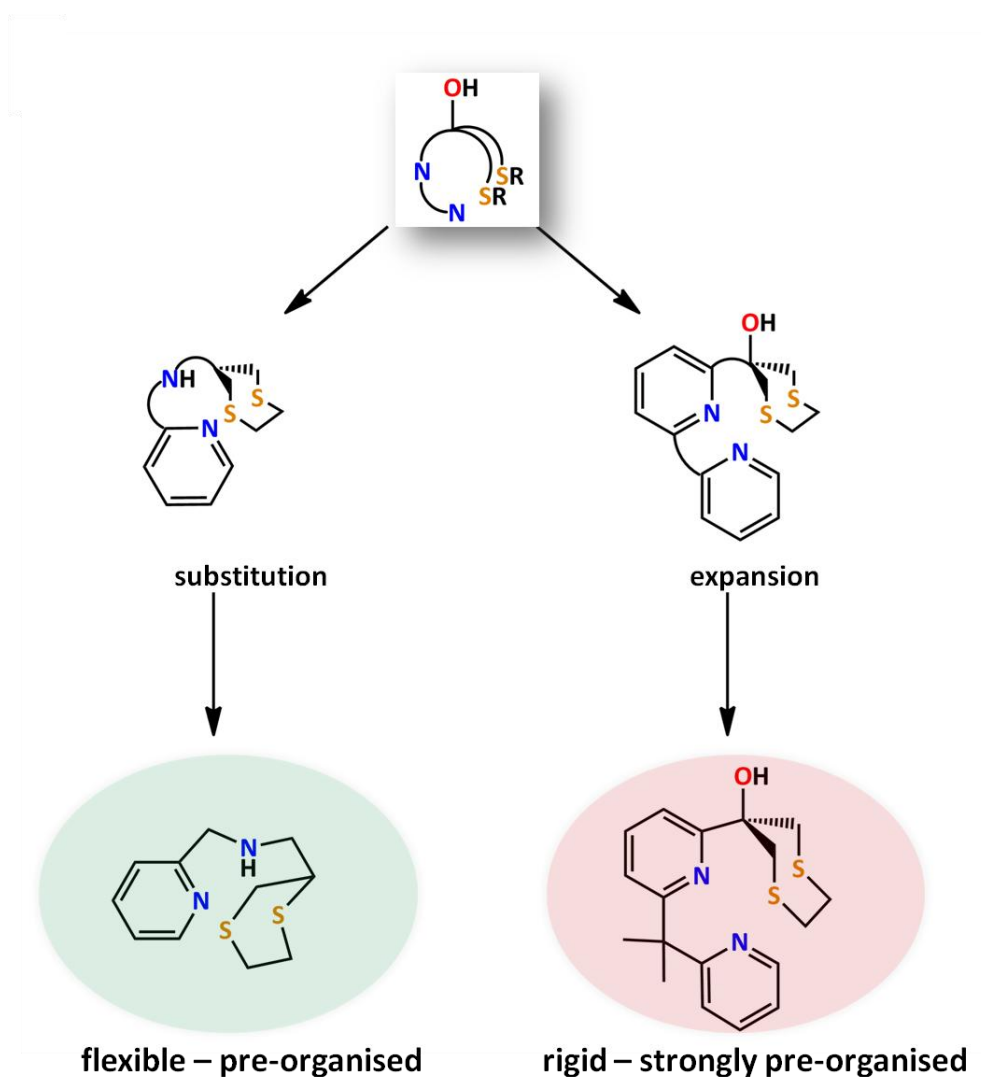
4.1 Introduction

Tridentate ligands with promising properties for applications in AD were described in the previous chapter. Under non-aqueous conditions model complexes with Cu^+ as well as Cu^{2+} could be synthesised and completely characterised. The structural parameters in solid state indicate that the rigid ligand **L^{3H}** is the most promising candidate, since it forms a mononuclear Cu^+ complex. However, the synthesis of Cu^{2+} complexes illustrates that the tripodal system are not selective to Cu^+. To obtain a higher affinity and more stable complexes, the ligand design was changed to tetradentate ligands. Introduction of a fourth sidearm carrying another donor atom should furthermore remarkably increase the inertness towards oxidation, due to the closed coordination sphere, while the desired high affinity towards Cu^+ is maintained. Thus, an additional functional group, containing a strong σ-donor was attached to **L^{3H}**. This was done in two ways, either by substitution of the tertiary alcohol by an amine or *via* expansion of the ligand through another pyridine sidearm (Figure 17).
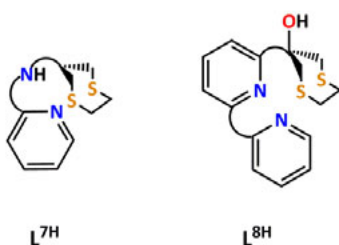
*Figure 17 Schematic representation of the desired tetradentate ligands **L^{7H}** and **L^{8H}**.*

4.2 Attempts to Synthesise Tetradentate Ligands

4.2.1 Synthesis of L^{7H}

Retrosynthetic analysis of **L^{7H}** suggests reductive amination as the simplest synthetic route towards the desired molecule (Scheme 10).
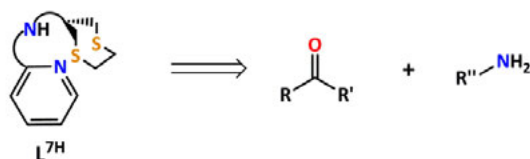
*Scheme 10 Retrosynthetic analysis of **L^{7H}**.*

Although a number of different reaction conditions were applied to couple ketone **II** and the commercially available 2-aminomethyl pyridine, like high temperatures or catalytic amounts of HCl or TiCl$_4$[266], no imine formation could be observed neither by ^{1}H-NMR spectroscopy nor MS. Instead the reagent could be recovered in most of the reactions or, in case of TiCl$_4$, only a side reaction, probably the complexation of the Ti^{4+} ion by 2-aminomethyl pyridine analogous to the literature, could be observed.[267] Reason for the unsuccessfully amination is most likely the low reactivity of the reactants. Reductive amination of a ketone is more hindered then in case of an aldehyde. Furthermore, the nucleophilic character of the amine is weakened by the electron withdrawing pyridine.
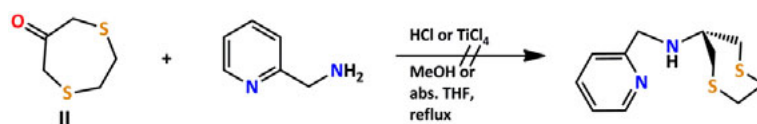
Scheme 11 Synthetic approach to L^{7H}.

To maintain the reductive amination as coupling reaction, the functionalities on the molecules were exchanged. Instead of 2-aminomethyl pyridine the commercially available 2-pyridinecarboxaldehyde could be used, which changes the electrophile from a ketone to a more reactive aldehyde. Thus, the coupling reaction should be more favoured. For the synthesis of the amine group, two different approaches were carried out (Scheme 12). In a first attempt, a direct pathway was chosen, letting **II** react with NH_4Cl in the presence of $[Ti(O^iPr)_4]$.[268] Even at higher temperature no reaction with the ketone **II** could be observed and thus it could be completely recovered. Another procedure to convert a ketone into an amine proceeds over an oxime intermediate. The oxime **III** could be synthesised in good yields (87 %) by the reaction of **II** with hydroxylamine[269], but the following reduction of **III** with $LiAlH_4$ or $NaBH_4$ in THF were performed without success.[270] According to the literature $NiCl_2$ can promote the reduction.[271] However, the desired amine could not be obtained. After addition of a concentrated sodium EDTA solution, to remove the Ni^{2+} ion, the reactant could be extracted with DCM. Therefore the reductive amination was discarded and in a new approach, a nucleophilic substitution was carried out instead.
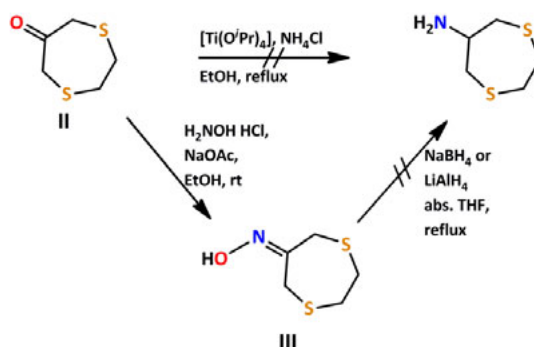
*Scheme 12 Synthetic approach of the conversion of the ketone of **II** to a primary amine, a precursor for reductive amination.*

The required electrophile **V** was synthesised according to literature in two steps (Scheme 13).[272] The first step was the reduction of ketone **II** with $NaBH_4$ in THF, followed by chlorination of the generated alcohol with thionyl chloride. Noteworthy is that the underlying mechanism results in an intramolecular arrangement, reducing the thioether ring size from a seven-membered to a six-membered ring. The last step of the ligand synthesis was the nucleophilic attack by 2-aminomethyl pyridine forming the hydrochloride. The product was *in situ* deprotonated by a second equivalent of the pyridine. The ligand **L^{7H}** could be obtained in good yields (80 %) as a brown liquid.
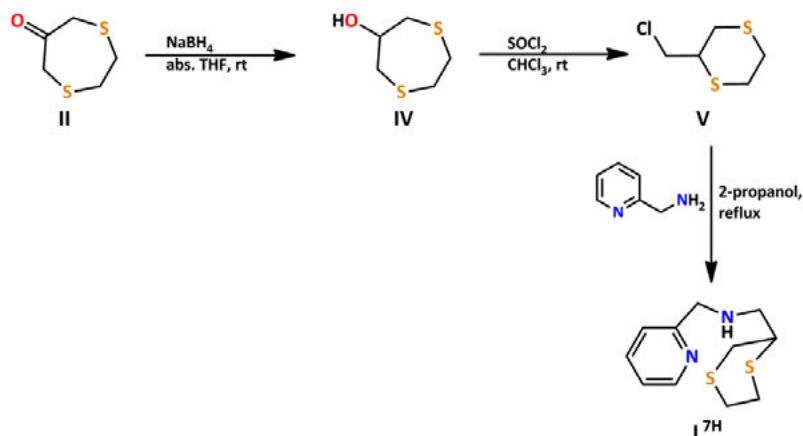
*Scheme 13 Synthesis of the tetradentate ligand **L^{7H}**.*

4.2.2 Synthesis of L^{8H}

Since **L^{3H}** was the most promising tripodal ligand for Cu$^+$ coordination, the tetradentate ligand **L^{8H}** was developed with the intention to preserve the present coordination motive as much as possible. The easiest way to achieve this was simple expansion of the ligand by a further pyridine comprising sidearm. This can either be done by coupling the pyridine directly to a derivative of **L^{3H}** or by introducing the additional group in the first step of the ligand synthesis. For the former, the general synthetic route of the tridentate ligand was preserved. In the first step, 2,6-dibromo pyridine was coupled to ketone **II** using ^{n}BuLi at -78 °C to provide **VI** in low yields (23 %) (Scheme 14). Before the second pyridine could be attached, the alcohol had to be protected, which was done by methylation. The alcohol was therefore deprotonated with sodium hydride and afterwards methyl iodide was added. The last reaction, the attachment of 2-methyl pyridine, was attempted by treating **VII** with ^{n}BuLi at -78 °C and also at higher temperature (up to room temperature). However, the final product could not be obtained. The reason for this is either the insufficient reactivity of **VII**, which prevents the transmetalation with ^{n}BuLi or chelation of the formed lithium-organyl intermediate by another ligand molecule, which would shield the reactive centre.
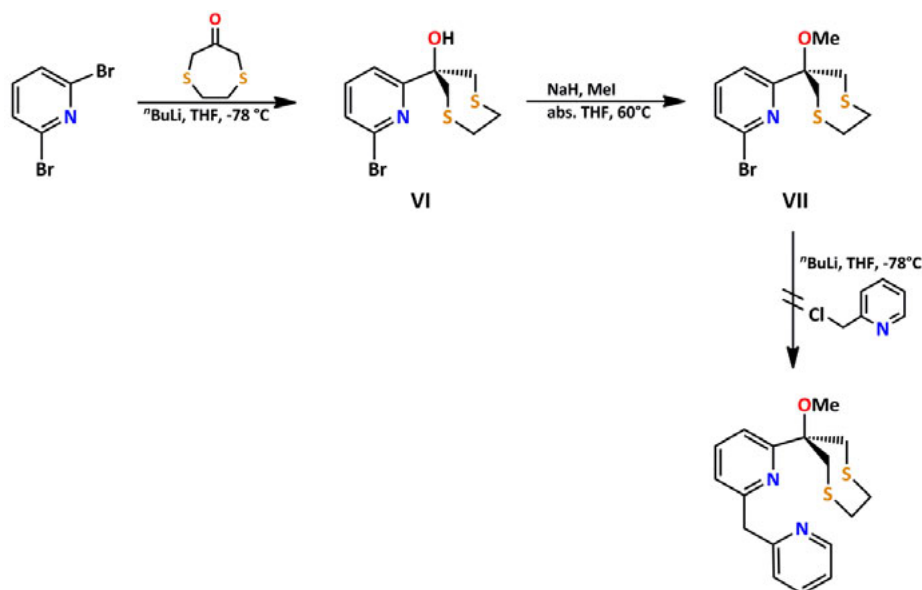
Scheme 14 Synthetic approaches to a tetradentate ligand.

The second strategy for the synthesis of L^{8H} starts with the synthesis of the {N_2} sidearm (Scheme 15). Therefore, a solution of 2-methyl pyridine in THF is prepared at -78 °C. Successive addition of ^{n}BuLi and 2,6-dibromo pyridine provides **VIII**. The formed methylene bridge is relatively acidic, due to the two electron withdrawing pyridine substituents and would therefore hinder the transmetalation in the next step. In addition to this, it is known that such electron deficient bridging groups can be activated and oxidised by transition metals like copper.[273–277] In order to prevent such reactions and also enable the last synthetic step, the hydrogen atoms of the methylene bridge were substituted by two methyl groups. Therefore methyl iodide was reacted with **VIII** in the presence of K^tOBu. Afterwards the {N_2} sidearm was attached to **II** under standard ^{n}BuLi conditions at -78 °C. L^{8H} could only be obtained in moderate yields (67 %) in small scales. Attempts to increase the yield by changing the transmetalation reagent to ^{t}BuLi, LDA, magnesium-organyls and zinc-organyls did not work.
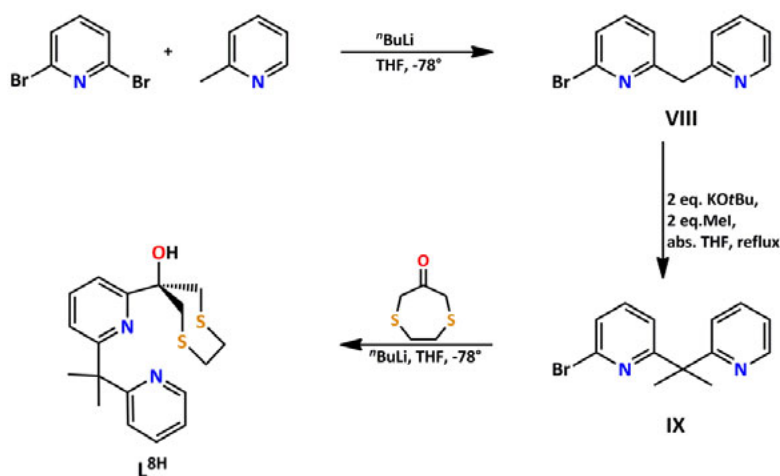
Scheme 15 Synthetic approaches in the synthesis of L^{8H}.

In addition to the synthesis of **L^8H**, further attempts were carried out using a bipyridine sidearm (Scheme 16). Bipyridine is a strongly coordinating bidentate chelating agent, which should provide an even higher affinity than the {N$_2$} sidearm used in **L^8H**. The first step of the ligand synthesis is the attachment of a methyl group to the commercially available 2,2-bipyridine *via* MeLi.[278] The product **X** could be obtained in good yields (54 %, Lit.: 59 %[278]) after reoxidation of the aromatic system with MnO$_2$. Although **X** is quite similar to 2-methyl pyridine, a direct coupling with BuLi analogue to the synthesis of **L^2H** and **L^4H** did not afford the desired ligand. Even usage of other transmetalation reagents (^{t}BuLi, LDA) could not provide the desired ligand. Thus, the reaction was optimised by favouring the transmetalation reaction. This was done by modification of **X** to 6-chloromethyl-2,2-bipyridine **XI** and 6-bromomethyl-2,2-bipyridine **XII**.[279,280] Unfortunately, the desired ligand could not be obtained. Nevertheless, with **L^7H** and **L^8H** two tetradentate ligands were synthesised which should be able to coordinate Cu$^+$. Especially the latter one, **L^8H**, is a promising candidate due to the strong tetrahedrally pre-organised geometry.
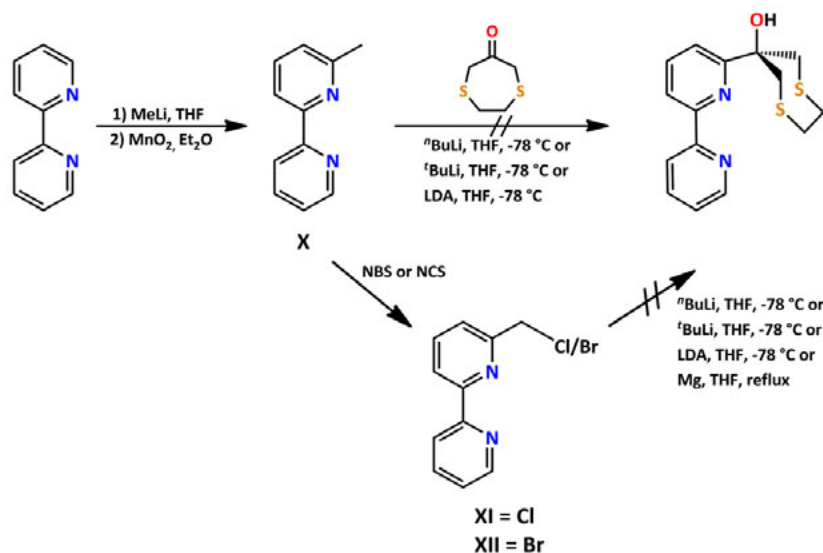
Scheme 16 Synthetic approaches to a 2,2-bipyridine-based tetradentate ligand.

4.3 Complex Formation with Tetradentate Ligands

The tetradentate ligands **L^7H** and **L^8H** were investigated with respect to their complexation properties for Cu$^+$, Cu^{2+} and Zn^{2+}. [**L^7H**Cu(MeCN)]OTf **10** could be synthesised by addition of **L^7H** under inert atmosphere to a solution of [Cu(MeCN)]OTf in MeCN. A white complex powder could be obtained by evaporation of the solvent under reduced pressure. To verify the ligand to metal ratio MS and NMR studies were performed. In the ESI-MS only the expected mononuclear species with a 1 : 1 ligand to metal ratio was recorded, thus, mononuclear complex formation seems to be favoured in solution. ^{1}H-NMR spectroscopy supports this finding. The complex was dissolved in MeOD-d$_4$ and equimolar amounts of CHCl$_3$ were added as reference. Comparison of the intensities showed only mononuclear complex formation. By this procedure only one ligand molecule could be determined in the complex. Unfortunately, no crystalline material suitable for X-ray crystallography could be provided, therefore the solid state structure of **10** is unknown.

The redox-stability of **10** was tested by stirring it for 24 h under ambient atmosphere. Within 15 minutes the Cu^+ starts to become oxidised, which can be followed by a colour change of the complex solution from yellow to blue. By ether diffusion in a saturated complex solution in MeCN purple crystals of the complex [**L$^{7H}_2$**Cu]OTf$_2$ · 2MeCN (**11**) could be obtained (Figure 18). Complex **11** crystallises in a monoclinic crystal system in the space group P21/c. The structure reveals an octahedral coordination of the metal centre by two ligands. Of the four possible donors only the pyridine, the amine and one sulphur atom of the thioether sidearm are coordinating per ligand. The strong nitrogen donors are roughly located in a plane and the sulphur atoms coordinate in the axial positions, resulting in a stretched octahedron. With 80.82 ° the N1-Cu1-N2 bite angle deviates most clearly from the ideal angle of 90 °. Thus, the complex is strongly distorted from an ideal octahedral geometry. Prominent structural features of the complex are summarised in Table 12 and Table 13. From the present 2 : 1 coordination motif containing a coordinatively saturated Cu^{2+} and from the fast oxidation of the Cu^+ complex **10** it can be assumed, that the ligand **L^{7H}** is not selective for Cu^+.

11

*Figure 18 Molecular structure of **11**. Hydrogen atoms and counterions were omitted for a better structural overview.*

Nevertheless, also the Zn^{2+} complexation was studied in solution. The complex solution was prepared by dropwise addition of Zn(ClO$_4$)$_2$ · 6 H$_2$O, dissolved in MeOH, to a 0.3 M solution of **L^{7H}** in MeOH. By the successive addition of Zn^{2+} the formation of a precipitate could be observed, which reaches its maximum at a ligand to metal ratio of approximately 2 : 1 and gets partially dissolved by further addition of Zn^{2+}. The mixture was stirred over night to complete the reaction. The formed precipitate was separated by filtration and analysed by ESI-MS in MeCN. The spectrum contains a peak at 302.9 (m/z), which can be assigned to [**L^7**Zn]$^+$ and also a peak at 272.1 (m/z), which can be assigned to [(**L^{7H}**)$_2$Zn]$^+$. Thus, it can be assumed that in the presence of excess **L^{7H}** most likely a [**L$^{7H}_2$**Zn]$^{2+}$ complex analogue to the [**L$^{7H}_2$**Cu]$^{2+}$ complex **11** is formed. Further addition of Zn^{2+} could then lead to the mononuclear [**L^{7H}**Zn]$^{2+}$ species. Thus, **L^{7H}** can form Zn^{2+} complexes not only in a 1 : 1 but also in a 2 : 1 ratio. For the desired application selectivity of the ligands is essential. Due to the characterisation of the Cu^+, Cu^{2+} and Zn^{2+} complexes no satisfying selectivity could be found. The molecular structure of **11** even indicates the opposite. **L^{7H}** seems to be relatively flexible in its structure and formation of undesired [**L$^{7H}_2$**M]$^{2+}$ complexes

takes place. Thus, the chance is high that in aqueous solution **L**^{7H} shows no selectivity towards Cu$^+$ and also coordinates Cu^{2+} and Zn^{2+}. Thus, the ligand is not useful for the desired application.

L^{8H}, in contrast to **L**^{7H}, is more tetrahedrally pre-organised and should therefore not be able to form octahedral bis(ligand) complexes with Cu^{2+} or Zn^{2+}. To prove this hypothesis, complexes were synthesised with the relevant transition metals. First of all the monovalent complex [**L**^{8H}Cu]PF$_6$ (**12**) was synthesised analogous to the previously described Cu$^+$ complexes. **12** could be crystallised by slow ether diffusion into a saturated complex solution in MeCN at 4 °C. The coordination sphere of the Cu$^+$ is completely saturated by the four donor atoms of the ligand in a strongly distorted tetrahedral geometry. Since N1 is almost orthogonal to the other donor atoms the complex geometry could also be described as a distorted trigonal pyramid. Bond lengths of 2.2506 Å and 2.3822 Å for the Cu-S bonds are present in the complex and are in the same range as for the tripodal ligands presented in chapter 3. Also the Cu–N bond lengths with 1.9780 Å and 2.0549 Å are in the same range as in the tripodal complexes (Table 12). The hexafluorophosphate counterion forms a hydrogen bond with the alcohol function of the ligand and can therefore be found close to the core structure. With 149.26 ° the N2–Cu–S2 bite angle clearly deviates from the ideal tetrahedron angle of 109.47 ° (Table 13). The distortion has its origin in the short bridging unit between the two pyridines in the sidearm. Thus, the sidearms are not able to fully reach around the Cu$^+$.

12

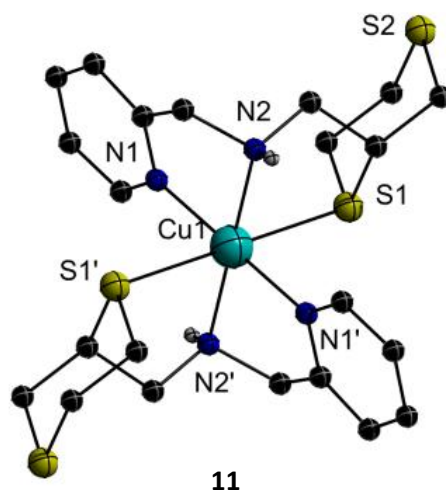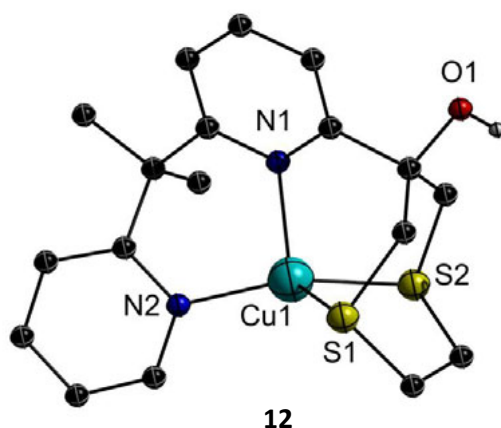*Figure 19 Molecular structure of **12**. Hydrogen atoms and counterions were omitted for a better structural overview.*

Complex **12** was oxidised on air by stirring the complex solution in MeCN in an open vessel over night. By introduction of the forth binding site the ligand should remarkably increase the stability of the Cu$^+$ complexes but the experiment indicates that oxidation to Cu^{2+} is still possible under aerobic conditions. Within 2 h the solution starts to become green, indicating oxidation of the metal. Unfortunately, no crystalline material suitable for X-ray crystallography could be obtained. Instead only crystals with an amorphous structure or non-diffracting substances could be prepared. In the ESI-MS of the oxidised complex powder the most intensive peak at 408.9 [m/z] could be assigned to the [**L**^{8}Cu]$^+$ species. This leads to the assumption that the deprotonated alcohol is involved in the coordination similar to the Cu^{2+} complexes with the tripodal ligands (**7**, **8** and **9**). Furthermore a peak at 470.9 [m/z] was assigned to the [**L**^{8}Cu$_2$]$^+$ species, which indicates the formation of a multinuclear complex.

*Table 12 Selected bond lengths of **11** and **12**.*

Complex	Cu–S [Å]	Cu–N$_{Py}$ [Å]	Cu–NH [Å]
11	2.7517(11)	2.0359(39)	2.0469(35)
12	2.3822(10)	2.0549(23)	-
	2.2506(8)	1.9780(24)	-

*Table 13 Selected bond angles of **11** and **12**.*

Complex	S–Cu–S [°]	N1–Cu–N2[°]	S1–Cu–N1 [°]	S2–Cu–N1 [°]
11	180.00(0)	80.82(14)	94.90(10)	-
12	87.67(3)	97.56(9)	98.33(7)	101.66(7)

The previously described experiments were all performed in organic solvent, thus it has to be proven that the expected selectivity of **L^{8H}** is also effective in aqueous solution. To define the Cu$^+$ and Cu^{2+} complexation abilities in aqueous solution a ^{1}H-NMR experiment was performed. The experimental conditions were 300 µM Cu^{2+} and 300 µM **L^{8H}** in 0.2 M deuterated phosphate buffer (pH 7.4). For the ligand a stock solution (10 mM) in DMSO-d$_6$ was prepared and as copper source a stock solution of CuSO$_4$ (10 mM) was used. The low concentrations were necessary due to the poor solubility of **L^{8H}**. First the spectrum of the free ligand was recorded and then Cu^{2+} added to the sample. The addition of Cu^{2+} does not induce a shift of the signals, but the spectra changes after the addition of dithionite as reductant (Figure 20). The *in situ* generated Cu$^+$ is coordinated by the ligand, which can be easily followed by a low field shift of the pyridine signals and also by a signal shift of the aliphatic protons. Thus, in aqueous solutions **L^{8H}** can coordinate Cu$^+$ but does not chelate Cu^{2+}. The coordination of the bivalent and highly solvated Cu^{2+} seems to be disfavoured due to the structural pre-organisation of the ligand and the relatively soft donor set.
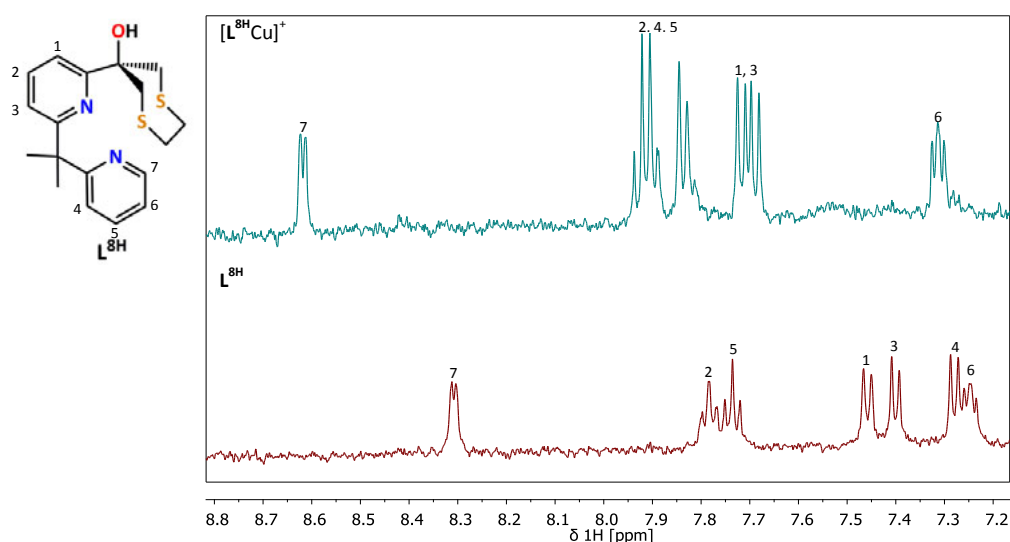

*Figure 20 Aromatic region of the ^{1}H-NMR spectra of **L^{8H}** (300 µM) and **[L^{8H}Cu]$^+$** (300 µM) in 0.2 M deuterated phosphate buffer (pH 7.4).*

As mentioned in the introduction, zinc is another important transition metal, which is postulated to play an important role in AD. Since Zn^{2+} is isoelectronic with Cu^+ it shows similar reactivity in its complexation behaviour. Both metals can form stable complexes with tetradentate ligands and also prefer similar donor atoms. From complex **11**, it can be anticipated that the ligand **L^8H** should also be suitable for Zn^{2+} complexation. The smaller ionic radius of Zn^{2+} (74 pm) in comparison to Cu^+ (77 pm) should even slightly favour tetrahedral metal complex formation.[281] Zn^{2+} complexes were synthesised by adding a solution of $Zn(ClO_4)_2 \cdot 6 H_2O$ in MeOH to a solution of **L^8H** in MeOH. To complete the reaction the mixture was stirred for 12 h. After removal of the solvent under reduced pressure and washing the crude product with diethyl ether, a white complex powder could be provided. To confirm the structure of the synthesised complex, crystals were produced by dissolving the complex powder in a mixture of MeCN/MeOH and subsequent slow evaporation of the solvent. The molecular structure of $[\mathbf{L^8}_2Zn_3(\mu\text{-}OH)MeOH(MeCN)_{0.5}(H_2O)_{0.5}]ClO_4 \cdot 1.5$ MeOH (**13**) is shown in Figure 21. Interestingly, no monomeric, but a trinuclear complex structure is formed, where each metal ion has a distinct individual environment. Zn1 is coordinated by the pyridine sidearms of one ligand, one μ-OH group and the deprotonated alcohol of the ligand, which bridges two Zn^{2+} ions. The trigonal pyramidal coordination sphere is saturated by a disordered water and acetonitrile molecule, with the same occupation. In contrast to Zn1, Zn2 is found in a rather soft donor set. The octahedral coordination is constituted by the two deprotonated alcohol groups and all four sulphur atoms of the thioether sidearms. Zn3 is coordinated by the pyridine sidearms of the second ligand, the μ-OH bridge, one MeOH molecule and also by one bridging alcoholate group.

13
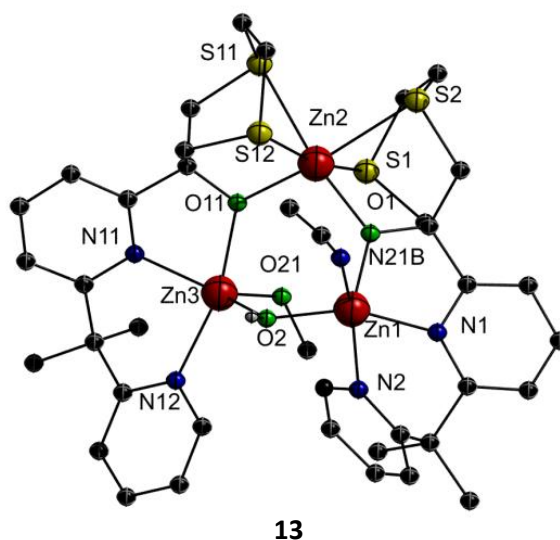
*Figure 21 Molecular structure of **13** with a coordinating MeCN molecule. Hydrogen atoms and the counterion were omitted for a better structural overview.*

Zn1 and Zn3, the two Zn^{2+} ions which are coordinated by hard donor molecules, are found in a trigonal pyramidal geometry, whereas Zn2 is found in an octahedral environment with six donors. Structural parameters of **13** are summarised in Table 14. The complex **13** was further characterised by ESI-MS. The peak with the highest *m/z* ratio could be assigned to a $[\mathbf{L^{8H}}Na]^+$ species. No indication for a zinc complex was observed. Thus, the formed complex is probably not stable enough for the ESI-MS measurements. However, the solid state structure of **13** shows that **L^8H** can coordinate Zn^{2+}. Although coordination of the $\{N_2S_2\}$ moiety is possible, the Zn^{2+} ions

prefer the coordination of the *in situ* formed alcoholates. The reasons for this binding motif are most likely the compensation of the charge and that the $\{N_2S_2\}$ moiety is too soft for Zn^{2+}. In the targeted final multifunctional tool, the chelator is coupled to a spacer, which is attached to a benzothiazole derivative. The alcohol function of the ligand in this final molecule is than no longer available for coordination, therefore Zn^{2+} coordination should be disfavoured. Furthermore, Zn^{2+} is stabilised in aqueous solution by formation of the $[Zn(H_2O)_6]^{2+}$ complex. Therefore, a coordination of the Zn^{2+} under cellular conditions should not be possible. Nevertheless, model complexes have to be synthesised, where the alcohol is protected, to define the metal binding affinities in the targeted multifunctional compound.

*Table 14 Selected bond lengths in the molecular structures of **13**.*

Complex	Cu–S [Å]	Cu–N$_{Py}$ [Å]	Cu–O$_{Ligand}$ [Å]	Cu–μ–OH [Å]
13	2.5411(16)	2.0996(45)	2.0156(33)	1.9483(35)
	2.6281(14)	2.1681(56)	1.9763(35)	1.9778(32)
	2.6405(18)	2.0956(46)	1.9665(26)	-
	2.5227(18)	2.1474(52)	2.0252(38)	-

4.4 Conclusion

Two tetradentate ligands **L^{7H}** and **L^{8H}** could be synthesised and evaluated with respect to their complexation properties. The flexible less pre-organised ligand **L^{7H}** can not only coordinate to Cu^+ but can also form stable complexes with Zn^{2+} and Cu^{2+}. In these octahedral complexes a $[\textbf{L}^{7H}{}_2M]^{2+}$ species is formed, which could be completely characterised in case of Cu^{2+}. For the desired application, selectivity towards Cu^+ is essential. The fast oxidation and complex formation of $[\textbf{L}^{7H}{}_2Cu]^{2+}$ indicates that Cu^{2+} can as well be coordinated by **L^{7H}**. In contrast to this, the strongly tetrahedrally pre-organised ligand **L^{8H}** does not coordinate Cu^{2+}, but Cu^+ in an aqueous buffer solution. The Cu^+ complex could also be prepared in organic solvents and structural analysis of the complex showed that the coordination sphere is completely saturated by the ligand. Although a Zn^{2+} complex could be synthesised with **L^{8H}**, coordination in aqueous solution can be excluded for several reasons. Thus, with **L^{8H}** a Cu^+ selective ligand was synthesised, which reveal the targeted promising binding properties.

Chapter 5

Model Systems Mimicking the Multifunctional Tools

Ligand

Spacer

Benzothiazole

tridentate model systems

tetradentate model system
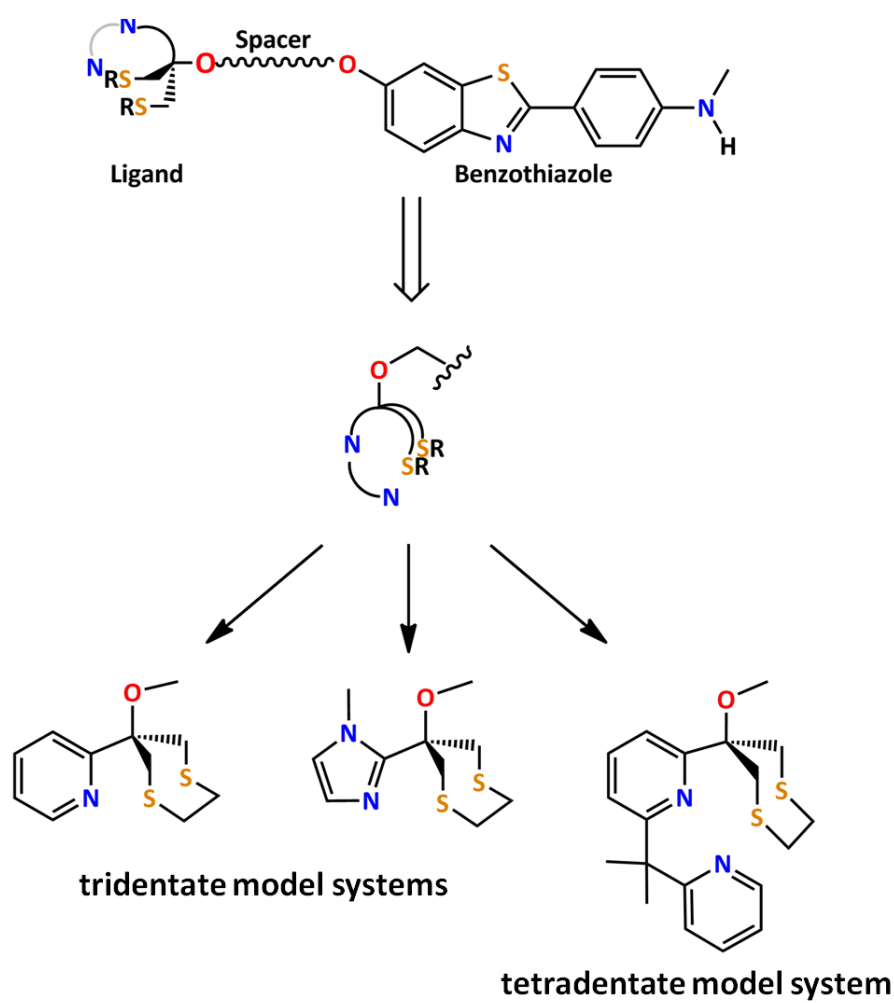
5.1 Introduction

The aim of this study is the synthesis and characterisation of multifunctional tools with a Cu^+ selective chelator and an Aβ-plaque sensitive subunit. In the two previous chapters ligand systems were presented which are promising candidates to fulfil this aim. The structural analyses of the tripodal ligands have shown good results for L^{3H}. Here, formation of mononuclear Cu^+ complexes in solution as well as in the solid state could be observed. Thus, the ligand was chosen for further investigations. Since L^{5H} is structurally similar to L^{3H}, it was also selected and will be further analysed. From the two tetradentate ligand systems, only L^{8H} has shown the desired selectivity for Cu^+ and was therefore used in the synthesis of model complexes. In the targeted final molecules the alcohol group of the ligands is attached to a spacer, linking the chelator with the Aβ-plaque attracting benzothiazole moiety. To gain first insights into the behaviour of these compounds, model ligands will be synthesised, were the alcohol group is protected. The synthesised model ligands were evaluated in terms of their ability to selective coordinate Cu^+ in organic solvents as well as in aqueous solution.

5.2 Synthesis of Model Ligands

To evaluate the complexation properties of the multifunctional tools, model ligands have to be synthesised, which structurally mimic the chelator subunit. The chelator will be attached to a spacer, which could be an aliphatic alkyl chain, a polyether chain or another bridging molecule. However, the alcohol will be directly coupled to a secondary carbon atom. Thus, a methyl group was attached to provide simple model ligands. The attachment was done *via* Williamson ether synthesis by stirring L^{3H}, L^{5H} and L^{8H} with methyl iodide in THF at 60 °C in the presence of sodium hydride (Scheme 17).
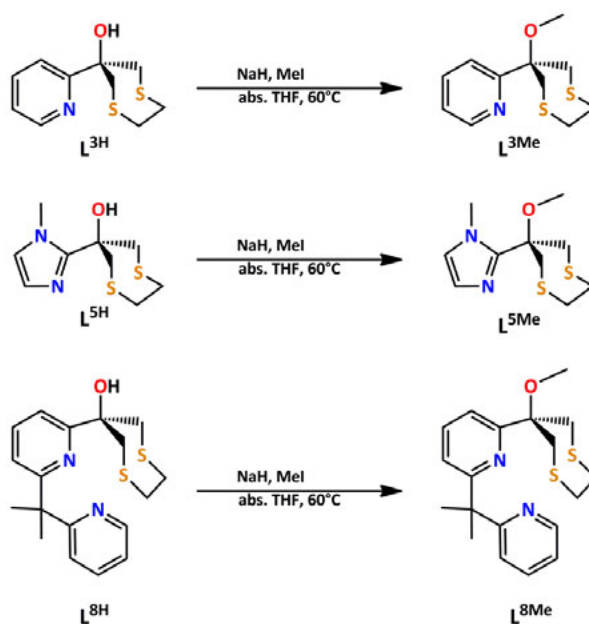
Scheme 17 Synthesis of model ligands (L^{3Me}, L^{5Me} and L^{8Me}), which mimic the coordination motif of the final product.

The underlying reaction is a nucleophilic attack (S_N2) by the deprotonated alcoholate of the ligand at the methyl iodide. After quenching with water and extraction with Et_2O the crude products could be obtained. Further purification by column chromatography on silica leads to the final products in high yields (95 % - 100 %). A solid state crystal structure of **L^{3Me}** could be provided by slow ether diffusion in a concentrated solution of **L^{3Me}** in DCM at 4 °C. **L^{3Me}** crystallises as a neutral molecule in the space group P 21/c with two molecules per unit cell (Figure 22). By introduction of the methyl group, the donor ability of the oxygen atom is reduced significantly. Thus, after modification, the Cu^+ complexes should be more inert against oxidation.
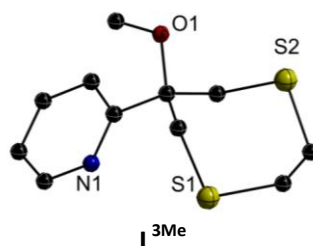
L^{3Me}

*Figure 22 Molecular structure of **L^{3Me}**. For a better overview hydrogen atoms were omitted.*

5.3 Influence of a CO as Strong Donor

The tripodal ligands are special, with respect to their tripodal character and the resulting vacant binding site on the complex. In the presented complexes these binding sites were always occupied by weakly coordinating solvent molecules, which can easily be substituted by other donor molecules. In neuronal cells a great number of different donors are present, which can replace the solvent and bind to the metal centre more tightly. Possible candidates would be sulphydryl, hydroxyl, carboxyl, imidazole and amino residues of proteins, amino acids (e.g. glutamate, which is released in high concentrations[82,83]), oxygen and nitrogen donors of heterocyclic bases or small molecules. To get a first impression of the influence of a stronger donor saturating the coordination sphere, metal carbonyl complexes of the type [**L^{XMe}**Cu(CO)]⁺ were synthesised. Furthermore, the stretching vibration can be used as an indirect measure for the binding properties of the ligands. Synthesis and characterisation of the metal carbonyl complexes will be discussed in detail in the appendix A.

Table 15 summarise the observed stretching vibration $\tilde{\nu}$ and determined force constants k for **L^{3Me}**Cu(CO)]⁺ and [**L^{5Me}**Cu(CO)]⁺. Comparison of the vibrational modes shows only a difference of $\tilde{\nu}$ = 4 cm⁻¹ between. Thus it can be assumed that the electronic structures in the complexes and thus the binding properties of both ligands are almost the same.

*Table 15 Stretching vibration ($\tilde{\nu}$) and force constant (k) of [**L^{3Me}**Cu(CO)]⁺ and [**L^{5Me}**Cu(CO)]⁺.*

	$\tilde{\nu}_{CO}$ [cm⁻¹]	k [N m⁻¹]
[**L^{3Me}**Cu(CO)]⁺	2118	1813
[**L^{5Me}**Cu(CO)]⁺	2114	1806

5.4 Synthesis of Model Complexes with Tripodal Ligands Systems

To gain insight into the reactivity and selectivity of the chelators, model complexes were synthesises with the in AD relevant transition metals, namely Cu^+, Cu^{2+} and Zn^{2+}. Model complexes with Cu^+ were synthesised by adding equimolar amounts of ligand to a solution of either $[Cu(MeCN)_4]PF_6$ or $[Cu(MeCN)_4]OTf$ in MeCN. The reaction solutions were stirred over night to complete the complex formation. Precipitation by addition of Et_2O afforded the complexes $[\mathbf{L^{3Me}}CuMeCN]OTf$ (**14**) and $[\mathbf{L^{5Me}}CuMeCN]PF_6$ (**15**) as colourless powders in very good yields (63 % / 76 %). The compounds were characterised by ESI-MS and NMR spectroscopy. The ESI-MS analysis of the products indicates only mononuclear complex formation. Further proof for the formation of mononuclear complexes is given by the ^{1}H- and ^{13}C-NMR spectra. The spectra obtained from the Cu^+ complexes with the unprotected ligand systems **3** and **4** were compared with **14** and **15** to prove that the methylation of the chelators has no significant influence on the Cu^+ coordination. The ^{1}H-NMR spectra show a remarkable similarity. Thus, it can be assumed that the modification has no influence on the Cu^+ coordination in solution. Crystalline material suitable for X-ray crystallography could be obtained from saturated solutions of **14** and **15** in MeCN by slow ether diffusion at 4 °C or at room temperature. In the molecular structure of **14**, the Cu^+ is coordinated in a distorted tetrahedral fashion by the {NS_2} moiety of the ligand and one MeCN molecule (Figure 23). Due to the protective group, hydrogen bond formation is no longer possible and the triflate counterion is separated from the cation structure. Although the introduction of the methyl group should not influence the coordination of the Cu^+, minor deviations can be observed in solid state by overlaying **14** and **3.** The nitrogen donor of the pyridine (N1), one sulphur atom of the thioether sidearm (S1) and the metal centre were taken as fixed points for creating a structural overlay. The bridging methylene and the ethylene groups in the cyclic thioether sidearm differ in the molecular structures. In **14** the MeCN molecule is bend stronger and thus the geometry is also distorted more clearly from the ideal tetrahedron, than in the case of **3**. The small differences in the structures are most likely induced by the arrangement of the molecules in the solid state. Bond lengths and bond angles presented in **14** are similar to those of **3**. The structural features of **14** are summarised in Table 16 and Table 17.

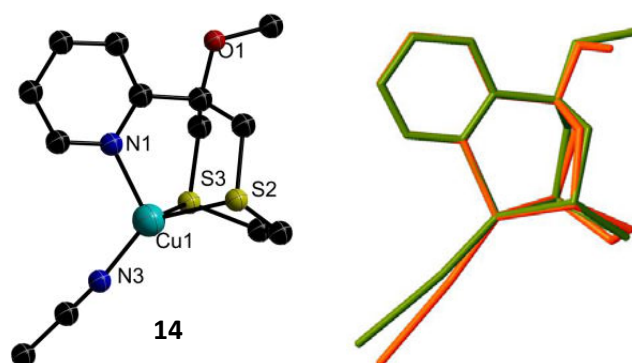*Figure 23 Molecular structure of **14** (left) and structural overlay (right) of **3** (orange) with **14** (green). Hydrogen atoms and counterions were omitted for a better structural overview.*

In contrast to compound **5**, where a chain structure was obtained utilising $\mathbf{L^{5H}}$, the complex **15** crystallises as a mononuclear complex similar to **3** and **14** (Figure 24). The metal is coordinated

by the {NS$_2$} moiety of the tridentate ligand and the tetrahedral coordination sphere is again saturated by one MeCN molecule. The missing alcohol leads to a clear separation of the counterion. Since there is no difference in the binding mode between **L^{5Me}** and **L^{5H}**, the assumption presented in chapter 3 that the molecular structure in solid state strongly depends on the crystallisation conditions and also on the molecule arrangement in the crystal seems to be right. Nevertheless the mononuclear structure obtained for **5** demonstrates also that **L^{5Me}** and **L^{5H}** may be suitable ligands for further investigation. In order to compare the structural features of the two obtained model complexes **14** and **15,** an overlay was prepared. The best overlay could be provided by using both sulphur atoms and the metal centre as fixed points. The overlay clearly illustrates, that only in the region of the thioether sidearm **14** resembles **15**. The orientations of the MeCN molecules and also of the methyl groups are clearly different. Furthermore, the N–Cu–N bite angle in **15** is with 136.781 ° larger than in **14** by more than 20 ° (Table 17). Although small differences are present, all bond lengths are quite similar and comparable to other Cu$^+$ complexes discussed in the previous chapters. Table 16 summarises prominent bond lengths of **14** and **15**. Thus, it can be assumed that **L^{3Me}** and **L^{5Me}** have a similar reactivity and affinity towards Cu$^+$. An analogous result could be obtained by studying the Cu$^+$ carbonyl complexes (see appendix A). Thus, both ligands have presumably the same reactivity.

15
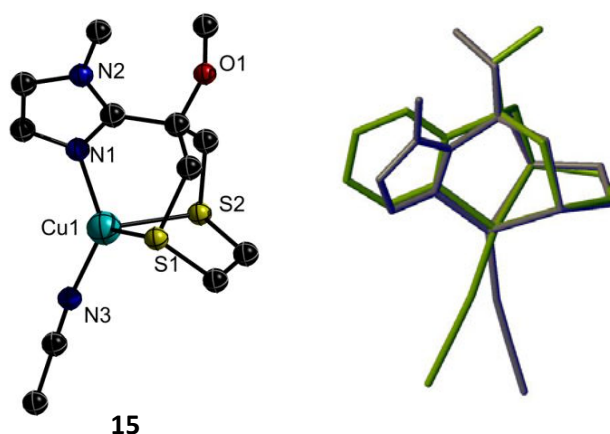
*Figure 24 Molecular structure of **15** (left) and structural overlay (right) of **14** (green) and **15** (blue). Hydrogen atoms and counterions were omitted for a better structural overview.*

Mainly all studies carried out so far were prepared in an anaerobic and non-aqueous environment due to the better solubility of the compounds and the facilitated preparation of the compounds. Information provided by X-ray crystallography and obtained from the MS and the NMR experiments have shown promising results for an application of the ligands. However, it is still unclear if these results can be easily transferred to aqueous solutions or even to cellular conditions. As a first step in this direction **14** was dissolved in MeOH under inert conditions and crystallised by ether diffusion at 4 °C by overlayering the saturated solution with diethyl ether. Thus, the solvent was changed from polar aprotic to polar protic, which is more similar to the aqueous medium. MeOH was used instead of water, because complex **14** is not soluble in water. The main idea behind this experiment was to study the complexation behaviour of **L^{3Me}** in a polar protic medium. Especially, the fate of the free fourth coordination side was of great interest: Can the binding side also be saturated by weaker co-ligands like MeOH or water? Crystals could be obtained and the molecular structure of [**L^{3Me}**Cu(MeOH)]OTf (**16**) could be refined. Surprisingly, **16** did not crystallise in a mononuclear structure like **3** or **13**. Instead, **16** crystallises in a chain

structure. Similar to earlier obtained chain structures, the thioether sidearm bridges two Cu$^+$. Again the metal is coordinated by the nitrogen atom and one sulphur atom of the same ligand and one sulphur atom of a second ligand. The free coordination side of the complex is saturated by one MeOH molecule that completes the distorted tetrahedral geometry. The angle, which deviates most from an ideal tetrahedron, is the S—Cu—S angle with 127.90 °. This expansion is caused by the steric demand of the neighbouring ligand. Although this might be possible, no hydrogen bond is present in the molecular structure. The counterion can be found separated from the chain structure.

16
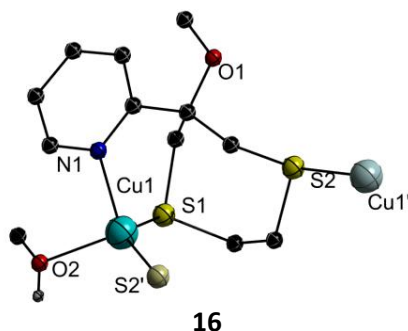
*Figure 25 Molecular structure of **16**. Hydrogen atoms and counterions were omitted for a better structural overview.*

*Table 16 Selected bond lengths of the molecular structures of **14**, **15** and **16**.*

	Cu—S [Å]	Cu—N$_{MeCN}$/O$_{MeOH}$ [Å]	Cu—N$_{Py/Im}$ [Å]
14	2.3163(6)	2.0192(6)	1.9094(7)
	2.3125(8)	-	-
15	2.5322(4)	1.8980(4)	1.9698(5)
	2.3698(4)	-	-
16	2.2383(6)	2.1272(18)	2.0583(18)
	2.2193(6)	-	-

*Table 17 Selected bond angles of the molecular structures of **14**, **15** and **16**.*

	S—Cu—S [°]	N—Cu—N/O [°]	S1—Cu—N1 [°]
14	87.103(18)	111.949(17)	99.081(15)
15	81.549(7)	136.781 (14)	92.931(9)
16	127.90(2)	97.47(7)	98.97(5)

NMR and ESI-MS studies performed with **16** indicate that upon dissolving the complex, the chain structure is cleaved and a mononuclear species is present in solution. Thus, with **16** the first example is given for complex formation in protic solutions. However complex formation with **L^{3Me}** and **L^{5Me}** in aqueous solution has still to be evaluated and will be discussed in chapter 5.7. Analogous to the complexes with the unprotected ligands, solutions of **14** and **15** were dissolved in MeCN and exposed to air in order to study the redox stability. After a few hours the reaction solutions turned green. After stirring for 24 h, to ensure that the oxidation was completely finished, different attempts were carried out to crystallise Cu^{2+} complexes. All crystals and complex powders obtained could be assigned to a [Cu(MeCN)$_n$]$^{2+}$ species; no complex formation with the ligands could be observed. Thus, the hypothesis that the methylation stabilises Cu$^+$ and

hindered oxidation was not confirmed. The conclusion form the empirical observation could be verified by cyclic voltammetry. Voltammograms were recorded of **3** and **14** and the potential for the oxidation was determined against ferrocen. For a better comparison were these values converted against the standard hydrogen electrode. For both complexes was a non-reversible oxidation recorded with a potential of 1.47 V vs. HNE for **3** and 1.40 V vs. HNE for **14.** The protection of the alcohol has therefore no influence on the stability of the Cu$^+$ complexes, which leads to the assumption that oxidation of the metal and formation of bi-and tetra-nuclear Cu^{2+} complexes is a stepwise process (Scheme 18). However, more important than the formation of the Cu^{2+} complexes is the fact that the modified ligands are no longer able to coordinate Cu^{2+} even in organic solvents. Thus, selectivity is given for Cu$^+$ in the presence of Cu^{2+}.

$$2\ [\mathbf{L^X Cu}]^+ \xrightarrow{\text{oxidation}} 2\ \mathbf{L} + 2\ [\mathbf{Cu(solv)_5}]^{2+} \xrightarrow[\text{deprotonation}]{\text{coordination}} [\mathbf{L^X_2 Cu_2(solv)_2}]^{2+}$$
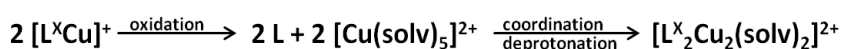
Scheme 18 Stepwise oxidation and formation of the dinuclear Cu²⁺ complexes

The unprotected tripodal ligands were not examined with respect to their ability to coordinate Zn^{2+}, since a huge number of Zn^{2+} complexes are known in the literature, where an alcohol function becomes deprotonated *in situ* due to the acidifying effect of the zinc.[282–284] Di- and multi-nuclear complex formation similar to the Cu^{2+} complexes is therefore most likely. The methylated ligands are not able to form these kinds of complexes. Thus, with **L^{3Me}** and **L^{5Me}** a first impression on the zinc-coordination behaviour of the {NS$_2$} donor set can be gained by the synthesis of the corresponding Zn^{2+} complexes. [(**L^{3Me}**)$_2$Zn](OTf)$_2$ (**17**) and [(**L^{5Me}**)$_2$Zn](OTf)$_2$ (**18**) were prepared by addition of ZnOTf$_2$ to the ligand solutions in methanol. The reactions were stirred over night at room temperature and the products were precipitated by the addition of diethyl ether. Complexes **17** and **18** could be obtained as grey solids. ESI-MS analysis of **17** and **18** indicated formation of mononuclear complexes coordinated by one ligand and one sulfonate counterion. Surprisingly, the ^{1}H-NMR spectra recorded in MeCN-d$_4$ show the formation of a [**L$^X_2$**Zn] species, indicating that **L^{3Me}** and **L^{5Me}** cannot only coordinate Cu$^+$ but also Zn^{2+}.

5.5 Synthesis of Model Complexes with a Tetradentate Ligand

A Cu$^+$ model complex with a tetradentate ligand was synthesised by stirring [Cu(MeCN)$_4$]OTf with **L^{8Me}** in MeCN over night at room temperature. The product [**L^{8Me}**Cu]OTf (**19**) was precipitated by the addition of diethyl ether and then characterised by NMR spectroscopy and ESI-MS spectrometry. Both analytic techniques indicate formation of a mononuclear complex similar to **13**. Unfortunately no solid state structure could be obtained during this study. Although complex formation of **L^{8H}** with Cu^{2+} could not be observed, neither in organic nor in aqueous solution, it has to be proven that **L^{8Me}** can also not coordinate Cu^{2+}. For the synthesis of a Cu^{2+} complex were equimolar amounts of **L^{8Me}** and Cu(ClO$_4$)$_2\cdot$6 H$_2$O stirred together for 12 h in MeCN. To increase the chance of metal coordination was the reaction heated at 60 °C. The solvent of the green coloured solution was removed under reduced pressure. The residue was taken up in diethyl ether and the resulting suspension was filtrated. The filtrate as well as the residue was characterised by ESI-MS analysis. The spectra of the filtrate show only the free ligand, whereas the spectra of the residue show no traces of neither the ligand or of the targeted Cu^{2+} complex. Thus, Cu^{2+} complex formation is probably prevented due to the strong

pre-organisation of the ligand. In addition to the Cu$^+$ complex **19**, also attempts to synthesise a Zn^{2+} complex using **L^{8Me}** as ligand were performed. Therefore, Zn(ClO$_4$)$_2 \cdot$ 6 H$_2$O was dissolved in different solvents (ethanol, methanol and water) and added to a ligand solution of **L^{8Me}** dissolved in methanol.

The solutions were stirred over night at room temperature. After removal of the solvent under reduced pressure a slightly yellow solid could be obtained, which was analysed by ESI-MS. The measured spectra showed only the protonated ligand and its fragments. In the negative region only the perchlorate anion was detected. Thus, the MS analysis indicates no complex formation. To verify the result, ^{1}H-NMR spectrum was recorded. The spectrum showed no shift of the pyridine signals compared to the free ligand and also the aliphatic proton signals did not change. With this experiment evidence is given that the tetradentate model ligand cannot coordinate Zn^{2+} in protic solvents. Since Zn^{2+} coordination is even more unlikely in aqueous solution due to the relative high stability of the [Zn(H$_2$O)$_6$]$^{2+}$ complex, **L^{8Me}** should be selective for Cu$^+$.

5.6 Attempts to Prepare Water-Soluble Ligand Systems

Ligand design was done with according to "Lipinski's Rule of Five"[231], which resulted in nonpolar compounds. On one hand, this increases the chance of the compounds to cross the BBB and to permeate the cells. However, on the other hand the nonpolar character reduces its solubility in water. Thus, analytic measurements in aqueous solutions become more difficult and are performed in the presence of DMSO. In the case of **L^{8Me}** the ligand becomes so insoluble in water, after protection of the hydroxide function, that even 10 % DMSO is not enough to keep it in solution at ≈200 mM. For further investigation of the ligand systems, especially when cells or proteins are involved, the solvent plays an important role. Dynamics, reactivity and protein folding strongly depend on the solvent. A value equal or smaller than 5 % of DMSO should not influence the measurement, but larger amounts could affect the reactivity of the Aβ protein and also of the compounds. Water-soluble ligands would be therefore most suited for metal exchange experiments, cell viability tests and ROS-inhibition studies. In particular for the determination of the metal exchange NMR experiments with **L^{8Me}** would be an increased solubility desirable. The solubility of compounds is influenced by their functional groups. Polar groups like –OH, –SH or –NH$_2$ increase the polarity and thus the solubility in water. In the ligand systems only one alcohol function is present, which is insufficient to dissolve the ligands in water. Thus, the ligand systems have to be attached to molecules with more polar groups or ionic groups like sulfonate (–SO$_3^-$). Herein different approaches for the synthesis of water-soluble model ligand systems will be presented. Reactions were carried out using **L^{3H}**.

In the first approach towards water-soluble ligand systems the host-guest principle of β-cyclodextrine was used. β-Cyclodextrine is a water-soluble cyclic oligosaccharide.[285] The hydrophilic exterior is responsible for the solubility and bioavailability and through the hydrophobic cavity on the inside formation of inclusion complexes with hydrophobic guest molecules, like 4-dimethylaminoazobenzene-4-sulfonyl, is possible.[286] Therefore β-cyclodextrine becomes a drug carrier molecule.[287] In this study an attempt was carried out to attach 4-dimethylaminoazobenzene-4-sulfonyl chloride to **L^{3H}** (Scheme 19). The sodium salt of the ligand was prepared in THF *via* sodium hydride and afterwards a small excess of the chloride

was added. After stirring the reaction solution for 24 h under reflux at 70 °C no product formation could be observed. Increasing the temperature to 100 °C and extension of the reaction time to 3 d had no influence on the reaction. The low reactivity, most likely results from the steric demand of the ligand. In the second approach, **L³ᴴ** should be directly coupled to β-D-glucose. β -Glucose is one of the few polar molecules which can cross the BBB. Therefore it can also be used as a drug carrier and even applications for the treatment of AD are known.[288] For the coupling reaction of **L³ᴴ**, the activated and protected β-D-glucose pentaacetate was used. Reaction was performed at different temperatures in THF and also in DMF, but no glucose-conjugated product was observed. This observation supports the hypothesis that the steric demand of the ligand prevents the attachment of other bulky molecules. However, attachment of small molecules should be possible. Thus, attempts were carried out to couple **L³ᴴ** with sodium 2-chloroethylsulfonate and sodium 2-bromoethylsulfonate. After stirring for 3 d under reflux no product could be obtained. Instead, the ligand could be completely recovered. Due to the low reactivity of the ligands further attempts to synthesise water-soluble ligands were forfeited and analytic measurements, described in the following chapter, were carried out in the presence of DMSO.
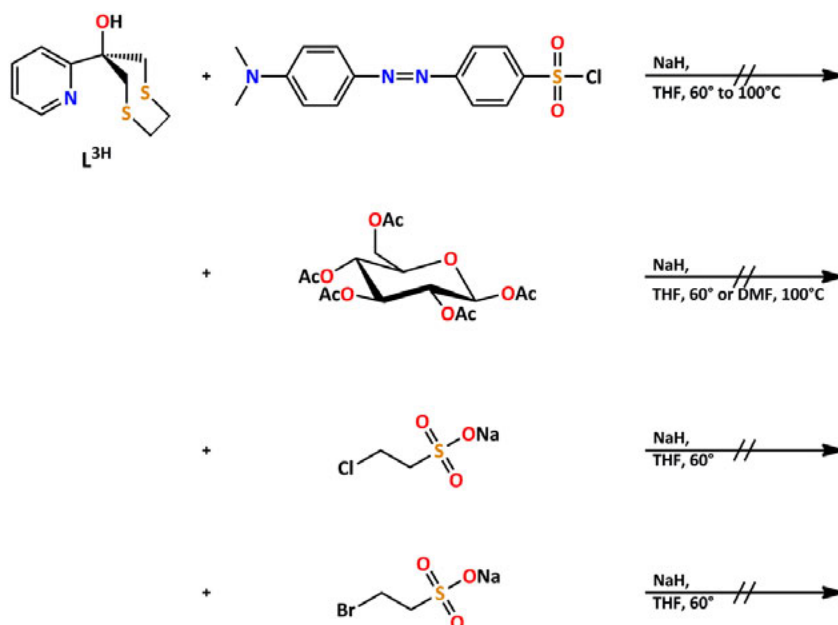
Scheme 19 Synthetic attempts to water-soluble ligands.

5.7 Selectivity and Metal Exchange Studies

5.7.1 Metal Selectivity

In the synthetic approaches presented so far only the chelating capabilities towards Cu^+, Cu^{2+} and Zn^{2+} have been tested, since these transition metals are postulated to play an important role in AD. However, in general a coordination of all metals present in cells has to be considered. As mentioned in chapter 2 the coordination of most transition metals can theoretically be excluded due to the specific equilibrium, and concentration control in cells.

Nevertheless, one attempt to prove the expected reactivity was carried out. Therefore were the ligands **L^{3H}** and **L^{5H}** coupled to *N*-ethyl-1,8-naphthalimide (NCLs, appendix B), because analogous systems are known as fluorescence sensors for transition metals.[256,289] Figure 26 illustrates one of the literature known systems and the systems synthesised in this study. To follow the metal coordination UV/Vis spectra and fluorescence spectra were recorded in water and in 0.1 M HEPES buffer (7.4). Coordination of the following metals were tested: Cu^+, Cu^{2+}, Zn^{2+}, Fe^{2+}, Ag^+, Co^{2+}, Ni^{2+}, Hg^{2+},Na^+, K^+, Cr^{3+}, Zr^{4+} and Mn^{2+}. Unfortunately, no changes of the absorbance or fluorescence bands could be observed. Comparison with the literature known system shows, that in case of the synthesised compounds, the linker chain is elongated by one ether function. The distances to the next coordinating atoms are even larger, since coupling was done over the ligand backbone. Therefore, the conjugated π-system of the detector is separated from the chelating unit and does not respond upon metal coordination. However, as mentioned before, the coordination of a transition metal in aqueous solution and especially in cells is restricted by many factors and from the structural features of the ligands should the ligands be selective for Cu^+. Thus, in the following only the selectivity of Cu^+ in the presence of Cu^{2+} and Zn^{2+} will be examined.
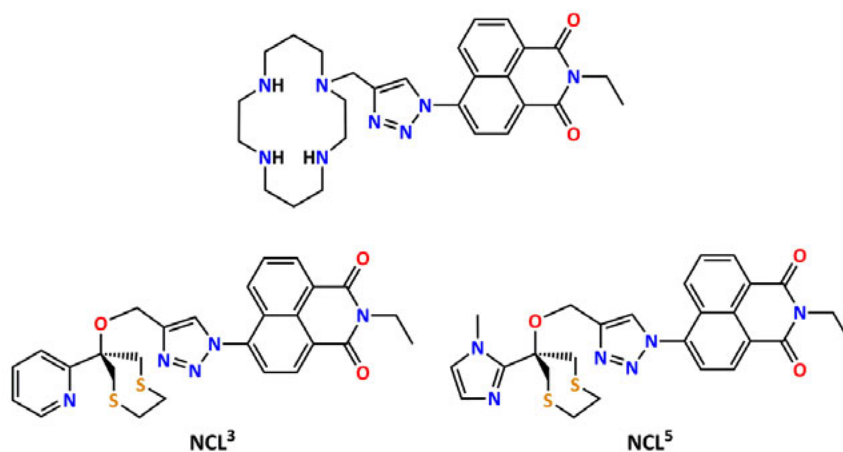
*Figure 26 The literature known cyclam-based Zn^{2+} sensor (top)$^{[290]}$ and **NCL^3** and **NCL^5** synthesised in this study (bottom).*

5.7.2 Cu$^+$ vs. Cu^{2+}

None of the experiments presented so far for the tripodal ligands were conducted in aqueous solution and extrapolation of the obtained results to other solvents is not always possible. To prove that the ligands can also coordinate copper in aqueous solution, in the presence of buffer, ^{1}H-NMR experiments were performed (Figure 27). **L^{8Me}** could not be used in this experiment due to its low solubility in aqueous buffer solution. However, the preparation of the model complexes as well as the ^{1}H-NMR experiment performed with the unprotected ligand proved that the Cu$^+$ selectivity for the tetradentate ligand system. First of all Cu$^+$ coordination was followed. The experimental conditions for this study were 1 mM Cu$^+$, 1 mM **L^{3Me}**/**L^{5Me}** in 0.2 M deuterated phosphate buffer (pH 6.9). A stock solution of $CuSO_4 \cdot 5\,H_2O$ in D_2O was used, which was reduced with dithionite *in situ*. For the ligands a stock solution in DMSO-d$_6$ (10 mM) was prepared due to the insolubility of the compounds in water. The insolubility results from the

plain, nonpolar ligand design, which favours the crossing of the BBB and permeation of the cells, but also makes them insoluble in water. Figure 27 shows the ^{1}H-NMR spectra recorded in the course of the experiment. Upon addition of Cu$^+$ all proton signals of the ligands are shifting. The aromatic signals of the pyridine and imidazole sidearm shift towards lower field, whereas the aliphatic signals are shifted to higher field. In common is the observed broadening of all resonances. This could be an indication for a dynamic process of the donating atoms. Thus, Cu$^+$ coordination takes place, but may be rather weak. To ensure this hypothesis either temperature-dependend NMR studies could be performed or stability constants have to be determined. The latter was done and the results will be presented in the next chapter. As mentioned before Cu$^+$ selectivity has to be ensured and Cu^{2+} coordination has to be excluded. With the same set-up, no signal shift could be observed by addition of one equivalent of Cu^{2+} to the ligand. Thus, the assumption from the synthetic approach of the Cu^{2+} complexes with **L^{3Me}** and **L^{5Me}** could be proven by NMR studies: The tripodal ligands are able to coordinate Cu$^+$, but not Cu^{2+}. These results show that the target orientated ligand design results in the desired selectivity.
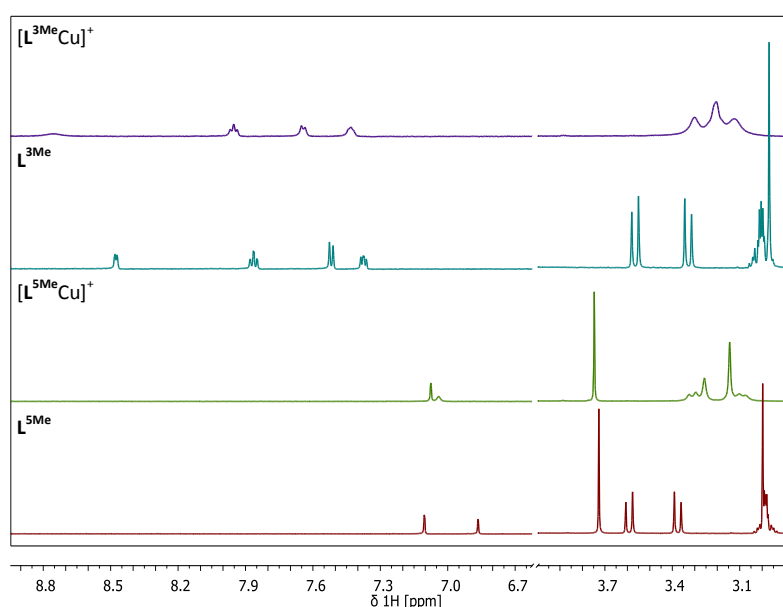
*Figure 27 ^{1}H-NMR spectra of **L^{3Me}**, **L^{5Me}** and their corresponding Cu$^+$ complexes. Experiment was conducted with 1 mм Cu$^+$, 1 mM **L^{3Me}**/**L^{5Me}** in 0.2 м deuterated phosphate buffer (pH 6.9).*

5.7.3 Cu$^+$ vs. Zn^{2+}

In AD afflicted brain and also in the Aβ plaques, not only copper but also elevated zinc levels have been detected. Thus, the synthesised ligands have to selectively coordinate Cu$^+$ in the presence of Cu^{2+} and also Zn^{2+}. As mentioned in chapter 2, a distinction between Cu$^+$ and the isoelectronic Zn^{2+} through targeted ligand design is not as simple as with Cu^{2+}. Both metal ions prefer tetrahedral coordination geometry and form the most stable complexes with a mixed {N$_x$S^-_y} donor set. However, they differ by their charge and therefore also by their acid character after the Pearson concept.[232] Cu$^+$ is softer than Zn^{2+} and prefers softer donors, whereas Zn^{2+} is harder and forms stable complexes with harder ligands. In the ligand systems soft thioether donors are present, which should be better suited for Cu$^+$ than for Zn^{2+} coordination. To prove this ^{1}H-NMR titration experiments of **L^{3Me}** and **L^{5Me}** were performed focusing on the metal exchange reactivity. Analogous to the synthetic procedure, metal selectivity was first

determined in organic solutions. Figure 28 shows the ^{1}H-NMR spectra of successive addition of Zn^{2+} to a solution of 0.40 mm **9** (left) and **10** (right) in MeCN-d_3. A stepwise replacement of Cu^+ by Zn^{2+} is visible for both complexes. Surprisingly, even a tenfold excess of Zn^{2+} to **9** does not lead to the spectra of the $[(\mathbf{L^{3Me}})_2Zn]^{2+}$ complex. The H_6 pyridine proton shifts further to higher field, but does not reach the same shift as in the pure Zn^{2+} complex. After addition of 0.5 eq. of Zn^{2+}, $[\mathbf{L^{5Me}}Cu(MeCN)]^+$ is completely transformed into the $[(\mathbf{L^{5Me}})_2Zn]^{2+}$ complex. Additional Zn^{2+} does not cause any further changes in the spectra. Although complete conversion of the Cu^+ complexes can be observed small deviations from the pure zinc-complexes are still present. The differences in the shifts are most likely induced by the presence of water from the utilised $Zn(ClO_4)_2 \cdot 6\ H_2O$ salt. However, the metal exchange experiment shows that $\mathbf{L^{3Me}}$ and $\mathbf{L^{5Me}}$ are selective for Zn^{2+} in MeCN, forming $[\mathbf{L}_2Zn]^{2+}$ complexes. Driving force of this reaction is not only the formation of the $[\mathbf{L}_2Zn]^{2+}$ complexes, but also the stabilisation of the replaced Cu^+ ion by formation of $[Cu(MeCN)_4]^+$.
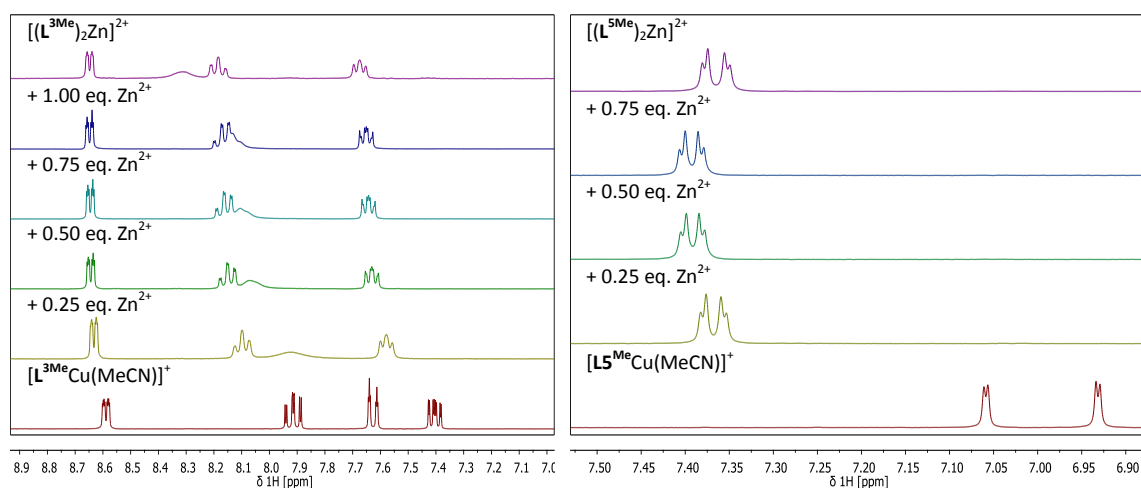

*Figure 28 ^{1}H-NMR spectra of the low field region in the metal exchange experiment. Successive addition of Zn^{2+} [$\mathbf{L^{3Me}}Cu(MeCN)]OTf$ (**9**, left) and $[\mathbf{L^{5Me}}Cu(MeCN)]PF_6$ (**10**,right).*

The experiment was also carried out under more cellular like conditions in 0.1 m deuterated tris (2-amino-2-hydroxymethyl-propane-1,3-diol) buffer (pH 7.4). Tris buffer was used instead of the phosphate buffer, since phosphate can coordinate to Zn^{2+}. From the NMR studies in MeCN-d_3 it is known that Zn^{2+} complexes are formed with a ligand to metal ratio of 2 : 1. Thus, a stock solution of $ZnSO_4 \cdot 7\ H_2O$ in D_2O was added stepwise and ^{1}H-NMR spectra were recorded with 0, 0.5 and 1.0 eq. of Zn^{2+} (Figure 29). Instead of the spectra of **17,** respectively **18,** only the signals of the free ligands could be observed. Thus, $\mathbf{L^{3Me}}$ and $\mathbf{L^{5Me}}$ cannot coordinate to Zn^{2+} in aqueous solution. This finding is completely different from the result obtained in MeCN, where Zn^{2+} could displace Cu^+. Reason for the different results is the different coordination properties of the used solvents. MeCN is a good ligand for Cu^+, which stabilises it by forming a $[Cu(MeCN)_4]^+$ complex, which can even protect Cu^+ against oxidation.[252] Zn^{2+} ions instead prefer harder ligands, such as water, resulting in the formation of a $[Zn(H_2O)_6]^{2+}$ complex. The $[Zn(H_2O)_6]^{2+}$ complex is even better stabilised than $[\mathbf{L^{3Me}}_2Zn]^{2+}$ and $[\mathbf{L^{5Me}}_2Zn]^{2+}$ respectively, although the latter are entropically favoured. Other metal ions like iron were not tested since they should be strongly disfavoured according to the concept of Pearson and the Irving-Williams series.[232,233] Thus, the metal exchange experiments prove that the synthesised ligands are *in vitro* selective for Cu^+ and can therefore be used for further investigation with respect to applications in AD.
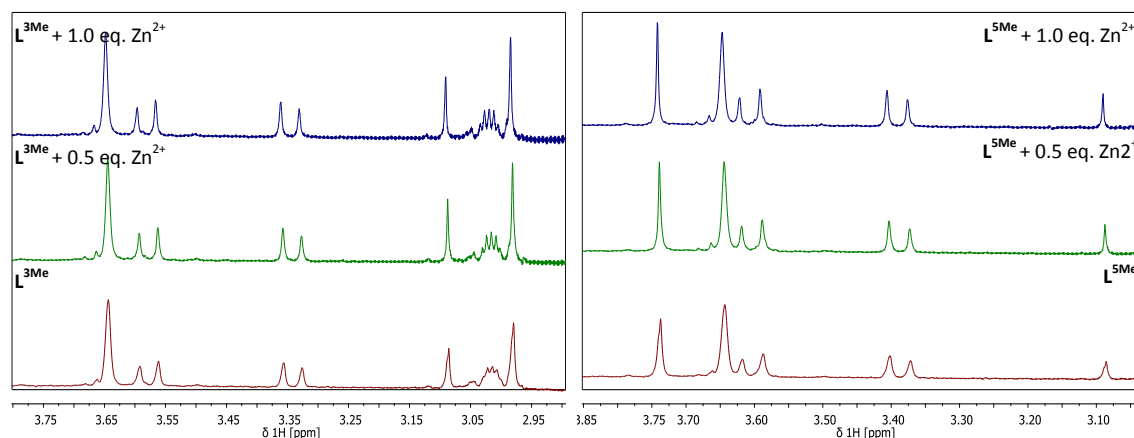
*Figure 29 Aliphatic region of the ¹H-NMR spectra of the successive addition of Zn²⁺ to 300 μm **L³ᴹᵉ** (left) and **L⁵ᴹᵉ** (right) in 0.1 m deuterated tris buffer (pH 7.4).*

5.8 Conclusion

The ligands were modified in order to mimic the structural features of the targeted multifunctional tool by attaching a methyl protective group to the backbone alcohol group. With these altered ligands, model complexes could be synthesised and characterised in solution and in solid state. The characterisation in solid state revealed formation of mononuclear complexes for both tripodal ligands. Furthermore, first attempts were carried out to determine the complexation properties in aqueous solution in the presence of buffer. Metal exchange experiments, show a selective coordination of Cu⁺ in aqueous solution. Consequently both ligands **L³ᴴ** and **L⁵ᴴ** seem to be suitable candidates to be coupled to the benzothiazole. For the tetradentate ligand **L⁸ᴴ**, metal selectivity could already be proven with the unprotected ligand. Nevertheless, also the methylated system was synthesised and evaluated with respect to its coordination properties, which are in agreement with the previous described results. Thus, besides the two tripodal ligand systems also **L⁸ᴴ** is a suitable candidate for the chelator subunit in the targeted multifunctional tool. However, **L⁸ᴴ** and especially **L⁸ᴹᵉ** are slightly soluble in water, which is a big disadvantage and has to be reconsidered in further experimental assemblies.

Chapter 6

Ligand Systems Targeting the Cu(Aβ) Complex
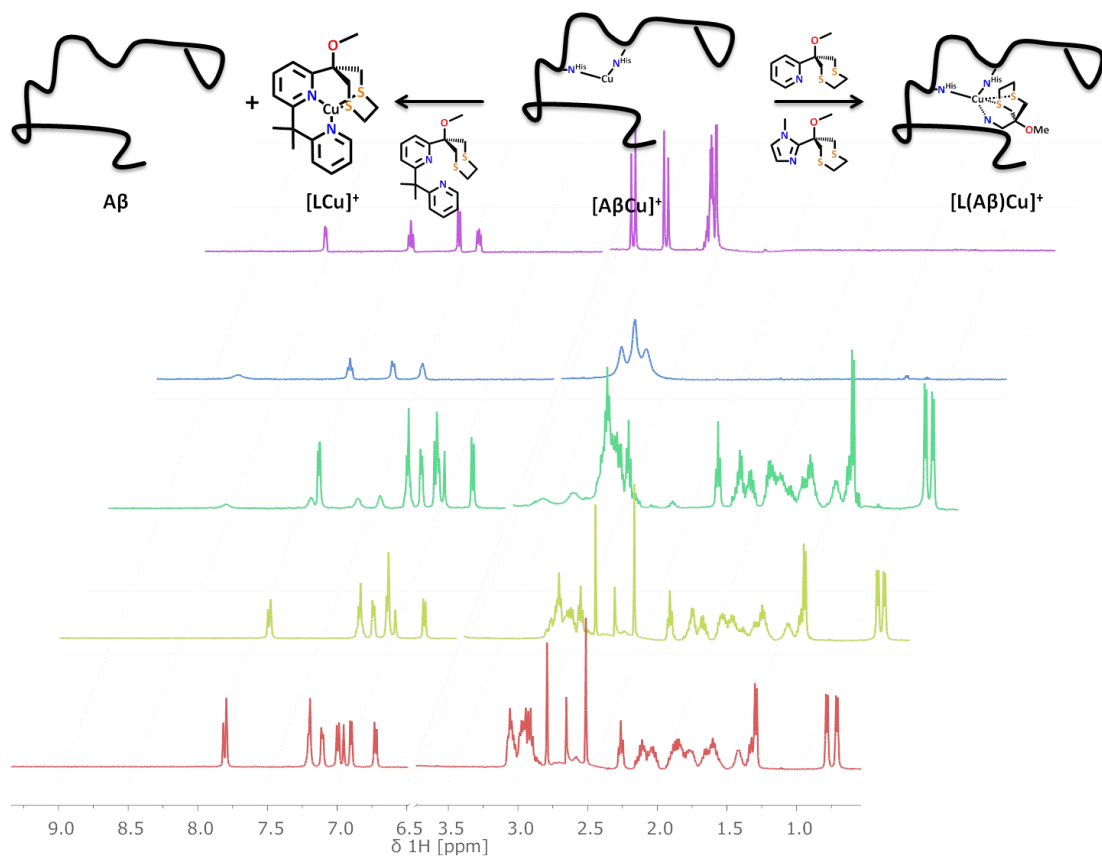
6.1 Introduction

The selectivity of the developed ligand systems could be proven in buffer solution. However, to be suitable for application in AD research, ligands have to comply with the following conditions:

i) The chelators should be able to not only coordinate Cu^+, but extract the Cu^+ from the Aβ protein. To do this, the ligand systems need higher Cu^+ affinities than Aβ.

ii) Metal induced oxidative stress is proposed to be the main event in AD progression, which damages the cell and finally leads to neuronal loss especially in the entorhinal cortex, hippocampus and basal forebrain.[5] Intercepting the reaction through chelating of Cu^+ *in vivo* would give evidence, whether the proposed $Cu^{2+/+}$ redox cycle is operative or not. Thus, the ligand should be able to inhibit metal induced ROS generation.

iii) The synthesised compounds must be nontoxic and be able to protect cells against metal induced oxidative stress.

In this chapter the synthesised chelators will be investigated with respect to these conditions.

6.2 Determination of Stability Constants

Recently association constants for different $Cu^+(Aβ)$ complexes were published.[145] The stability constants were determined by following the characteristic UV/Vis band of the chromophoric $[Cu(Fz)_2]^{3-}$ complex (Fz = ferrozine, 5,6-diphenyl-3-(2-pyridyl)-1,2,4-triazine-4,4''-disulfonic acid) at 470 nm (ε = 4320 $M^{-1} cm^{-1}$) upon successive addition of different types of Aβ proteins. For a successful inhibition of the proposed redox cycle (presented in chapter 1) the ligands have to possess a greater affinity and thus a greater stability constant than Aβ. Therefore the determination of the stability constants for the ligands is necessary. Association constants for L^{3Me}, L^{5Me} and also their unprotected precursor were determined similar to the literature known procedure (see experimental section for further information). Figure 30 shows exemplary the UV/Vis spectrum of the titration experiments with L^8. The shoulder at 562 nm (ε = 2600 $M^{-1} cm^{-1}$) is assignment to the $[Fe(Fz)_2]^{4-}$ complex, which is formed by trace amounts of iron in the used chemicals. In contrast to the literature was a $CuSO_4$ stock solution *in situ* reduced as Cu^+-source, instead of $[Cu(MeCN)_4]BF_4$. Upon coordination, the tridentate ligands leave a vacant binding site on the metal, which could in case of $[Cu(MeCN)_4]BF_4$ be saturated by one MeCN molecule and thus influence the determined stability constants. To reduce the Cu^{2+}, a freshly prepared dithionite solution (100 mM) was used. The conducted experiment is very sensitive, since all solutions have to be degassed and used under inert atmosphere. Additional dithionite was added after each titration experiment to determine the amount of Cu^{2+} which was formed during the experiment. For the calculation of the stability constants only measurements were taken into account with less than 5 % increase in the absorption band of the $[Cu(Fz)_2]^{3-}$ complex. The partially oxidation of Cu^+ was considered in the listed errors.
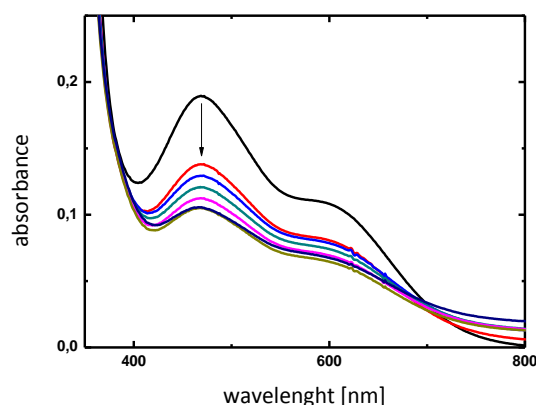
*Figure 30 UV/Vis spectrum of the titration of the [Cu(Fz)₂]³⁻ (50 μM) with **L⁸ᴴ** (20 μM/per step) in HEPES (0.1 M, pH 7.4). The band at 470 nm corresponds to the absorbance of the [Cu(Fz)₂]³⁻ complex and the band at 562 nm corresponds to the [Fe(Fz)₃]⁴⁻ complex.*

Table 18 summarises the calculated values. Comparison of the results leads to different conclusions. There are only minor differences between the ligands with and without a methyl group. No significant difference could be observed for **L³ᴴ** and **L⁵ᴴ**, thus substitution of pyridine by imidazole has no big influence on the affinity towards Cu⁺. Indication of this was already given by the structural comparison of the model complexes and also by the synthesised [**L**ˣᴹᵉCu(CO)]⁺ complexes (see appendix A). However, with this metal exchange experiment further proof is given. The obtained values for the tridentate ligands **L³ᴴ** and **L⁵ᴴ** are with 5.40 to 6.37 one magnitude lower than the reported one for the Cu⁺(Aβ) complex. As consequence the tripodal ligands **L³ᴴ** and **L⁵ᴴ** should not be able to extract Cu⁺ from Aβ under equimolar conditions. In contrast **L⁶ᴴ** should with a log β value of 7.51 be able to displace the protein. Furthermore, this result shows that substitution of the sulphur donor by stronger σ-donors results in a stronger Cu⁺ affiniy. Therefore, **L⁶ᴴ** would be a better candidate for further applications than **L³ᴴ** or **L⁵ᴴ**. Unfortunately, **L⁶ᴴ** shows also a high affinity towards Cu²⁺ and thus lack the essential selectivity. The ability of **L⁶ᴴ** to coordinate to Cu²⁺ and form stable complexes could also be indirectly represented in this experiment. By using **L⁶ᴴ** the highest amounts of Cu²⁺ could be determined at the end of the experiment. However, all measurements showed less than 5 % increase of the [Cu(Fz)₂]³⁻ absorption.

Table 18 Determined brutto stability constants (log β values) of the [LˣCu]⁺ species in presence of 0.1 M HEPES buffer (pH 7.4) by competition with Fz.

	log β		log β
L³ᴴ	6.37 ± 0.3	**L³ᴹᵉ**	5.40 ± 0.6
L⁵ᴴ	6.22 ± 0.3	**L⁵ᴹᵉ**	5.56 ± 0.4
L⁶ᴴ	7.51 ± 0.5	-	-
L⁸ᴴ	7.31 ± 0.2	**L⁸ᴹᵉ**	7.05 ± 0.2
Aβ₁₋₁₆	≈ 6.9	Aβ₁₋₄₂	≈ 7.3

L⁸ᴴ forms with a log β value of 7.31 also more stable Cu⁺ complexes than the tripodal ligands **L³ᴴ** and **L⁵ᴴ**. In theory, **L⁸ᴴ** and also **L⁸ᴹᵉ** should be able to remove Cu⁺ not only from the truncated Aβ₁₋₁₆ but also from the natural Aβ₁₋₄₂ if an excess of ligand is used. The strong increase in the binding constant is due to the second pyridine, which not only saturates the coordination sphere

of Cu^+ but also stabilises the complex through its strong σ-donor and π-acceptor character. Surprisingly, the determined value is still lower than the stability constant determined for **L**[6H], although **L**[8H] is entropic favoured; three *vs.* four donor atoms. Thus, the experiment not only elucidated, which ligands should be able to remove Cu^+ from the Aβ protein complex, but also illustrates the influence of the different donating groups in the ligands, and this provides an outlook for further ligand design. Thus, investigation of a $\{N_4\}$-ligand generation would be interesting.

6.3 Metal Exchange Studies on Aβ$_{1\text{-}16}$

6.3.1 Metal Exchange with Tridentate Ligands

In order to confirm the result from the Fz competition experiment a metal exchange ^{1}H-NMR experiment was performed for **L**[3Me] and **L**[5Me]. Set up for the experiment were 1 mM ligand, 1 mM Aβ$_{1\text{-}16}$ and 1 mM Cu^+ in 0.2 M phosphate buffer (pH 6.9). For verification of the result both the **L**[X]Cu^+ and the Cu^+(Aβ) complex were supplied and the corresponding compound added yielding in the same spectra. Since there are some overlapping signals of the ligand with the protein in the high field only the aromatic regions are shown in Figure 31. All pyridine signals of **L**[3Me] shift to low field upon coordination, whereas the aliphatic signals of the thioether sidearm shift to high field. The broadening of the ligand signals indicates a fast exchange of the donor atoms. The proton signals of the [**L**[3Me]Cu]$^+$ complex shift back towards the free ligand spectrum upon addition of the Aβ$_{1\text{-}16}$. However, they do not reach the same values as the free ligand. Furthermore, the broadening is kept. The Aβ protein behaves analogously. Coordination of the complex yields in a shift of the involved amino residues, such as His[13] and His[14]. In the mixed spectra these groups still deviate from their original metal-free values. This leads to the conclusion that a ternary ligand-Cu^+-Aβ complex is formed under the given conditions. Under consideration of the determined stability constants it is very likely that the metal is mostly localised on the protein and the different donor atoms of the ligands are in a fast exchange.
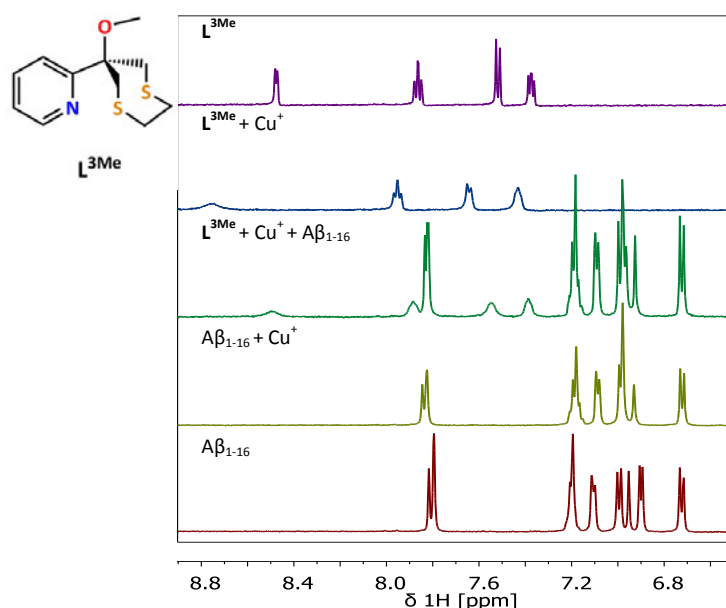
*Figure 31 ^{1}H-NMR spectra of the metal exchange experiment between **L^{3Me}** and Aβ$_{1-16}$. Spectra were recorded with 1 mM **L^{3Me}**, 1 mM Aβ$_{1-16}$ and 1 mM Cu$^+$ in 0.2 M phosphate buffer (pH 6.9).*

The experiment was also performed with **L^{5Me}** as competitor to Aβ$_{1-16}$ (Figure 32). The prediction from the determined stability constant would be again that the ligand is not able to remove Cu$^+$ from the protein. **L^{5Me}** has only two aromatic signals from the imidazole sidearm. Thus, coordination can be followed by detection of their shift. Especially, the nitrogen-neighboured proton signal shifts to higher ppm values upon metal coordination (marked with *). After addition of Aβ$_{1-16,}$ ternary complex formation can be observed similar to **L^{3Me}**. Thus, under physiological conditions, both tridentate ligands cannot extract Cu$^+$ from the Aβ$_{1-16}$ protein. Instead ternary complexes were most likeyl formed. For the desired application of this study a Cu$^+$ selective ligand is necessary, which can extract Cu$^+$ from the Cu$^+$(Aβ$_{1-42}$) complex. In this experiment it could be proven that neither of the two tripodal ligands is capable of this. Nevertheless, the utilised ligands can interact with the Cu$^+$(Aβ) complex and it would be interesting to study their influence, e. g. on the protein aggregation. It could be possible that the steric demand of the ligand prevents the formation of oligomers or even favour fibril formation.
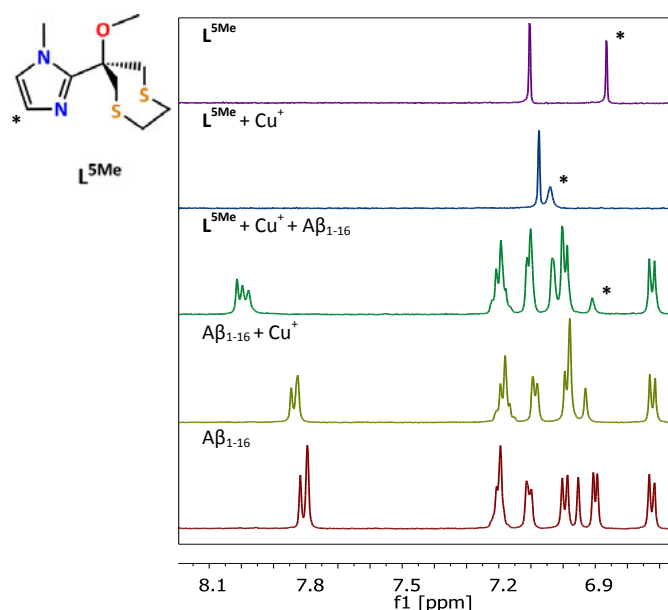
Figure 32 ^{1}*H-NMR spectra of the metal exchange experiment between* **L**^{5Me} *and Aβ$_{1-16}$. Spectra were recorded with 1 mM* **L**^{5Me}*, 1 mM Aβ$_{1-16}$ and 1 mM Cu$^+$ in 0.2 M phosphate buffer (pH 6.9).*

6.3.2 Metal Exchange with Tetradentate Ligands

The metal exchange experiment which was performed with the tridentate ligands was also carried out with the tetradentate ligand. **L**^{8H} was used instead of **L**^{8Me} due to the low solubility of the methylated ligand. However, the determined stability constant already proved that there is no difference between the protected and unprotected system. Although **L**^{8H} is better soluble the used ligand concentration had to be decreased. Thus, the specified set up for the ^{1}H-NMR experiment were 300 µM ligand, 300 µM Aβ$_{1-16}$ and 300 µM Cu$^+$ in phosphate buffer (pH 7.4). Unfortunately trace amounts of Cu^{2+} lead to a broadening of the histidine signals of the Aβ$_{1-16}$ and the ligand signals are diminished due to the bad solubility of the ligand and its complex. Thus, as indicator for the replacement of the protein were the aliphatic signals of the Val^{12} residue used. By coordination of Cu$^+$ the Val^{12} signals shift due to structural reorganisation of the protein (Figure 33). Addition of equimolar amounts ligand causes a shift, back to the free protein. In combination with the determined stability constants indicates this result, that the ligand can extracted the Cu$^+$ from the protein. Thus, it seems that in contrast to the tripodal ligands, **L**^{8H} is able to partially compete with Aβ$_{1-16}$, but not able to completly displace the protein. However, the detection of the Val^{12} shift is only an indirect measurement, since it is not directly involved in metal binding. To verify the results additional measurements are necessary and this experiment should be rather seen as a first indication of the reactivity.
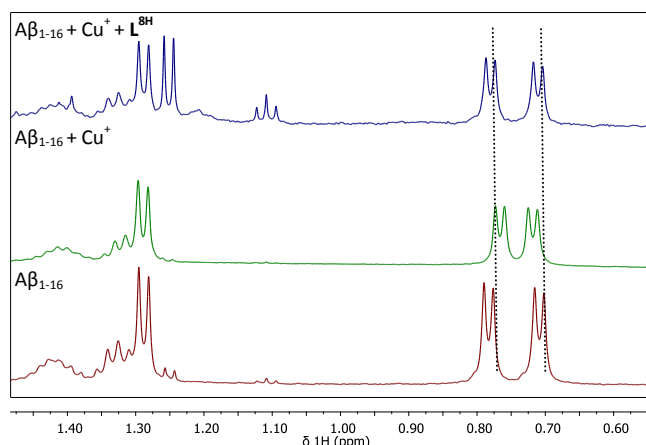
*Figure 33 ^{1}H-NMR spectra of the aliphatic region of the metal exchange experiment between **L^{8H}** and Aβ$_{1-16}$. The two duplets corresponds to the amino acid residue Val^{12}. The dotted lines better demonstrate the shifts. Spectra were recorded with 300 μM **L^{8H}**, 300 μM Aβ$_{1-16}$ and 300 μM Cu$^+$ in 0.2 M phosphate buffer (pH 7.4).*

6.4. Ascorbate Reduction as Extent of the Ligand Interception in ROS Origin

To study the capacity of the ligands to intercept in a Cu$^{2+/+}$ redox cycle, analogous to the one which is proposed for ROS generation in AD[173], time dependent ascorbate consumption was monitored by UV spectroscopy. The standard set up for the experiment was 100 μM sodium ascorbate, 5 μM Cu^{2+} and 7 μM of ligand or Aβ$_{1-16}$ in 50 mM phosphate buffer. The order of addition was buffer, ascorbate, ligand/protein, copper. The ascorbate stock solution was freshly prepared and no longer used than 5 h. The excess of ligand was used in order to make sure that no free Cu$^+$ is present. Ascorbate consumption was followed over a time period of 5 minutes and evaluation was graphically done by plotting the absorption (265 nm, Ɛ = 14500 M^{-1} cm^{-1}) against time. The metal becomes re-oxidised by O$_2$ from the air. The experiment was performed with both the methylated and the not methylated ligands to verify the results obtained in the Fz experiment (chapter 6.2). Each measurement was repeated at least three times to minimise errors and quantify the results. The detected ascorbate consumption should be slow in case of a strong Cu+ chelator and fast in case of weakly coordinating ligand systems. Thus, the following order could be assumed according to the determined stability constants: **L^{6H}** (slow) < **L^{8H}** < Aβ$_{1-16}$ << **L^{3H}** ≈ **L^{5H}** (fast).

Figure 37 shows the time depended ascorbate consumption for the methylated and not methylated ligand systems. Between the methylated and the not methylated systems no significant difference could be recorded. The biggest deviation could be observed for **L^{3H}** and

L^{3Me}. However, the experiment is very sensitive, so that the deviation lies within the error margin. Overall, the experiment again proves that the alcohol is not involved in metal coordination and methylation has no influence on the Cu$^+$ affinity. The slowest ascorbate consumption could be observed for **L^{8H}**, followed by Aβ$_{1-16}$. **L^{6H}**, which even has a higher Cu$^+$ affinity than **L^{8H}**, is only the third most active compound. **L^{3H}** and **L^{5H}** have according to the determined stability constants only a small inhibition of the metal mediated redox cycle.
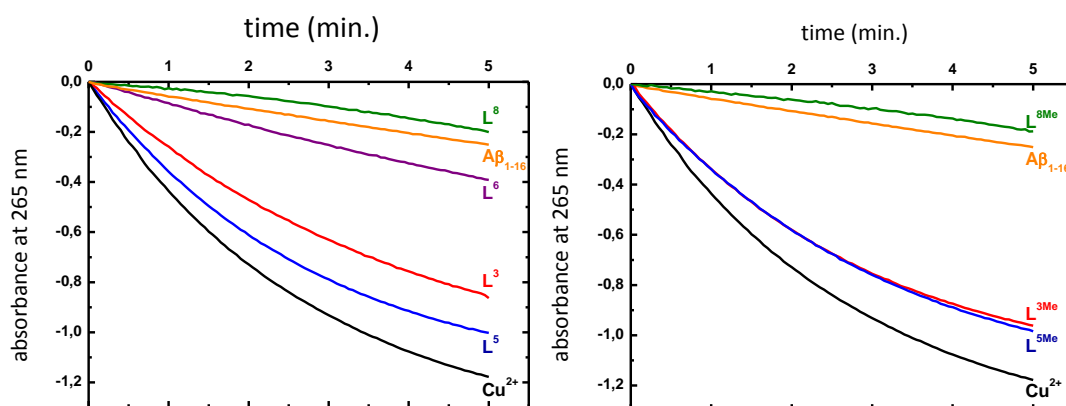
Figure 34 Time depended ascorbate consumption at 265 nm. Conditions were 100 μM sodium ascorbate, 5 μM Cu^{2+} and 7 μM L^x or Aβ$_{1-16}$ in 50 mM phosphate buffer (pH 7.4). Left the not modified ligands and right the methylated ligands.

The different inhibition capacities of **L$^{6H/Me}$** compared to the stability constants can be explained by different redox pairs formed during the experiment and should also be considered by the interpretation for the other ligand systems(Scheme 20). Aβ$_{1-16}$ has a relatively strong affinity to Cu^{2+} and binds it in the nM range.[113,114] Thus, after addition of Cu^{2+}, the Cu^{2+}(Aβ$_{1-16}$) complex is formed, which gets reduced by the ascorbate leading to Cu$^+$(Aβ$_{1-16}$). Thus, in case of Aβ$_{1-16}$ the observed redox pair is [Aβ$_{1-16}$Cu]$^{2+}$/[Aβ$_{1-16}$Cu]$^+$. The oxidation as well as the reduction requires reorganisation of the protein. The single redox states are therefore stabilised and the re-oxidation hindered. As a consequence the protein shows a remarkably strong inhibition in the ascorbate oxidation. The ligands **L^{3Me}**, **L^{5Me}** and **L^{8Me}** are in contrast only selective for Cu$^+$. The observed redox partners are therefore the [L^{x}Cu]$^+$ complex and the ligand free [Cu(H$_2$O)$_5$]$^{2+}$ complex and thus the ascorbate experiment resembles the determined stability constants. As mentioned before **L^{6H}** can not only coordinate to Cu$^+$, but also form a stable complex with Cu^{2+}. The formed redox pair is likely 2 [L^{6H}Cu]$^+$/[(L^{6H})$_2$Cu]$^{2+}$ + [Cu(H$_2$O)$_5$]$^{2+}$. The low activity of **L^{6H}** is most likely induced due to the stabilisation of the oxidised [(L^{6H})$_2$Cu]$^{2+}$ species. As a consequence the Ligand **L^{6H}** shows a higher activity than **L^{3Me}** and **L^{5Me}** but still much less active than the Aβ$_{1-16}$, although the determined stability constant is higher.

$$[Cu(H_2O)_5]^{2+} \xrightarrow{A\beta_{1-16}} [A\beta_{1-16}Cu]^{2+} \underset{O_2}{\overset{S_2O_4^{2-}}{\rightleftharpoons}} [A\beta_{1-16}Cu]^{+}$$

$$\downarrow S_2O_4^{2-}$$

$$[Cu]^{+} \xrightarrow{L^X} [L^XCu]^{+} \underset{O_2}{\overset{S_2O_4^{2-}}{\rightleftharpoons}} L^X + [Cu(H_2O)_5]^{2+}$$

$$\downarrow L^6$$

$$[L^6Cu]^{+} \underset{O_2}{\overset{S_2O_4^{2-}}{\rightleftharpoons}} \tfrac{1}{2}[Cu(H_2O)_5]^{2+} + \tfrac{1}{2}[(L^6)_2Cu]^{2+}$$
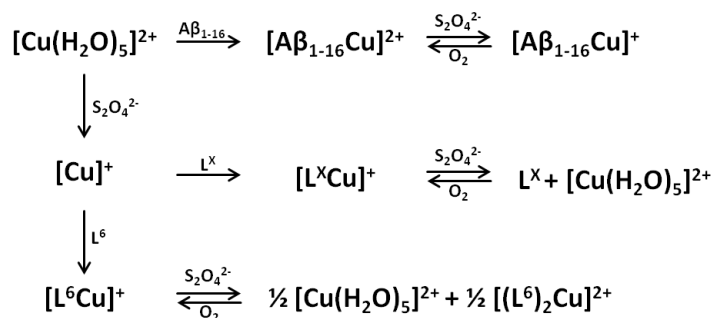
Scheme 20 Reaction pathways in the ascorbate consumption experiment. L^X can be L^{3H}, L^{5H}, L^{8H} or their corresponding methylated derivatives.

The experiment was repeated at different conditions to further investigate the inhibition capacity of the most active chelator, L^{8H}. Figure 35 shows the ascorbate consumption at 2.5 μM and 7 μM in the presence of $A\beta_{1-16}$ and without. By lowering the concentration of ligand to equimolar concentration of the copper a remarkable increase of the ascorbate consumption could be observed. One reason for this increase could be the presence of free Cu^+. Even small inaccuracies in the pipettes or minimal impurities in the used compounds could lead to an excess of copper and thus a significant increase in the ascorbate consumption. Further decrease of the ligand concentration, to 2.5 μM, results in a loss of the protective function. Besides low ligand concentration higher concentration were tested. However, increase to 10 μM or higher (15 μM, 20 μM) have no significantly influence on the ascorbate oxidation.
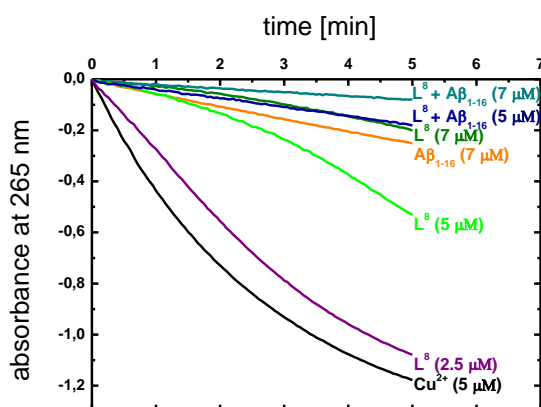
Figure 35 Time depended ascorbate consumption at 2.5 μM, 5 μM and 7 μM of L^{8H} in the presence of $A\beta_{1-16}$ and without. Spectra were recorded in 50 mM phosphate buffer (pH 7.4).

The experiment was also carried out in the presence of Aβ to study the influence of the protein on the sensitive redox system. The addition of $A\beta_{1-16}$ leads to a further decrease of the ascorbate oxidation. One possible explanation for this increased inhibition would be that a ternary complex is formed where the Cu^+ is tightly bound by the protein and the chelator. However, formation of such a complex is unlikely because it was not observed in the NMR metal exchange experiment. In Scheme 21 is a proposed redox cycle presented, which comprises all important intermediates and could explain the observed reactivity's. The redox cycle starts with the free Cu^{2+}, which becomes coordinated by the $A\beta_{1-16}$. In the next step takes the reduction place and generates the $[A\beta_{1-16}Cu]^+$ complex. The higher affinity of L^{8H} should than lead to a replacement of the protein

and coordination of the ligand, like observed in the NMR experiment. This $[\mathbf{L^8}Cu]^+$ complex becomes then oxidised by air and releases the Cu^{2+}, which can again be coordinated by the $A\beta_{1-16}$. Since no studies were done concerning the kinetics, it can only be conjectured what the rate determining step is. The reduction and oxidation of the metal is more or less known from the previous experiments and in both cases faster ascorbate consumption was observed. The metal exchange rate instead, is not specified. However, it could be seen in the ferrozine experiment (see chapter 6.2) that such a metal exchange can be relatively slow. Thus, the increased inhibition activity is not induced by a stronger coordination, but most likely due to an intermediate were the $A\beta_{1-16}$ gets replaced by the ligand.
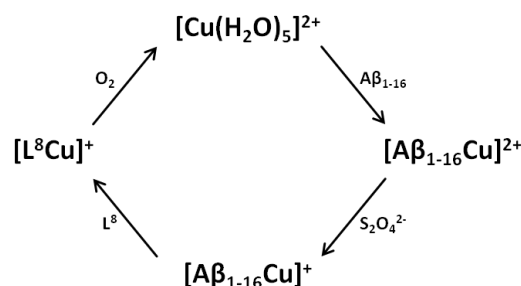
Scheme 21 Proposed redox cycle for the ligand inhibited ascorbate consumption in the presence of Aβ1-16.

The ^{1}H-NMR experiment showed that $\mathbf{L^{3Me}}$ and $\mathbf{L^{5Me}}$ can, together with $A\beta_{1-16}$, probably form ternary Cu^+ complexes. Thus, the ascorbate consumption experiment in the presence of $A\beta_{1-16}$ was also repeated for $\mathbf{L^{3Me}}$ and $\mathbf{L^{5Me}}$ to study the influence of these complexes. A higher inhibition capacity was expected, since an additional ligand is involved in the coordination of the Cu^+. However, the comparison with the $A\beta_{1-16}$ alone showed no significant deceleration of the ascorbate consumption. This leads to the assumptions that either no ternary complex is formed or that the coordination of the ligand is too weak and does not influence the re-oxidation of the Cu^+. The latter hypothesis is disfavoured by the fact that the tripodal ligands have already shown an activity. Thus, coordination should induce a change in the inhibition.

6.5 Cell Viability Tests

Cell viability tests or viability assays are studies which determine the ability of cells to maintain or recover their viability.[291] The cultured cells can be used to determine the cytotoxicity of chemical compounds and for drug screening. The synthesised ligands and also the final multifunctional tools should be at least suitable for *in vivo* studies or in best case used as drugs. Thus, the toxicity of the compounds had to be determined. The utilised test was a colorimetric MTT (3-(4,5-Dimethylthiazol-2-yl)-2,5-diphenyltetrazolium bromide) test for cell viability based on the activity of the mitochondrion of living cells. Cell viability was determined by a mitochondria enzyme dependent reaction of MTT as described elsewhere.[292] MTT (a yellow tetrazole) is reduced by the mitochondrial reductase to a purple farmazan (Scheme 22). The mitochondria play an important role in the respiration cycle of living cells and thus their activity can be used as a measure of enzymatic activity and cell viability, respectively. The colour change, induced by the metabolised MTT, can be measured by UV/Vis-spectroscopy. The purple farmazan has an absorption maximum at 570 nm, which can be shifted by solvatochromism

(500-600 nm). MTT was added to the neuronal cells (human tumor cells SH-SY5Y) at final concentration of 5 mg/ml at 37 °C for 4 h, 24 h after testing the compound. Undifferentiated human neuroblastoma SH-SY5Y cells were grown under standard culture conditions in an incubator containing a humidified atmosphere with 5 % CO_2 at 37 °C. The medium used was DMEM (Dubelcoo's Modified Eagle's Medium) supplemented with 15 % foetal bovine serum (FBS). The reaction was terminated by removal of the supernatant and addition of 1.5 ml DMSO to dissolve the formazan product and afterwards, the absorbance was measured. The experiment was performed three times with three batches per measurement. The error margin for cell studies like the presented MTT assay can be up to 20 % and in this study only a low number of batches were conducted. Thus, the cell studies should be reconsidered as a first indication of the reactivity of the compounds with respect to cellular conditions. The Cell studies were performed by Isabelle Sasaki in the laboratories of the *Institut de Pharmacologie et de Biologie Structurale* (IPBS) in Toulouse, France.
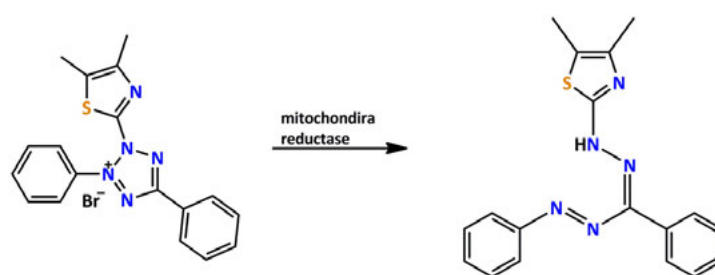
Scheme 22 Reduction of MTT (3-(4,5-Dimethylthiazol-2-yl)-2,5-diphenyltetrazolium bromide) by mitochondria.

The toxicity of the ligands L^{3Me}, L^{5Me} and L^{8H} (L^{8H} was used due to the better solubility than L^{8Me}) were determined by the MTT viability assay (Figure 36). L^{3Me} and L^{5Me} show no toxic behaviour. Mainly all cells survived in the case of L^{3Me} and L^{5Me}. Unfortunately, the ligand L^{8H}, which has the highest affinity towards Cu^+ and also shows the highest activity in the inhibition of ascorbate consumption, seems to by cytotoxic. The reason for the toxic behaviour of L^{8H} is not known and can only be speculated. The comparison with L^{3Me} and L^{5Me} leads to the hypothesis that the specific toxic behaviour could be induced by the alcohol function of L^{8H}. After coupling with the benzothiazole, the alcohol function would be protected and probably the generated multifunctional compound would show no cytotoxicity. Since no measurements were available to follow the pathway of the ligand, the cytotoxic mode of action remains unknown. One hypothesis is that since the ligand L^{8H} is relative nonpolar and highly lipophilic, it should be able to penetrate the cells and react with proteins or enzymes in the cell. Such reactivity could disturb the natural respiration of the cell and could than lead to cell death. Another possibility for the low survival rate is an interaction of L^{8H} with the FBS and a disturbance of the sensitive cell environment.
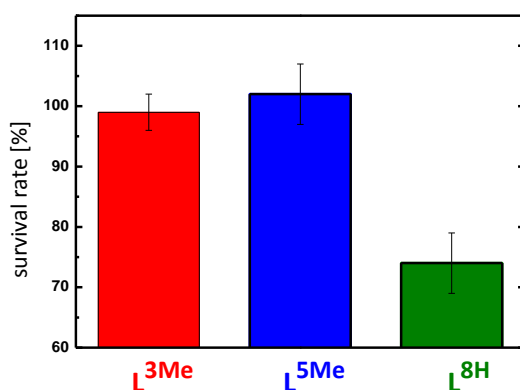
*Figure 36 Viability assays with **L³ᴹᵉ**, **L⁵ᴹᵉ** and **L⁸**. Percentage of living cells after the treatment with 10 uM of the compounds.*

By modification of the experiment it could be used to measure the protective function against metal induced ROS. The ROS can be artificially generated by adding Cu^{2+} and ascorbate to the cell medium (Figure 37). In this experiment only the ligands were examined, which have shown no toxic behaviour. Thus, the experiment was only performed with **L³ᴹᵉ** and **L⁵ᴹᵉ**. The first, black bar is the average survival rate of cells treated with ascorbate and copper, and serves as reference. The results show for both chelators a slight protective function. This result directly corresponds with the determined stability constants and also with the performed ascorbate consumption experiment. Thus, **L³ᴹᵉ** and **L⁵ᴹᵉ** seem to be able, even though only weakly, to stabilise Cu^+ in aqueous solution. Thus, with this study a first impression is given for the metal-induced ROS protective function of the tridentate ligand systems.
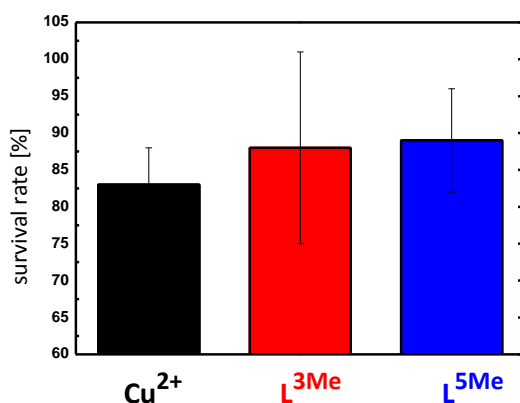
*Figure 37 Modified viability assays to with **L³ᴹᵉ** and **L⁵ᴹᵉ**. Percentage of living cells after the treatment with 5 uM Cu⁺, 100 uM ascorbate and 10 uM of the compounds.*

6.6 Conclusion

For **L^{3H}**, **L^{5H}**, **L^{8H}** and their methyl protected derivatives were brutto stability constants determined. The values indicated that all ligands should be able to compete with Aβ$_{1-16}$. However, in the performed ^{1}H-NMR metal exchange experiment only **L^{8H}** was able to extract the copper from the Cu$^+$(Aβ$_{1-16}$) complex. The tripodal ligand system can interact with the metallo protein complex, but their affinity is too low to displace the Aβ$_{1-16}$. The ligands and their derivatives were further investigated with respect to their redox-inhibition capacity in an metal mediated ascorbate consumption experiment. Out of the series only **L^{8H}** is able to slow down the ascorbate consumption more than the Aβ$_{1-16}$. For **L^{3H}** and **L^{5H}** only a minor deceleration of the ascorbate consumption could be observed. Since the final aim is an *in vivo* application, the ligand systems were tested of their cytotoxicity. The performed cell viability test revealed that **L^{3Me}** and **L^{5Me}** are not toxic, whereas **L^{8H}** shows a toxic behaviour. The specific toxic mechanisms are not known, but it is possible that the free alcohol function is responsible for this reactivity and therefore it could be possible that the final molecule shows a different behaviour. However, the obtained results in the ascorbate consumption experiment and the determined stability constants are very promising. All three ligands were therefore introduced in a multifunctional tool.

Chapter 7

Synthesis and Characterisation of Multifunctional Tools for Applications in AD
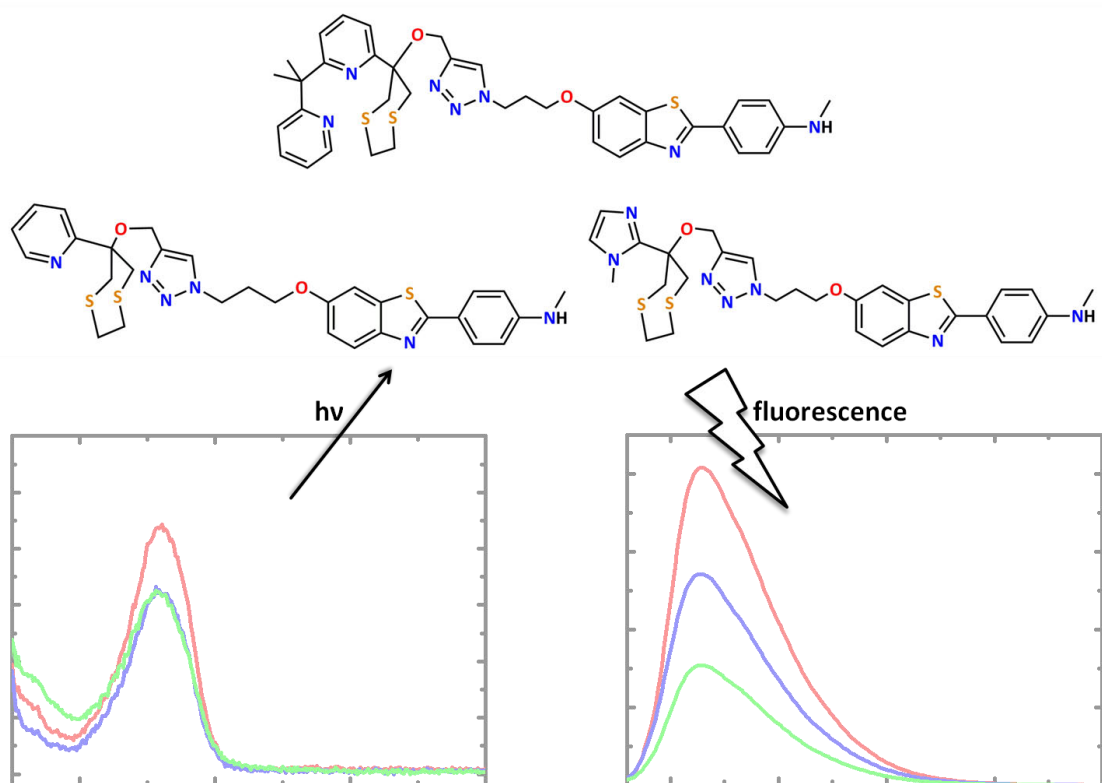
7.1 Introduction

Since the discovery of Aβ plaques as one of the main features of AD, several dyes have been developed for Aβ plaques to ensure an early AD-therapy. Small fluorescent molecules like Congo red, Thioflavin or Stilbene and their derivatives become of great interest in this context, since they can intercalate in the β-sheet structure of the Aβ plaques and allow the use of tomographic techniques (PET or SPECT).[56,64,293] One of the best known representatives of these Aß dyes is Thioflavin T, which stands out due to its spectral alteration upon binding to Aβ fibrils. Free ThT absorbs at 342 nm and has a characteristic fluorescence excitation at 430 nm. Binding to the fibrils induces a red shift of the absorbance to 442 nm and also a shift of the fluorescence excitation to 482 nm.[62,294] One further developed ThT derivative is the Pittsburgh Compound B (PIB), where the benzothiazole moiety is slightly modified (Figure 38). However, this small variation remarkably increases the binding affinity to Aβ plaques and provides other advantages, such as a short clearance time from healthy brain tissues.[57,58] Responsible for the different affinity and improved intercalation is most likely the combination of aromatic π-π-interactions and hydrogen bridges between PIB and the fibrils.
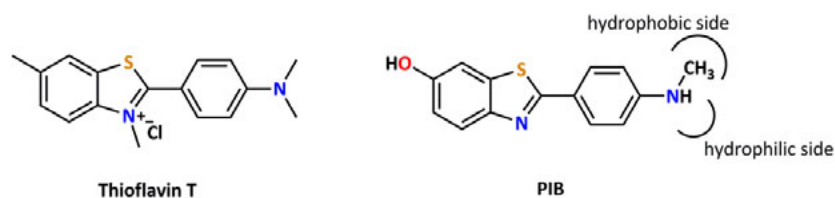
Figure 38 Hydrophobic and hydrophilic sides of PIB

AD is a very complex disease with various hallmarks like miss-regulation and dyshomeostasis of transition metals, formation of Aβ plaques, hyperphosphorylation of the tau protein. Classical therapeutic strategies which target only one of the hallmarks have shown low efficiency.[217] Certain symptoms can be treated with these drugs, but not the cause of AD. Thus, the trend goes to drugs, which do not target the symptoms but the cause itself.[222,227] In order to provide these therapeutic strategies, a more profound understanding of the disease is necessary. To enlighten the specific mechanisms involved in the AD, molecules become favoured that comprising more than one active functional group.[295] Thus, the compounds can modulate multiple targets that characterise the neurodegenerative disease. In the last decade multifunctional systems of different types were synthesised and evaluated for their efficiency in the treatment of AD (Figure 39). For the first type a proven active molecule gets an additional functionalisation to increase its activity or introduce a new beneficial property (e.g. solubility increase or crossing the BBB). The second type consists of single molecules which combine multiple functions, to allow interaction with more than one target. The third and last type are compounds with two molecules or functional groups with intrinsic activity, which are bridged by a linker, resulting in hybrid molecules. Depending on the nature of the spacer both active sites can interact or react completely independently.
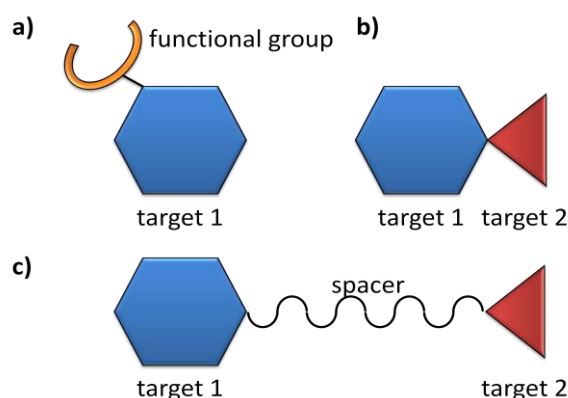
Figure 39 General representation of different multifunction types developed in the last decade. a) functionalisation, b) incorporation and c) coupling over an spacer.

The second type of multifunctional systems has high potential for applications due to its ability to "kill two birds with one stone".[295] Therefore, they were announced as most promising compounds in comparison with the other types.[295] Their advantage to interact with multiple targets, is a major disadvantage in medical applications, since the observed activity cannot be assigned to a certain functional group or target.

Aim of this study is the synthesis of a multifunctional tool which can enlighten the interaction of Cu^+ with Aβ. For this task, a multifunctional type three system was developed, containing a Cu^+ chelator and an Aβ plaque sensitive unit. The synthesis and characterisation of suitable chelators for Cu^+ recognition was reported in the previous chapters. Due to the promising results for L^{3H}, L^{5H} and L^{8H}, these systems will be used in the multifunctional tools. In this chapter, the synthesis of the Aβ recognition subunit —a benzothiazole analogue of PIB —and coupling attempts with the ligands will be presented. Coupling of these two molecules *via* a linker, should form a hybrid with the following attributes: i) selective coordination of Cu^+, ii) selectivity towards Aβ plaques and iii) luminescence properties.

7.2 Synthetic Approach to Benzothiazole Derivatives

Although many different approaches for the synthesis of benzothiazole derivatives are known in the literature, most of the synthetic routes lack flexibility.[242,243] In this study, a synthetic route was developed with *Suzuki Coupling* as the key step, which offers the possibility to combine different building blocks, leading to various benzothiazoles (Scheme 23).[296,297] Nevertheless, in this study only one benzothiazole derivative (**BTA**) was synthesised. The synthetic route starts with the synthesis of the precursors for *Suzuki Coupling* reactions: a halogenated benzothiazole and a boron derivative which can either be a boronic acid or boronic ester.
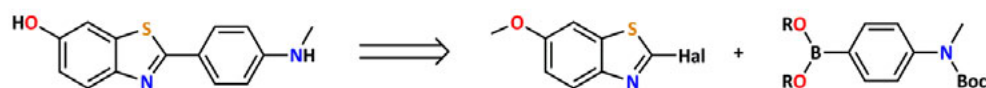
Scheme 23 Retrosynthetic analysis of the targeted benzothiazole derivative.

The halide can be synthesised by a two-step synthesis from 4-methoxyanilin. In the first step 2-amino-6-methoxybenzothiazole **XIII** is generated by reaction of 4-methoxyanilin with potassium

thiocyanate and elemental bromine in acetic acid (Scheme 24).[298] During the reaction the temperature has to be kept lower than 20 °C to ensure a high yield. The amine can be activated with a nitrite and then substituted to a halide. In the first approach the literature known substitution to 2-bromo-6-methoxybenzothiazole (**XIV**) was carried out.[299] The amine was therefore activated with *tert*-butyl nitrite. Further reaction of the activated intermediate with CuBr$_2$ provided **XIV** in good yields (74 % Lit.: 79 %[299]). Unfortunately, the synthesis could only be used in small scales, since upscaling would require a few litres of solvent and HCl. The aim was to find a simple pathway, which also works on bigger scale. Thus, the last step was changed and instead of a bromide an iodide was attached to the benzothiazole. Activation of **XIII** was achieved with sodium nitrite and potassium iodide was used as halide transfer agent. In the presence of catalytic amounts of *para*-toluenesulfonic acid, 2-iodo-6-methoxybenzothiazole **XV** could be synthesised in moderate yields (58 %).
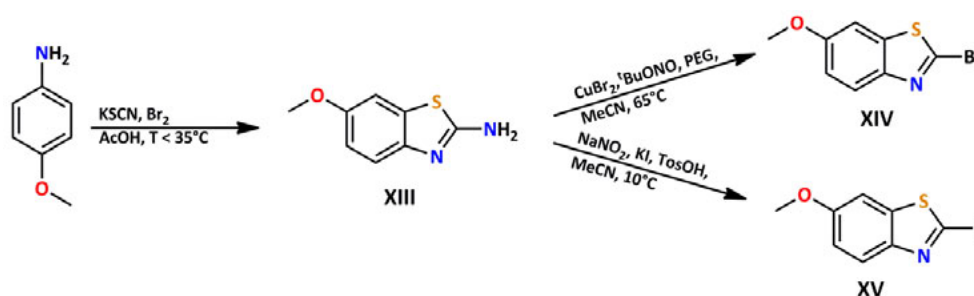
Scheme 24 Synthetic pathway of the halides XIV and XV as precursor for Suzuki coupling.

The boronic acid or ester was synthesised starting from the commercially available 4-bromoanilin. According to the scaffold in Figure 38, a methyl group has to be introduced on the amine to create a hydrophobic and a hydrophilic side. This is needed for a good intercalation of the multifunctional tool in the Aβ fibrils. Two approaches were carried out providing the mono methylated compound **XVIII** (Scheme 25). In the first approach 4-bromoaniline was methylated with methyl iodide in the presence of Et$_3$N. After attachment of the first methyl group the pK_a value of the remaining secondary amines increased only slightly and therefore the amine became methylated twice. Thus, the main product of this reaction was 4-bromo-*N*,*N*-dimethylaniline and the desired mono methylated product **XVI** could only be obtained in low yields (40 %). The second approach proceeds over the *boc*-protected intermediate **XVII**, which could be synthesised by reaction of 4-bromoaniline with di-*tert*-butyl dicarbonate. In the next step, the methyl group could be attached by treating **XVII** with methyl iodide after deprotonation with sodium hydride. The desired boron functionality was afterwards introduced *via* transmetalation with ^{n}BuLi and addition of the trimethoxyborane. The mild acidic workup with NH$_4$Cl partially cleaves the ester providing not only **XIX** but also **XX** as a side product. However, **XIX** as well as **XX** can be used in the cross coupling reactions. Thus, the products were not separated.
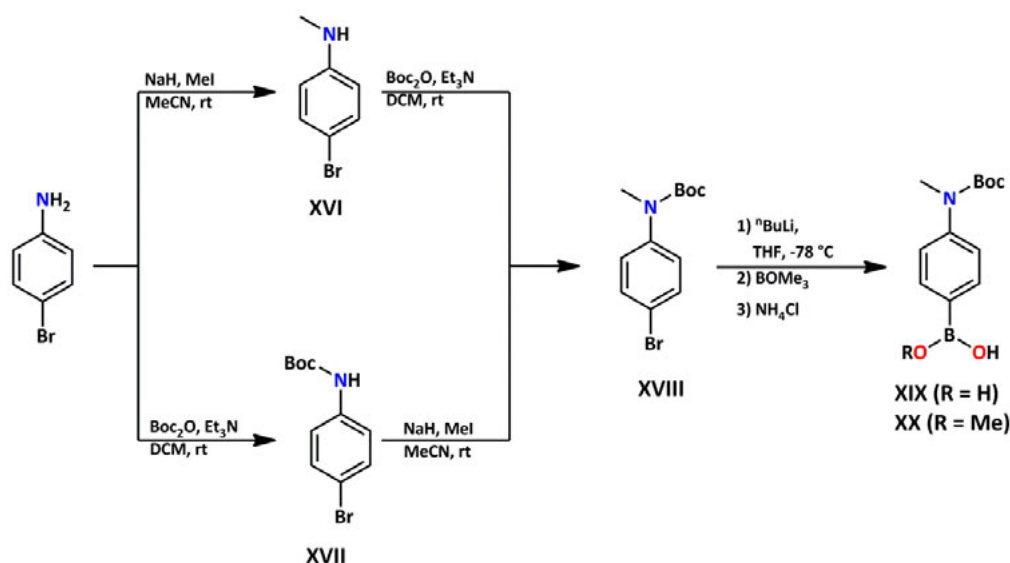
*Scheme 25 Synthesis of the boron-precursors **XIX** and **XX** for Suzuki coupling.*

Suzuki Cross Coupling reactions were carried out with both the bromide **XIV** and the iodide **XV**. As coupling partner, the mixture of **XIX** and **XX** was used (Scheme 26). Reaction conditions for the cross coupling were stoichiometric amounts of the provided precursors and catalytic amounts of $CuSO_4$ and $Pd(PPh_3)_4$. The reaction was stirred under reflux for 24 h - 48 h at 120 °C. Yields up to 98 % could be achieved utilising both halides, but the iodide requires a longer reaction time. The reaction time could be shortened to 0.5 h to 1 h by microwave irradiation (250 W). The last step of the benzothiazole synthesis was the cleavage of the protection groups, namely the *boc* protection group on the amine and the methoxy group on the alcohol. Both groups can be cleaved in one step *via* BBr_3 in DCM, providing **XXII** in very good yields (98 %). As mentioned before, the utilised synthetic strategy theoretically provides a fast excess to a broad variety of different benzothiazoles and with *Suzuki Coupling* as key step, many functional groups are tolerated.[296,297] With 2-(4-(methylamino)phenyl)benzo[*d*]thiazol-6-ol **XXII** (**BTA**) the second molecule for the synthesis of multifunctional tools is provided. Thus, in the following, different approaches to introduce a spacer and couple the Cu^+ chelator subunit with **BTA** will be discussed in more detail.
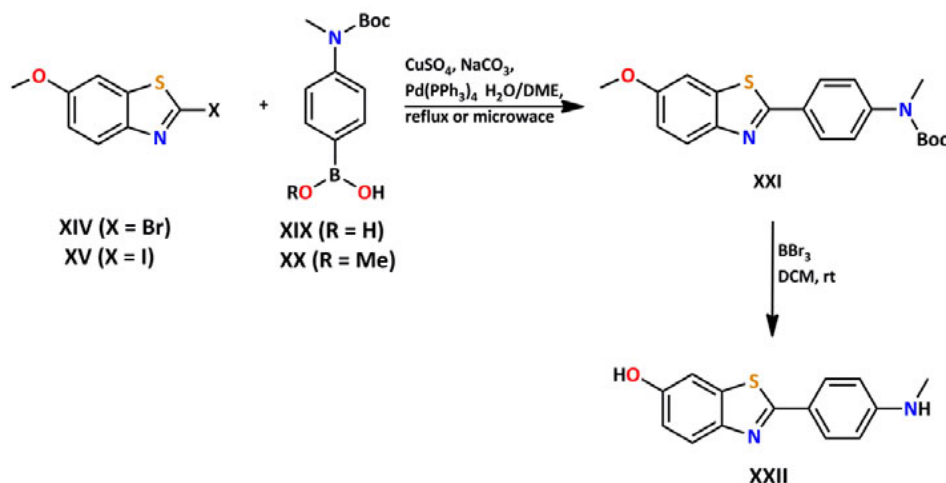
*Scheme 26 Synthesis of Benzothiazole **XXII**.*

7.3 Synthetic Approach to Multifunctional Systems *via* Nucleophilic Substitution

The use of PIB in multifunctional systems has already been investigated.[295] Often the derivatives have been modified on the amine function. As has been explained before, this function is announced to be essential for an effective binding to the fibrils. In contrast to that modifications on the benzylic alcohol are rare. One reason for this could be, that little is known about its influence on the intercalation. In the few literature known systems, where the alcohol was substituted, only small groups like iodide, a methyl group or a methoxy group were implemented.[58,243] Since these derivatives show overall a high activity, the benzylic alcohol was in this work chosen as coupling position for the spacer.

7.3.1 Attempts for an Ethylene Linker

In the first approach towards a multifunctional system an ethylene bridge was chosen as spacer between the two functional groups. The small bridging unit should allow an intramolecular interaction of the chelator with the fluorescence sensor. Upon metal coordination, a shift or a change in the intensity of the fluorescence signal should therefore be observed, providing a tool to detect not only the intercalation into the fibrils but also metal coordination. Introduction of the ethylene bridge on the benzothiazole was done by reacting the alcohol with ethylene epoxide in the presence of stoichiometric amounts of potassium hydroxide (Scheme 20). In addition to this, attempts to introduce the spacer on the ligand were carried out. Only the reaction with the benzothiazole yielded the desired product **XXIII**. A reason for this might be the steric demand of the bulky residues on the tertiary alcohol, which shield it and prevent a nucleophilic attack. The benzothiazole provides, in contrast to that, a high reactivity due to the phenolic proton and missing steric demand of the sp^2-hybridised C-atom. Thus, the product was obtained in good yields (81 %).
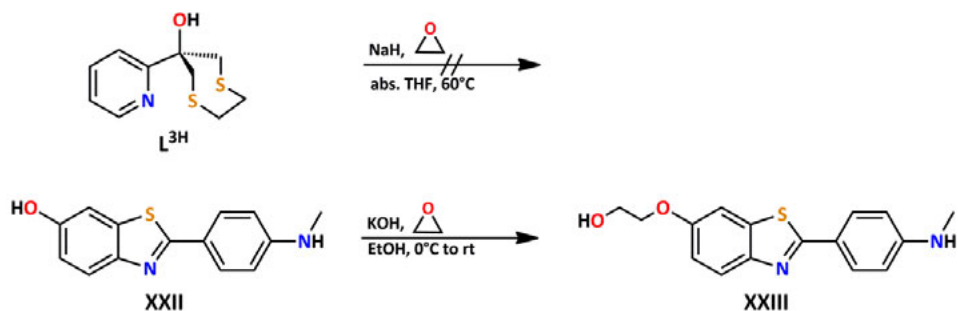
Scheme 27 Synthetic attempts to introduce an ethylene spacer on the ligand **L³ᴴ** *and on the benzothiazole* **XXII***.*

Different synthetic approaches to couple **XXIII** with the ligands were carried out. The first attempt was an activation of the ligands. **L³ᴴ** was therefore heated under reflux with an excess of hydrobromic and hydrochloric acid in the presence of H_2SO_4 (Scheme 28). The reaction was performed at different conditions but no products could be obtained. With ^{1}H-NMR spectroscopy, protonation of the pyridine could be observed.
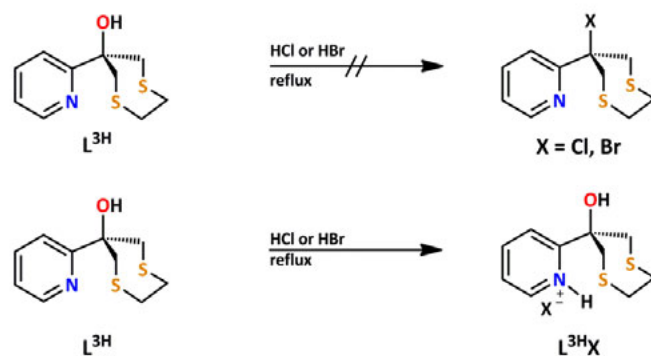
Scheme 28 Synthetic attempts to activate **L³ᴴ** *by halogenations.*

Since activation of the ligands did not succeed, attempts to activate the **BTA** were carried out (Scheme 29). Activation of the benzothiazole *in situ* with stoichiometric amounts and an excess of HCl or PPh₃ did not lead to the desired coupled product. In a different attempt, *Mitsunobu* reaction conditions were used. Equimolar amounts of **L³ᴴ**, benzothiazole, PPh₃ and DIAD (diisopropyl azodicarboxylate) in the absence and presence of benzoic acid were stirred at different temperatures. Although formation of triphenylphosphine oxide could be observed *via* TLC, no product could be isolated nor detected by ^{1}H-NMR.
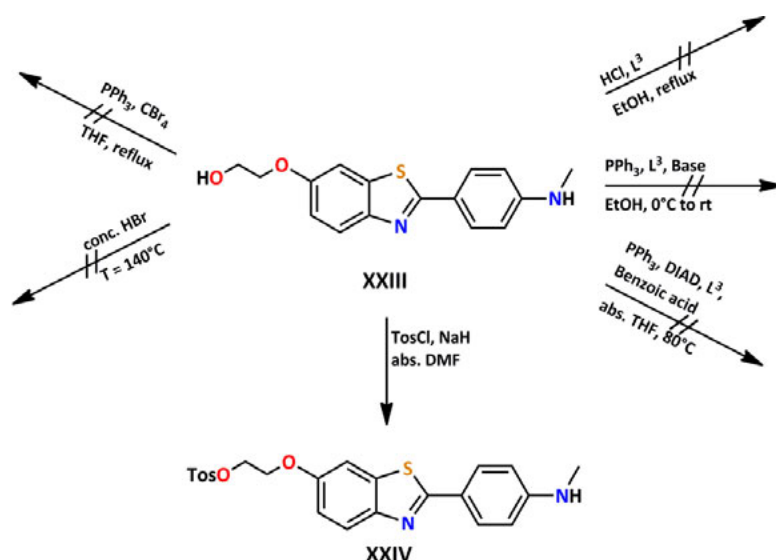
*Scheme 29 Synthetic attempts to activate and couple **XXIII** with the Ligand **L³ᴴ**. On the right side are attempts of the in situ activation of the alcohol. On the left side are different activation trials shown.*

The synthetic pathway was changed to a stepwise process in order to gain more control over the reaction. The attachment of the ligand should proceed *via* a nucleophilic attack. Thus, good leaving groups on the spacer should promote the coupling reaction. The alcohol of **XXIII** was therefore substituted by a chloride, a bromide and a tosylate group. At high temperatures normally used in the substitution of alcohols to halides, no product formation could be observed. An intramolecular attack of the ether group and formation of an oxonium intermediate would explain the observed result.[300] The subsequent reaction with water could then result in the recovery of the reactant. **XXII** was treated with 1,2-dibromoethane and successively heated from room temperate to 60 °C to verify the hypothesis (Scheme 30). The reaction was monitored *via* TLC. After increasing the temperature over 40 °C, formation of a **XXIII** could be observed. As a consequence of this experiment, activation of **XXIII** has to be done at room temperature. Thus, activation of **XXIII** with *para*-toluenesulfonyl chloride could be quantitatively achieved at room temperature providing **XXIV**.
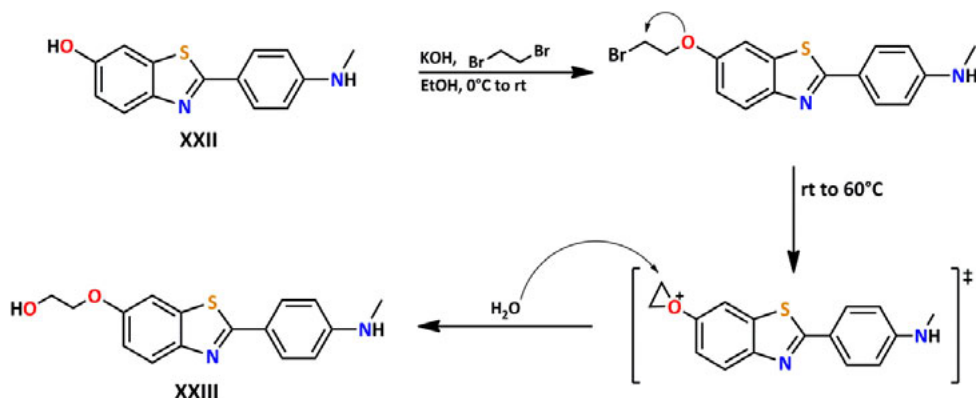
Scheme 30 Mechanism of the intramolecular nucleophilic attack of the ether and formation of the oxonium intermediate.

For the nucleophilic attack of the ligand, the sodium salt of **L³ᴴ** was prepared by addition of sodium hydride to a ligand solution in THF. **XXIV** was added afterwards and the reaction was

stirred at room temperature to avoid side reactions. Monitoring with TLC showed no conversion after 24 h. Thus, temperature was slowly increased over an interval of 4-5 hours to enhance the reactivity. Over 40 °C, formation of the oxonium intermediate could again be observed. The reaction was further heated up to 60 °C to investigate if the ligand could react with the oxonium species (Scheme 31). However, only **XXIII** and minor amounts of an elimination side product could be obtained after aqueous workup. Due to the various side reactions and the low reactivity of the ligand, the introduction of an ethylene spacer was forfeited.
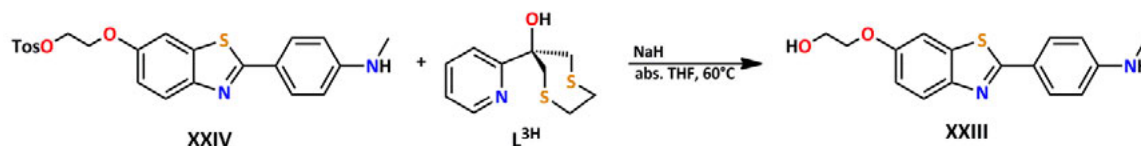
*Scheme 31 Synthetic attempt to couple **XXIV** with **L³ᴴ**.*

7.3.2 Attempts for a Propylene Linker

The fast intramolecular formation of the hydroxonium species prevented the successful coupling of the ligand to the spacer. Thus, the spacer was extended by a further -CH$_2$- group. For the attachment of the propylene spacer **XXII** was treated with 1,3-dibromopropane under basic conditions (Scheme 32). The nucleophilic attack of the benzylic alcohol provided **XXV** in good yields (88 %).
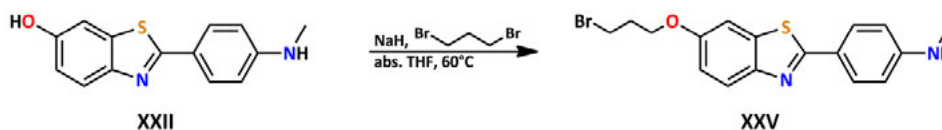
*Scheme 32 Synthesis of **XXV**.*

For the coupling reaction of **XXV** the sodium salt of **L³ᴴ** was used again and the reaction temperature successively increased. The reaction was again monitored by TLC and ^{1}H-NMR. No reaction could be observed at room temperature and upon raising the temperature over 40 °C, the benzothiazole was fast converted to the elimination product **XXVI** (Scheme 33). ^{1}H-NMR indicated a complete transformation of the reactant to **XXVI** within 30 min. To promote the nucleophilic attack over the elimination, potassium iodide was added to the reaction (Finkelstein reaction[301]), but no change in the reaction outcome could be observed. Thus, it can be assumed that the nucleophilic character of the ligands is not sufficient, likely due to the steric demand.
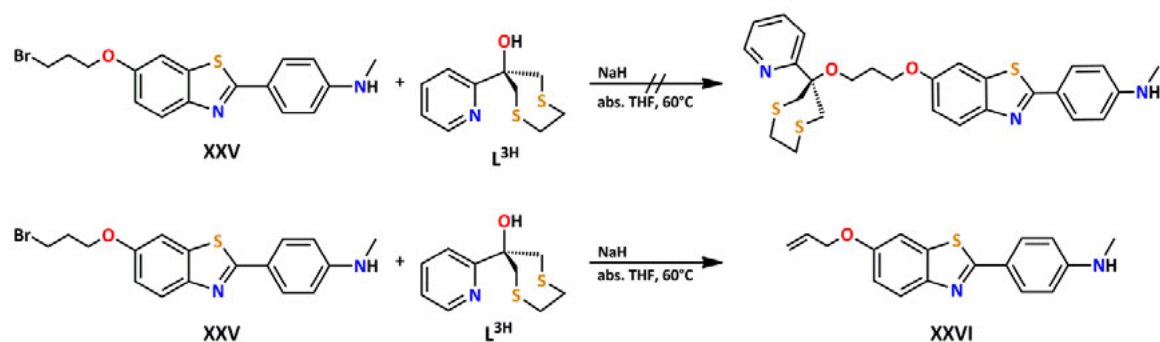
Scheme 33 Synthetic attempt to couple XXV with L³ᴴ.

7.4 Synthetic Approach to Multifunctional Systems *via* Click Chemistry

Since attempts *via* nucleophilic substitutions have failed due to the low reactivity of the ligands and other side reactions, an alternative synthetic pathway had to be provided. The protection of the alcohol function of the ligands with methyl iodide has shown that small molecules can be attached to the ligand. Therefore, it should also be possible to attach a propargyl group. With this a terminal acetylene group can be introduced, giving acces to click chemistry. Indeed, reaction with propargyl bromide, under basic reaction conditions, led to the desired compounds (Scheme 34).
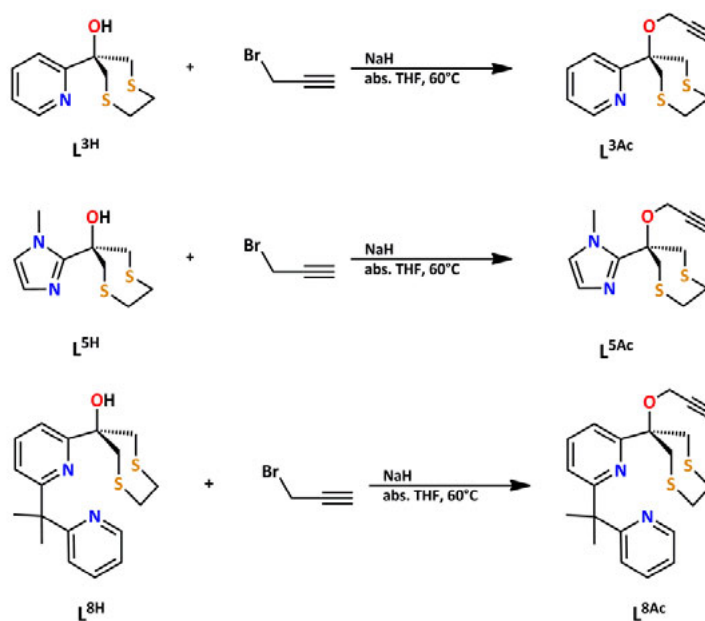
Scheme 34 Synthesis of acetylene derivatives of L³ᴴ, L⁵ᴴ and L⁸ᴴ.

For the click chemistry, the benzothiazole had to be further functionalised to an azide. Since activation of the ethylene bridged derivative often resulted in side reactions, only the bromo-propylene derivative **XXV** was further used. The necessary azide group was introduced by treatment of **XXV** with sodium azide in THF (Scheme 35).
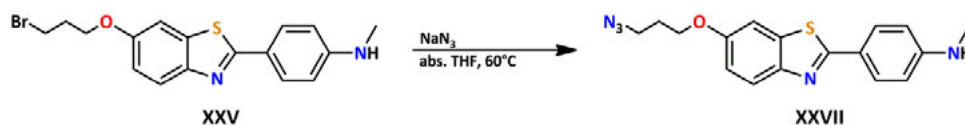
*Scheme 35 Conversion of the bromide **XXV** to the azide **XXVII**.*

Click reactions were carried out under inert atmosphere with equimolar amounts of Cu^{2+} and tenfold excess of sodium ascorbate (Scheme 36). The unusual high amount of catalyst was used, since the ligand can reduce the concentration of free Cu$^+$ by coordination. After heating the solution for 24 h under reflux, the reaction was allowed to cool to room temperature. A concentrated solution of sodium EDTA was added, to remove the copper. The resulting solution was poured into brine (200 ml) and cooled to 4 °C. The precipitate was separated by filtration and suspended in methanol. The resulting suspension was filtrated and the solvent of the filtrate removed under reduced pressure. The crude products were purified by column chromatography on silica. With this synthetic route, the coupling of all three ligands to the benzothiazole was possible in low to moderate yields (16 % - 54 %). For the desired application and the measurements a high purity has to be ensured. Thus, purification was done by column chromatography on silica and the products were recrystallisation in DCM/Et$_2$O prior to use.
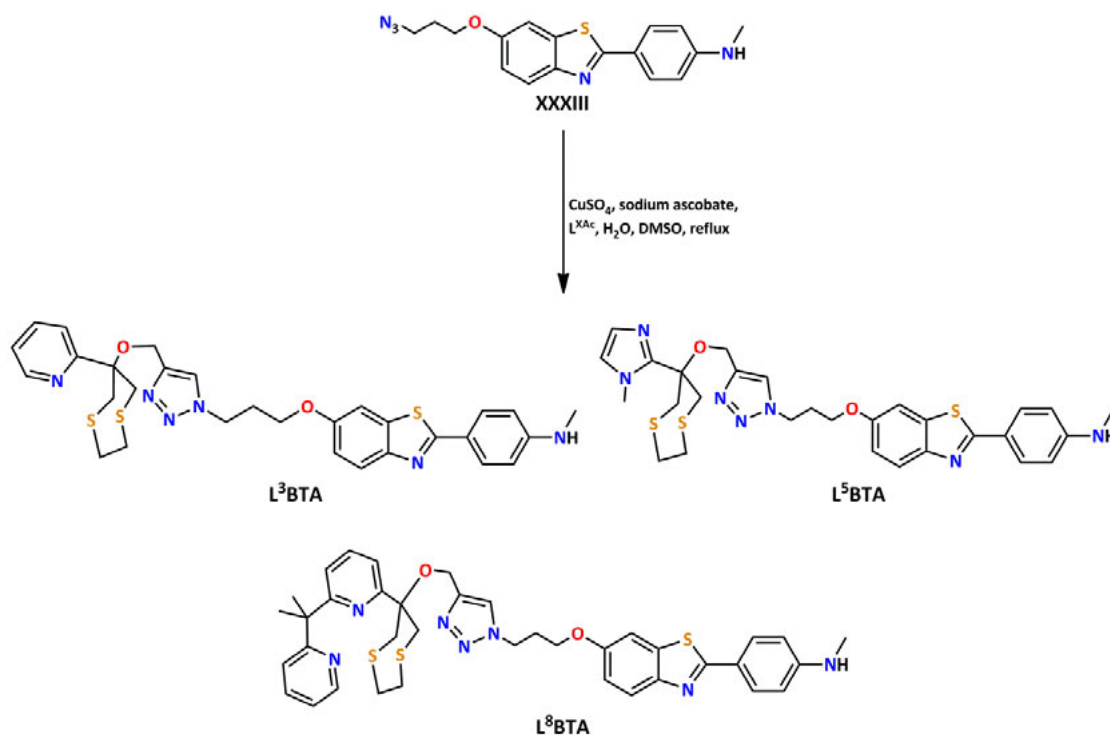
*Scheme 36 Synthesis of **L^{3}BTA**, **L^{5}BTA** and **L^{8}BTA** via click chemistry.*

7.5 Characterisation of the Multifunctional Tools

The synthesised multifunctional tools were characterised by various analytic techniques. The specific spectroscopic behaviour of the **L^{X}BTA** compounds, their solubility in water, as well as their purity, will be discussed in more detail.

7.5.1 Characterisation by NMR Spectroscopy

Purity of the compounds had to be ensured for highly sensitive experiments such as binding studies to Aβ fibrils or viability assays. Exemplary only the characterisation of **L³BTA** will be discussed. Figure 40 shows the ¹H-NMR spectrum of **L³BTA** recorded in DMSO-d_6. All signals could be assigned, by the help of HH-COSY experiments and comparison with the precursors. The detected water signal at 3.34 ppm is an impurity of the deuterated DMSO-d_6 and vanishes when measured in CDCl₃. The –NH proton signal (6.42 ppm) can also not be observed in CDCl₃ likely due to broadening and/or H-D exchange. Although, clean spectra were also obtained for **L⁵BTA** and **L⁸BTA**, all compounds were recrystallised from DCM/Et₂O before use, to ensure their purity.
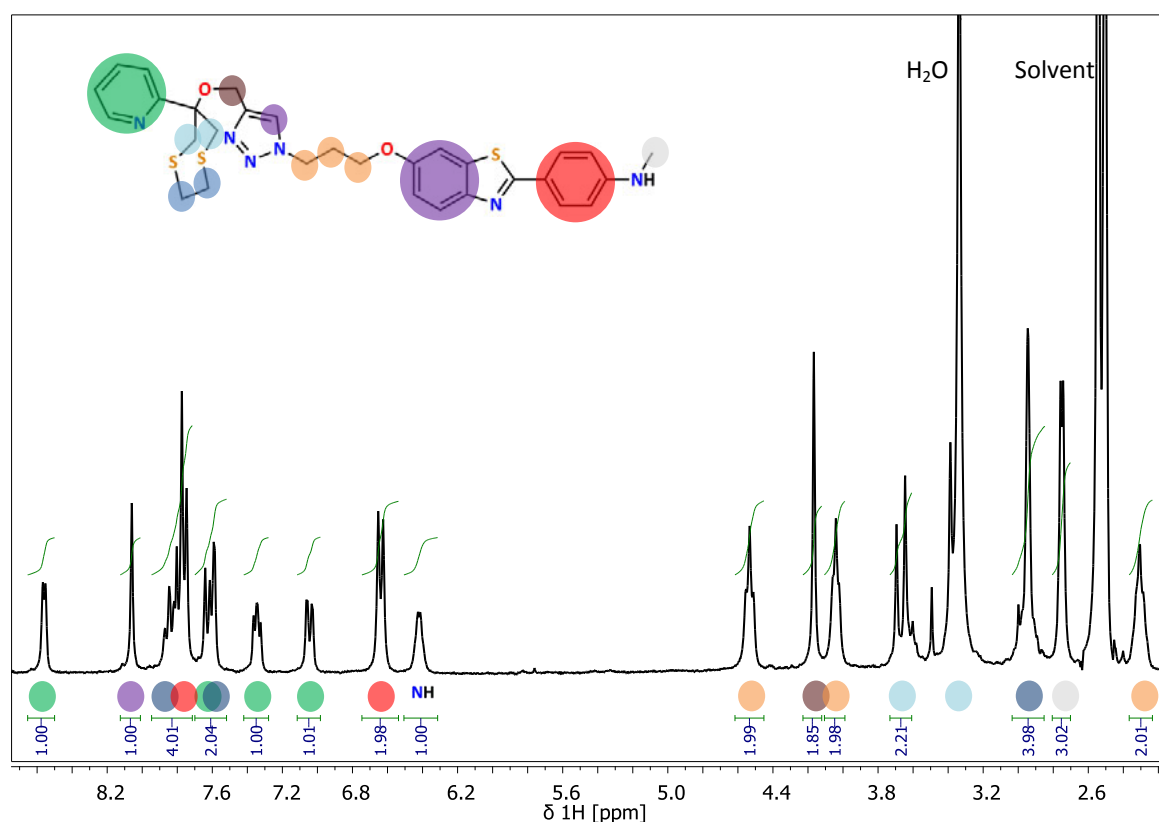
*Figure 40 ¹H-NMR spectrum of **L³BTA** after column chromatography on silica recorded in DMSO-d_6. Signals were assigned by comparison with the reactants and increment tables.*

7.5.2 Solubility of L^XBTA

The low solubility of the chelators impeded already the metal exchange experiments. After coupling the ligands to the rather nonpolar benzothiazole, the water-solubility should be further decreased. To prevent a falsification of the experiments due to precipitation of the compounds, the water-solubility was tested *via* UV/Vis-spectroscopy. Stock solutions of the compounds were prepared in DMSO and samples were prepared in 0.1 M HEPES buffer at different concentrations. The UV/Vis spectrum was measured directly after addition of the compounds, and after 5 minutes in a centrifuge. Even at low concentrations (10 µM) all three compounds precipitated from the buffer solution. By a stepwise increase of the amount of DMSO the

compounds could be kept in solution and a solubility order was determined: **L⁸BTA** << **L⁵BTA** < **L³BTA**. This order directly correlates with the solubility of the corresponding ligands. The least soluble ligand is **L⁸ᴴ** respectively **L⁸ᴹᵉ**. The second in order is **L⁵ᴴ** which could also be easily precipitated out of DMSO by addition of water. In contrast to this, **L³ᴴ** is quit soluble in a water-DMSO mixture, most likely due to the pyridine group, which can form strong hydrogen bonds in water. As a consequence of the poor water-solubility, measurements in neutral buffer solutions were not possible. Two different approaches were used to avoid the precipitation of the **LˣBTA** compounds. One way is the increase of the DMSO concentration up to 5-15 % (v/v). However, in case of studying the intercalating abilities of the compounds into fibrils, the amount of DMSO should be limited. A high concentration of DMSO, around 80 % (v/v), might cleave the bonds between the single Aβ molecules and dissolve the fibrils.[302] But also smaller amounts can influence the intermolecular fibril bonding and favour formation of small oligomers.[303] The other way to keep the **LˣBTA** in solution would be lowering the pH value. In an acidic solution a water-soluble charged **HLˣBTA⁺** species is formed. The pH value has to be chosen carefully, since only the chelator unit should be protonated and not the intercalating benzothiazole moiety, which also bears two basic nitrogen atoms. Table 19 summarises the different relevant pK_a values. The upper limit for the pH value is given by the pyridine group (pK_a = 5.25) and the lower limit is given by the **BTA** moiety (pK_a = 3.0). To ensure the protonation of the chelator, but not of the benzothiazole the pH value has to be in this range. Thus, a pH value of 4.5 was chosen and adjusted with HCl. Unfortunately, this method cannot be used in case of studying the coordination abilities, due to the protonation of the chelator subunit.

Table 19 pK_a values of organic bases. The number in brackets corresponds to the protonated imidazole.

	pK_a
⁺NH₂CH₃-BTA	3.0[304]
⁺NHR₂-BTA	1.2[305]
Triazole	2.44
Pyridine	5.25[306]
Imidazole	7.05, (14.5)[307]

It is worth mentioning that both approaches comprise the disadvantage that they do not resemble biological conditions, which has to be reconsidered for the data interpretation.

7.5.3 Characterisation by UV/Vis- and Fluorescence Spectroscopy

To completely characterise the multifunctional tools UV/Vis spectra were recorded in DMSO and in water at pH 4.5 (Figure 41). The spectra recorded in DMSO show only one absorption band around 358 – 364 nm. The absorption band can be assigned to the π-π* transition of the BTA. The pyridine band of **L³BTA** and **L⁸BTA**, which is normally observed at around 260 nm, is not visible due to the absorption of the solvent (λ_{DMSO} = 265 nm). Since water does not absorb in the UV/Vis range, the pyridine absorption could be obtained by performing the experiment in water at pH 4.5. Since water is more polar than DMSO, due to the higher dielectric constant, a positive solvatochromism (red shift in more polar solvents) is present. The observed shift is not equal for all three compounds. Table 20 summarises the observed **LˣBTA** absorption bands in the different solvents.
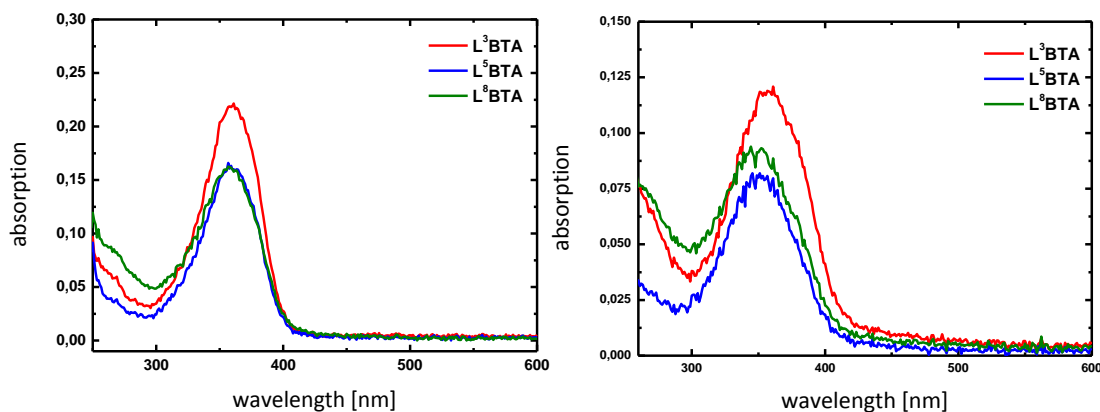
*Figure 41 UV/Vis absorption spectra of 20 μM **L³BTA**, **L⁵BTA** and **L⁸BTA** in DMSO (left) and in water at pH 4.5 (right).*

*Table 20 UV/Vis- and fluorescence parameter of **L³BTA**, **L⁵BTA** and **L⁸BTA**.*

	DMSO absorption [nm]	ε [M^{-1}cm^{-1}]	emission (excitation) [nm]	pH 4.5 excitation [nm]	ε [M^{-1}cm^{-1}]	emission (excitation) [nm]
L³BTA	364	10872	415 (364)	361	6850	428 (361)
L⁵BTA	360	8072	413 (360)	325	4144	418 (325)
L⁸BTA	358	8194	414 (358)	341	4744	414 (341)

The fluorescence spectra were recorded after irradiation at the determined absorption wavelengths. The measurements were performed in DMSO and at pH 4.5 (Figure 42). The compounds were irradiated at their absorption wavelengths. **L³BTA** has the strongest fluorescence in DMSO, followed by **L⁵BTA**. The lowest intensity was thus observed for **L⁸BTA**. The order changes at pH 4.5, where **L⁵BTA** has the highest intensity in its fluorescence band. Comparison of the two measurements shows that in general the intensity decreases at pH 4.5, which could be either the result of the protonation or a solvatochromism effect.
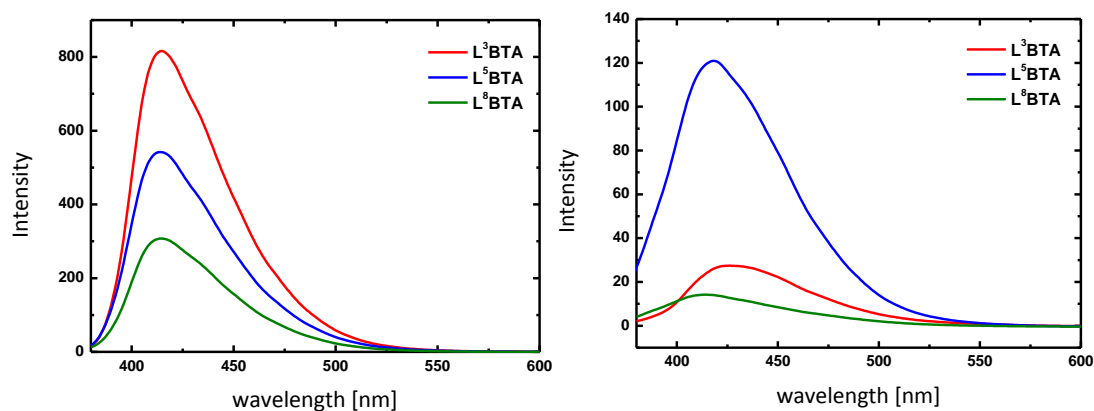
*Figure 42 Fluorescence spectra of 10 μM **L³BTA**, **L⁵BTA** and **L⁸BTA** in DMSO (left) and in water at pH 4.5 (right).*

Compounds were further examined with respect to their metal detecting ability. Therefore, different metals (Cu^+, Cu^{2+}, Zn^{2+}, Fe^{2+}, Ag^+, Co^{2+}, Ni^{2+}, Hg^{2+}, Na^+, K^+, Cr^{3+}, Zr^{4+} and Mn^{2+}) were added to the **L^{X}BTA** compounds and the UV/Vis- and fluorescence spectra were recorded. The spectra were recorded with 10 µM **L^{X}BTA,** 10 µM and 20 µM metal in 50 mM HEPES buffer (pH 7.4). No visible changes could be observed, even in case of Cu^+, where an interaction is known from the NMR and ferrozine experiment. Thus, it can be assumed that the spacer unit is too long to allow an interaction of the chelator with the fluorescent **BTA** system.

7.6 Conclusion

A convenient pathway for the synthesis of **BTA** derivatives *via* cross coupling reaction as key step was developed and established for the synthesis of the **BTA** compound **XXIII**. In a first step towards the desired multifunctional tools, a set of different ethylene and propylene spacers were attached to **XXIII**. Unfortunately, nucleophilic attachment of the ligand was not possible due to various side reactions. Therefore, a coupling reaction was chosen, where the low nucleophilic character of the ligand becomes irrelevant. Finally, the three multifunctional tools **L^{3}BTA**, **L^{5}BTA** and **L^{8}BTA** could be synthesised *via* click chemistry and were characterised with various methods. Especially the solubility of these compounds was studied by UV/Vis-spectroscopy. All three compounds are unfortunately insoluble in water, even in the presence of 3 % DMSO. Therefore, modified experimental conditions have to be used to further investigate the activity of the **L^{X}BTA** compounds. One modification consists of an increase of the DMSO concentration, whereas another targets the pH value. At low pH values (< 5) the chelator unit gets protonated and with this the compounds become water soluble.

Chapter 8

Multifunctional Tools Targeting Amyloid
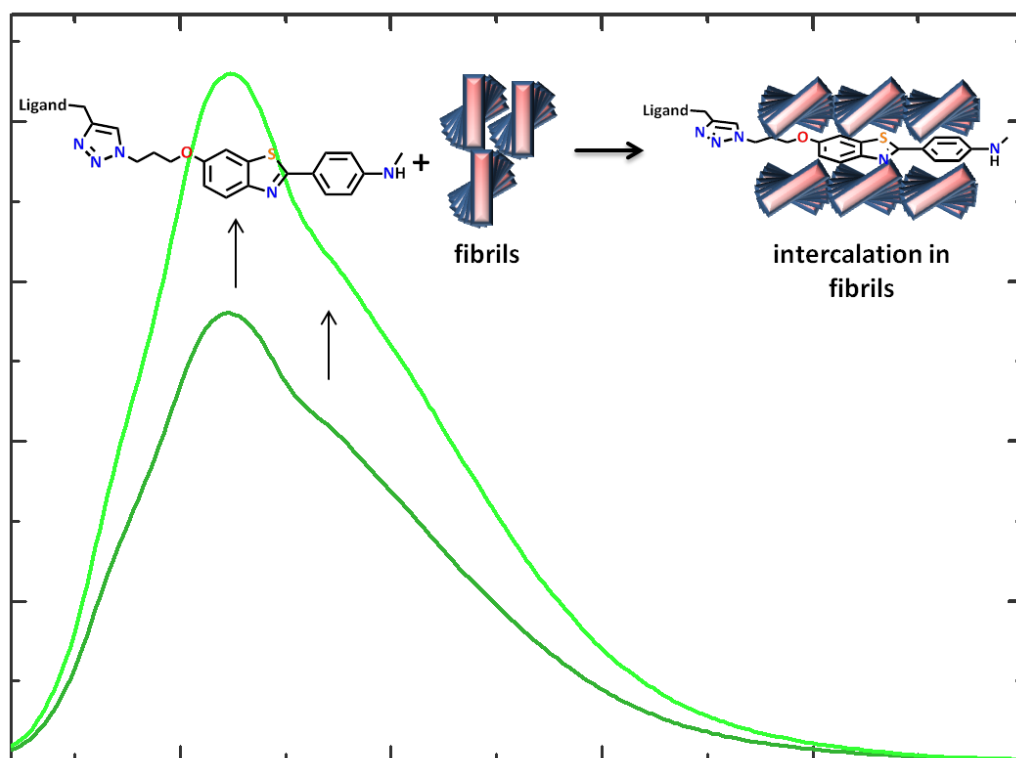
8.1 Introduction

The 10 step synthesis of the three multifunctional tools **L³BTA**, **L⁵BTA** and **L⁸BTA** for applications in AD research and their characterisation was presented in the previous chapter. Although, these compounds were called as *multifunctional* so far no prove was given that they really can fulfil the assigned tasks, namely selective chelation of Cu⁺ and thus inhibition of metal induced oxidative stress and intercalation in Aβ fibrils. Thus, in this chapter, the reactivity of the multifunctional tools will be discussed.

8.2 Binding Studies

The beta sheet structure of Aβ fibrils and also in the Aβ plaques creates a cavity, where conjugated, aromatic compounds like Congo red or Thioflavin T (ThT) can interact.[60,61] Due to the chromophoric abilities of these compounds, they have become of great interest as dyes in AD.[294,308] Until today, ThT is the most common dye for Aβ plaques, since its absorption band dramatically red shifts upon intercalation. The shift of the UV band is accompanied by a change in its fluorescence excitation. The exact mechanisms, that lead to the 115 nm hypochromic spectral shift are still unknown, but it is most likely induced by the lipophilic environment in the plaques.[62,63]

The multifunctional compounds **L³BTA**, **L⁵BTA** and **L⁸BTA** were investigated with respect to their intercalating ability in Aβ plaques. The main question is, if the compounds can still interact with the fibril structure or not? Although the spacer is relatively long a hindrance due to the bulky ligands cannot be excluded. As mentioned above, the change in the environment of ThT and its derivatives can be easily followed by UV/Vis- and fluorescence spectroscopy. Thus to study the intercalation properties of the synthesised compounds was a combined UV/Vis-fluorescence experiment performed.

The synthesised compounds are insoluble in neutral buffer solutions (pH 7). Thus, experimental conditions for the binding studies have to be modified to keep the compounds in solution. As discussed in chapter 7.5.2, either the amount of DMSO can be increased or the pH value can be lowered to achieve the desired solubility. Since DMSO is able to cleave the bonds between the single Aβ molecules in the fibrils, measurements were performed at pH 4.5. UV/Vis-samples were prepared at 10 μM **LˣBTA** and 20 μM fibrils. The pH value was adjusted with HCl before the addition of the fibrils. UV/Vis spectra were recorded before and after the addition of the fibrils. Upon addition of the fibrils no spectral changes could be observed, indicating that the compounds are not intercalating in the fibrils. However, the recorded fluorescence spectra proved the opposite. After addition of the fibrils an increase in the fluorescence intensity could be observed. This elevation of the fluorescence is most likely induced by an intercalation of the compounds in the rather lipophilic β sheet structure of the fibrils.[62,63] Nevertheless, the interaction seems to be relatively week, since it does not affect the absorbance spectra, such as in case of PIB or ThT.[69,294] Thus, a simple interaction with the fibril surface could be as well possible. However, the experiment showed that the benzothiazole subunit keeps an affinity for the fibrils even when coupled to a bulky ligand system.
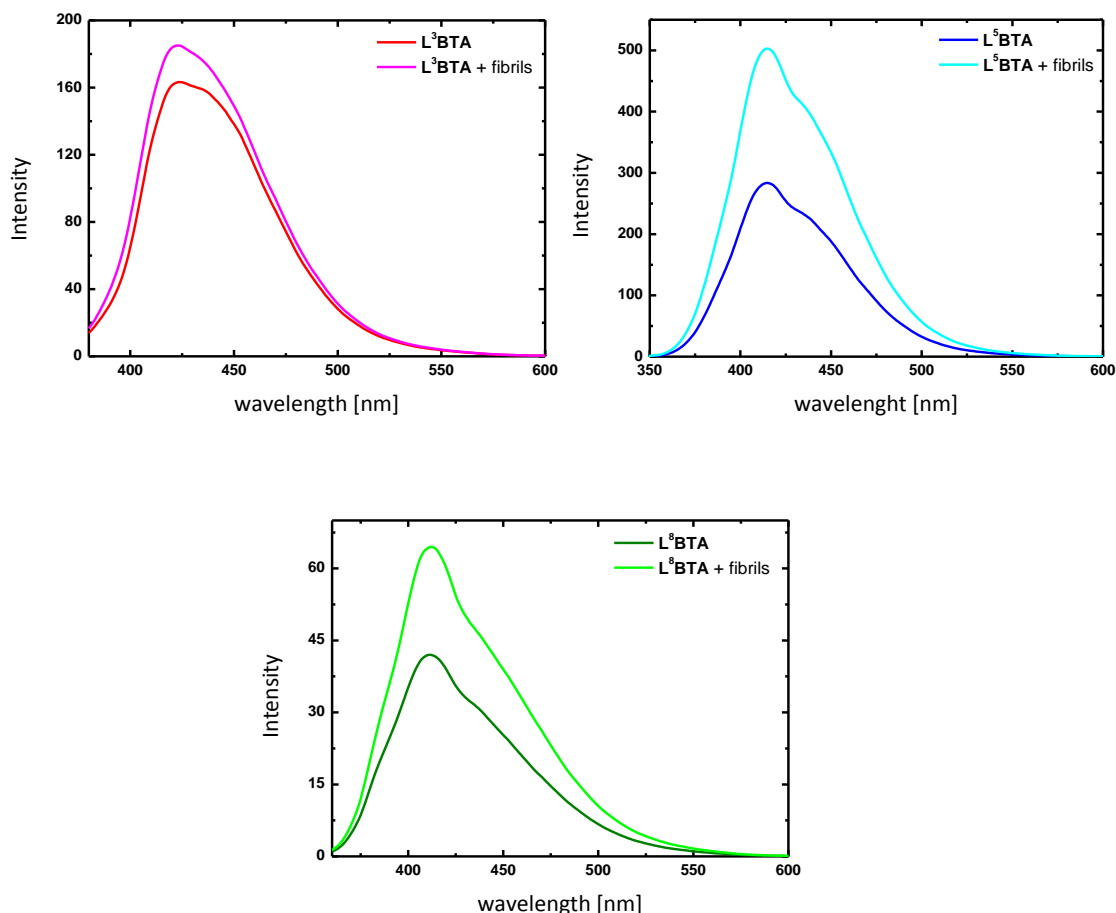
*Figure 43 Fluorescence spectra of 3.33 μM **L³BTA** (top left), **L⁵BTA** (top right) and **L⁸BTA** (bottom) before and after the addition of 6.66 μM fibrils at pH 4.5.*

8.3 Determination of the Cytotoxicity *via* Cell Viability Tests

In the viability assay with the ligands, the chelators **L^{3Me}** and **L^{5Me}** already have shown no cytotoxic behaviour, whereas **L^{8H}** was toxic to the cells (see chapter 6.6). Since the exact toxic mechanism of **L^{8H}** is unknown, it could also be induced by the alcohol function of **L^{8H}**. The alcohol function is in **L^{8}BTA** not available for side reaction and thus, the viability assay with **L^{8}BTA** could probably enlighten the toxic reactivity of the ligand. Unfortunately, **L^{8}BTA** could not be used in this study due to its low solubility. However, the experiment was performed with **L^{3}BTA** and **L^{5}BTA** to study the influence of the coupling to the **BTA**. The precise experimental set up is described in detail in chapter 11.5.4. Two samples were measured for each compound. With this the test has to been seen as a first indication of the reactivity. To determine the toxicity of the final multifunctional compounds, cells were incubated with the **L^{X}BTA** compounds. Comparison with the reference shows an increased survival rate of the **L^{X}BTA**-treated cells (Table 21). In case of **L^{3}BTA** 118 % of the cells have survived and in case of **L^{5}BTA** the value is 105 %. Since **L^{3Me}** and **L^{5Me}** did not increase the survival rate of the cells is this effect most likely induced by the benzothiazole moiety. The nonpolar character of the **L^{X}BTA** compounds favours cell penetration and therefore the uptake of the multifunctional tools in the cells. Thus, it is most likely that the protection function evolves in the cells. As mentioned before, methods to determine the

metabolism of the compounds in the cell were not available. Thus, the exact protective function of the **L^{X}BTA** compounds remains unknown. More important than the slightly increased survival rate is, that after coupling with the benzothiazole, the compounds are still not toxic and thus useable for *in vivo* studies.

*Table 21 Cell viability test performed with 10 µM **L³BTA** and **L⁵BTA**. 100 % corresponds to the average survival rate of reference cells.*

	L^{3}BTA	L^{5}BTA
Living cells [%]	105	118

After conformation of the non-toxic character of the **L^{X}BTA** compounds, also a modified viability assay was performed to determine their inhibition capacity in metal induced ROS. The model ligands **L^{3Me}** and **L^{5Me}** have shown a slight protection function against ROS. However, the reactivity has to be tested again after coupling to the **BTA** subunit. Oxidative stress was artificially induced by incubation of ascorbate and copper in the cell medium. Figure 44 shows the results of the modified viability assay for the **L^{X}BTA** compounds. The observed protective function for **L^{3}BTA** and **L^{5}BTA** corresponds with the result obtained for the model ligands. The small differences between the **L^{X}BTA** compounds and their corresponding model ligands as well as between **L^{3H}** and **L^{5H}** are within the error margin and therefore negligible. Thus, the experiment indicates that the ligand subunit keeps, although coupled, its chelating properties and can therefore protect the cells against oxidative stress.
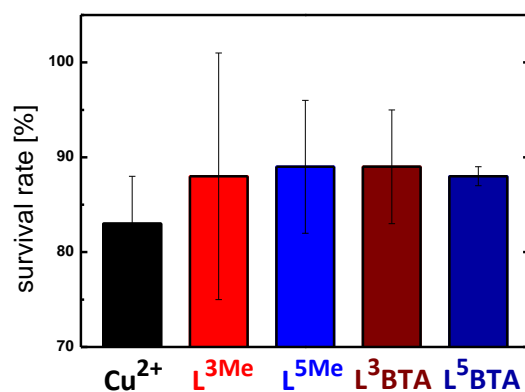
Figure 44 Modified viability assay with metal induced ROS. Percentage of living cells after the treatment with 5 µM Cu$^+$, 100 µM ascorbate and 10 µM of the compounds.

8.4 Ascorbate Consumption

Different attempts were carried out to perform the ascorbate consumption experiment, which was already presented in chapter 6.4 for the model ligands. In the main focus of this experiment was **L^{8}BTA**, since **L^{8H}** was the only system which has shown higher inhibition activity than Aβ$_{1-16}$. The experiment had to be modified due to the poor solubility of **L^{8}BTA**. Experimental conditions like in the binding studies cannot be used, since the ligand becomes protonated and cannot coordinate Cu$^+$. Thus, instead of the pH value the amount of DMSO was increased. To keep

L⁸BTA in solution a DMSO content of 5 – 10 % was necessary. Unfortunately, no experimental conditions could be found, where the ascorbate consumption could be determined. It is known, that even low DMSO concentrations can interact with the ascorbate radical and generate the ascorbyl free radical (AFR)*DMSO complex.[309,310] Thus, DMSO cannot be used in measurements in which radicals are formed, due to its scavenging effect.[311,312] Attempts were carried out with other organic solvents such as methanol. However, also methanol and the other solvents are radical scavenger and disturb in the measurements.[313] During this study, no solvent was found which does not interact with the ascorbyl radical.

8.5 Conclusion

The synthesised multifunctional tools were examined with respect to their intercalation capacity in Aβ fibrils, their inhibition of ascorbate consumption and their cytotoxicity. In the binding study, an intercalation of the **LˣBTA** compounds could be observed. Thus, the affinity of the **BTA** could be successfully implemented in the multifunctional tool. Although many attempts and various conditions were tried no conditions could be found to perform the ascorbate experiment with the final multifunctional tools. Nevertheless, coupling of the chelator should not influence its coordination capabilities. Thus, it can be assumed that the inhibition ability of the final systems resembles the model complexes. This hypothesis is supported by the results of the modified viability assay, where the same reactivity could be observed for **L³BTA**, **L⁵BTA** and their corresponding model ligands. Furthermore, could the viability assay show that neither **L³BTA** nor **L⁵BTA** is cytotoxic and thus both compounds are suitable for *in vivo* studies. Unfortunately, the solubility of the most promising multifunctional tool, **L⁸BTA**, has to be improved before useable in such studies, for example: through the attachment of a sulfonate alkyl at the triazole backbone according to the literature.[314]

Chapter 9

From the Blueprints to Multifunctional Tools- Summary and Outlook

1. Synthesis and characterization of Cu⁺ selective ligands considering inorganic and biological aspects.
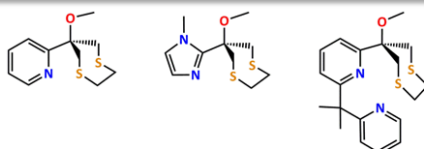
2. Exploring the complexation abilities of the designed ligands with respect to selectivity, stability and metal exchange properties.
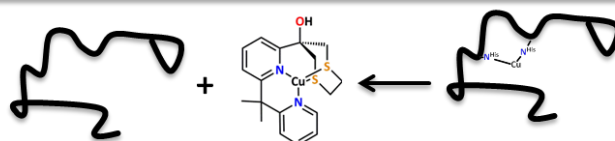
3. Studies of the inhibition of ROS generation.
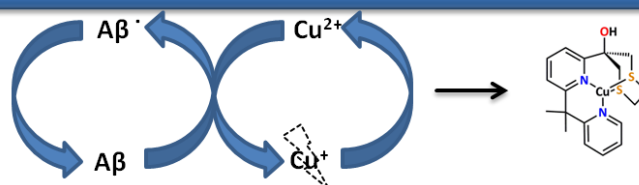
4. Synthesis of benzothiazole derivatives as Aβ-plaque markers and coupling with the evaluated ligands.
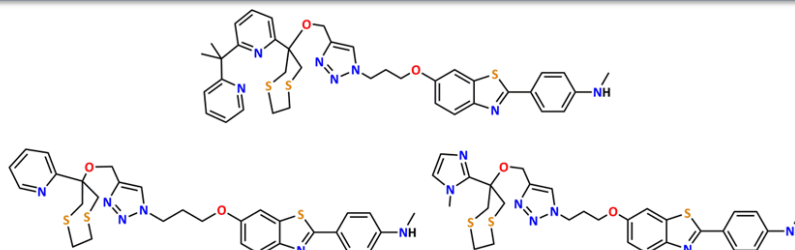
5. Binding studies of the final compounds with Aβ-plaques.
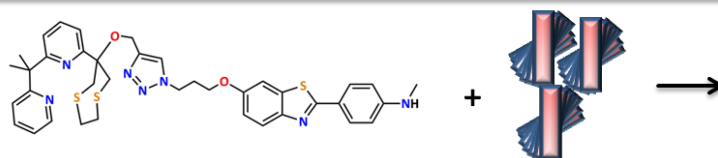
9.1 Summary

AD is the most common neuro-degenerative disease in the world.[1] AD is clinically characterised by a decreased cognitive performance resulting from neuronal losses in different cognitive domains, and can pathologically be characterised by formation of β-amyloid plaques (Aβ plaques) and intracellular neurofibrillary tangles (NFTs).[3,4,7] Although AD is the most frequent form of dementia, no therapeutic strategy which can cure the disease or restore the cellular losses is yet available.[217] The main reason for this lack is that AD is a very complex disease with various hallmarks and the current understanding of its origin and progression is only limited. Evidence exists that these processes may be copper-mediated.[99] Specifically, neuronal losses may originate from metal induced oxidative stress.[216] Thus, different reaction pathways and redox cycles have been proposed which may play a significant role in AD.[173] However, involvement of Cu^+ in AD has yet to be proven as most analytic methods and techniques cannot detect it. Thus, the aim of this study was the development, synthesis and characterisation of a multifunctional tool, which can be used *in vivo* and *in vitro* to gain a more profound understanding of the Cu^+ chemistry in AD. This multifunctional compound should consist of two subunits: a Cu^+-selective chelating moiety and an Aβ-plaques sensitive benzothiazole derivative. In order to achieve this goal, a five-stage plan was developed and will be evaluated in this chapter.

1. Synthesis and characterisation of Cu^+ selective ligands considering inorganic and biological aspects.

The ligand design was undertaken with consideration of the Irving-Williams series[233] and the concept of Pearson[232], resulting in a mixed $\{N_XS_Y\}$ donor set for selective Cu^+ coordination. The second aspect considered in the ligand design was the complex geometry. LFSE does not contribute to Cu^+ coordination. Thus, complex geometry is defined by the steric demand of the ligands, which for four donor atoms results in a preferred tetrahedral geometry. Ligands were therefore designed to be pre-organised towards tetrahedral cooridnation. Taking these aspects into account eight ligands were synthesised in moderate to good yields were in two different approaches. The first approach consisted of five tripodal ligands with an $\{NS_2\}$ moiety (**L^{1H}-L^{5H}**) and one ligand with an $\{N_3\}$ moiety (**L^{6H}**). In the second approach two tetradentate ligands were synthesised with an $\{N_2S_2\}$ moiety (**L^{7H}** and **L^{8H}**). Ligand design was kept as simple as possible in order to follow "Lipinski's Rule of Five" and ensure their absorption and permeation of cell membranes.

2. Exploring the complexation abilities of the designed ligands with respect to selectivity, stability and metal exchange properties.

The synthesised ligands were investigated with respect to their complexation behaviour towards Cu^+ and Cu^{2+} on order to determine their selectivity. Most of the obtained metal complexes could be characterised in solution as well as in the solid state, indicating that, only the rigid chelators, **L^{3H}** and **L^{5H}** from the tripodal systems, and **L^{8H}** from the tetradentate ligands, are suitable for the desired application. In ^{1}H-NMR experiments it could be demonstrated that these three ligands can selectively coordinate Cu^+ in buffer solution. The stability constants of the three compounds were determined by UV/Vis ligand replacement experiments in order to study their affinity

towards Cu^{+}. Furthermore, the ability of chelators to extract Cu^{+} from the Cu(Aβ)[+] complex was evaluated. Thus, a ^{1}H-NMR metal exchange experiment was conducted, indicating that only **L**[8H] can compete with the protein, whereas the tripodal systems form ternary complexes. Nevertheless, the three ligand systems can interact with the Cu(Aβ)[+] complex and should therefore be able to alter the progression of AD.

3. Studies of the inhibition of ROS generation.

Since metal induced ROS is proposed to be involved in AD progression, ligands were investigated with respect to their protective function against ROS. This was done *via* time dependent ascorbate consumption and cell viability tests. Although all ligand systems showed a protective functionality in the ascorbate consumption experiment, only the tetradentate ligand **L**[8] was more active than Aβ. Unfortunately, this result could not be extended to the cell viability tests as **L**[8H] showed toxic behaviour. In contrast to this, **L**[3Me] and **L**[5Me] were not toxic and even showed a slight protective functionality against metal induced ROS.

4. Synthesis of benzothiazole derivatives of Aβ-plaque markers and coupling with the evaluated ligands.

Although many different approaches for the synthesis of benzothiazole derivatives are known in the literature, most of the synthetic routes lack flexibility.[242,243] In this study a convenient pathway was established, which offers the possibility to combine different building blocks *via* *Suzuki Coupling* as the key step, leading to various benzothiazoles.[296,297] In a first approach towards the target multifunctional tools, a set of different ethylene and propylene spacers were attached to the synthesised **BTA**. Unfortunately, nucleophilic attachment of the ligand was not possible due to various side reactions. Finally, the three multifunctional tools **L**[3]**BTA**, **L**[5]**BTA** and **L**[8]**BTA** could be synthesised *via* click chemistry and were characterised with various methods, including UV/Vis-spectroscopy and NMR spectroscopy. In cell viability tests, **L**[3]**BTA** and **L**[5]**BTA** showed the same reactivity as the corresponding ligands, whereas **L**[8]**BTA** could not be used most likely due to its poor solubility.

5. Binding studies of the final compounds with Aβ-plaques.

The synthesised multifunctional tools were examined with respect to their intercalation capacity in Aβ fibrils, to prove if the affinity of the **BTA** could be successfully implemented. No intercalation could be detected at neutral pH due to the low solubility of the compounds. However, at a pH of 4.5 the intercalation could be followed by fluorescence spectroscopy. As no changes were visible in the UV/Vis spectra, it can be assumed that the interaction between fibrils and **L**[X]**BTA** is rather weak.

9.2 Conclusion and Outlook

The aim of this study was the synthesis and characterisation of a multifunctional tool suitable for selective coordination of Cu^{+}, which could be achieved in a five-stage plan. Besides the synthesis of Cu^{+} selective chelators, a new synthetic pathway to benzothiazoles was established. Coupling

of the evaluated ligands with such a benzothiazole afford three multifunctional tools, **L³BTA**, **L⁵BTA** and **L⁸BTA,** which are not only metal selective but also contain an Aβ plaque sensitive unit.

In according with "Lipinski's Rule of Five", the final molecules are relatively nonpolar and should be able to cross the BBB and cell walls. However, this also resulted in poor aqueous solubility of the compounds, which complicates the analytics. Specifically, the most promising system **L⁸BTA** is poorly soluble in water and therefore could not be used in the cell viability tests. Thus, increasing the solubility would be the next step in the project progress. This could be achieved by the introduction of a water soluble group, e.g. a sulfonate group, on the ligand, the benzothiazole, or on the triazole.[314] This would allow for cell viability tests and also binding studies in neutral buffer solution. Furthermore, water soluble compounds would allow studies on their alteration of the Aβ aggregation. Nevertheless, two multifunctional tools, **L³BTA** and **L⁵BTA**, could be synthesised, which show protective functionality against metal induced ROS and which are not toxic. Thus, these two compounds are suitable for preliminary *in vivo* testing.

Chapter 10

CO-Releasing Molecules
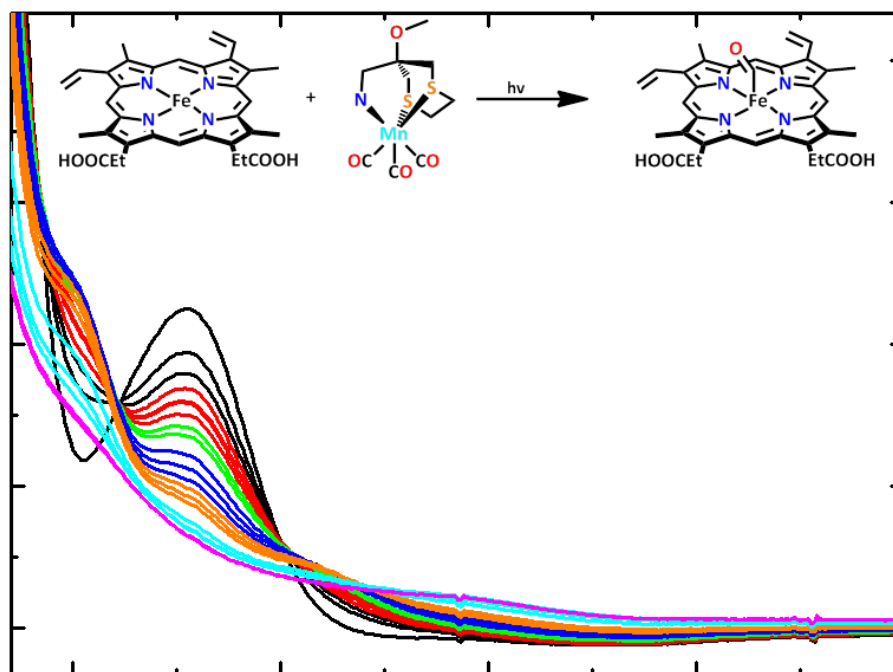
10.1 Introduction

Carbon monoxide (CO) is a stable, highly toxic gas, which is endogenously produced in plants, bacteria and animals by heme oxygenase enzymes.[315] CO serves as a natural detoxicate and can protect cells against oxidative stress.[316–318] *In vivo* CO can bind tightly to heme-containing targets (e.g. soluble guanylate cyclase, cytochrome c oxidase, NADPH oxidase, and BK potassium channels). It has been demonstrated that besides nitric oxide[319] and hydrogen sulphide,[320] CO is involved in the intracellular signal transduction.[321] Furthermore, CO participation in important biological activities such as resolution of inflammatory states, vasorelaxation, anti-apoptotic, and cyto-protective actions could be shown.[322,323] In low doses even a protective function against ROS could be proven.[322] Thus, the growing interest for pharmaceutical applications of CO in the last decades is no surprise, but implementation is not a simple task, since overdoses are highly toxic. The discovery of CO-releasing molecules (CORMs), compounds that serve as carriers and can release CO in a controlled fashion finally opened a pathway to new therapies.[324,325] In general two different types of CORMs can be distinguished. The first type of CORMs consists of boranocarbonates with sodium boranocarbonate (CORM-A1) as representative. These boranocarbonates can spontaneously release CO under physiological conditions, which make them superior for medical applications. [326–328] The second type comprises of metal carbonyl complexes with different transition metals, mainly ruthenium, rhodium, iron or manganese.[322,329] The most famous representatives of this group are the lipid-soluble tricarbonyldichlororuthenium(II) dimer (CORM-2) and the water-soluble tricarbonylchloro(glycinato)ruthenium(II) (CORM-3) (Figure 45).[324,325]
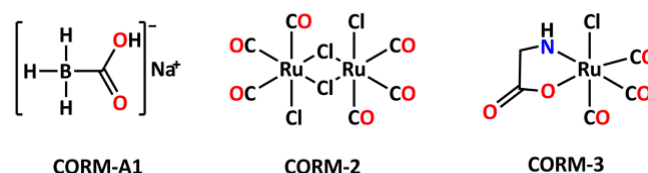
Figure 45 Literature known CO-releasing molecules (CORMs).

The aim of the current research mainly lies in the development of CORMs, which can under physiological conditions achieve a beneficial delivery of CO. To provide this, the compounds have to release CO in specific amounts over an extended time period or by an external trigger. Photoactive CORMs fulfil these requirements and are announced as potential therapeutics.[330–333] Especially the manganese-containing systems have already shown remarkable cytotoxicity against cancer cells. Investigation of the take-out of HT-29 and MCF-7 human cancer cells with [CpMn(CO)$_3$] (cymantrene) and its conjugate with cell-penetrating peptides (CPP) have shown a good activity. However, the long half-life of several hours and slow photolytic release alleviate the results (Figure 46).[334,335] The next generation, the [Mn(CO)$_3$(tpm)]$^+$ (tpm = tris(pyrazolyl)methane) complex and its derivatives have a shorter half-life and feature by a higher activity, e.g. cytotoxicity on human colon cancer cells.[244–246] Nevertheless, for pharmaceutical applications the irradiation has to be done at high wavelengths were the skin becomes permeable and so far no CORM is available, which combines all requirements.

cymantrene $[Mn(CO)_3(tpm)]^+$ $[Mn(CO)_3(tpp)]^+$
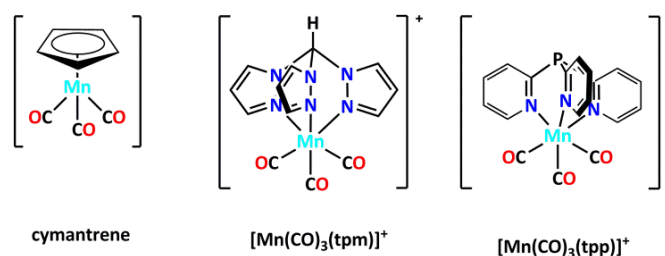
Figure 46 Manganese based light induced CORMs (tpm = tris(pyrazolyl)methylene, tpp = tris(pyridine-2yl)-phosphane).

Thus, most of the new developed CORMs consist of aromatic donor groups, such as pyridine or pyrazol. Fine-tuning of the physical and chemical properties of the CORMs is normally done by different substituent on the aromatic system. Variation of the donor set is only rarely done, since prognosis of the resulting CORMs behaviour is not easy, because it depends on various factors. Although there is a broad variation of reported CORMs in literature, up to date no mixed donor system with a {NS$_2$} binding motif is known. The tripodal ligands **L^{3Me}** and **L^{5Me}** consist of two relatively weak thioether donors and one strong pyridine donor. The prepared Cu$^+$ complex, presented in appendix A, shows that relatively few electron density is provided by the ligand. In case of manganese-based CORMs should this result in a weak Mn-CO bonding, which could induce a short half-life and a fast CO release. Thus the chelators stand out from previously reported systems. Furthermore, it could be demonstrated, that the synthesised ligands can be easily modified to precursors for *click* chemistry, allowing the coupling of the ligands to CPP or other molecules. **L^{3Me}** and **L^{5Me}** are therefore perfect candidates for the synthesis of CORMs. In the following chapter, the synthesis and characterisation of four new CORMs and first studies of their capabilities as CO suppliers will be presented. The main focus of this work lies in answering the question: Does the {NS$_2$} moiety lead to a new type of CORMs? Besides **L^{3Me}** and **L^{5Me}** also **L^{6H}** was used to have a direct comparison. With its three pyridines, **L^{6H}** is similar to the previously reported tpp (tris(pyridine-2yl)-phosphane) chelator.[336] However, in contrast to the literature known system, **L^{6H}** has the advantage, that it can be easily modified on the amine and thus coupling e.g. to CPPs is possible.

10.2 Synthetic Approach to New CO–Releasing Complexes

The first step of the synthesis of the {NS$_2$}-CORMs is the preparation of the manganese precursor (Figure 47). The commercially available dimanganese decacarbonyl was therefore halogenated with elemental bromine. After sublimation, the precursor [Mn(CO)$_5$Br] could be obtained as fine yellow crystals in very good yields (65 %) according to literature (58-67 %).[337]
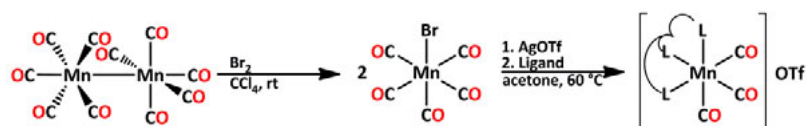
Figure 47 Synthesis of manganese based CO-releasing molecules.

The manganese complex was activated *in situ* by treating [Mn(CO)$_5$Br] with silver triflate in acetone.[334,335] After 1.5 h heating under reflux was the salt metathesis completed and the

precipitated silver bromide was separated by filtration. To the filtrate equimolar amounts of ligand were added and the reaction heated for further 90 min. The reaction solution was reduced to a few ml and afterwards the final complexes were crystallised from dichloromethane/diethyl ether. The products could be obtained as yellow crystals. All reactions were carried out under light exclusion to avoid decomposition. By crystallisation only moderate yields could be achieved (Table 22). Higher yields could be provided without crystallisation, by precipitating the complexes with diethyl ether directly out of the reaction solution.

Table 22 Synthesised CORMs and their yields. The numbers in brackets corresponds to yields obtained by crystallisation.

	Complex	Yield [%]
20	[**L^{3Me}**Mn(CO)$_3$]OTf	92 (65)
21	[**L^{5Me}**Mn(CO)$_3$]OTf	97 (71)
22	[**L^{6H}**Mn(CO)$_3$]OTf	95 (28)

10.3 CORM Characterisation in Solid State

Molecular structures of all three complexes could be elucidated by X-ray crystallography, revealing an interesting behaviour in solid state (Figure 48). Expected was manganese coordination by the {NS$_2$} moiety of **L^{3Me}** and **L^{5Me}**, which was indeed observed for **21**. However the structural refinement of **20** reveals coordination by the two sulphur atoms of the thioether sidearm and, instead of the pyridine, the methoxy group is coordinated. One explanation for this unexpected binding motive could be that the ether coordination allows a tighter bonding of the CO molecule in *trans* position. Ether groups are weakly coordinating donor groups without π acceptor properties. Thus, the *trans* CO has no competitor for the d-orbitals and can form a strong π-backbond. Indeed, comparison of the bond lengths shows that the CO opposing the ether group is most strongly bond to the manganese (1.8010 Å *vs.* 1.8215 Å and 1.8234 Å). The CO molecules *trans* to the thioether groups are longer most likely due to their, though weak, π-acceptor character.[338] The CO molecules in **21** are with Mn–CO bond lengths between 1.8057 Å and 1.8146 Å in general slightly tighter bound then in **20**. Prominent bond length are summarised in Table 23. Both molecular structures reveal an almost ideal octahedral complex geometry for the Mn$^+$ ion. The square planes are in each case constituted by the two sulphur atoms and two CO molecules. Important bond angles are summarised in Table 24.

20   **21**
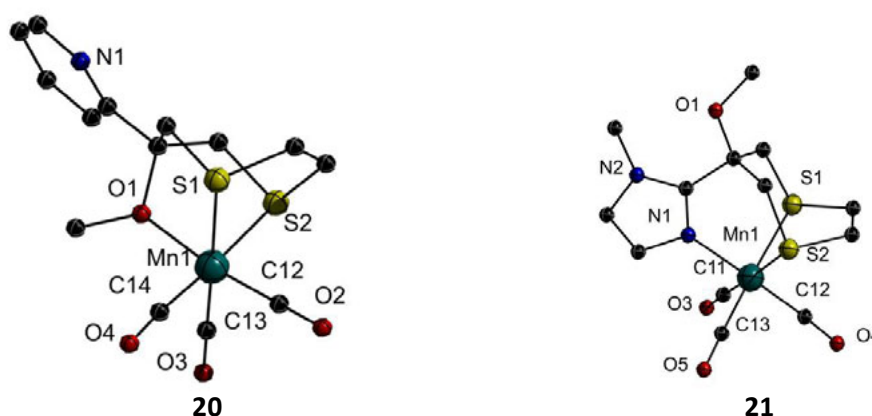
Figure 48 Molecular structure of 20 (left) and 21 (right). Hydrogen atoms and the counterion were omitted for a better structural overview.

For the molecular structure of **22** was a coordination of the three pyridine groups expected. However, similar to **20**, one pyridine is not coordinated and the octahedral complex geometry is saturated by the amine. Another similarity is the short M–CO bond length of the *trans* CO molecule, which is with 1.7859 Å more tightly bound than the other two CO molecules (1.8054 Å and 1.8210 Å).

22   **23**
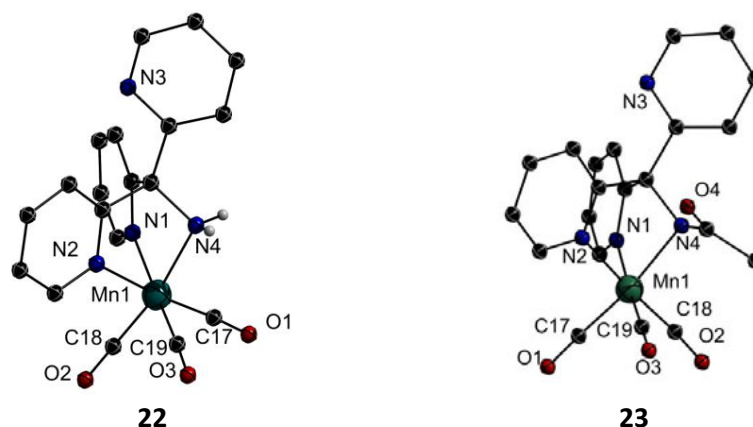
*Figure 49 Molecular structure of **22** (left) and **23** (right). Hydrogen atoms and the counterion were omitted for a better structural overview.*

To disfavour the coordination of the amine and forcing the coordination of the third pyridine, **L**^{6H} was acetylated. **L**^{6H} was treated with acetic anhydride to synthesise **L**^{6Acet}.[339] According to the literature **L**^{6Acet} could be synthesised in good yields (71 %, Lit.: 71 %[339]) and with the standard procedure for the synthesis of CORMs also [**L**^{6Acet}Mn(CO)$_3$]OTf (**23**) could be provided. Surprisingly, even in the molecular structure of **23** is the amine still coordinated instead of the pyridine, although the acetyl group withdraws electron density from the amine and thus weakens its donor capacity. The shortest Mn–CO bond is again found for the CO in *trans* position of the amine (1.8044 Å). The octahedral complexes **22** and **23** are in the square plane each constituted by two pyridine groups, and two CO molecules, and in the axial positions by the amine group and one CO molecule.

*Table 23 Selected bond lengths in the molecular structures of **20-24**. Numbers marked with a) refer to the amine.*

	Mn–S [Å]	Mn–N/O [Å]	Mn–CO [Å]
20	2.3483(10)	2.0938(19)	1.8010(29)
	2.3336(9)	-	1.8215(29)
	-	-	1.8234(27)
21	2.3479(15)	2.0346(27)	1.8096(56)
	2.3664(10)	-	1.8146(37)
	-	-	1.8057(35)
22	-	2.0419(40)	1.7859(50)
	-	2.0416(41)	1.8210(53)
	-	2.0725(42)$^{a)}$	1.8054(50)
23	-	2.0469(24)	1.8044(30)
	-	2.0506(24)	1.8075(35)
	-	2.1114(23)$^{a)}$	1.8185(34)

*Table 24 Selected bond angles of the molecular structures of **20-24**.*

	S1—Mn—S2 [°]	S1—Mn—N/O[°]	S2—Mn—N/O [°]
20	82.93(3)	83.89(6)	81.09(6)
21	81.07(4)	90.58(9)	88.65(9)
	N1—Mn—N4 [°]	N4—Mn—N2 [°]	N1—Mn—N2 [°]
22	77.03(13)	78.17(14)	84.47(9)
23	75.72(9)	78.52(9)	84.65(14)

10.4 DFT Calculations of CORMs

To get an impression whether the coordination of the weak donor groups is thermodynamically induced by stabilisation of the CO or induced by other effects, theoretical calculations were performed by Prof. Ulrich Schatzschneider (*Institut für Anorganische Chemie* der *Julius-Maximilians-Universität* Würzburg, Germany). Basis of the calculations were the atom coordinates from the structure refinement. The relative energies for the crystallised binding mode and for the corresponding alternative binding mode were calculated. In Figure 50 and Figure 51 the optimised structures and their energies are illustrated. The energies calculated for the binding modes, which crystallised were set to zero for a better comparison. The structure of **20** revealed a coordination of the $\{OS_2\}$ moiety. However, the theoretical calculation shows that the coordination of $\{NS_2\}$ moiety should be energetically favoured (+82.0 kJmol^{-1}). An analogous result was obtained for **21** with an energy difference of 55.4 kJmol^{-1}. Although, the energy difference between the two possible modes in **22** is only minor (9.5 kJmol^{-1}), the coordination of the amine is energetically favoured. With the electron withdrawing acetyl group of **L^{6Acet}** is coordination of the amine unlikely, which could also be shown in the calculation. The coordination of the three pyridine groups is strongly favoured (-58.1 kJmol^{-1}). Thus, the hypothesis from the structural characterisation, that the coordination of the weak donor groups stabilises the complexes due to the formation of strong π-backbonding to the *trans* CO molecule seems only to apply to **22**. Consequently, the coordination of the rather weak ether in case of **20** or amine group, in case of **22** and the resulting loss in energy must be compensated by packing effects in the crystal structures. Since in **20** and also in **23,** the crystallised binding modes are strongly disfavoured, the crystal structures were further examined, to get more information about how the loss in energy could be balanced.

20 (0.0 kJmol^{-1})   **20b** (+82.0 kJmol^{-1})

21 (0.0 kJmol^{-1})   **21b** (-55.4 kJmol^{-1})
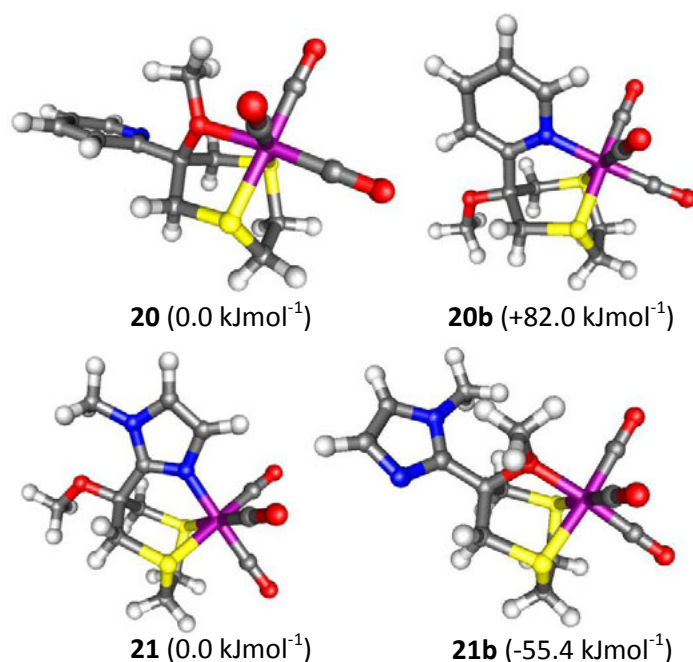
*Figure 50 Optimised structures and relative energies of **20**, **20b**, **21** and **21b** (RI-BP86). Structures marked with b correspond to the alternative binding mode.*

22 (0.0 kJmol^{-1})   **22b** (+9.5 kJmol^{-1})

23 (0.0 kJmol^{-1})   **23b** (-58.1 kJmol^{-1})
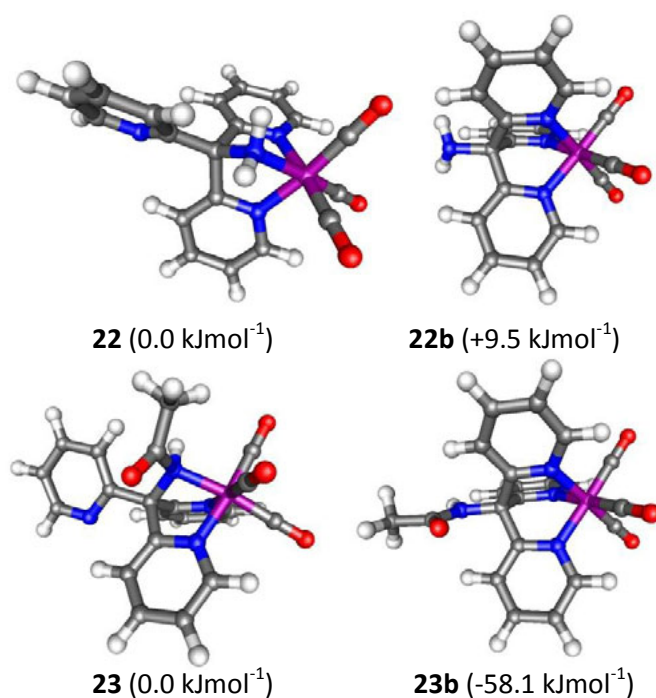
*Figure 51 Optimised structures and relative energies of **22**, **22b**, **23** and **23b** (RI-BP86). Structures marked with b correspond to the alternative binding mode.*

The view of the molecular arrangement revealed a π-π stacking of the unbound pyridine rings in case of **20**, **22** and **23** (Figure 52). Even energetically disfavoured binding modes, like the observed ones, can be stabilised by π-π stacking, since electron deficient aromatic rings, such as pyridine, can form strong π-π interactions due to the polarisation induced by the heteroatom.[340] For pyridine rings are two different π-π stacking modes possible: i) face to face, with perfect alignment of the aromatic rings, or ii) offset, with a parallel displacement.[341] In the latter case, one carbon atom of each ring is often found orthogonal to the centre of the other ring. The distance between two parallel molecular planes reaches between 3.3 Å for strong

interactions to 3.8 Å for rather weak interactions.[341] In the molecular structure of **20** is each pyridine neighboured by two other pyridine. The closer one is in a centroid-centroid distance of around 4.7 Å and shows only a minor overlap were only two carbons are parallel aligned (3.6 Å). The long distance and large displacement of the aromatic rings indicate a rather weak π-π interaction. The second pyridine is offset aligned in a centroid-centroid distance of 5.2 Å. Although a fitting overlay is present, in which one carbon atom of each ring is aligned orthogonal to the centre of the other aromatic ring, is the interaction diminished due to the long distance.
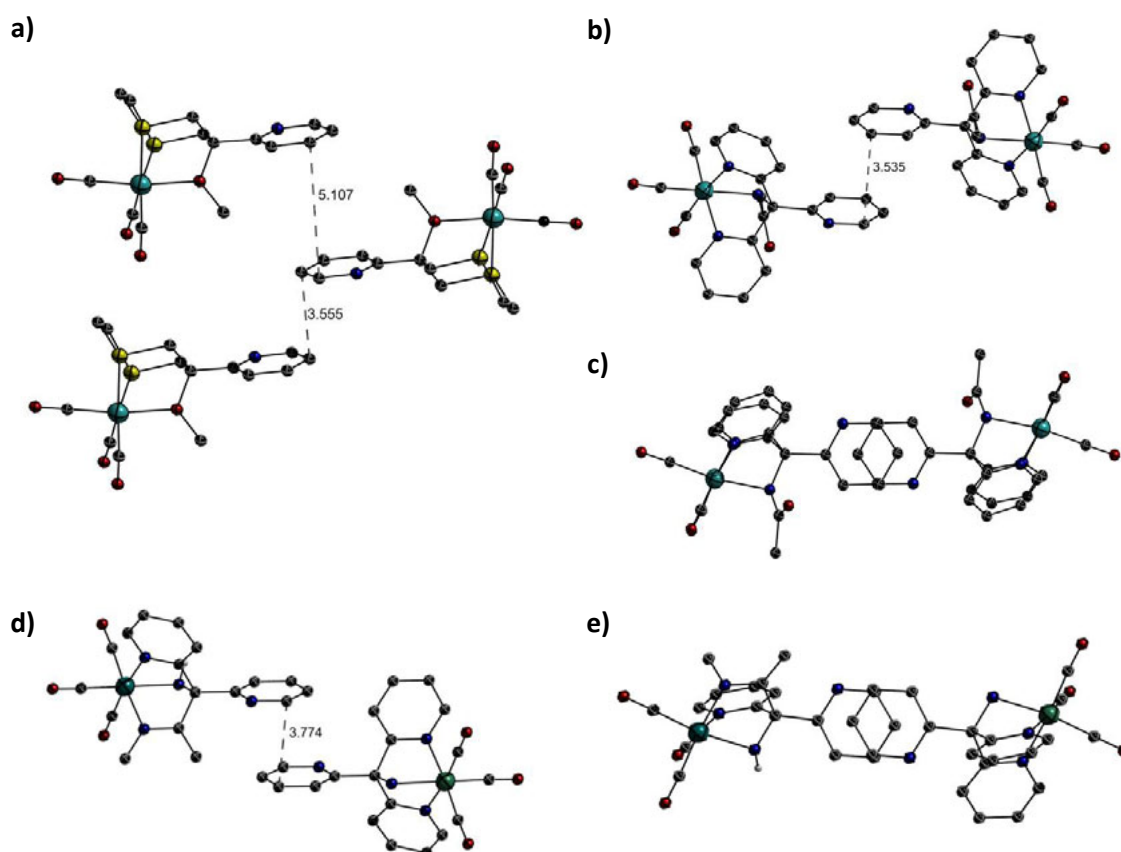
*Figure 52 Molecular structures of **20** (a), **22** (b, c) and **23** (d, e). Counterions and hydrogen atoms are omitted for a better overview.*

The structure of **22** and **23** showed completely separated pyridine pairs. Two pyridine rings are in **22** aligned in a centroid-centroid distance of approximately 3.8 Å. The displaced arrangement is typical for pyridine-pyridine stacking with one carbon atom orthogonal to the ring centre. The same arrangement could also be found in the structure of **23** with a centroid-centroid distance of 3.8 Å. Besides the characterisation in solid state, the complexes were also characterised in solution by ESI-MS and NMR techniques. In solution π-π interaction are hindered due to the formed solvent shell. Thus, the thermodynamically most stable binding mode should be formed. The ^{1}H-NMR spectrum of **21** shows a broadening of all resonances which could be either induced by a fast exchange or by paramagnetic impurities. However, the imidazole signals are shifted, indicating their coordination. For complex **22** was calculated, that the coordination of the amine is slightly favoured over the coordination of the pyridine. Accordingly, the ^{1}H-NMR spectrum shows two sets of pyridine resonances with a relative intensity of 2 : 1. In contrast to this, the

spectrum of **23** shows separated resonances for each pyridine. Furthermore, the signals are broadened, indicating a fast exchange or paramagnetic impurities.

10.5 Spectroscopic Behaviours of the Synthesised CORMs

In order to study the potential of **20** - **23** as photo active CORMs their spectroscopic behaviour were examined. First of all, UV/Vis spectra were recorded to determine the excitation wavelengths and the extinction coefficients. Figure 53 shows the spectra of 0.5 μм complex in 0.1 м phosphate buffer (pH 7.4). Direct comparison of the four complexes shows that **21** has the highest excitation wavelength (379 nm) and thus contains the lowest LFSE (141 kJmol^{-1}); than follows **20** with a LFSE of 151 kJmol^{-1}. The complexes **22** and **23** have the highest LFSE (155 kJmol^{-1} and 159 kJmol^{-1}) and the lowest excitation wavelengths. The order can be reasoned by the different donor groups in the ligands. As mentioned before, pyridine is a strong σ-donor with π-acceptor character and causes a larger orbital splitting.
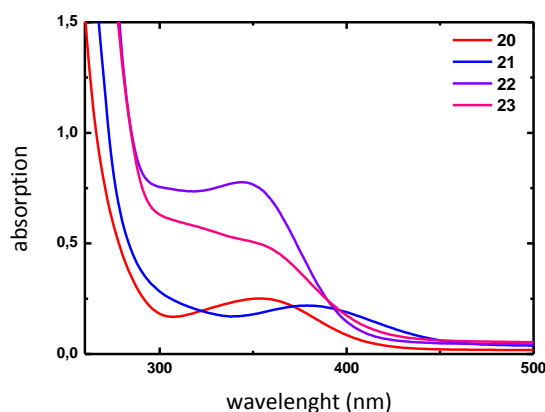
*Figure 53 UV/Vis spectra of **20**, **21**, **22** and **23** at 0.5 μм n 0.1 м phosphate buffer (pH 7.4).*

The weak {NS$_2$} donor set in **21** and **20** barely provides electron density to the metal and thus the ligands induce only a low LFSE. The small deviation between **22** and **23** is most likely induced by the acetyl group, which causes a slightly higher LFSE. However, all complexes have their excitation in the short wavelength range, which is a typical region for many manganese containing CORMs.[342,343] The determined extinction coefficients for **20** and **21** are low and only one-third of the extinction coefficients for **22** and **23**. The larger values most likely results from the different electronic structures in the complexes. Table 25 summarises the determined excitation wavelengths, extinction coefficients and LFSEs of the synthesised CORMs. The LFSE is inversely proportional to the excitation wavelength and was calculated by equation 7 (N$_L$ = Loschmidt constant, h = Planck constant, c = velocity of light).[281]

$$\Delta_O = N_L h v = N_L h \frac{c}{\lambda} \tag{7}$$

*Table 25 Excitation wavelengths, extinction coefficients and determined LFSE of **20-24**.*

	excitation wavelengths [nm]	extinction coefficient [$M^{-1}cm^{-1}$]	Δ_O [kJmol^{-1}]
20	380	730	140
21	355	759	150
22	345	2304	155
23	335	2193	159

The compounds were further characterised by IR spectroscopy (Figure 54). In solution (dichloromethane) one strong IR band (A_1 mode) at around 2050 cm^{-1} and two additional bands (A_2 mode, B_2 mode) between 1933 cm^{-1} and 1980 cm^{-1} could be observed.
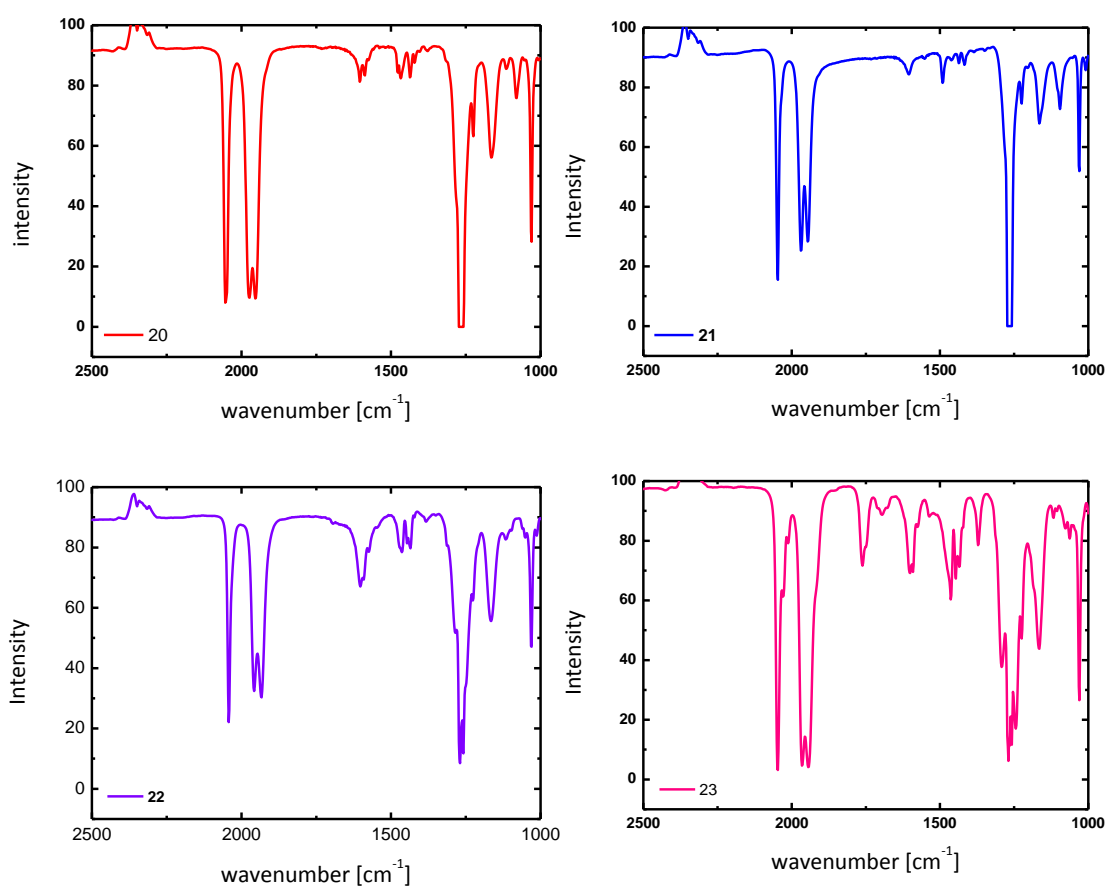
*Figure 54 IR spectra of **20** (red), **21** (blue), **22** (violet) and **23** (pink) in dichloromethane.*

This is an expected pattern for *fac*-Mn(CO)$_3$ complexes with C$_s$ symmetry. The measurements in solution are essential, since in solid state a different binding mode is present. Table 26 summaries the CO vibration bands of the synthesised CORMs. Stretching vibrations decrease in the series according to **20 > 21 ≈ 23 > 22** and results from the electronic structure in the complex. Thus, the IR spectroscopic analysis is similar to the measured UV/Vis spectra. Furthermore, the recorded CO stretching vibrations are in accordance with comparable literature known CORMs.[330,336]

*Table 26 CO stretching vibrations $\tilde{v}_{co}$ of **20-24** and literature known complexes (tpm = tris(pyrazolyl)methylene, tpp = tris(pyridine-2yl)-phosphane). For the spectra in solution compounds were dissolved in dichloromethane.*

	$\tilde{v}_{CO}$ [cm^{-1}]	
	in solution	*in solid state*
20	2052, 1974, 1953	2047, 1967, 1944
21	2047, 1967, 1945	2043, 1980, 1954
22	2042, 1958, 1933	2046, 1960, 1940
23	2047, 1964, 1944	2046, 1960, 1940
[Mn(CO)$_3$tpm]OTf[330]	2050, 1950	-
[Mn(CO)$_3$tpp]OTf[336]	2042, 1951	-

10.6 Photoinduced Time Dependent CO Release

As mentioned above, the stability of CORMs in the dark and selective CO release upon irradiation are essential features for therapeutic applications.[245,330] In order to study the stability in solution, UV/Vis spectra were recorded after 12 h and 24 h incubation time of the compound under light exclusion. All four complexes are stable in solution and do not release CO in the dark. Photolytic activity of the compounds was followed by UV/Vis. Figure 55 shows the time-dependent changes of the UV/Vis spectra of **21** as an example. The specific complex absorption at 380 nm vanishes upon irradiation at 365 nm and a new band appears at around 500 nm. Since no isosbestic points could be observed, it can be assumed that a stepwise CO release takes place.
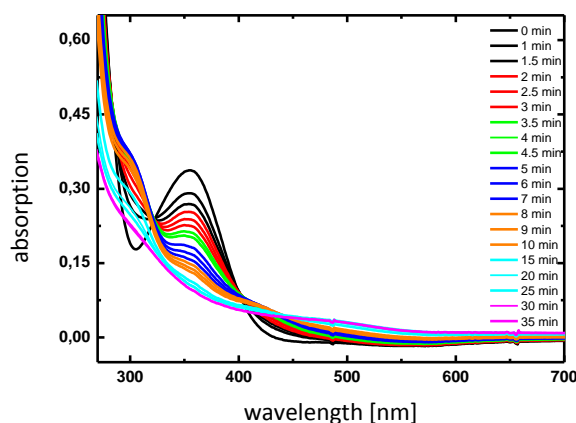
*Figure 55 Photolysis experiment of **21** in 0.1 M phosphate buffer (pH 7.4). The sample was irradiated at 365 nm.*

In order to study the photoactivity, a myoglobin was assay performed.[329,344,345] Horse skeletal muscle myoglobin was dissolved in degassed 0.1 M phosphate buffer (pH 7.4). The myoglobin was reduced *in situ* by a freshly prepared dithionite solution and afterwards the CORM complex in DMSO was added. The experiment was at least repeated three times with different incubation durations in the dark (between 1 h and 21 h). However, before determining the CO release, a dark measurement was carried out to verify again the stability of the CORMs in solution. The samples were therefore kept in the dark for 16 h or 21 h at 8 °C and every 5 min the absorption at 510 nm, 540 nm, 557 nm and 577 nm were measured. Again, no CO release was detected. In

the second step, the samples were irradiated for 5 min at 365 nm. After 1 h, the irradiation-time was expanded to 10 min. Figure 56 exemplary shows the CO release of **21**.
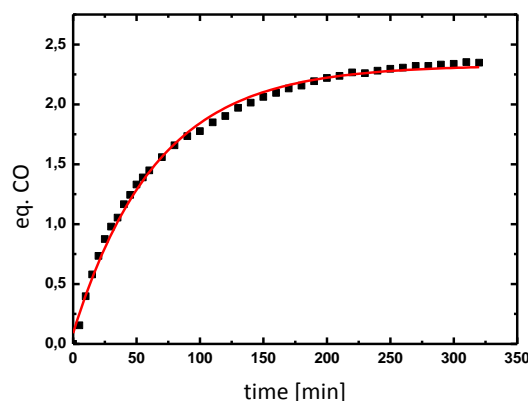
*Figure 56 CO release of 10 μM **21** after 2 h in the dark. The fit corresponds to the equation: y = A·exp(x/t$_{1/2}$)+y$_0$.*

21 and also the other synthesised CORMs can release up to approximately two CO molecules upon irradiation (Table 27). Comparison with other CORMs shows that only systems with bulky ligands release one equivalent CO.[336] Small ligands like **L^{3Me}**, **L^{5Me}**, **L^{6H}** and **L^{6Acet}** should be able to release up to two mole CO per mole CORM. Thus, the myoglobin assay supports the hypothesis from the photolysis experiment, that a stepwise CO release is taking place. Another important value, besides the number of released CO molecules (n_{CO}), is the half-life ($t_{1/2}$), which were also determined.

*Table 27 Determined half-lifes ($t_{1/2}$) and number of released CO (n_{CO}) of **20 – 24** (tip^{iPr2} = tris(1,4-diisopropylimidazol-2-yl)phosphane).*

	incubation time [h]	$t_{1/2}$ [min]	n_{CO}
20	16	41.16	2.23
20	1	87.03	2.11
20	2	74.31	1.52
21	16	14.68	2.18
21	1	49.2	1.77
21	1	24.13	1.48
21	2	42.68	2.34
22	16	9.55	1.95
22	2	15.64	1.27
22	1	18.2	1.49
23	2	21.95	2.45
23	2	13.56	2.05
23	21	5.558	2.79
[Mn(CO)$_3$tpm]OTf[330]	-	20	1.96
[Mn(CO)$_3$tpp]OTf[336]	-	17	2.28
[Mn(CO)$_3$tip^{iPr2}]OTf[336]	-	13	1.04

The longest half-life and thus the most stable complex was found for **20** (41 - 87 min). **21** follows with a half-live of 15 - 49 min. **22** and **23** show a similar reactivity and have a similar half-life (6 - 22 min) and are the only systems which can compete with literature known complexes. Both complexes show a higher activity than [Mn(CO)$_3$tpm]$^+$, but not surpass the currently known CORMs. Nevertheless, this synthesised CORMs show good results for a first generation and provide a good starting point for further developments. The Myoglobin assay illustrates that the measurement of the number of released CO is no simple task and depends on various factors. The comparison of the results shows that the longer the incubation times, the shorter are the observed half-lifes. The shortened half-lifes are probably due to an interaction between the myoglobin and the CORMs. However, studies on the kinetics were not done. Thus, the mechanism of the exact CO release is not known and can only be speculated about. Scheme 37 illustrates possible reaction pathways in the CO release experiment. The first step is the irradiation of the CORMs, which results in an excited complex. This complex can either release one CO molecule or react back to the not ground state *via* relaxation. After release of one CO molecule, a vacant position is left on the metal, which should be saturated by a solvent molecule. For this new complex are three reaction pathways possible. The complex could either also be irradiated by light or it could dimerise or decompose. All three pathways could lead to the release of another CO molecule. The performed experiments only indicate a stepwise CO release, but do not provide any information on the origin of the second CO molecule. Thus, without further studies on the intermediates which are formed during the experiments, it is impossible to define the right reaction pathway. It is noteworthy to mention that also more than just one reaction pathway could take place. Thus, the systems would become even more complicated.
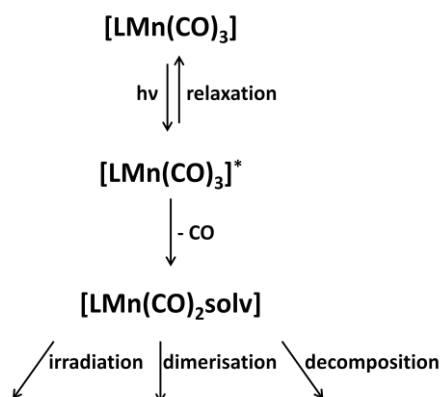
Scheme 37 Possible reaction pathways for the CORMs upon irradiation.

10.7 Conclusion

Besides the two trispyridyl-CORMs **22** and **23**, with **20** and **21** a new class of manganese-based CORMs were developed. The two complexes contain a unique {NS$_2$} binding moiety, which had not been tested before in this context. All four CORMs were characterised by several spectroscopic techniques and in solid state. The structural analysis revealed an interesting switch in the binding mode due to the formation of π-π stacking of the pyridines in solid state. This interaction stabilises the system in a fashion which allows the substitution of the strong

pyridine donors by rather weak methoxy or amine groups. The synthesised complexes were used for first studies of their CO-release capability. It could be demonstrated that all four complexes can release up to two equivalents of CO upon irradiation by light. Only the irradiation wavelength under 400 nm and the long half-lifes of **20** and **21** compromise the overall good results. Nevertheless, the two complexes **20** and **21** are the first examples of thioether-containing CORMs and should be useful as starting point for a next generation. Especially the substitution of the sulphur atoms by a heavy atom such as selenium would be very interesting.

Chapter 11

Experimental Section

11.1 General Remarks

Reactions Under Inert Atmosphere

Reactions, which were carried out under inter atmosphere were performed in an anaerobic and anhydrous atmosphere of dry nitrogen flashed over copper catalyst, by employing standard Schlenk techniques. Solvents were dried as follows: Et_2O over sodium benzophenone ketyl; THF over potassium benzophenone ketyl; MeCN, DMSO over CaH_2; CH_2Cl_2 and $CHCl_3$ over P_4O_{10} and MeOH over Mg. The deuterated solvents were dried and distilled analogous. Glassware was cleaned by passing through an ethanolic KOH bath followed by HCl bath (in each 24 h) and dried over night at 100 °C.

Preparation of Metal Precursors

$[Cu(MeCN)_4]OTf$ and $[Cu(MeCN)_4]PF_6$ were synthesised according to the literature.[346] The metal salts were crystallised from $MeCN/Et_2O$ and stored under N_2-atmosphere to prevent oxidation. $[Mn(CO)_5Br]$ for the synthesis of the CORMs was synthesised according to the literature.[337] The complex was stored under exclusion of light.

Utilised Analytical Methods and Devices for the Synthetic Part

^{1}H-NMR and ^{13}C-NMR spectra of the synthesised compounds were recorded on *Bruker Avance* 200 MHz, 300 MHz and 500 MHz spectrometers. No internal standard was used in the measurements, thus calibration is based on the residual signal of the solvent ($CDCl_3$ = 7.24 ppm and 77.1 ppm, $MeCN\text{-}d_3$ = 1.94 ppm and 118.3 ppm, $MeOH\text{-}d_4$ = 3.31 ppm and 49.1 ppm, $DMSO\text{-}d_6$ = 2.46 ppm and 29.9 ppm). The abbreviations s (singlet), d (doublet), t (triplet) indicate the spin multiplicity and *J* corresponds to the coupling constants. The assignment of the signals takes place according to the IUPAC numbering of the molecules. Sample preparation for IR spectra of the solids were done by grounding the sample with KBr in a mortar and then pressing under vacuum at 100 Kg/cm^2 into a tablet. Liquid samples were homogeneously applied between two KBr windows and directly measured. The used IR spectrometer was a *Digilab Excalibur*. The abbreviations are s (strong), m (medium), w (weak), b (broad signal). EI mass spectra were measured on a *Finnigan MAT 8200* and ESI mass spectra were recorded on a *Thermo Finnigan Trace LCQ* spectrometer. UV/Vis spectra were recorded in quartz cuvettes with an *Analytik Jena Specord S100* spectrometer and the fluorescence spectra were recorded with a *Jasco FP-6200* spectrofluorometer. Temperature-dependent magnetic susceptibilities of crystalline material were recorded on *a Quantum Design MPMS-5S* SQUID magnetometer at 0.5 T. Recorded data were corrected for the underlying diamagnetism by using tabulated Pascal constants (incremental method) and for temperature independent paramagnetism (TIP). Elemental analysis was performed by the *Analytical Laboratory at the Institute of Inorganic Chemistry at the Georg-August University* on a *Vario EL II* from *Elementar*. Melting points were determined on a *SRS OptiMelt*. The microwave used for the Suzuki coupling reaction was a *CEM Discovery*, which was used with 250 W.

Utilised Analytical Methods and Devices for the Metal Selectivity and Affinity Studies

The ^{1}H-NMR metal exchange experiments were carried out on *Bruker Avance* 500 MHz spectrometer equipped with a 5 mm triple resonance inverse Z-gradient probe (TBI ^{1}H, ^{31}P, BB). Spectra were collected at 298 K in deuterated buffer solution. The water signal was suppressed

in the measurements. UV/Vis spectra were recorded in quartz cuvettes with an *Analytik Jena Specord S100* or a *Hewlett Packard Agilent 8453* spectrometer at 25 °C. The fluorescence spectra were recorded with a *Jasco FP-6200* spectrofluorometer. All UV/Vis and NMR experiments were performed in argon-degassed solutions and under argon atmosphere.

Utilised AnalyticalMmethods and Devices for the CO Release Studies

For the CO release studies UV/Vis spectra were recorded with the kinetic function of an *Agilent 8453* spectroscopy system. The measurements were performed in argon-degassed solutions and under argon atmosphere.

Theoretical Calculations of the CORMs

Density functional theory (DFT) calculations were carried out on the Linux cluster of the *Leibniz-Rechenzentrum* (LRZ) in Munich with *ORCA* version 2.8[347] using the BP86 functional with the resolution-of-the-identity (RI) approximation, a def2-TZVP/def2-TZVP/J basis set,[348,349] the tightscf and grid4 options, and the COSMO solvation model with DMSO as the solvent for geometry optimisations. The DFT calculations were performed by Prof. Dr. Ulrich Schatzschneider (*Institute of Inorganic Chemistry at the Julius-Maximilians-University of Würzburg*, Germany).

11.2 Synthesis of the Ligands

I

II

III

IV

V

VI

VII

VIII

IX

X

XI

XII

L^{1H}

L^{2H}

L^{3H}

L^{4H}

L^{5H}

L^{3Me}

L^{5Me}

L^{3Ac}

L^{5Ac}

L^{6H}

L^{6Acet}

L^{7H}

L^{8H}

L^{8Me}

L^{8Ac}
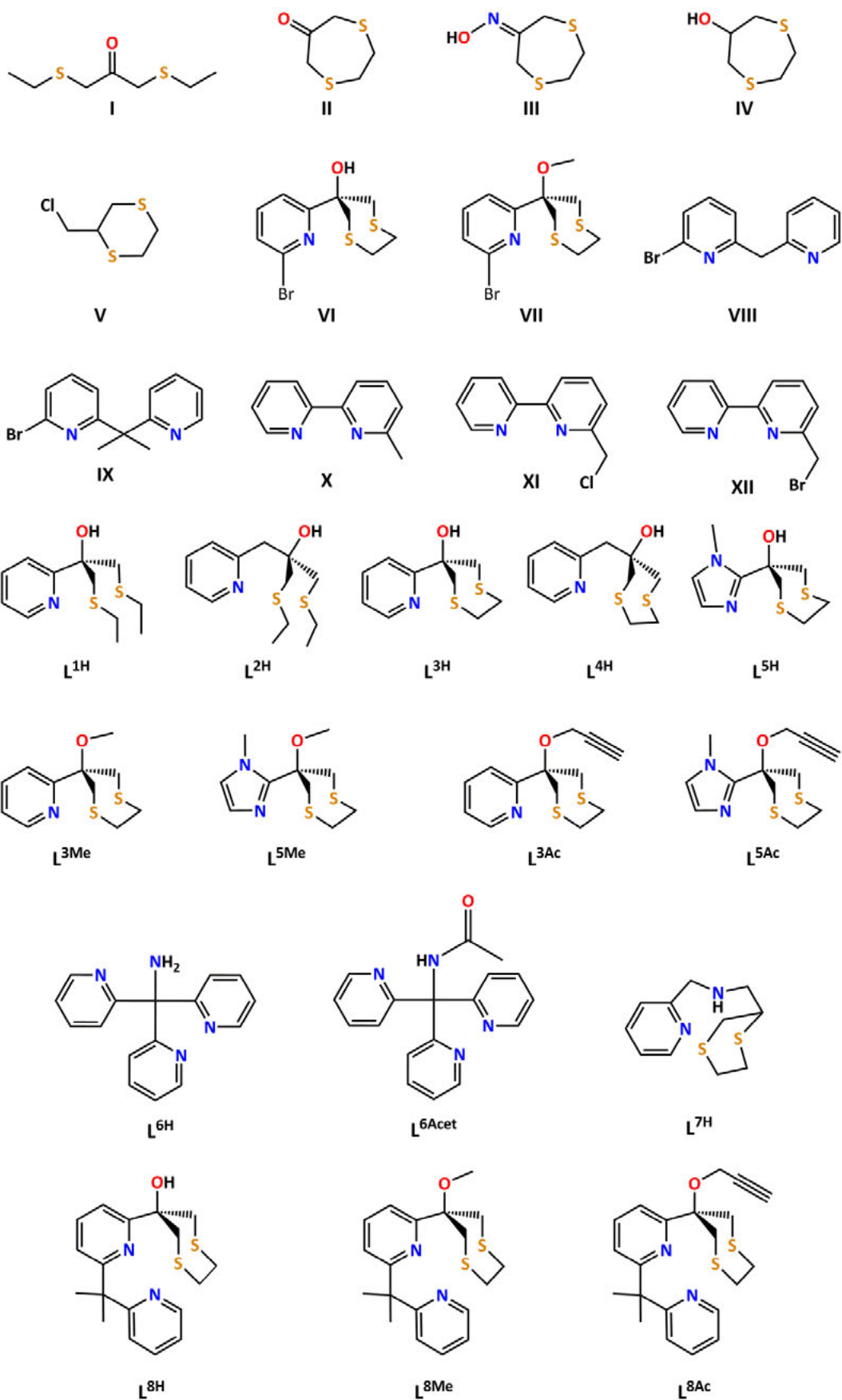
Synthesis of 1,3-*bis*(ethylsulfanyl)acetone (I)

Ethanethiol (10.3 g, 12.4 ml, 167 mmol, 2.0 eq.) was added to a solution of potassium hydroxide (8.64 g, 167 mol, 2.0 eq.) in water and stirred for 30 min at room temperature. The solution was then cooled to 0°C and a solution of 1,3-dichloro acetone (10.5 g, 82.9 mmol, 1.0 eq.) in diethyl ether (100 ml) was slowly added. The reaction was stirred over night and allowed to warm to room temperature. The phases were separated and the aqueous phase was washed with diethyl ether (100 ml). The combined organic solutions were dried over Na_2SO_4 and the solvent removed under reduced pressure. The crude product was purified by column chromatography on silica to give the product as yellow oil.

Yield:	11.8 g (66.1 mmol, 80 %)
R$_f$:	0.48 (hexane : ethyl acetate / 6 : 1)
^{1}H-NMR	(300 MHz, CDCl$_3$)
δ [ppm]:	3.41 (s, 4 H, CH$_2$), 2.50 (q, $^3J_{(H,H)}$ = 7.4 Hz, 4 H, CH$_2$CH$_3$), 1.22 (t, $^3J_{(H,H)}$ = 7.4 Hz, 6 H, CH$_2$CH$_3$)
^{13}C-NMR	(75 MHz, CDCl$_3$)
δ [ppm]:	200.2 (C=O), 38.0 (CH$_2$), 26.1 (CH$_2$CH$_3$), 14.0 (CH$_2$CH$_3$)
Mass spectrometry	ESI$^+$ (70 eV, MeOH)
m/z (%):	178 (100) [M]$^+$, 152 (65.6) [M - C$_2$H$_2$]$^+$, 117 (48.8) [M - C$_2$H$_5$S]$^+$
IR	KBr
$\tilde{v}$ [cm^{-1}]:	2969 (m), 2928 (m), 2872 (w), 1703 (s), 1451 (m), 1408 (w), 1354 (m), 1257 (m), 1187 (w), 1146 (w), 1078 (w), 1051 (w), 972 (w), 783 (w), 756 (w), 570 (w), 492 (w)
Elemental analysis	C$_7$H$_{14}$OS$_2$ (178.32 gmol^{-1})
Calculated (%):	C: 47.15, H: 7.91, S: 35.96
Found (%):	C: 46.97, H: 7.28, S: 34.25

Synthesis of 1,4-dithiepan-6-one (II)

In a 500 ml flask, 1,2-ethandithiol (22.20 g, 19.75 ml, 236 mmol, 1.0 eq.) was added to a solution of potassium hydroxide (26.45 g, 314 mmol, 2.0 eq.) in water. After 30 min stirring at room temperature the solution was cooled to 0 °C and a solution of 1,3-dichloro acetone (30.00 g, 236 mmol, 1.0 eq.) in diethyl ether (250 ml) was slowly added. The reaction mixture was stirred over night and allowed to warm to room temperature. The phases were separated and the aqueous phase was washed with diethyl ether (100 ml). The combined organic solutions were dried over Na_2SO_4 and the solvent removed under reduced pressure. The product could be obtained as yellow oil.

Yield:	28.43 g (191.7 mmol 84 %)
R$_f$:	0.23 (hexane : ethyl acetate / 6 : 1)
^{1}H-NMR	(300 MHz, CDCl$_3$)
δ [ppm]:	3.65 (s, 4 H, CH$_2$), 3.09 (s, 4 H, SCH$_2$CH$_2$S)
^{13}C-NMR	(75 MHz, CDCl$_3$)
δ [ppm]:	204.8 (C=O), 40.6 (CH$_2$), 38.2 (SCH$_2$CH$_2$S)
Mass spectrometry	ESI$^+$ (70 eV, MeOH)
m/z (%):	148 (100) [M]$^+$, 106 (17) [C$_3$H$_6$S]$^+$
IR	KBr
$\tilde{\nu}$ [cm^{-1}]:	2905 (m), 1750 (w), 1699 (s), 1406 (s), 1279 (w), 1236 (m), 1161 (m), 1088 (w), 912 (m), 830 (w), 763 (w), 679 (w), 525 (w), 454 (w), 427 (m)
Elemental analysis	C$_5$H$_8$OS$_2$ (148.25 gmol^{-1})
Calculated (%):	C: 40.51, H: 5.44, S: 43.26
Found (%):	C: 40.32, H: 5.60, S: 43.35

Synthesis of 1,4-dithiepan-6-one oxime (III)

Hydroxylamine hydrochloride (0.47 g, 6.75 mmol) and **II** (1.00 g, 6.75 mmol) were dissolved in ethanol (50 ml) and sodium acetate (0.55 g, 6.75 mmol) was added. The reaction was stirred for 24 h at room temperature. Afterwards, the solvent was evaporated under reduced pressure and the solid residue was purified by column chromatography on silica to provide the product as white solid.

Yield: 0.96 g (5.87 mmol, 87 %)

R$_f$: 0.43 (hexane : ethyl acetate / 2 : 1)

^{1}H-NMR (300 MHz, CDCl$_3$)

δ [ppm]: 3.84 (s, 2 H, C$\underline{H}$H), 3.74 (s, 2 H, CH$\underline{H}$), 3.10-3.01 (m, 4 H, SC$\underline{H}_2$C$\underline{H}_2$S)

^{13}C-NMR (75 MHz, CDCl$_3$):

δ [ppm]: 160.48 ($\underline{C}$=O), 39.27 ($\underline{C}$HH), 37.12 ($\underline{C}$HH'), 35.34 (S$\underline{C}$H$_2$CH$_2$S), 29.72 (SCH$_2$$\underline{C}H_2$S)

Mass spectrometry EI$^+$

m/z (%): 163 (100) [M]$^+$, 146 (23) [M - OH]$^+$

IR KBr

$\tilde{\nu}$[cm^{-1}]: 3268 (w), 2904 (w), 1485 (w), 1447 (m), 1403 (s), 1381 (s), 1284 (m), 1250 (m), 1231 (m), 1186 (m), 1142 (m), 1102 982 (s), 926 (s), 892 (m), 857 (m), 817 (m), 746 (m), 677 (m), 613 (m), 494 (m), 422 (s)

Elemental analysis C$_5$H$_9$NOS$_2$ (163.26 gmol^{-1})

Calculated (%): C: 36.78, H: 5.56, N: 8.58, S: 39.28

Found (%): C: 36.79, H: 5.37, N: 8.29, S: 38.92

Synthesis of 1,4-dithiepan-6-ol (IV)

A solution of **II** (1.00 g, 6.75 mmol) and sodium borohydride (0.26 g, 6.75 mmol) in abs. THF (50 ml) was stirred for 16 h at room temperature. The reaction was quenched by the addition of water (20 ml). The solution was adjusted to pH 7, using HCl and afterwards extracted with DCM. The combined organic phases were dried over Na_2SO_4. After evaporation of the solvent under reduced pressure, the product was re-crystallised from ethanol/hexane and could be obtained as white solid.

Yield:	1.01 g (6.75 mmol, 100 %)
R$_f$:	0.33 (hexane : ethyl acetate / 2 : 1)
^{1}H-NMR	(300 MHz, $CDCl_3$)
δ [ppm]:	4.99 (d, $^3J_{(H,H)}$ = 6 Hz, 1 H, CHO<u>H</u>), 4.08-3.99 (m, 1 H, C<u>H</u>OH), 3.03 (dd, $^2J_{(H,H)}$ = 6 Hz, $^3J_{(H,H)}$ = 9 Hz, 2 H, C<u>H</u>H), (dd, $^2J_{(H,H)}$ = 6 Hz, $^3J_{(H,H)}$ = 9 Hz, 2 H, CH<u>H</u>), 2.87 (q, $^3J_{(H,H)}$ = 3 Hz, 4 H, SC<u>H</u>$_2$C<u>H</u>$_2$S)
^{13}C-NMR	(75 MHz, $CDCl_3$)
δ [ppm]:	71.16 (<u>C</u>HOH), 37.49 (CHH), 38.96 (S<u>C</u>H$_2$<u>C</u>H$_2$S)
Mass spectrometry	EI$^+$
m/z (%):	150 (100) [M]$^+$, 132 (40) [M - H$_2$O]$^+$, 104 (22) [C$_3$H$_4$S$_2$]$^+$
IR	KBr
$\tilde{v}$[cm^{-1}]:	3271 (w), 2897 (w), 1455 (s), 1411 (s), 1397 (s), 1344 (s), 1326 (m), 1293 (s), 1269 (s), 1230 (m), 1204 (m), 1183 (m), 1163 (m), 1132 (m), 1095 (m), 1032 (s), 998 (m), 949 (m), 918 (m), 848 (s), 802 (s), 755 (w), 698 (w), 667 (s), 598 (w), 552 (w)
Elemental analysis	C$_5$H$_{10}$OS$_2$ (150.26 gmol^{-1})
Calculated (%):	C: 39.97, H: 6.71, S: 42.68
Found (%):	C: 39.84, H: 6.39, S: 42.19

Synthesis of 2-(chloromethyl)-1,4-dithiane (V)

Compound **V** was synthesised according to the literature.[272]

Yield:	71 % (Lit.: 75 %)
^{1}H-NMR	(300 MHz, CDCl$_3$)
δ [ppm]:	4.09 (dd, $^3J_{(H,H)}$ = 12 Hz, $^3J_{(H,H)}$ = 9 Hz, 1 H, C$\underline{H}^2$), 3.84 (dd, $^3J_{(H,H)}$ = 12 Hz, $^3J_{(H,H)}$ = 6 Hz, 1 H, C$\underline{H}$H^3), 2.94 (m, 7 H, C$\underline{H}_2^{5,6,7}$, CH$\underline{H}^3$)
^{13}C-NMR	(75 MHz, CDCl$_3$)
δ [ppm]:	46.04 (C$\underline{H}^2$), 39.19 (C$\underline{H}_2^7$), 30.45 (C$\underline{H}_2^3$), 27.91 (C$\underline{H}_2^5$), 26.43 (C$\underline{H}_2^6$)
Mass spectrometry	EI$^+$
m/z (%):	168 (100) [M]$^+$, 133 (68) [M - Cl]$^+$, 119 (35) [M - CH$_2$Cl]$^+$
IR	KBr
$\tilde{v}$ [cm^{-1}]:	2947 (m), 2906 (s), 2803 (w), 1431 (m), 1411 (s), 1323 (w), 1281 (m), 1220 (m), 1163 (w), 1127 (w), 1070 (w), 999 (w), 926 (w), 908 (m), 886 (m), 860 (m), 829 (w), 745 (m), 703 (s), 673 (s), 631 (m)
Elemental analysis	C$_5$H$_9$ClS$_2$ (168.71 gmol^{-1})
Calculated (%):	C: 35.60, H: 5.38, S: 38.01
Found (%):	C: 35.60, H: 5.38, S: 37.38

Synthesis of 6-(6-bromopyridin-2-yl)-1,4-dithiepan-6-ol (VI)

Under a N_2-atmosphere 2.5 M ^{n}BuLi (20.4 ml, 0.51 mmol, 1.5 eq.) was slowly added to a -78 °C cooled solution of 2,6-dibromopyridine (11.98 g, 0.51 mmol, 1.5 eq.) in abs. THF (300 ml). The solution was stirred for 1 h at this temperature. Afterwards the solution was added to a cooled solution of **II** (5.00 g, 0.34 mmol, 1.0 eq.) in THF (50 ml). After 4 h at -78 °C the reaction was quenched by the addition of brine (30 ml). The THF was removed under reduced pressure and the solution was extracted with chloroform after adjusting to a pH value of 7. The combined organic phases were dried over Na_2SO_4 and the solvent was removed under reduced pressure. After column chromatography on silica the product could be obtained as brown oil, which solidified at 4 °C.

Yield:	2.39 g (78 mmol, 23 %)
R$_f$:	0.34 (hexane : ethyl acetate / 2 : 1)
^{1}H-NMR	(300 MHz, CDCl$_3$)
δ [ppm]:	7.57 (dd, $^3J_{(H,H)}$ = 6 Hz, $^3J_{(H,H)}$ = 6 Hz, 1 H, C$\underline{H}^{Py, 4}$), 7.45 (d, $^3J_{(H,H)}$ = 6 Hz, 1 H, C$\underline{H}^{Py, 5}$), 7.41 (d, $^3J_{(H,H)}$ = 6 Hz, 1 H, C$\underline{H}^{Py, 3}$), 5.54 (s$_{br}$, 1 H, CO$\underline{H}$) 3.59 (d, $^2J_{(H,H)}$ = 15 Hz, 2 H, C$\underline{H}$H), 3.18 (d, $^2J_{(H,H)}$ = 15 Hz, 2 H, CH$\underline{H}$), 3.02 (s, 4 H, SC$\underline{H_2}$C$\underline{H_2}$S)
^{13}C-NMR	(75 MHz, CDCl$_3$)
δ [ppm]:	163.27 ($\underline{C}^{Py, 6}$), 141.11 ($\underline{C}^{Py, 2}$), 138.98 ($\underline{C}H^{Py, 4}$), 127.23 ($\underline{C}H^{Py, 3}$), 120.25 ($\underline{C}H^{Py, 5}$), 68.34 ($\underline{C}$OH), 41.34 ($\underline{C}$HH), 38.98 (S$\underline{C}H_2\underline{C}H_2$S)
Mass spectrometry	ESI$^+$ (70 eV, MeOH)
m/z (%):	345.9 (7) [M + K]$^+$, 329.9 (100) [M + Na]$^+$, 308.0 (14) [M + H]$^+$, 290.0 (39) [M - OH]$^+$
General Information	$C_{10}H_{12}BrNOS_2$ (306.24 gmol^{-1})
Calculated (%):	C: 39.22, H: 3.95, N: 4.57, S: 20.94

Synthesis of 2-bromo-6-(6-methoxy-1,4-dithiepan-6-yl)pyridine (VII)

Under a N_2-atmosphere **VI** (350 mg, 1.14 mmol, 1.0 eq.) was dissolved in abs. THF (30 ml) and NaH (60 %, 54 mg, 1.37 mmol, 1.2 eq.) was added. The reaction was heated under reflux for 30 min and afterwards methyl iodide (195 mg, 1.37 mmol, 1.2 eq.) was added. The reaction was heated for further 14 h under reflux and then quenched with water (5 ml). The THF was removed under reduced pressure and the residue was extracted with chloroform. The combined organic phases were dried over Na_2SO_4 and the solvent was removed under reduced pressure. The crude product was purified by column chromatography on silica and the product was obtained as yellow solid.

Yield:	227 mg (0.71 mmol, 62 %)
R_f:	0.39 (hexane : ethyl acetate / 5 : 1)
^{1}H-NMR	(300 MHz, CDCl$_3$)
δ [ppm]:	7.59 (dd, $^3J_{(H,H)}$ = 6 Hz, $^3J_{(H,H)}$ = 6 Hz, 1 H, C$\underline{H}^{Py, 4}$), 7.43 (d, $^3J_{(H,H)}$ = 6 Hz, 1 H, C$\underline{H}^{Py, 5}$), 7.42 (d, $^3J_{(H,H)}$ = 6 Hz, 1 H, C$\underline{H}^{Py, 3}$), 3.61 (d, $^2J_{(H,H)}$ = 15 Hz, 2 H, C$\underline{H}$H), 3.21 (d, $^2J_{(H,H)}$ = 15 Hz, 2 H, CH$\underline{H}$), 3.08 (s, 3 H, COC$\underline{H}_3$), 3.03 (s, 4 H, SC$\underline{H}_2$C$\underline{H}_2$S)
^{13}C-NMR	(75 MHz, CDCl$_3$)
δ [ppm]:	163.13 ($\underline{C}^{Py, 6}$), 141.06 ($\underline{C}^{Py, 2}$), 138.99 ($\underline{C}H^{Py, 4}$), 127.18 ($\underline{C}H^{Py, 3}$), 120.23 ($\underline{C}H^{Py, 5}$), 68.30 ($\underline{C}OCH_3$), 51.47 (CO$\underline{C}H_3$), 41.28 ($\underline{C}HH$), 38.94 (S$\underline{C}H_2CH_2S$)
Mass spectrometry	ESI$^+$ (70 eV, MeOH)
m/z (%):	342.0 (100) [M + Na]$^+$, 321.0 (12) [M + H]$^+$, 288.0 (14) [M - OMe]$^+$
General Information	C$_{11}$H$_{14}$BrNOS$_2$ (320.27 gmol^{-1})
Calculated (%):	C: 41.25, H: 4.41, N: 4.37, S: 20.02

Synthesis of 2-bromo-6-(pyridin-2-ylmethyl)pyridine (VIII)

Under a N_2-atmosphere 2.5 M ^{n}BuLi (20.0 ml, 50.0 mmol, 2.0 eq.) was slowly added to a -20 °C cooled solution of 2-methylpyridine (5.0 ml, 50.0 mmol, 2.0 eq.) in THF (50 ml). After stirring for 120 min at -20 °C, a solution of 2,6-dibromopyridine (5.92 g, 25.0 mmol, 1.0 eq.) in THF (50 ml) was added and the reaction was allowed to warm up to room temperature. The reaction was then stirred under reflux for further 90 min at 50 °C. The reaction was quenched by the addition of iced water (10 ml) and THF was removed under reduced pressure. The aqueous phase was extracted with DCM and the combined organic phases were dried over Na_2SO_4. After removal of the solvent under reduced pressure the product was purified by column chromatography on silica. The product could be obtained as brown oil.

Yield: 8.58 g (34.4 mmol, 69 %)

R_f: 0.05 (hexane : ethyl acetate / 5 : 1)

^{1}H-NMR (300 MHz, $CDCl_3$)

δ [ppm]: 8.56 (ddd, $^3J_{(H,H)}$ = 6 Hz, $^4J_{(H,H)}$ = 3 Hz, $^5J_{(H,H)}$ = 1 Hz, 1 H, C$\underline{H}^{Py, 10}$), 7.64 (ddd, $^3J_{(H,H)}$ = 6 Hz, $^3J_{(H,H)}$ = 6 Hz, $^4J_{(H,H)}$ = 3 Hz, 1 H, C$\underline{H}^{Py, 12}$), 7.47 (dd, $^3J_{(H,H)}$ = 9 Hz, $^3J_{(H,H)}$ = 9 Hz, 1 H, C$\underline{H}^{Py, 4}$), 7.35 (dd, $^3J_{(H,H)}$ = 9 Hz, $^4J_{(H,H)}$ = 1 Hz, 1 H, C$\underline{H}^{Py, 5}$), 7.30 (d, $^3J_{(H,H)}$ = 6 Hz, $^4J_{(H,H)}$ = 1 Hz, 1 H, C$\underline{H}^{Py, 3}$), 7.22 (dd, $^3J_{(H,H)}$ = 6 Hz, $^4J_{(H,H)}$ = 1 Hz, 1 H, C$\underline{H}^{Py, 13}$), 7.16 (ddd, $^3J_{(H,H)}$ = 6 Hz, $^4J_{(H,H)}$ = 1 Hz, $^5J_{(H,H)}$ = 1 Hz, 1 H, C$\underline{H}^{Py, 11}$), 4.33 (s, 2 H, C$\underline{H}_2$)

^{13}C-NMR (75 MHz, $CDCl_3$)

δ [ppm]: 160.93 ($\underline{C}^{Py, 6}$), 158.56 ($\underline{C}^{Py, 8}$), 149.49 ($\underline{C}H^{Py, 10}$), 141.51 ($\underline{C}^{Py, 2}$), 138.83 ($\underline{C}H^{Py, 4}$), 136.72 ($\underline{C}H^{Py, 3}$), 125.86 ($\underline{C}H^{Py, 12}$), 123.75 ($\underline{C}H^{Py, 11}$), 122.40 ($\underline{C}H^{Py, 5}$), 121.73 ($\underline{C}H^{Py, 13}$), 46.75 ($\underline{C}H_2$)

Mass spectrometry EI^+

m/z (%): 250 (32) $[M+H]^+$, 249 (100) $[M]^+$, 168 (22) $[M - HBr]^+$

IR KBr

$\tilde{V}$[cm^{-1}]: 3396 (m), 3061 (s), 3008 (m), 2930 (m), 2303 (w), 1974 (w) 1589 (s), 1554 (s), 1474 (s), 1433 (s), 1404 (s), 1297 (w), 1152 (m), 1117 (s), 986 (s), 924 (w), 864 (m), 781 (s), 749 (s), 673 (s)

Elemental analysis $C_{11}H_9BrN_2$ (249.11 gmol^{-1})

Calculated (%): C: 53.04, H: 3.64, N: 11.25

Found (%): C: 52.70, H: 3.68, N: 11.68

Synthesis of 2-bromo-6-(pyridin-2-ylmethyl)pyridine (IX)

Potassium *tert*-butanolate (3.52 g, 31.0 mmol, 1.5 eq.), methyl iodide (0.52 g, 31.0 mmol, 1.5 eq.) and **VIII** (5.21 g, 20.9 mmol, 1.0 eq.) were dissolved in abs. THF (100 ml) and stirred at room temperature. After 8 h, additional potassium *tert*-butanolate (3.52 g, 31.0 mmol, 1.5 eq.) and methyl iodide (0.52 g, 31.0 mmol, 1.5 eq.) were added and the reaction was stirred for additional 16 h. The reaction was quenched by the addition of brine, THF was removed under reduced pressure and the aqueous residue was extracted with chloroform. The combined organic phases were combined and dried over Na_2SO_4. After removal of the solvent under reduced pressure, the product was purified by column chromatography on silica. The product could be obtained as yellow oil.

Yield: 3.95 g (14.3 mmol, 68 %)

R_f: 0.48 (hexane : ethyl acetate / 2 : 1)

^{1}H-NMR (300 MHz, $CDCl_3$)

δ [ppm]: 8.57 (ddd, $^3J_{(H,H)}$ = 6 Hz, $^4J_{(H,H)}$ = 3 Hz, $^5J_{(H,H)}$ = 1 Hz, 1 H, C$\underline{H}^{Py, 10}$), 7.62 (ddd, $^3J_{(H,H)}$ = 6 Hz, $^3J_{(H,H)}$ = 6 Hz, $^4J_{(H,H)}$ = 3 Hz, 1 H, C$\underline{H}^{Py, 12}$), 7.41 (dd, $^3J_{(H,H)}$ = 9 Hz, $^3J_{(H,H)}$ = 9 Hz, 1 H, C$\underline{H}^{Py, 4}$), 7.30-7.24 (m, C$\underline{H}^{Py, 3, 5}$), 7.14 (dd, $^3J_{(H,H)}$ = 6 Hz, $^4J_{(H,H)}$ = 1 Hz, 1 H, C$\underline{H}^{Py, 13}$), 7.07 (ddd, $^3J_{(H,H)}$ = 6 Hz, $^4J_{(H,H)}$ = 1 Hz, $^5J_{(H,H)}$ = 1 Hz, 1 H, C$\underline{H}^{Py, 11}$), 1.80 (s, 6 H, C$\underline{H}_3$)

^{13}C-NMR (75 MHz, $CDCl_3$)

δ [ppm]: 169.34 ($\underline{C}^{Py, 6}$), 166.82 ($\underline{C}^{Py, 8}$), 148.70 ($\underline{C}H^{Py, 10}$), 141.02 ($\underline{C}^{Py, 2}$), 138.37 ($\underline{C}H^{Py, 4}$), 136.28 ($\underline{C}H^{Py, 12}$), 125.29 ($\underline{C}H^{Py, 3}$), 121.31 ($\underline{C}H^{Py, 11}$), 121.16 ($\underline{C}H^{Py, 5}$), 120.41 ($\underline{C}H^{Py, 13}$), 48.19 ($\underline{C}C_4$), 28.30 ($\underline{C}H_3$)

Mass spectrometry EI$^+$

m/z (%): 278 (27) [M(Br^{81})]$^+$, 276 (28) [M(Br^{79})]$^+$, 263 (97) [M(Br^{81}) -Me]$^+$, 261 (100) [M(Br^{79}) -Me]$^+$, 120 (30) [$C_8H_{10}N$]$^+$

IR KBr

$\tilde{V}$[cm^{-1}]: 3051 (m), 2972 (s), 2931 (s), 2872 (m), 1586 (m), 1553 (m), 1472 (m), 1423 (m), 1396 (m), 1295 (w), 1174 (m), 1118 (m), 1049 (w), 984 (m), 931 (w), 825 (s), 786 (s), 744 (s), 664 (s), 601 (m), 561 (w)

Elemental analysis $C_{13}H_{13}BrN_2$ (277.16 gmol^{-1})

Calculated (%): C: 56.34 H: 4.73 N: 10.11

Found (%): C: 56.34 H: 3.96 N: 10.19

Synthesis of 6-methyl-2,2'-bipyridine (X)

Compound **X** was synthesised according to the literature.[278]

Yield:	54 % (Lit.: 59 %)
R$_f$:	0.39 (hexane : ethyl acetate / 2 : 1)
^{1}H-NMR	(500 MHz, CDCl$_3$)
δ [ppm]:	8.64 (d, $^3J_{(H,H)}$ = 5 Hz, $^4J_{(H,H)}$ = 2 Hz,, 1 H, C$\underline{H}$$^{Py, 12}$), 8.37 (d, $^3J_{(H,H)}$ = 8 Hz, 1 H, C$\underline{H}$$^{Py, 3}$), 8.14 (d, $^3J_{(H,H)}$ = 8 Hz, 1 H, C$\underline{H}$$^{Py, 9}$), 7.77 (ddd, $^3J_{(H,H)}$ = 8 Hz, $^3J_{(H,H)}$ = 8 Hz, $^4J_{(H,H)}$ = 2 Hz, 1 H, C$\underline{H}$$^{Py, 11}$), 7.66 (dd, $^3J_{(H,H)}$ = 8 Hz, $^3J_{(H,H)}$ = 8 Hz, 1 H, C$\underline{H}$$^{Py, 4}$), 7.26-7.23 (mC$\underline{H}$$^{Py, 10}$), 7.13 (d, $^3J_{(H,H)}$ = 8 Hz, 1 H, C$\underline{H}$$^{Py, 5}$), 2.60 (s, 3 H, C$\underline{H}_3$)
^{13}C-NMR	(125 MHz, CDCl$_3$)
δ [ppm]:	157.88 ($\underline{C}$$^{Py, 2}$), 156.43 ($\underline{C}$$^{Py, 7}$), 155.50 ($\underline{C}$$^{Py, 6}$), 149.08 ($\underline{C}H^{Py, 9}$), 137.01 ($\underline{C}H^{Py, 4}$), 136.79 ($\underline{C}H^{Py, 11}$), 123.44 ($\underline{C}H^{Py, 3}$), 123.20 ($\underline{C}H^{Py, 5}$), 121.12 ($\underline{C}H^{Py, 10}$), 118.05 ($\underline{C}H^{Py, 12}$), 24.60 ($\underline{C}H_3$)
Mass spectrometry	EI$^+$
m/z (%):	170 (100) [M]$^+$, 155 (17) [M - CH$_3$]$^+$
IR	KBr
$\tilde{V}$[cm^{-1}]:	3061 (m), 3012 (w), 2923 (w), 1677 (w), 1580 (s), 1516 (w), 1460 (s), 1428 (s), 1374 (w), 1256 (m), 1152 (w), 1083 (m), 1043 (m), 994 (m), 897 (w), 818 (w), 771 (s), 745 (m), 640 (m), 621 (m), 603 (w), 553 (w)
Elemental analysis	C$_{11}$H$_{10}$N$_2$ (170.21 gmol^{-1})
Calculated (%):	C: 77.62, H: 5.92, N: 16.46
Found (%):	C: 76.14, H: 5.97, N: 16.66

Synthesis of 6-chloromethyl-2,2'-bipyridine (XI)

Compound **XI** was synthesised according to the literature.[279]

Yield: 39 % (Lit.: 60 %)

^{1}H-NMR   (200 MHz, CDCl$_3$)

δ [ppm]:   8.63 (d, $^3J_{(H,H)}$ = 6 Hz, 1 H, C$\underline{H}^{Py,\ 12}$), 8.39 (d, $^3J_{(H,H)}$ = 6 Hz, 1 H, C$\underline{H}^{Py,\ 3}$), 8.15 (d, $^3J_{(H,H)}$ = 6 Hz, 1 H, C$\underline{H}^{Py,\ 9}$), 7.82 (d, $^3J_{(H,H)}$ = 6 Hz, $^3J_{(H,H)}$ = 6 Hz, 1 H, C$\underline{H}^{Py,\ 11}$), 7.67 (dd, $^3J_{(H,H)}$ = 6 Hz, $^3J_{(H,H)}$ = 6 Hz, 1 H, C$\underline{H}^{Py,\ 4}$), 7.28 (dd, $^3J_{(H,H)}$ = 6 Hz, $^3J_{(H,H)}$ = 6 Hz, C$\underline{H}^{Py,\ 10}$), 7.15 (d, $^3J_{(H,H)}$ = 6 Hz, 1 H, C$\underline{H}^{Py,\ 5}$), 4.72 (s, 3 H, C$\underline{H}_3$)

Mass spectrometry   EI$^+$

m/z (%):   206 (33) [M(^{35}Cl)]$^+$, 204 (100) [M(^{37}Cl)]$^+$, 170 (75) [M - Cl]$^+$

General Information C$_{11}$H$_9$ClN$_2$ (204.66 gmol^{-1})

Calculated (%):   C: 64.56, H: 4.43, N: 13.69

Synthesis of 6-bromomethyl-2,2'-bipyridine (XII)

Compound **XII** was synthesised according to the literature.[280]

Yield: 45 % (Lit.: 60 %)

^{1}H-NMR (200 MHz, CDCl$_3$)

δ [ppm]: 8.62 (d, $^3J_{(H,H)}$ = 6 Hz, 1 H, C$\underline{H}^{Py, 12}$), 8.45 (d, $^3J_{(H,H)}$ = 6 Hz, 1 H, C$\underline{H}^{Py, 3}$), 8.25 (d, $^3J_{(H,H)}$ = 6 Hz, 1 H, C$\underline{H}^{Py, 9}$), 7.82-7.68 (m, 2 H, C$\underline{H}^{Py, 11, 4}$), 7.43 (d, $^3J_{(H,H)}$ = 6 Hz, C$\underline{H}^{Py, 10}$), 7.33-7.28 (m, 1 H, C$\underline{H}^{Py, 5}$), 4.61 (s, 3 H, C$\underline{H}_3$)

Mass spectrometry EI$^+$

m/z (%): 247 (100) [M(^{81}Br)]$^+$, 245 (97) [M(^{79}Br)]$^+$, 170 (83) [M - Br]$^+$, 155 (14) [M - CH$_3$]$^+$

General Information C$_{11}$H$_9$BrN$_2$ (249.11 gmol^{-1})

Calculated (%): C: 53.04, H: 3.64, N: 11.25

Synthesis of 1,3-*bis*(ethylthio)-2-(pyridin-2-yl)propan-2-ol (L^{1H})

Under an atmosphere of dry N_2 a 2.5 M solution of ^{n}BuLi in hexanes (8.6 ml, 21.6 mmol, 1.5 eq.) was slowly added to a solution of 2-bromopyridine (3.41 g, 21.6 mmol, 1.5 eq.) in THF (50 ml) at -78 °C. After 30 min stirring, the reaction mixture was allowed to warm to room temperature. After 10 min at room temperature the solution was again cooled to -78 °C and slowly added to a solution of **1** (2.13 g, 14.4 mmol, 1.0 eq.) in THF (50 ml). After 3 h at -78 °C the reaction was quenched by the addition of water (10 ml). The solvent THF was removed under reduced pressure. Chloroform (30 ml) was added and with diluted HCl a pH value of 7 was adjusted. The resulting emulsion was extracted with chloroform. The combined organic phases were dried over Na_2SO_4 and the solvent was removed under reduced pressure. After column chromatography on silica the product could be obtained as dark brown oil.

Yield:	2.89 g (11.2 mmol, 52 %)
R$_f$:	0.27 (hexane : ethyl acetate / 4 : 1)
^{1}H-NMR	(500 MHz, CDCl$_3$)
δ [ppm]:	8.53 (ddd, $^3J_{(H,H)}$ = 4.9 Hz, $^4J_{(H,H)}$ = 1.8 Hz, $^5J_{(H,H)}$ = 1.0 Hz, 1 H, C$\underline{H}^{Py,\,6}$), 7.73 (ddd, $^3J_{(H,H)}$ = 8.0 Hz, $^4J_{(H,H)}$ = 7.4 Hz, $^3J_{(H,H)}$ = 1.8 Hz, 1 H, C$\underline{H}^{Py,\,4}$), 7.58 (ddd, $^3J_{(H,H)}$ = 8.0 Hz, $^4J_{(H,H)}$ = 1.2 Hz, $^5J_{(H,H)}$ = 1.1 Hz, 1 H, C$\underline{H}^{Py,\,3}$), 7.20 (ddd, $^3J_{(H,H)}$ = 7.4 Hz, $^4J_{(H,H)}$ = 4.9 Hz, $^5J_{(H,H)}$ = 1.2 Hz, 1 H, C$\underline{H}^{Py,\,5}$), 4.60 (s$_{br}$, 1 H, O$\underline{H}$), 3.24 (d, $^2J_{(H,H)}$ = 13.5 Hz, 2 H, C$\underline{H}$H), 3.07 (d, $^2J_{(H,H)}$ = 13.5 Hz, 2 H, CH$\underline{H}$), 2.37 (q, $^3J_{(H,H)}$ = 7.4 Hz, 4 H, C$\underline{H}_2$CH$_3$), 1.13 (t, $^3J_{(H,H)}$ = 7.4 Hz, 6 H, CH$_2$C$\underline{H}_3$)
^{13}C-NMR	(125 MHz, CDCl$_3$)
δ [ppm]:	162.4 ($\underline{C}^{Py,\,2}$), 147.9 ($\underline{C}H^{Py,\,6}$), 136.8 ($\underline{C}H^{Py,\,4}$), 122.4 ($\underline{C}H^{Py,\,3}$), 120.6 ($\underline{C}H^{Py,\,5}$), 77.1 ($\underline{C}$OH), 42.8 ($\underline{C}H_2$), 27.5 ($\underline{C}H_2CH_3$), 14.8 (CH$_2\underline{C}H_3$)
Mass spectrometry	ESI$^+$ (70 eV, MeOH)
m/z (%):	280.2 (100) [M + Na]$^+$, 264.3 (10) [M]$^+$, 258.1 (17) [M + H]$^+$, 240.2 (10) [M - OH]$^+$
IR	KBr
$\tilde{v}$ [cm^{-1}]:	3429 (m), 3054 (w), 2964 (s), 2924 (s), 2870 (m), 2359 (w), 1703 (w), 1590 (s), 1571 (m), 1451 (m), 1434 (s), 1402 (m), 1376 (m), 1343 (m), 1294 (m), 1263 (m), 1244 (m), 1193 (w), 1153 (m), 1113 (m), 1077 (m), 1051 (m), 996 (m), 972 (m), 845 (w), 784 (m), 752 (s), 717 (w), 618 (m), 565 (w), 469 (w)
Elemental analysis	C$_{12}$H$_{19}$NOS$_2$ (257.42 gmol^{-1})
Calculated (%):	C: 55.99, H: 7.44, N: 5.44, S: 24.91
Found (%):	C: 54.74, H: 7.26, N: 6.26, S: 23.90

Synthesis of 1,3-*bis*(ethylthio)-2-(pyridin-2-ylmethyl)propan-2-ol (L^{2H})

Under an atmosphere of dry N_2 a 2.5 M solution of ^{n}BuLi in hexanes (9.6 ml, 24.0 mmol, 1.5 eq.) was slowly added to a solution of 2-metylpyridine (2.23 g, 24.0 mmol, 1.5 eq.) in THF (50 ml) at -78 °C. After 30 min stirring the reaction mixture was allowed to warm to room temperature. After 10 min at room temperature the solution was again cooled to -78 °C and slowly added to a solution of **1** (2.37 g, 16.0 mmol, 1.0 eq.) in THF (50 ml). After 3 h at -78 °C the reaction was quenched by the addition of water (10 ml). The THF was removed under reduced pressure. DCM (30 ml) was added and with diluted HCl a pH value of 7 was adjusted. The solution was extracted with DCM until the organic phase becomes colourless. The combined organic phases were dried over Na_2SO_4 and the solvent was removed under reduced pressure. After column chromatography on silica the product could be obtained as dark brown oil.

Yield:	4.3 g (15.8 mmol, 66 %)
R$_f$:	0.33 (hexane : ethyl acetate / 2 : 1)
^{1}H-NMR	(500 MHz, CDCl$_3$):

δ [ppm]: 8.48 (d, $^3J_{(H,H)}$ = 5.0 Hz, 1 H, C$\underline{H}^{Py, 6}$), 7.63 (ddd, $^3J_{(H,H)}$ = 7.0, $^3J_{(H,H)}$ = 7.0 Hz, $^4J_{(H,H)}$ = 2.0 Hz, 1 H, C$\underline{H}^{Py, 4}$), 7.22 (d, $^3J_{(H,H)}$ = 7.0 Hz, 1 H, C$\underline{H}^{Py, 3}$), 7.16 (ddd, $^3J_{(H,H)}$ = 7.0 Hz, $^3J_{(H,H)}$ = 5.0 Hz, $^4J_{(H,H)}$ = 2.0 Hz, 1 H, C$\underline{H}^{Py, 5}$), 6.25 (s$_{br}$, 1 H, O$\underline{H}$), 3.10 (s, 2 H, C^{Py}C$\underline{H}_2$), 2.81 (d, $^2J_{(H,H)}$ = 13.1 Hz , 2 H, C$\underline{H}$H), 2.67 (d, $^2J_{(H,H)}$ = 13.1 Hz, 2 H, CH$\underline{H}$), 2.57 (q, $^3J_{(H,H)}$ = 7.5 Hz, 4 H, $\underline{CH}_2$CH$_3$), 1.19 (t, $J_{(H,H)}$ = 7.5 Hz, 6 H, CH$_2$$\underline{CH}_3$)

^{13}C-NMR	(125 MHz, CDCl$_3$)

δ [ppm]: 159.0 ($\underline{C}^{Py, 2}$), 148.3 ($\underline{C}H^{Py, 6}$), 137.0 ($\underline{C}H^{Py, 4}$), 124.9 ($\underline{C}H^{Py, 3}$), 121.7 ($\underline{C}H^{Py, 5}$), 76.2 ($\underline{C}$OH), 43.2 (2 C, $\underline{C}H_2$), 40.7 ($C^{Py}\underline{C}H_2$), 27.7 ($\underline{C}H_2$CH$_3$), 14.9 (CH$_2\underline{C}H_3$)

Mass spectrometry	ESI$^+$ (70 eV, MeOH)

m/z (%): 294.2 (100) [M + Na]$^+$, 272.2 (64) [M + H]$^+$, 254.2 (58) [M - OH]$^+$, 210 (9) [M - SC$_2$H$_5$]$^+$, 192.2 (73) [M - C$_5$H$_5$N]$^+$

IR	KBr

$\tilde{v}$[cm^{-1}]: 3308 (m), 3058 (w), 3013 (w), 2963 (s), 2925 (s), 2869 (m), 1737 (w), 1595 (s), 1569 (m), 1474 (s), 1439 (s), 1375 (m), 1331 (w), 1261 (m), 1195 (m), 1150 (m), 1100 (w), 1050 (w), 1001 (w), 971 (w), 906 (w), 865 (w), 811 (w), 756 (m), 725 (w), 629 (w), 549 (w), 496 (w), 474 (w)

Elemental analysis	C$_{13}$H$_{21}$NOS$_2$ (271.44 gmol^{-1})
Calculated (%):	C: 57.52, H: 7.80, N: 5.16, S: 23.63
Found (%):	C: 57.12, H: 8.23, N: 4.94, S: 22.73

Synthesis of 6-(pyridin-2-yl)-1,4-dithiepan-6-ol (L^{3H})

Under an atmosphere of dry N_2 a 2.5 M solution of ^{n}BuLi in hexanes (8.6 ml, 21.6 mmol, 1.5 eq.) was slowly added to a solution of 2-bromopyridine (3.41 g, 21.6 mmol, 1.5 eq.) in THF (50 ml) at -78 °C. After 30 min stirring the reaction mixture was allowed to warm to room temperature. After 10 min at room temperature the solution was again cooled to -78 °C and slowly added to a solution of 2 (2.13 g, 14.4 mmol, 1.0 eq.) in THF (50 ml). After 3 h at -78 °C the reaction was quenched by the addition of water (10 ml). The solvent THF was removed under reduced pressure. Chloroform (30 ml) was added and with diluted HCl a pH value of 7 was adjusted. The resulting emulsion was extracted with chloroform. The combined organic phases were dried over Na_2SO_4 and the solvent was removed under reduced pressure. After column chromatography on silica the product could be obtained as orange solid.

Yield:	1.83 g (8.06 mmol, 56 %)
R$_f$:	0.23 (hexane : ethyl acetate / 2 : 1)
^{1}H-NMR	(300 MHz, $CDCl_3$)
δ [ppm]:	8.51 (ddd, $^3J_{(H,H)}$ = 4.9 Hz, $^4J_{(H,H)}$ = 1.7 Hz, $^5J_{(H,H)}$ = 1.0 Hz, 1 H, C$\underline{H}^{Py, 6}$), 7.82-7.70 (m, 2 H, C$\underline{H}^{Py, 4}$, C$\underline{H}^{Py, 3}$), 7.25 (ddd, $^3J_{(H,H)}$ = 7.1 Hz, $^4J_{(H,H)}$ = 4.9 Hz, $^5J_{(H,H)}$ = 1.5 Hz, 1 H, C$\underline{H}^{Py, 5}$), 5.51 (s$_{br}$, 1 H, O$\underline{H}$), 3.33 (d, $^2J_{(H,H)}$ = 14.6 Hz, 2 H, C$\underline{H}$H), 3.11 (d, $^2J_{(H,H)}$ = 14.6 Hz, 2 H, CH$\underline{H}$), 3.08 (s, 4 H, SC$\underline{H_2}$C$\underline{H_2}$S)
^{13}C-NMR	(75 MHz, $CDCl_3$)
δ [ppm]:	162.8 ($\underline{C}^{Py, 2}$), 147.5 ($\underline{C}H^{Py, 6}$), 137.4 ($\underline{C}H^{Py, 4}$), 122.9 ($\underline{C}H^{Py, 3}$), 119.8 ($\underline{C}H^{Py, 5}$), 78.1 ($\underline{C}OH$), 45.4 ($\underline{C}H_2$), 38.7 (S$\underline{C}H_2\underline{C}H_2$S)
Mass spectrometry	EI$^+$
m/z (%):	227.1 (13) [M]$^+$, 209.1 (17) [M - OH]$^+$, 121.1 (100) [C$_7$H$_7$NO]$^+$, 79.1 (41) [pyridine]$^+$
IR	KBr
$\tilde{\nu}$ [cm^{-1}]:	3367 (m), 2924 (w), 2903 (w), 1680 (w), 1589 (s), 1569 (m), 1474 (s), 1431 (s), 1400 (s), 1375 (s), 1307 (w), 1283 (w), 1262 (m), 1217 (m), 1167 (m), 1119 (m), 1100 (w), 1048 (s), 995 (m), 971 (w), 924 (m), 898 (w), 857 (m), 800 (w), 764 (s), 714 (w), 679 (m), 640 (m), 617 (m), 567 (w), 532 (s), 481 (m), 442 (w), 410 (m)
Elemental analysis	$C_{10}H_{13}NOS_2$ (227.35 gmol^{-1})
Calculated (%):	C: 52.83, H: 5.76, N: 6.16, S: 28.21
Found (%):	C: 52.29, H: 5.95, N: 5.73, S: 28.74

Synthesis of 6-(pyridin-2-yl)-1,4-dithiepan-6-ol (L^{4H})

Under an atmosphere of dry N_2 a 2.5 M solution of ^{n}BuLi in hexanes (9.6 ml, 24.0 mmol, 1.5 eq.) was slowly added to a solution of 2-methylpyridine (2.23 g, 24.0 mmol, 1.5 eq.) in THF (50 ml) at -78 °C. After 30 min stirring, the reaction mixture was allowed to warm to room temperature. After 10 min at room temperature the solution was again cooled to -78 °C and slowly added to a solution of **2** (2.85 g, 16.0 mmol, 1.0 eq.) in THF (50 ml). After 3 h at -78 °C the reaction was stirred for 24 h at room temperature. The reaction was then quenched by the addition of brine (50 ml) and with diluted HCl a pH value of 7 was adjusted. The solution was extracted with chloroform until the organic phase becomes colourless. The combined organic phases were dried over Na_2SO_4 and the solvent was removed under reduced pressure. After column chromatography on silica the product could be obtained as orange solid.

Yield:	2.16 g (9.00 mmol, 56 %)
M$_P$:	54.3 °C
R$_f$:	0.23 (hexane : ethyl acetate / 2 : 1)
^{1}H-NMR	(500 MHz, CDCl$_3$)
δ [ppm]:	8.44 (d, 1 H, $^3J_{(H,H)}$ = 4.8 Hz, C$\underline{H}$$^{Py, 6}$), 7.61 (ddd, 1 H, $^3J_{(H,H)}$ = 7.7 Hz, $^4J_{(H,H)}$ = 7.7 Hz, $^5J_{(H,H)}$ = 1.8 Hz, C$\underline{H}$$^{Py, 4}$), 7.24-7.13 (m, 2 H, C$\underline{H}$$^{Py, 3}$, C$\underline{H}$$^{Py, 5}$), 6.25 (s$_{br}$, 1 H, O$\underline{H}$), 3.02 (s, 2 H, C^{Py}C$\underline{H_2}$), 2.97-2.83 (m, 8 H, C$\underline{H_2}$, SC$\underline{H_2}C\underline{H_2}$S)
^{13}C-NMR	(125 MHz, CDCl$_3$)
δ [ppm]:	158.5 ($\underline{C}$$^{Py, 2}$), 148.5 ($\underline{C}H^{Py, 6}$), 137.1 ($\underline{C}H^{Py, 4}$), 124.6 ($\underline{C}H^{Py, 3}$), 121.8 ($\underline{C}H^{Py, 5}$), 78.9 ($\underline{C}$OH), 44.4 (C^{Py}$\underline{C}H_2$), 43.5 ($\underline{C}H_2$), 38.3 (S$\underline{C}H_2$$\underline{C}H_2$S)
Mass spectrometry	ESI$^+$ (70 eV, MeOH)
m/z (%):	505.1 (17) [M$_2$ + Na]$^+$, 280.2 (10) [M + K]$^+$, 264.2 (100) [M + Na]$^+$, 242.2 (51) [M + H]$^+$, 224.1 (50) [M - OH]$^+$
IR	KBr
$\tilde{v}$[cm^{-1}]:	3328 (m), 2920 (w), 2901 (w), 1697 (w), 1591 (s), 1564 (m), 1472 (s), 1441 (s), 1420 (s), 1406 (s), 1323 (w), 1273 (m), 1179 (w), 1148 (m), 1098 (m), 1038 (s), 997 (w), 972 (w), 941 (w), 906 (m), 895 (m), 854 (m), 814 (m), 795 (m), 768 (s), 719 (w), 679 (w), 621 (m), 546 (w), 534 (w), 480 (m), 452 (w), 413 (w)
Elemental analysis	C$_{11}$H$_{15}$NOS$_2$ (241.37 gmol^{-1})
Calculated (%):	C: 54.74, H: 6.26, N: 5.80, S: 26.57
Found (%):	C: 54.34, H: 6.19, N: 5.58, S: 27.06

Synthesis of 6-(1-methyl-1*H*-imidazol-2-yl)-1,4-dithiepan-6-ol (L^{5H})

Under an atmosphere of dry N_2 a 1.6 M solution of ^{n}BuLi in hexanes (12.6 ml, 20.2 mmol, 1.5 eq.) was slowly added to a solution of 2-methylimidazole (1.66 g, 20.2 mmol, 1.5 eq.) in THF (50 ml) at -78 °C. After 30 min stirring the reaction mixture was allowed to warm to room temperature. After 10 min at room temperature the solution was again cooled to -78 °C and slowly added to a solution of **1** (2.00 g, 13.5 mmol, 1.0 eq.) in THF (50 ml). After 3 h at -78 °C the reaction was quenched by the addition of water (10 ml). The solvent THF was removed under reduced pressure. Chloroform (30 ml) was added and with diluted HCl a pH value of 7 was adjusted. The solution was extracted with chloroform and the combined organic phases were dried over Na_2SO_4 and the solvent was removed under reduced pressure. After column chromatography on silica the product could be obtained as yellow solid.

Yield:	2.55 g (11.1 mmol, 82 %)
R$_f$:	0.17 (methanol : chloroform / 1 : 6)
M$_P$:	181 °C
^{1}H-NMR	(500 MHz, CDCl$_3$)
δ [ppm]:	6.93 (s, 1 H, C$\underline{H}^{Im, 5}$), 6.82 (s, 1 H, C$\underline{H}^{Im, 4}$), 3.87 (s, 3H, NC$\underline{H}_3$), 3.57 (d, $^2J_{(H,H)}$ = 15.0 Hz, 2 H, C$\underline{H}$H), 3.14 (d, $^2J_{(H,H)}$ = 15.0 Hz, 2 H, CH$\underline{H}$), 3.03 (s, 4 H, SC$\underline{H}_2$C$\underline{H}_2$S)
^{13}C-NMR	(125 MHz, CDCl$_3$):
δ [ppm]:	148.2 ($\underline{C}^{Im, 2}$), 126.6 ($\underline{C}H^{Im, 4}$), 123.1 ($\underline{C}H^{Im, 5}$), 75.8 ($\underline{C}OH$), 44.3 ($\underline{C}H_2$), 36.8 (S$\underline{C}H_2\underline{C}H_2$S), 35.1 (N$\underline{C}H_3$)
Mass spectrometry	EI$^+$
m/z (%):	230 (9) [M]$^+$, 213 (4) [M - OH]$^+$, 183 (42) [M -SCH$_3$]$^+$, 156 (84) [C$_6$H$_8$N$_2$OS]$^+$, 124 (60) [C$_6$H$_8$N$_2$O]$^+$, 114 (100) [C$_5$H$_{10}$N$_2$O]$^+$, 82 (28) [C$_4$H$_6$N$_2$]$^+$
IR	KBr
$\tilde{V}$[cm^{-1}]:	3104 (m), 2923 (m), 2902 (m), 1599 (w), 1526 (w), 1473 (s), 1406 (s), 1370 (m), 1337 (w), 1300 (w), 1275 (s), 1251 (m), 1221 (w), 1192 (m), 1181 (w), 1145 (w), 1106 (m), 1036 (s), 999 (m), 979 (m), 938 (w), 918 (s), 854 (w), 806 (m), 787 (w), 763 (s), 732 (s), 689 (m), 658 (m), 555 (w), 492 (w), 470 (w), 431 (w)
Elemental analysis	C$_9$H$_{14}$N$_2$OS$_2$ (230.35 gmol^{-1})
Calculated (%):	C: 46.93, H: 6.13, N: 12.16, S: 27.84
Found (%):	C: 47.60, H: 6.00, N: 11.54, S: 27.18

Synthesis of tris(2-pyridylmethyl)amine (L^6H)

The ligand **L^6H** was synthesised according to the literature.[251]

Yield:	87 % (Lit.: 99 %)
R_f:	0.42 (chloroform : methanol / 9 : 1)
M_p:	60.8 °C
^{1}H-NMR	(300 MHz, CDCl$_3$)

δ [ppm]: 8.59 (d, $^3J_{(H,H)}$ = 3 Hz, 3 H, C$\underline{H}^{Py, 3,3',3''}$), 7.63 (t, $^3J_{(H,H)}$ = 6 Hz, 3 H, C$\underline{H}^{Py, 4,4',4''}$), 7.38 (d, $^3J_{(H,H)}$ = 6 Hz, 3 H, C$\underline{H}^{Py, 6,6',6''}$), 7.17 (t, $^3J_{(H,H)}$ = 6 Hz, 3 H, C$\underline{H}^{Py, 5,5',5''}$), 3.19 (s, 2 H, CN$\underline{H}_2$)

^{13}C-NMR (75 MHz, CDCl$_3$)

δ [ppm]: 165.02 ($\underline{C}^{Py, 2,2',2''}$), 148.76 ($\underline{C}H^{Py, 3,3',3''}$), 136.21 ($\underline{C}H^{Py, 4, 4',4''}$), 123.07 ($\underline{C}H^{Py, 6,6',6''}$), 121.83 ($\underline{C}H^{Py, 5,5',5''}$), 70.20 ($\underline{C}NH_2$)

Mass spectrometry EI$^+$

m/z (%): 262 (46) [M]$^+$, 184 (100) [M - pyridine]$^+$, 80 (26) [pyridine + H]$^+$

IR KBr

$\tilde{V}$[cm^{-1}]: 3363 (w), 3295 (w), 3051 (w), 3004 (w), 1983 (w), 1949 (w), 1874 (w), 1678 (w), 1585 (s), 1467 (s), 1427 (s), 1324 (w), 1291 (m), 1237 (w), 1147 (m), 1117 (m), 1097 (m), 1049 (m), 994 (s), 903 (m), 874 (s), 785 (s), 772 (s), 747 (s), 659 (s), 617 (s), 584 (m), 504 (m), 457 (w), 405 (s)

Elemental analysis C$_{16}$H$_{14}$N$_4$ (262.31 gmol^{-1})

Calculated (%): C: 73.26, H: 5.38, N: 21.36

Found (%): C: 72.35, H: 5.36, N: 21.00

Synthesis of *N*-((1,4-dithian-2-yl)methyl)-*N*-(methylpyridin-2-yl)amine (L^{7H})

(2-Aminomethyl)pyridine (1.27 g 11.97 mmol, 1.5 eq.) and **V** (1.32 g, 7.86 mmol, 1 eq.) were dissolved in propane-2-ol (50 ml). The reaction was stirred under reflux at 120 °C for 6 d. The solvent was removed under reduced pressure and the product was purified by gradient column chromatography on silica. The product was obtained as brown oil.

Yield:	1.51 g (6.29 mmol, 80 %)
R$_f$:	0.44 (chloroform : methanol / 9 : 1)
^{1}H-NMR	(300 MHz, CDCl$_3$)

δ [ppm]:   8.52 (dd, $^3J_{(H,H)}$ = 9 Hz, $^4J_{(H,H)}$ = 3 Hz, 1 H, C$\underline{H}^{Py, 6}$), 7.67-7.60 (m, 1 H, C$\underline{H}^{Py, 4}$), 7.32 (d, $^3J_{(H,H)}$ = 9 Hz, 1 H, C$\underline{H}^{Py, 3}$) 7.15 (ddd, $^3J_{(H,H)}$ = 12 Hz, $^4J_{(H,H)}$ = 6 Hz, 1 H, C$\underline{H}^{Py, 5}$), 4.01-3.91 (m, 2 H, C$\underline{H}_2$), 3.50-2.63 (m, 11 H, C$\underline{H}_2$, C$\underline{H}_2^{Cylc}$, C$\underline{H}^{Cylc}$)

^{13}C-NMR   (75 MHz, CDCl$_3$)

δ [ppm]:   158.66 ($\underline{C}^{Py, 2}$), 149.29 ($\underline{C}H^{Py, 6}$), 136.55 ($\underline{C}H^{Py, 4}$), 122.19 ($\underline{C}H^{Py, 3, 5}$), 54.46 ($\underline{C}H_2{}^9$), 52.47 ($\underline{C}H_2{}^7$), 40.61 ($\underline{C}H^{10}$), 37.48 ($\underline{C}H_2{}^{14}$), 28.39 ($\underline{C}H_2{}^{11}$), 28.92 ($\underline{C}H_2{}^{13}$)

Mass spectrometry   ESI$^+$ (70 eV, MeOH)

m/z (%):   263 (64) [M + Na]$^+$, 241 (100) [M + H]$^+$

IR   KBr

$\tilde{\nu}$ [cm^{-1}]:   3306 (s), 3051 (m), 3007 (m), 2902 (s), 2825 (s), 1725 (w), 1672 (w), 1591 (s), 1569 (s), 1474 (m), 1434 (m), 1411 (m),1355 (w), 1283 (m), 1146 (m), 1124 (m), 1048 (m), 995 (m), 887 (w), 849 (w), 758 (m)

Elemental analysis   C$_{11}$H$_{16}$N$_2$S$_2$ (240.39 gmol^{-1})

Calculated (%):   C: 54.96, H: 6.71, N; 11.65, S: 26.68

Found (%):   C: 53.55, H: 6.73, N: 11.38, S: 24.94

Synthesis of 6-(6-(2-(pyridin-2-yl)propan-2-yl)pyridin-2-yl)-1,4-dithiepan-6-ol (L^{8H})

Under a N$_2$-atmosphere 1.6 M ^{n}BuLi (1.81 ml, 2.89 mmol, 1.2 eq.) was slowly added to a -78 °C cooled solution of **IX** (0.80 g, 2.89 mmol, 1.2 eq.) in THF (120 ml) and stirred for 45 min. Then the mixture was allowed to warm to room temperature, stirred for 10 min at this temperature before it was recooled to -78 °C and **II** (0.36 g, 2.41 mmol, 1.0 eq.) was slowly added. After 4 h at -78 °C the reaction was allowed to warm to room temperature and quenched by the addition of brine (30 ml). THF was removed under reduced pressure and the pH was adjusted to 7. The solution was extracted with chloroform, the combined organic phases were dried over Na$_2$SO$_4$ and the solvent was removed under reduced pressure. After column chromatography on silica the product could be obtained as yellow oil.

Yield: 0.56 g (1.62 mmol, 67 %)

R$_f$: 0.38 (hexane : ethyl acetate / 2 : 1)

^{1}H-NMR (300 MHz, CDCl$_3$)

δ [ppm]: 8.56 (ddd, $^3J_{(H,H)}$ = 6 Hz, $^4J_{(H,H)}$ = 1 Hz, $^5J_{(H,H)}$ = 1 Hz, 1 H, C$\underline{H}^{Py, 10}$), 7.67-7.57 (m, 3 H, C$\underline{H}^{Py, 4, 5, 12}$), 7.21 (dd, $^3J_{(H,H)}$ = 9 Hz, $^4J_{(H,H)}$ = 1 Hz, 1 H, C$\underline{H}^{Py, 3}$), 7.13 (m, 2 H, C$\underline{H}^{Py, 11, 13}$), 5.79 (s, 1 H, O$\underline{H}$), 3.26 (d, 2 H, $^3J_{(H,H)}$ = 15 Hz, C$\underline{H}$H), 3.26 (d, 2 H, $^3J_{(H,H)}$ = 15 Hz, CH$\underline{H}$), 3.04 (s, 4 H, SC$\underline{H}_2$C$\underline{H}_2$S) 1.81 (s, 6 H, C$\underline{H}_3$)

^{13}C-NMR (75 MHz, CDCl$_3$)

δ [ppm]: 166.00 ($\underline{C}^{Py, 2}$), 164.63 ($\underline{C}^{Py, 6}$), 160.05 ($\underline{C}^{Py, 8}$), 147.68 ($\underline{C}H^{Py, 10}$), 136.74 ($\underline{C}H^{Py, 4}$), 135.18 ($\underline{C}H^{Py, 12}$), 120.16 ($\underline{C}H^{Py, 13}$), 120.15 ($\underline{C}H^{Py, 11}$), 119.45 ($\underline{C}H^{Py, 5}$), 118.98 ($\underline{C}H^{Py, 3}$), 77.45 ($\underline{C}OH$), 47.10 ($\underline{C}C_4$), 44.37 ($\underline{C}HH$), 38.10 (S$\underline{C}H_2\underline{C}H_2$S), 27.43 ($\underline{C}H_3$)

Mass spectrometry ESI$^+$ (70 eV, MeOH)

m/z (%): 369.1 (100) [M + Na]$^+$, 347.1 (52) [M + H]$^+$, 329.1 (33) [M - OH]$^+$

IR KBr

$\tilde{V}$[cm^{-1}]: 3328 (w), 2968 (w), 2922 (w), 1574 (s), 1472 (m), 1452 (m), 1429 (m), 1408 (m), 1265 (w), 1181 (w), 1174 (s), 1115 (m), 1049 (m), 993 (m), 790 (m), 749 (s), 609 (w), 560 (w), 500 (w)

Elemental analysis C$_{18}$H$_{22}$N$_2$OS$_2$ (346.51 gmol^{-1})

Calculated (%): C: 62.39, H: 6.40, N: 8.08, S: 18.51

Found (%): C: 61.90, H: 6.38, N: 7.86, S: 17.56

Synthesis of 2-(6-methoxy-1,4-dithiepan-6-yl)pyridine (L^{3Me})

L^{3H} (300 mg, 1.33 mmol, 1.0 eq.) and NaH (60 %, 63 mg, 1.59 mmol, 1.2 eq.) were dissolved in abs. THF (25 ml) and heated under reflux at 60 °C for 30 min. Methyl iodide (226 mg, 1.59 mmol, 1.2 eq.) was added to the formed suspension and heating was continued for an additional 1 h. Then the reaction was allowed to cool to room temperature and quenched by the addition of brine (20 ml). The solution was extracted with chloroform, the combined organic phases were dried over Na_2SO_4 and the solvent was removed under reduced pressure. After column chromatography on silica the product could be obtained as brown solid.

Yield: 313 mg (1.30 mmol, 98 %)

R$_f$: 0.38 (hexane : ethyl acetate / 2 : 1)

M$_P$: 120.2 °C

^{1}H-NMR (300 MHz, CDCl$_3$)

δ [ppm]: 8.62 (ddd, $^3J_{(H,H)}$ = 6 Hz, $^4J_{(H,H)}$ = 1 Hz, $^5J_{(H,H)}$ = 1 Hz, 1 H, C$\underline{H}^{Py, 6}$), 7.73 (ddd, $^3J_{(H,H)}$ = 9 Hz, $^3J_{(H,H)}$ = 9 Hz, $^4J_{(H,H)}$ = 1 Hz, 1 H, C$\underline{H}^{Py, 4}$), 7.49 (ddd, $^3J_{(H,H)}$ = 9 Hz, $^3J_{(H,H)}$ = 3 Hz, $^4J_{(H,H)}$ = 1 Hz, 1 H, C$\underline{H}^{Py, 3}$), 7.23 (ddd, $^3J_{(H,H)}$ = 9 Hz, $^3J_{(H,H)}$ = 3 Hz, $^4J_{(H,H)}$ = 1 Hz, 1 H, C$\underline{H}^{Py, 5}$), 3.71 (d, $^2J_{(H,H)}$ = 15 Hz, 2 H, C$\underline{H}$H), 3.35 (d, $^2J_{(H,H)}$ = 15 Hz, 2 H, CH$\underline{H}$), 3.09 (s, 4 H, SC$\underline{H}_2$C$\underline{H}_2$S), 3.04 (s, 3 H, OC$\underline{H}_3$)

^{13}C-NMR (75 MHz, CDCl$_3$)

δ [ppm]: 161.43 ($\underline{C}$OCH$_3$), 148.70 ($\underline{C}^{Py, 2}$), 136.71 ($\underline{C}$H$^{Py, 6}$), 122.75 ($\underline{C}$H$^{Py, 4}$), 121.35 ($\underline{C}$H$^{Py, 3}$), 86.58 ($\underline{C}$H$^{Py, 5}$), 51.37 (O$\underline{C}$H$_3$), 41.37 ($\underline{C}$HH), 38.99 (S$\underline{C}$H$_2$$\underline{C}H_2$S)

Mass spectrometry ESI$^+$, (70 eV, MeOH)

m/z (%): 264.1 (33) [M + Na]$^+$, 242.1 (43) [M + H]$^+$, 210.1 (100) [M - OMe]$^+$, 150.1 (33) [C$_8$H$_8$NS]$^+$

IR KBr

$\tilde{V}$[cm^{-1}]: 3047 (w), 2981 (m), 2948 (m), 2932 (m), 2901 (m), 2827 (m), 1972 (w), 1872 (w), 1849 (w), 1730 (w), 1669 (w), 1584 (s), 1566 (m), 1470 (s), 1431 (s), 1407 (s), 1296 (m), 1270 (m), 1236 (m), 1190 (m), 1178 (m), 1153 (m), 1122 (m), 1096 (m), 1073 (s), 1009 (m), 995 (s), 982 (s), 930 (m), 850 (m), 802 (s), 775 (s), 763 (s), 740 (m), 712 (m), 682 (m), 638 (m), 614 (m), 492 (m), 465 (w), 436 (m), 403 (w)

Elemental analysis C$_{11}$H$_{15}$NOS$_2$ (241.37 g/mol)

Calculated (%): C: 54.74, H: 6.26, N: 5.80, S: 26.57

Found (%): C: 54.51, H: 6.18, N: 5.73, S: 26.38

Synthesis of 2-(6-methoxy-1,4-dithiepan-6-yl)-1-methyl-1H-imidazole (L^{5Me})

L^{5H} (300 mg, 1.30 mmol, 1.0 eq.) and NaH (60 %, 62 mg, 1.59 mmol, 1.2 eq.) were dissolved in abs. THF (25 ml) and stirred under reflux at 60 °C for 30 min. Methyl iodide (221 mg, 1.59 mmol, 1.2 eq.) was added to the formed suspension and heating was continued for an additional 1 h. The reaction was allowed to cool to room temperature and quenched by the addition of brine. The solution was extracted with chloroform, the combined organic phases dried over Na$_2$SO$_4$ and the solvent was removed under reduced pressure. After column chromatography on silica the product could be obtained as orange solid.

Yield:	318 mg (1.30 mmol, 100 %)
R$_f$:	0.50 (chloroform : methanol / 2 : 1)
M$_P$:	106.0 °C
^{1}H-NMR	(300 MHz, CDCl$_3$)
δ [ppm]:	6.69 (d, $^3J_{(H,H)}$ = 3 Hz, 1 H, C$\underline{H}^{Im, 5}$), 6.88 (d, $^3J_{(H,H)}$ = 3 Hz, 1 H, C$\underline{H}^{Im, 4}$), 3.79 (s, 3 H, NC$\underline{H}_3$), 3.75 (d, $^2J_{(H,H)}$ = 15 Hz, 2 H, C$\underline{H}$H), 3.43 (d, $^2J_{(H,H)}$ = 15 Hz, 2 H, CH$\underline{H}$), 3.08 (s, 4 H, SC$\underline{H}_2$C$\underline{H}_2$S), 3.02 (s, 3 H, OC$\underline{H}_3$)
^{13}C-NMR	(75 MHz, CDCl$_3$)
δ [ppm]:	146.42 (1 C, $\underline{C}^{Im, 2}$), 127.09 (1 C, $\underline{C}$H$^{Im, 4}$), 123.55 (1 C, $\underline{C}$H$^{Im, 5}$), 84.03 (1 C, $\underline{C}$OCH$_3$), 51.39 (O$\underline{C}$H$_3$), 40.08 ($\underline{C}$HH), 38.68 (S$\underline{C}$H$_2$$\underline{C}H_2$S), 33.99 (1 C, N$\underline{C}H_3$)
Mass spectrometry	EI
m/z (%):	244 (8) [M]$^+$, 213 (100) [M - OMe]$^+$
IR	KBr
$\tilde{v}$ [cm^{-1}]:	3127 (w), 3100 (m), 2976 (m), 2948 (w), 2934 (m), 2903 (m), 2826 (m), 1682 (w), 1599 (w), 1520 (w), 1472 (s), 1461 (s), 1443 (m), 1414 (s), 1396 (s), 1341 (w), 1302 (m), 1273 (s), 1254 (w), 1214 (m), 1185 (m), 1161 (m), 1140 (m), 1110 (m), 1073 (s), 1004 (w), 987 (w), 969 (s), 913 (m), 842 (m), 788 (m), 762 (s), 732 (w), 677 (m), 654 (m), 529 (m), 467 (w), 440 (w)
Elemental analysis	C$_{10}$H$_{16}$N$_2$OS$_2$ (244.38g/mol)
Calculated (%):	C: 49.15, H: 6.60, N: 11.46, S: 26.24
Found (%):	C: 48.96, H: 6.54, N: 11.42, S: 26.36

Synthesis of 2-(6-methoxy-1,4-dithiepan-6-yl)-6-(2-(pyridin-2-yl)propan-2-yl)pyridine (L^{8Me})

L^{8H} (50 mg, 0.14 mmol, 1.0 eq.) and NaH (60 %, 6 mg, 0.16 mmol, 1.1 eq.) were dissolved in abs. THF (5 ml) and stirred under reflux for 30 min. Methyl iodide (23 mg, 0.16 mmol, 1.1 eq.) was added to the formed suspension and heating was continued for an additional 1 h. Then the reaction was allowed to cool to room temperature and quenched by the addition of brine. The solution was extracted with chloroform, the combined organic phases dried over Na_2SO_4 and the solvent was removed under reduced pressure. After column chromatography on silica the product could be obtained as brown oil.

Yield:	48 mg (0.13 mmol, 95 %)
R$_f$:	0.51 (hexane : ethyl acetate / 2 : 1)
^{1}H-NMR	(300 MHz, CDCl$_3$)

δ [ppm]:   8.47 (ddd, $^3J_{(H,H)}$ = 6 Hz, $^4J_{(H,H)}$ = 3 Hz, $^5J_{(H,H)}$ = 1 Hz, 1 H, C$\underline{H}^{Py, 10}$), 7.54-7.44 (m, 2 H, C$\underline{H}^{Py, 4, 12}$), 7.21 (dd, $^3J_{(H,H)}$ = 6 Hz, $^4J_{(H,H)}$ = 1 Hz, 1 H, C$\underline{H}^{Py, 3}$), 7.18 (ddd, $^3J_{(H,H)}$ = 6 Hz, $^4J_{(H,H)}$ = 1 Hz, C$\underline{H}^{Py, 5}$), 7.03 (dd, $^3J_{(H,H)}$ = 6 Hz, $^4J_{(H,H)}$ = 1 Hz, 1 H, C$\underline{H}^{Py, 13}$), 6.98 (ddd, $^3J_{(H,H)}$ = 6 Hz, $^4J_{(H,H)}$ = 1 Hz, $^5J_{(H,H)}$ = 1 Hz, 1 H, C$\underline{H}^{Py, 11}$), 3.62 (d, $^2J_{(H,H)}$ = 15 Hz, 2 H, C$\underline{H}$H), 3.20 (d, $^2J_{(H,H)}$ = 15 Hz, 2 H, CH$\underline{H}$), 2.95-7.89 (m, 7 H,SC$\underline{H}_2$C$\underline{H}_2$S, OC$\underline{H}_3$), 1.74 (s, 6 H, C$\underline{H}_3$)

^{13}C-NMR	(75 MHz, CDCl$_3$)

δ [ppm]:   166.54 ($\underline{C}^{Py, 2}$), 165.65 ($\underline{C}^{Py, 6}$), 158.81 ($\underline{C}^{Py, 8}$), 147.42 ($\underline{C}H^{Py, 10}$), 135.93 ($\underline{C}H^{Py, 4}$), 135.02 ($\underline{C}H^{Py, 12}$), 120.06 ($\underline{C}H^{Py, 13}$), 119.89 ($\underline{C}H^{Py, 11}$), 118.85 ($\underline{C}H^{Py, 5}$), 117.28 ($\underline{C}H^{Py, 3}$), 85.76 ($\underline{C}OCH_3$), 47.26 ($\underline{C}C_4$), 40.46 ($\underline{C}HH$), 38.02 (S$\underline{C}H_2\underline{C}H_2$S), 27.29 (C$\underline{C}H_3$)

Mass spectrometry	ESI$^+$ (70 eV, MeOH)
m/z (%):	383.0 (52) [M + Na]$^+$, 361.0 (100) [M]$^+$, 329.0 (37) [M - OMe]$^+$
IR	KBr

$\tilde{V}$[cm^{-1}]:   3292 (w), 3057 (w), 2970 (m), 2927 (m), 2903 (m), 2861 (w), 1719 (w), 1574 (s), 1472 (s), 1448 (s), 1428 (s), 1409 (s), 1359 (m), 1293 (w), 1269 (w), 1165 (w), 114 (m), 1060 (s), 993 (m), 930 (w), 856 (w), 820 (m), 790 (m), 750 (s), 670 (w), 629 (m), 609 (m), 566 (w)

Elemental analysis	$C_{19}H_{24}N_2OS_2$ (360.54 gmol^{-1})
Calculated (%):	C: 63.30, H: 6.71, N: 7.77, S: 17.79
Found (%):	C: 65.07, H: 6.03, N: 6.78, S: 15.65

Synthesis of 2-(6-(prop-2-ynyloxy)-1,4-dithiepan-6-yl)pyridine (L^{3Ac})

L^{3H} (0.67 g, 2.96 mmol, 1.0 eq.) and NaH (60 %, 0.12 g, 4.44 mmol, 1.5 eq.) were dissolved in abs. THF (30 ml) and stirred under reflux for 30 min. Propargyle bromide (80 % in toluene, 0.12 g, 2.96 mmol, 1.0 eq.) was added to the formed suspension and the reaction was stirred over night at room temperature. Then then reaction was quenched by the addition of brine. The solution was extracted with DCM, the combined organic phases were dried over Na_2SO_4 and the solvent was removed under reduced pressure. After column chromatography on silica the product could be obtained as yellow solid.

Yield:	0.63 g (2.37 mmol, 80 %)
R$_f$:	0.19 (hexane : ethyl acetate / 5 : 1)
^{1}H-NMR	(300 MHz, CDCl$_3$)
δ [ppm]:	8.62 (ddd, $^3J_{(H,H)}$ = 6 Hz, $^4J_{(H,H)}$ = 1 Hz, $^5J_{(H,H)}$ = 1 Hz, 1 H, C$\underline{H}^{Py, 6}$), 7.74 (ddd, $^3J_{(H,H)}$ = 9 Hz, $^3J_{(H,H)}$ = 9 Hz, $^4J_{(H,H)}$ = 1 Hz, 1 H, C$\underline{H}^{Py, 4}$), 7.58 (ddd, $^3J_{(H,H)}$ = 9 Hz, $^3J_{(H,H)}$ = 3 Hz, $^4J_{(H,H)}$ = 1 Hz, 1 H, C$\underline{H}^{Py, 3}$), 7.25 (ddd, $^4J_{(H,H)}$ = 9 Hz, $^3J_{(H,H)}$ = 3 Hz, $^4J_{(H,H)}$ = 1 Hz, 1 H, C$\underline{H}^{Py, 5}$), 3.91 (d, $^4J_{(H,H)}$ = 3 Hz, 2 H, OC$\underline{H}_2$), 3.73 (d, $^2J_{(H,H)}$ = 15 Hz, 2 H, C$\underline{H}$H), 3.05 (d, $^2J_{(H,H)}$ = 15 Hz, 2 H, CH$\underline{H}$), 3.06-3.03 (m, 4 H, SC$\underline{H}_2$C$\underline{H}_2$S), 2.41 (t, 3 H, $^4J_{(H,H)}$ = 3 Hz, 1 H, CC$\underline{H}$)
^{13}C-NMR	(75 MHz, CDCl$_3$)
δ [ppm]:	160.88 ($\underline{C}$OCH$_2$), 148.61 ($\underline{C}^{Py, 2}$), 137.00 ($\underline{C}$H$^{Py, 6}$), 123.05 ($\underline{C}$H$^{Py, 4}$), 121.49 ($\underline{C}$H$^{Py, 3}$), 87.72 ($\underline{C}$H$^{Py, 5}$), 80.25 ($\underline{C}$CH), 74.15 (C$\underline{C}$H), 52.38 (O$\underline{C}$H$_2$), 41.38 ($\underline{C}$HH), 38.91 (S$\underline{C}$H$_2$$\underline{C}H_2$S)
Mass spectrometry	ESI$^+$ (70 eV, MeOH)
m/z (%):	266.11 (100) [M + H]$^+$, 210.1 (57) [M - OCH$_2$CCH]$^+$
Elemental analysis	C$_{13}$H$_{15}$NOS$_2$ (265.39 g/mol)
Calculated (%):	C: 58.83, H: 5.70, N: 5.28, S: 24.61
Found (%):	C: 58.36, H: 5.37, N: 4.34, S: 23.95

Synthesis of 1-methyl-2-(6-(prop-2-ynyloxy)-1,4-dithiepan-6-yl)-1*H*-imidazole (L^{5Ac})

L^{5H} (0.68 g, 2.96 mmol, 1.0 eq.) and NaH (60 %, 0.12 g, 4.44 mmol, 1.5 eq.) were dissolved in abs. THF (30 ml) and heated under reflux at 60 °C for 30 min. Propargyle bromide (80 % in toluene, 0.66 g, 2.96 mmol, 1.0 eq.) was added to the formed suspension and the mixture was stirred over night at room temperature. Then the reaction was quenched by the addition of brine. The solution was extracted with DCM, the combined organic phases were dried over Na_2SO_4 and the solvent was removed under reduced pressure. After column chromatography on silica the product could be obtained as yellow solid.

Yield: 0.52 g (1.92 mmol, 65 %)

R$_f$: 0.43 (hexane : ethyl acetate / 1 : 1)

M$_P$: 112.0 °C

^{1}H-NMR (300 MHz, $CDCl_3$)

δ [ppm]: 6.99 (d, $^3J_{(H,H)}$ = 1 Hz, 1 H, C$\underline{H}^{Im, 5}$), 6.89 (d, $^3J_{(H,H)}$ = 1 Hz, 1 H, C$\underline{H}^{Im, 4}$), 3.92 (d, $^4J_{(H,H)}$ = 3 Hz, 1 H, OC$\underline{H}_2$), 3.83 (s, 3 H, NC$\underline{H}_3$), 3.79 (d, $^2J_{(H,H)}$ = 15 Hz, 2 H, C$\underline{H}$H), 3.51 (d, $^2J_{(H,H)}$ = 15 Hz, 2 H, CH$\underline{H}$), 3.03-3.01 (m, 4 H, SC$\underline{H}_2$C$\underline{H}_2$S), 2.39 (t, $^4J_{(H,H)}$ = 3 Hz, 1 H, CC$\underline{H}$)

^{13}C-NMR (125 MHz, $CDCl_3$)

δ [ppm]: 145.87 ($\underline{C}^{Im, 2}$), 127.13 (1 C, $\underline{C}$H$^{Im, 4}$), 123.89 ($\underline{C}$H$^{Im, 5}$), 84.59 ($\underline{C}$OCH$_2$), 79.33 ($\underline{C}$CH), 74.34 (C$\underline{C}$H) 52.27 (1 C, OC$\underline{H}_2$), 40.16 ($\underline{C}$HH), 38.63 (S$\underline{C}$H$_2$$\underline{C}H_2$S), 34.45 (N$\underline{C}H_3$)

Mass spectrometry EI$^+$

m/z (%): 268 (8) [M]$^+$, 213 (52) [M - OCH$_2$CCH]$^+$, 113 (100) [C$_5$H$_{10}$S$_2$]$^+$

IR KBr

$\tilde{v}$[cm^{-1}]: 3188 (m), 2957 (w), 2928 (m), 2855 (m), 2119 (m), 1704 (w), 1612 (w), 1516 (w), 1479 (m), 1468 (m), 1411 (s), 1372 (m), 1343 (m), 1281 (m), 1264 (m), 1224 (m), 1196 (w), 1182 (w), 1136 (m), 1122 (m), 1058 (s), 997 (s), 912 (s), 853 (m), 806 (s), 762 (s), 720 (s), 695 (s), 662 (s), 626 (m), 580 (m), 486 (w), 446 (w)

Elemental analysis $C_{12}H_{16}N_2OS_2$ (268.40g/mol)

Calculated (%): C: 53.70, H: 6.01, N: 10.44, S: 23.89

Found (%): C: 55.37, H: 6.34, N: 9.71, S: 22.43

Synthesis of 2-(6-(prop-2-yn-1-yloxy)-1,4-dithiepan-6-yl)-6-(2-(pyridin-2-yl)propan-2-yl) pyridine (L^{8Ac})

L^{8H} (100 mg, 0.29 mmol, 1.0 eq.) and NaH (60 %, 12 mg, 0.32 mmol, 1.1 eq.) were dissolved in abs. THF (10 ml) and heated under reflux for 1 h at 60 °C. Propargyle bromide (80 % in toluene, 47 mg, 0.32 mmol, 1.1 eq.) was added to the formed suspension and the reaction was heated for an additional 1 h at 60 °C. The reaction was quenched by the addition of brine. Then the solution was extracted with DCM, the combined organic phases were dried over Na$_2$SO$_4$ and the solvent was removed under reduced pressure. After column chromatography on silica the product could be obtained as brown solid.

Yield:	102 mg (0.27 mmol, 91 %)
R$_f$:	0.45 (hexane : ethyl acetate / 2 : 1)
^{1}H-NMR	(300 MHz, CDCl$_3$)
δ [ppm]:	8.47 (ddd, $^3J_{(H,H)}$ = 6 Hz, $^4J_{(H,H)}$ = 3 Hz, $^5J_{(H,H)}$ = 1 Hz, 1 H, C$\underline{H}^{Py, 10}$), 7.56-7.50 (m, 2 H, C$\underline{H}^{Py, 4, 12}$), 7.22 (dd, $^3J_{(H,H)}$ = 6 Hz, $^4J_{(H,H)}$ = 1 Hz, 1 H, C$\underline{H}^{Py, 3}$), 7.21 (ddd, $^3J_{(H,H)}$ = 6 Hz, $^4J_{(H,H)}$ = 1 Hz, C$\underline{H}^{Py, 5}$), 7.05-7.00 (dd, $^3J_{(H,H)}$ = 6 Hz, $^4J_{(H,H)}$ = 1 Hz, 1 H, C$\underline{H}^{Py, 11, 13}$), 3.74 (d, 2 H, $^4J_{(H,H)}$ = 3 Hz, OC$\underline{H_2}$), 3.63 (d, $^2J_{(H,H)}$ = 15 Hz, 2 H, C$\underline{H}$H), 3.29 (d, $^2J_{(H,H)}$ = 15 Hz, 2 H, CH$\underline{H}$), 2.98-2.85 (m, 4 H, SC$\underline{H_2}$C$\underline{H_2}$S), 2.27 (t, $^4J_{(H,H)}$ = 3 Hz, 1 H, CC$\underline{H}$), 1.75 (s, 6 H, C$\underline{H_3}$)
^{13}C-NMR	(75 MHz, CDCl$_3$)
δ [ppm]:	166.54 ($\underline{C}^{Py, 2}$), 165.65 ($\underline{C}^{Py, 6}$), 158.81 ($\underline{C}^{Py, 8}$), 147.42 ($\underline{C}H^{Py, 10}$), 135.93 ($\underline{C}H^{Py, 4}$), 135.02 ($\underline{C}H^{Py, 12}$), 120.06 ($\underline{C}H^{Py, 13}$), 119.89 ($\underline{C}H^{Py, 11}$), 118.85 ($\underline{C}H^{Py, 5}$), 117.28 ($\underline{C}H^{Py, 3}$), 85.76 ($\underline{C}OCH_3$), 47.26 ($\underline{C}C_4$), 40.46 ($\underline{C}HH$), 38.02 (S$\underline{C}H_2\underline{C}H_2$S), 27.29 (C$\underline{C}H_3$)
Mass spectrometry	ESI$^+$ (70 eV, MeOH)
m/z (%):	423.1 (24) [M + K]$^+$, 407.1 (100) [M + Na]$^+$, 385.0 (49) [M + H]$^+$, 329.0 (35) [M - OAc]$^+$, 269.1 (13) [C$_{16}$H$_{17}$N$_2$S]$^+$
General Information	C$_{21}$H$_{24}$N$_2$SO$_2$ (384.56 gmol^{-1})
Calculated (%):	C: 65.59, H: 6.29, N: 7.28, S: 16.68

Synthesis of *N*-(tri(pyridin-2-yl)methyl)acetamide (L^{6Acet})

The ligand **L^{6Acet}** was synthesised according to the literature.[339]

Yield:	71 % (Lit.: 71 %)
R$_f$:	0.64 (chloroform: methanol / 9 : 1)
M$_P$:	145.4 °C
^{1}H-NMR	(300 MHz, CDCl$_3$)

δ [ppm]: 9.31 (s, 1 H, N$\underline{H}$), 8.53 (d, $^3J_{(H,H)}$ = 6 Hz, 3 H, C$\underline{H}^{Py, \ 3,3',3''}$), 7.62 (dd, $^3J_{(H,H)}$ = 6 Hz, $^3J_{(H,H)}$ = 6 Hz, 3 H, C$\underline{H}^{Py, \ 4,4',4''}$), 7.58 (d, $^3J_{(H,H)}$ = 6 Hz, 3 H, C$\underline{H}^{Py, \ 6,6',6''}$), 7.16 (dd, $^3J_{(H,H)}$ = 6 Hz, $^3J_{(H,H)}$ = 6 Hz, 3 H, C$\underline{H}^{Py, \ 5,5',5''}$), 2.19 (s, 3 H, C$\underline{H}_3$)

^{13}C-NMR	(75 MHz, CDCl$_3$)

δ [ppm]: 168.91 ($\underline{C}$=O), 160.89 ($\underline{C}^{Py, \ 2,2',2''}$), 147.85 ($\underline{C}H^{Py, \ 3,3',3''}$), 136.09 ($\underline{C}H^{Py, \ 4,4',4''}$), 124.47 ($\underline{C}H^{Py, \ 6,6',6''}$), 122.08 ($\underline{C}H^{Py, \ 5,5',5''}$), 70.74 ($\underline{C}NH$), 24.18 ($\underline{C}H_3$)

Mass spectrometry	EI$^+$

m/z (%): 304.1 (3) [M]$^+$, 261.1 (29) [M - C$_2$H$_3$O]$^+$, 246.0 (37) [M - C$_2$H$_4$NO]$^+$, 245.0 (39) [M - C$_2$H$_5$NO]$^+$, 209.0 (100) [C$_{12}$H$_9$N$_3$O]$^+$, 184.0 (42) [C$_{11}$H$_{10}$N$_3$]$^+$

IR	KBr

$\tilde{v}$ [cm^{-1}]: 3277 (s), 3076 (w), 3048 (w), 3007 (w), 2927 (w), 1670 (s), 1588 (m), 1568 (m), 1498 (s), 1466 (s), 1429 (s), 1369 (m), 1298 (w), 1281 (m), 1199 (w), 1152 (w), 1121 (w), 1093 (w), 1053 (m), 999 (m), 939 (w), 787 (m), 768 (m), 749 (s), 695 (w), 662 (m), 621 (m), 586 (m), 558 (m), 534 (w), 478 (w), 408 (w)

Elemental analysis	C$_{18}$H$_{16}$N$_4$O (304.35 gmol^{-1})
Calculated (%):	C: 71.04, H: 5.30, N: 18.41
Found (%):	C: 70.31, H: 5.26, N: 18.35

11.3 Synthesis of the Multifunctional Tools

XIII

XIV

XV

XVI

XVII

XVIII

XIX

XX

XXI

XXII

XXIII

XXIV

XXV

XXVI

XXVII

XXVIII

CNL³

CNL⁵

L³BTA

L⁵BTA

L⁸BTA
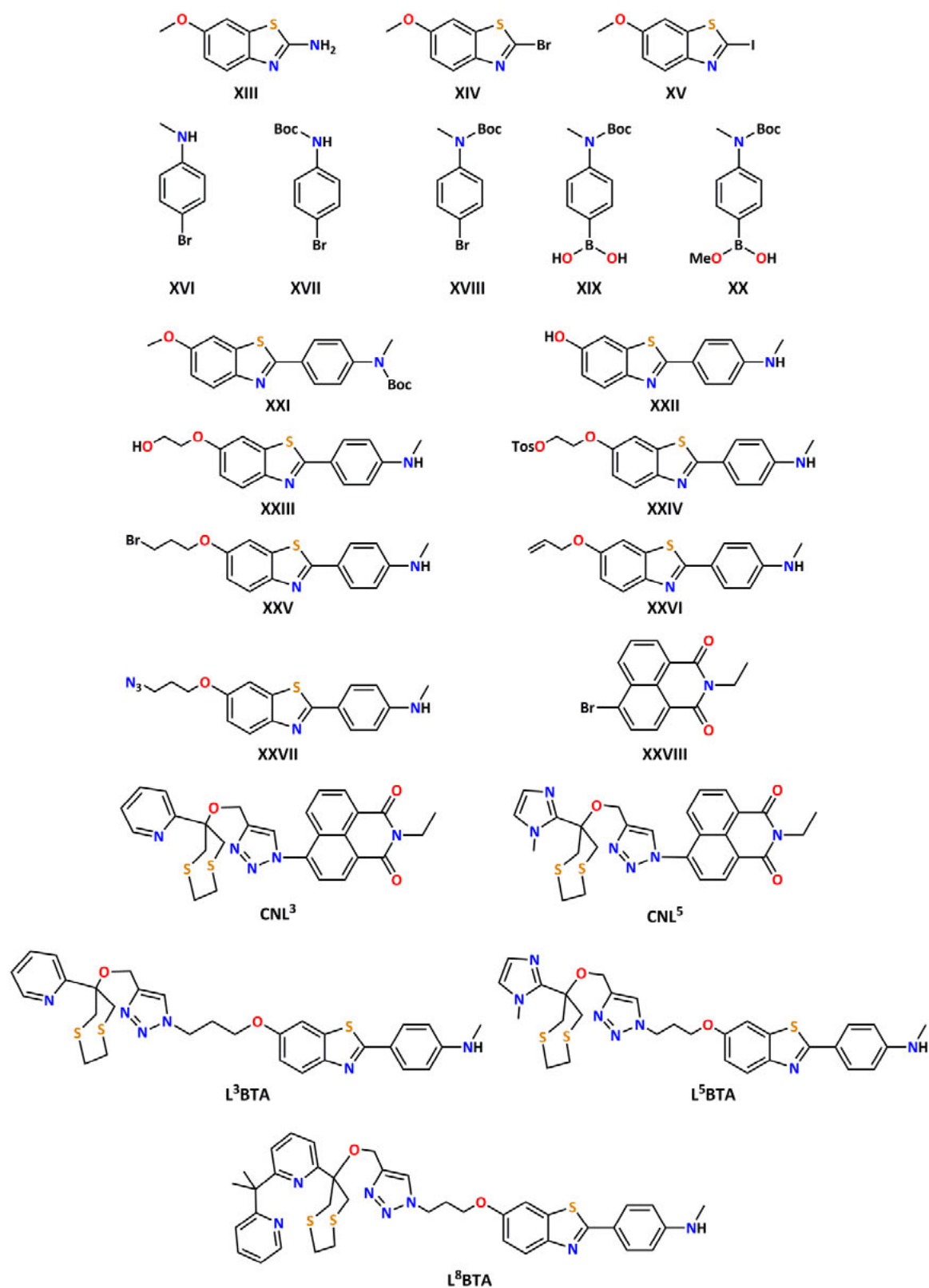
Synthesis of 6-methoxybenzo[*d*]thiazol-2-amine (XIII)

The compound **XIII** was synthesised according to the literature.[298]

Yield:	86 % (Lit.: 87 %)
R$_f$:	0.30 (hexane : ethyl acetate / 7 : 3)
M$_P$:	163.2 °C
^{1}H-NMR	(300 MHz, CDCl$_3$)
δ [ppm]:	7.46 (d, $^3J_{(H,H)}$ = 15 Hz, 1 H, C$\underline{H}^4$), 7.15 (s, 1 H, C$\underline{H}^7$), 6.92 (d, $^3J_{(H,H)}$ = 15 Hz, 1 H, C$\underline{H}^5$), 5.24 (sb, 2H, N$\underline{H}_2$) 3.84 (s, 3 H, OC$\underline{H}_3$)
^{13}C-NMR	(75 MHz, CDCl$_3$)
δ [ppm]:	164.67 ($\underline{C}^2$), 154.24 ($\underline{C}^6$), 146.81 ($\underline{C}^9$), 131.88 ($\underline{C}^8$), 118.04 ($\underline{C}H^4$), 112.84 ($\underline{C}H^5$), 105.50 ($\underline{C}H^7$), 55.51 (O$\underline{C}H_3$)
Mass spectrometry	EI$^+$
m/z (%):	180.1 (88) [M]$^+$, 165.1 (100) [M–NH$_2$]$^+$, 13.1 (16) [M–N-C-NH$_2$]$^+$
IR	KBr
$\tilde{V}$[cm^{-1}]:	3388 (s), 1641 (s), 1545 (s), 1462 (s), 1277 (s), 1205 (s), 1053 (s), 1021 (s), 806 (s), 3086 (m), 1338 (m), 1134 (m), 846 (m), 709 (m), 615 (m), 446 (m), 2744 (w), 2062 (w), 1849 (w), 904 (w), 545 (w)
Elemental analysis	C$_8$H$_8$N$_2$OS (180.23 gmol^{-1})
Calculated (%):	C: 53.31, H: 4.47, N: 15.54, S: 17.79
Found (%):	C: 52.88, H: 4.54, N: 15.47, S: 17.93

Synthesis of 2-bromo-6-methoxybenzo[*d*]thiazole (XIV)

The compound **XIV** was synthesised according to the literature.[299]

Yield:	74 % (Lit.: 79 %)
R$_f$:	0.61 (hexane : ethyl acetate / 2 : 1)
M$_P$:	52 °C
^{1}H-NMR	(300 MHz, CDCl$_3$)
δ [ppm]:	7.85 (d, $^3J_{(H,H)}$ = 9 Hz, 1 H, C$\underline{H}^4$), 7.24 (d, $^4J_{(H,H)}$ = 3 Hz, 1 H, C$\underline{H}^7$), 7.09 (dd, $^3J_{(H,H)}$ = 9 Hz, $^4J_{(H,H)}$ = 3 Hz, 1 H, C$\underline{H}^5$), 3.89 (s, 3 H, OC$\underline{H}_3$)
^{13}C-NMR	(75 MHz, CDCl$_3$)
δ [ppm]:	158.07 ($\underline{C}^6$), 150.13 ($\underline{C}^9$), 145.40 ($\underline{C}^8$), 137.40 ($\underline{C}^2$), 123.44 ($\underline{C}H^4$), 115.76 ($\underline{C}H^5$), 103.92 ($\underline{C}H^7$), 55.84 (O$\underline{C}H_3$)
Mass spectrometry	EI$^+$
m/z (%):	245 (100) [M + H]$^+$, 228 (56) [M - CH$_3$]$^+$
IR	KBr
$\tilde{V}$[cm^{-1}]:	3411 (w), 2987 (m), 2975 (m), 1607 (m), 1558 (m), 1493 (s), 1462 (s), 1437 (s), 1405 (m), 1318 (m), 1275 (s), 1252 (m), 1227 (w), 1210 (s), 1180 (m), 1152, 1074 (m), 1029 (s), 1012 (s), 886 (w), 843 (m), 807 (s), 223 (w), 700 (w), 673 (w), 601 (w), 575 (w), 527 (w), 471 (w), 426 (w)
General information	C$_8$H$_6$BrNOS (244.11 gmol^{-1})
Calculated (%):	C: 39.36, H: 2.48, N: 5.74, S: 13.14

Synthesis of 2-iodo-6-methoxybenzo[*d*]thiazole (XV)

To a cooled solution (10 °C) of *p*-toluene sulfuric acid (6.33 g, 33.3 mmol, 3.0 eq.) and 6-methoxy-2-benzothiazolamine (2.00 g, 11.1 mmol, 1.0 eq.) in MeCN (45 ml) was slowly added a solution of $NaNO_2$ (1.53 g, 22.2 mmol, 2 eq.) and KI (4.61 g, 27.8 mmol, 2.5 eq) in water (6.66 ml). During the reaction the temperature has to remain below 20 °C. After stirring an additional 3.5 h at this temperature, water (250 ml) was added and the pH value was adjusted to 9 by addition of a $NaHCO_3$ solution (1 M). Then an aqueous solution of $Na_2S_2O_3$ (2 M, 24 ml) were added to the reaction mixture and the crude product was obtained after extraction with chloroform (3 x 70 ml) and removal of the solvent under reduced pressure. Purification was done by column chromatography on silica. The product was obtained as brown solid.

Yield:	1.87 g (6.42 mmol, 58 %)
R$_f$:	0.59 (hexane : ethyl acetate / 2 : 1)
^{1}H-NMR	(500 MHz, CDCl$_3$)
δ [ppm]:	7.92 (d, $^3J_{(H,H)}$ = 15 Hz, 1 H, C$\underline{H}^4$), 7.30 (d, $^4J_{(H,H)}$ = 5 Hz, 1 H, C$\underline{H}^7$), 7.05 (dd, $^3J_{(H,H)}$ = 15 Hz, $^4J_{(H,H)}$ = 5 Hz, 1 H, C$\underline{H}^5$), 3.87 (s, 3 H, OC$\underline{H}_3$)
^{13}C-NMR	(125 MHz, CDCl$_3$)
δ [ppm]:	158.09 ($\underline{C}^6$), 149.02 ($\underline{C}^9$), 140.45 ($\underline{C}^8$), 123.00 ($\underline{C}H^4$), 115.62 ($\underline{C}H^5$), 103.09 ($\underline{C}H^7$), 101.45 ($\underline{C}^2$), 55.84 (O$\underline{C}H_3$)
Mass spectrometry	EI$^+$
m/z (%):	313.9 (16) [M + Na]$^+$, 291.9 (100) [M]$^+$, 165.2 (5) [M - I]$^+$
IR	KBr
$\tilde{v}$ [cm^{-1}]:	1598 (s), 1477 (s), 1406 (s), 1251 (s), 1223 (s), 952 (s), 812 (s), 1554 (m), 1319 (m), 1097 (m), 1055 (m), 663 (m), 599 (m), 3109 (w), 2961 (w), 2827 (w), 1878 (w), 514 (w)
Elemental analysis	C$_8$H$_6$INOS (291.11 gmol^{-1})
Calculated (%):	C: 33.01, H: 2.08, N: 4.81, S: 11.01
Found (%):	C: 32.25, H: 2.01, N: 4.74, S: 11.03

Synthesis of 4-bromo-*N*-methylaniline (XVI)

4-bromoaniline (3.02 g, 17.6 mmol, 1.0 eq.) was dissolved in acetonitrile (75 ml) and triethylamine (3.4 ml, 24.6 mmol, 1.4 eq.) was added. The solution was stirred for 1 h at room temperature before methyl iodide (2.50 g, 17.6 mmol, 1.0 eq.) was added. Then the reaction was heated at 60 °C and stirred for 16 h. The solvent was removed under reduced pressure and the crude product was purified by column chromatography on silica. The product could be obtained as white powder.

Yield:	1.31 g (7.0 mmol, 40 %)
R_f:	0.29 (hexane : ethyl acetate / 5 : 1)
^{1}H-NMR	(200 MHz, CDCl$_3$)
δ [ppm]:	7.28-7.20 (m, 2 H, C$\underline{H}^{3,5}$), 6.51-6.43 (m, 2 H, C$\underline{H}^{2,6}$), 3.78 (s, 1 H, N$\underline{H}$), 2.81 (s, 3 H, NC$\underline{H}_3$)
Mass spectrometry	EI$^+$
m/z (%):	187 (97) [M(^{81}Br)]$^+$, 185 (100) [M(^{79}Br)]$^+$, 105 [M - HBr]$^+$.
General Information	C$_7$H$_8$BrN (186.05 gmol^{-1})
Calculated (%):	C: 45.19, H: 4.33, N: 7.53

Synthesis of *tert*-butyl 4-bromophenylcarbamate (XVII)

A solution of 4-bromoaniline (2.00 g, 11.6 mmol, 1.0 eq) and di-*tert*-butyldicarbonate (4.2 g, 40.4 mmol, 3.5 eq.) in Et_3N/CH_3OH (10 %, 12 ml) was heated at 50 °C and stirred for 12 h. Then the volume was reduced to a small amount and dissolved in ethyl acetate (25 ml). After extraction with brine (3 x 15 ml), the organic phase was dried over Na_2SO_4 and the solvent was removed under reduced pressure. Column chromatography on silica provided a white powder.

Yield:	2.71 g (10.0 mmol, 87 %)
R$_f$:	0.30 (hexane : ethyl acetate / 5 : 1)
M$_P$:	104.1 °C
^{1}H-NMR	(300 MHz, CDCl$_3$)
δ [ppm]:	7.40 (d, $^3J_{(H,H)}$ = 6 Hz, 2 H, C$\underline{H}^{3,3'}$), 7.27 (d, $^3J_{(H,H)}$ = 6 Hz, 2 H, C$\underline{H}^{2,2'}$), 6.52 (s, 1 H, N$\underline{H}$), 1.53 (s, 9 H, C(C$\underline{H}_3$)$_3$)
^{13}C-NMR	(75 MHz, CDCl$_3$)
δ [ppm]:	152.53 ($\underline{C}O_2$), 137.49 ($\underline{C}^4$), 131.88 ($\underline{C}H^{2,2'}$), 120.08 ($\underline{C}H^{3,3'}$), 115.44 ($\underline{C}^1$), 88.91 ($\underline{C}(CH_3)_3$), 28.33 (C($\underline{C}H_3$)$_3$)
Mass spectrometry	ESI$^+$ (70 eV, MeOH)
m/z (%):	270.9 (14) [M]$^+$, 214.9 (48) [M - ^{t}Bu]$^+$, 170.9 (36) [M - Boc]$^+$, 57.0 (100) [^{t}Bu]$^+$
IR	KBr
$\tilde{v}$ [cm^{-1}]:	3370 (s), 2984 (s), 2934 (w), 1884 (w), 1696 (s), 1591 (m), 1518 (s), 1449 (m), 1395 (s), 1366 (s), 1306 (m), 1268 (m), 1238 (m), 1159 (m), 1116 (w), 1071 (m), 1053 (m), 1024 (m), 1007 (m), 931 (w), 905 (w), 816 (m), 765 (m), 693 (w), 635 (m), 613 (m), 498 (m), 433 (w)
General Information	$C_{11}H_{14}BrNO_2$ (272.14 gmol^{-1})
Calculated (%):	C: 48.55, H: 5.19, N: 5.15

Synthesis of *tert*-butyl 4-bromophenyl(methyl)carbamate (XVIII)

A suspension of **XVII** (2.50 g, 9.2 mmol, 1.0 eq.) (100 ml) and sodium hydride (60%, 0.67 g, 10.0 mmol, 1.1 eq.) in acetonitrile was stirred for 30 min at 60°C. Afterwards methyl iodide (1.42 g. 10.0 mmol, 1.1 eq.) was added and the reaction was stirred at 60°C for 20 h. The solvent was removed under reduced pressure and the residue was taken up in chloroform (20 ml) and filtered. Then the filtrate was concentrated under reduced pressure. The crude product could be obtained as yellow oil, which solidified at 4 °C.

Yield:	2.11 g (7.4 mmol, 80 %)
R_f:	0.59 (hexane : ethyl acetate / 2 : 1)
^{1}H-NMR	(300 MHz, CDCl$_3$)
δ [ppm]:	8.19 (d, $^3J_{(H,H)}$ = 9 Hz, 2 H, C$\underline{H}^{3,3'}$), 7.41 (d, $^3J_{(H,H)}$ = 6 Hz, 2 H, C$\underline{H}^{2,2'}$), 3.36 (s, 3 H, NC$\underline{H}_3$), 1.51 (s, 9H, C(C$\underline{H}_3)_3$)
^{13}C-NMR	(75 MHz, CDCl$_3$)
δ [ppm]:	154.47 ($\underline{C}O_2$), 147.80 ($\underline{C}^4$), 136.06 ($\underline{C}H^{3,3'}$), 134.04 ($\underline{C}^1$), 124.56 ($\underline{C}H^{2,2'}$), 80.77 ($\underline{C}(CH_3)_3$), 37.09 (N$\underline{C}H_3$), 28.36 (C($\underline{C}H_3)_3$)
Mass spectrometry	ESI$^+$ (70 eV, MeOH)
m/z (%):	594.9 (20) [2 M + Na]$^+$, 310 (100) [M + Na]$^+$, 253.9 (42) [M - ^{t}Bu + Na]$^+$, 230.0 (50) [M - ^{t}Bu]$^+$
IR	KBr
$\tilde{\nu}$ [cm^{-1}]:	3333 (w), 2976 (m), 2932 (w), 2834 (w), 1699 (s), 1600 (w), 1514 (s), 1456 (m), 1441 (m), 1366 (s), 1296 (m), 1247 (s), 1154 (s), 1110 (m), 1036 (m), 976 (w), 866 (w), 833 (m), 768 (w), 725 (w), 638 (w), 611 (w), 571 (w), 521 (w), 462 (w)
General Information	C$_{12}$H$_{16}$BrNO$_2$ (286.16 gmol^{-1})
Calculated (%):	C: 50.37, H: 5.64, N: 4.89

Synthesis of *tert*-butyl 4-(hydroxy(methoxy)boryl)phenyl(methyl)carbamate (XIX) and *tert*-butyl (4-(hydroxy(methoxy)boryl)phenyl)(methyl)carbamate (XX)

XVIII (2.00 g, 7.0 mmol, 1 eq.) was dissolved in abs. THF (80 ml) and 2.5 M ^{n}BuLi (3.08 ml, 7.7 mmol, 1.1 eq.) was slowly added at -78 °C. The reaction was stirred for 1.5 h at this temperature before trimethyl borate (2.39 ml, 21.0 mmol, 1.5 eq.) was added dropwise. After stirring at -78 °C for 30 min the reaction was allowed to warm up to room temperature and a saturated NH_4Cl-solution (80 ml) was added. Stirring for an additional 2 h at room temperature completed the reaction. The solution was extracted with DCM (4 x 100 ml), the combined organic layers were dried over Na_2SO_4 and the solvent was removed under reduced pressure. The crude product was obtained as a brown solid. The solid was purified by column chromatography on silica. First side products were removed by washing with hexane/ethyl acetate (2:1) and afterward the products were washed from the silica with methanol.

Analysis of **XIX**:

Yield:	351 mg (1.4 mmol, 20 %)
R$_f$:	0.08 (hexane : ethyl acetate / 2 : 1)
M$_P$:	125.3 °C
^{1}H-NMR	(200 MHz, $CDCl_3$)
δ [ppm]:	8.14 (d, $^3J_{(H,H)}$ = 8 Hz, 2 H, C$\underline{H}^{3,5}$), 7.36 (d, $^3J_{(H,H)}$ = 8 Hz, 2 H, C$\underline{H}^{2,6}$), 3.30 (s, 3 H, NC$\underline{H}_3$), 1.46 (s, 9 H, C(C$\underline{H}_3$)$_3$).
Mass spectrometry	EI$^+$
m/z (%):	251 (5) [M]$^+$, 151 (59) [M - *boc*]$^+$, 57 (100) [C_4H_9]$^+$
IR	KBr
$\tilde{v}$[cm^{-1}]:	3359 (s), 3038 (w), 2981 (m), 2936 (w), 2315 (w), 1682 (s), 1604 (m), 1567 (w), 1512 (w), 1480 (m), 1458 (m), 1429 (m), 1369 (s), 1332 (s), 1303 (m), 1261 (m), 1164 (m), 1112 (m), 1015 (m), 998 (m), 981 (m), 865 (m), 840 (s), 774 (s), 723 (m), 662 (m), 648 (s), 631 (m), 600 (w), 571 (w), 509 (w), 456 (w), 431 (w)
General Information	$C_{12}H_{18}BNO_4$ (251.09 gmol^{-1})
Calculated (%):	C: 57.40, H: 7.23, N: 5.58

Analysis of **XX**:

Yield:	4.0 g (14.0 mmol, 47 %)
R$_f$:	0.12 (hexane : ethyl acetate / 2 : 1)

M$_P$:	107.5 °C
^{1}H-NMR	(300 MHz, CDCl$_3$)
δ [ppm]:	7.98 (s, 1 H, BO$\underline{H}$), 7.73 (d, $^3J_{(H,H)}$ = 9 Hz, 2 H, C$\underline{H}^{2,2'}$), 7.21 (d, $^3J_{(H,H)}$ = 9 Hz, 2 H, C$\underline{H}^{3,3'}$), 3.33 (s, 3 H, NC$\underline{H}_3$), 3.17 (s, 3 H, BOC$\underline{H}_3$), 1.38 (s, 9 H, C(C$\underline{H}_3)_3$)
^{13}C-NMR	(75 MHz, CDCl$_3$)
δ [ppm]:	153.58 ($\underline{C}O_2$), 145.02 ($\underline{C}^4$), 134.34 (C$\underline{H}^{3,3'}$), 123.87 ($\underline{C}H^{2,2'}$), 79.57 ($\underline{C}(CH_3)_3$), 36.78 (N$\underline{C}H_3$), 27.89 (C($\underline{C}H_3)_3$)
Mass spectrometry	ESI$^+$ (70 eV, MeOH)
m/z (%):	288.1 (100) [M + Na]$^+$, 232.2 (46) [M - OMe]$^+$, 210.1 [M - ^{t}Bu]$^+$
IR	KBr
$\tilde{V}$[cm^{-1}]:	3318 (s), 2976 (s), 2913 (s), 2870 (s), 2791 (w), 2218 (s), 1665 (s), 1615 (s), 1565 (m), 1517 (w), 1478 (w), 1414 (m), 1369 (m), 1254 (m), 1198 (m), 1156 (s), 1109 (m), 1040 (w), 1018 (w), 977 (w), 928 (w), 865 (w), 940 (w), 770 (w), 723 (m), 652 (w), 573 (w), 535 (m), 505 (w), 465 (w), 428 (w)
General Information	C$_{12}$H$_{18}$BNO$_4$ (251.09 gmol^{-1})
Calculated (%):	C: 57.40, H: 7.23, N: 5.58

Synthesis of *tert*-butyl -4-(6-methoxybenzo[*d*]thiazol-2-yl)phenyl(methyl)carbamate (XXI)

Route A

$CuSO_4$ (0.67 g, 2.67 mmol, 1.3 eq.), tetrakis triphenylposphane palladium (0.12 g, 0.10 mmol, 0.05 eq.), potassium carbonate (0.57 g, 4.12 mmol, 1.5 eq.) and 1.0 eq. of the halogen **XIV** or **XV** were suspended in a mixture of DME (5 ml) and water (2 ml). 1.2-1.4 eq. of the mixture of **XIX**, and **XX** was added to the suspension and the reaction was heated under reflux at 100 °C for 24 h to 48 h. The solution was then cooled and ethyl acetate (5 ml) was added. The suspension was filtered through a thin layer of celite and the solvent of the filtrate was removed under reduced pressure. Column chromatography on silica gave the product as a yellow solid.

Yield: 0.94 g (2.54 mmol, 95 %)

Route B

$CuSO_4$ (0.67 g, 2.67 mmol, 1.3 eq.), tetrakis triphenylposphane palladium (0.12 g, 0.10 mmol, 0.05 eq.), potassium carbonate (0.57 g, 4.12 mmol, 1.5 eq.) and 1.0 eq. of the halogen **XIV** or **XV** were suspended in a mixture of DME (5 ml) and water (2 ml). 1.2-1.4 eq. of the mixture of **XIX**, and **XX** was added to the suspension and under microwave irradiation (250 W) stirred for 0.5 h-1 h. To the cooled solution ethyl acetate (5 ml) was added and the suspension was filtered through a thin layer of celite. The solvent of the filtrate was removed under reduced pressure. Column chromatography on silica gave the product as a yellow solid.

Yield: 0.97 g (2.62 mmol, 98 %)

R_f: 0.14 (hexane : ethyl acetate / 2 : 1)

M_P: 109.0 °C

^{1}H-NMR (300 MHz, $CDCl_3$)

δ [ppm]: 7.92 (d, $^3J_{(H,H)}$ = 9 Hz, 1 H, C$\underline{H}^7$), 7.91 (d, $^4J_{(H,H)}$ = 6 Hz, 1 H, C$\underline{H}^4$), 7.82 (d, $^3J_{(H,H)}$ = 9 Hz, 2 H, C$\underline{H}^{11,11'}$), 7.28 (dd, $^3J_{(H,H)}$ = 9 Hz, $^4J_{(H,H)}$ = 6 Hz, 1 H, C$\underline{H}^5$), 6.65 (d, $^3J_{(H,H)}$ = 9 Hz, 1 H, C$\underline{H}^{12,12'}$), 6.50 (q, $^3J_{(H,H)}$ = 6 Hz, 1 H, C$\underline{H}^{12,12'}$), 3.88 (s, 3 H, OC$\underline{H}_3$), 3.28 (d, 3 H, $^3J_{(H,H)}$ = 6 Hz, NC$\underline{H}_3$), 1.46 (s, 9 H, C(C$\underline{H}_3)_3$)

^{13}C-NMR (75 MHz, $CDCl_3$)

δ [ppm]: 168.67 ($\underline{C}^2$), 152.58 ($\underline{C}^6$), 151.79 ($\underline{C}O_2$), 147.21 ($\underline{C}^9$), 143.09 ($\underline{C}^{13}$), 134.23 ($\underline{C}^8$), 128.67 ($\underline{C}^{10}$), 121.96 ($\underline{C}H^{11,11'}$), 120.40 ($\underline{C}H^{12,12'}$), 119.73 ($\underline{C}H^4$), 111.48 ($\underline{C}H^5$), 99.51 ($\underline{C}H^7$), 80.39 ($\underline{C}(CH_3)_3$), 55.08 (OC$\underline{H}_3$), 29.27 (NC$\underline{H}_3$), 27.25 (C(C$\underline{H}_3)_3$)

Mass spectrometry ESI$^+$ (70 eV, MeOH)

m/z (%): 763.1 (49) [2M + Na]$^+$, 409.0 (34) [M + K]$^+$, 393.1 (74) [M + Na]$^+$, 371.1 (100) [M + H]$^+$, 315.0 (66) [M - ^{t}Bu]$^+$, 271.2 (53) [M - Boc]$^+$

IR KBr

| $\tilde{V}$ [cm^{-1}]: | 3007 (w), 2980 (m), 2939 (w), 2831 (w), 2875 (w), 1709 (s), 1605 (s), 1566 (m), 1524 (m), 1488 (m), 1463 (s), 1437 (m), 1425 (m), 1397 (w), 1367 (m), 1347 (m), 1318 (m), 1303 (m), 1283 (m), 1264 (m), 1225 (m), 1160 (m), 1117 (m), 1105 (m), 1060 (m), 1024 (m), 970 (m), 891 (w), 858 (m), 845 (m), 827 (s), 766 (m), 686 (w), 670 (m), 624 (w), 592 (m), 561 (w), 541 (w), 510 (w), 473 (w), 438 (w), 411 (w) |

Elemental analysis $C_{20}H_{22}N_2O_3S$ (370.14 gmol^{-1})

Calculated (%):   C: 64.84, H: 5.99, N: 7.56, S: 8.66

Found (%):   C: 64.44, H: 6.06, N: 7.17, S: 8.44

Synthesis of 2-(4-(methylamino)phenyl)benzo[*d*]thiazol-6-ol (XXII)

XXI (0.50 g, 1.35 mmol, 1.0 eq.) and boron tribromide (0.85 g., 3.37 mmol, 2.5 eq.) were dissolved in DCM (20 ml) and stirred at room temperature for 16 h. The reaction was quenched by addition of diluted HCl (5 %, 2 ml) and a pH value of 7 was adjusted with sodium carbonate. Extraction with ethyl acetate (3 x 10 ml), drying of the combined organic layers over Na_2SO_4 and removal of the solvent gave a yellow solid.

Yield:	0.97 g (3.07 mmol, 91 %)

^{1}H-NMR (300 MHz, CDCl$_3$)

δ [ppm]: 9.75 (sb, 1 H, CO$\underline{H}$), 7.75 (d, $^3J_{(H,H)}$ = 9 Hz, 2 H, C$\underline{H}^{11,11'}$), 7.70 (d, $^3J_{(H,H)}$ = 9 Hz, 1 H, C$\underline{H}^7$), 7.30 (d, $^4J_{(H,H)}$ = 6 Hz, 1 H, C$\underline{H}^4$), 6.91 (dd, $^3J_{(H,H)}$ = 9 Hz, $^4J_{(H,H)}$ = 3 Hz, 1 H, C$\underline{H}^5$), 6.64 (d, $^3J_{(H,H)}$ = 9 Hz, 2 H, C$\underline{H}^{12,12'}$), 2.75 (s, 3 H, NC$\underline{H}_3$)

^{13}C-NMR (75 MHz, CDCl$_3$)

δ [ppm]: 164.47 ($\underline{C}^2$), 159.79 ($\underline{C}^6$), 154.87 ($\underline{C}O_2$), 151.48 ($\underline{C}^9$), 147.17 ($\underline{C}^{13}$), 134.99 ($\underline{C}^8$), 128.14 ($\underline{C}^{10}$), 122.23 ($\underline{C}H^{11,11'}$), 120.45 ($\underline{C}H^{12,12'}$), 115.42 ($\underline{C}H^4$), 111.61 ($\underline{C}H^5$), 106.70 ($\underline{C}H^7$), 29.49 (N$\underline{C}H_3$)

Mass spectrometry ESI$^+$ (70 eV, MeOH)

m/z (%): 535.1 (6) [2M + Na]$^+$, 279.1 (11) [M + Na]$^+$, 257.0 (100) [M + H]$^+$, 242.0 (6) [M - CH$_3$]$^+$

IR KBr

$\tilde{v}$ [cm^{-1}]: 1610 (s), 1458 (s), 1240 (s), 1178 (s), 817 (s), 3394 (m), 1540 (m), 1487 (m), 1340 (m), 1279 (m), 1062 (m), 974 (m), 902 (m), 715 (m), 582 (m), 505 (m), 2870 (w), 2784 (w), 2662 (w), 538 (w)

Elemental analysis C$_{14}$H$_{12}$N$_2$OS (256.32 gmol^{-1})

Calculated (%): C: 65.60, H: 4.72, N: 10.93, S: 12.51

Found (%): C: 61.35, H: 4.83, N: 10.12, S: 11.78

Synthesis of 2-((2-(4-(methylamino)phenyl)benzo[*d*]thiazol-6-yl)oxy)ethanol (XXIII)

Potassium hydroxide (33 mg, 0.59 mmol, 1.5 eq.) and **XXII** (100 mg, 0.39 mmol, 1.0 eq.) were dissolved in aqueous ethanol (100 ml) and cooled to 0 °C. A large excess of ethane epoxide was added. After 30 min the reaction was allowed to warm to room temperature and stirred for an additional 1 h. A pH value of 7 was adjusted with diluted HCl and under reduced pressure the solution was reduced to a small amount. DCM was added and the phases were separated. The combined organic phases were dried over Na_2SO_4 and the solvent was removed under reduced pressure. The residue was purified by column chromatography on silica. The product was obtained as yellow solid.

Yield:	96 mg (0.32 mmol, 81 %)
R$_f$:	0.06 (hexane : ethyl acetate / 2 : 1)
M$_P$:	148.0 °C
^{1}H-NMR	(300 MHz, CDCl$_3$)
δ [ppm]:	7.78 (d, $^3J_{(H,H)}$ = 6 Hz, 1 H, C$\underline{H}^4$), 7. 76 (d, $^3J_{(H,H)}$ = 9 Hz, 2 H, C$\underline{H}^{11,11'}$), 7.62 (d, $^3J_{(H,H)}$ = 6 Hz, 1 H, C$\underline{H}^7$), 7.06 (dd, $^3J_{(H,H)}$ = 6 Hz, $^4J_{(H,H)}$ = 3 Hz, 1 H, C$\underline{H}^5$), 6.64 (d, $^3J_{(H,H)}$ = 9 Hz, 2 H, C$\underline{H}^{12,12'}$), 4.17 (t, $^3J_{(H,H)}$ = 6 Hz, 2 H, OC$\underline{H_2}$CH$_2$OH), 3.76 (t, $^3J_{(H,H)}$ = 6 Hz, 2 H, OCH$_2$C$\underline{H_2}$OH), 2.75 (s, 3 H, NC$\underline{H_3}$)
^{13}C-NMR	(75 MHz, CDCl$_3$)
δ [ppm]:	166.32 ($\underline{C}^2$), 156.10 ($\underline{C}^6$), 152.11 ($\underline{C}^9$), 142.91 ($\underline{C}^{13}$), 135.04 ($\underline{C}^8$), 128.24 ($\underline{C}^{10}$), 122.22 ($\underline{C}H^{11,11'}$), 120.25 ($\underline{C}H^{12,12'}$), 115.48 ($\underline{C}H^4$), 111.46 ($\underline{C}H^5$), 105.60 ($\underline{C}H^7$), 70.14 (O$\underline{C}H_2$CH$_2$OH), 59.55 (OCH$_2$$\underline{C}H_2$OH), 29.30 (N$\underline{C}H_3$)
Mass spectrometry	ESI$^+$ (70 eV, MeOH)
m/z (%):	623.1 (7) [2M + Na]$^+$, 345.1 (10) [M + K]$^+$, 323.1 (11) [M + Na]$^+$, 301.1 (100) [M + H]$^+$, 257.0 (8) [C$_{14}$H$_{13}$N$_2$OS]$^+$
IR	KBr
$\tilde{v}$ [cm^{-1}]:	3375 (w), 2938 (w), 2872 (w), 2817 (w), 2361 (w), 2341 (w), 1609 (s), 1560 (m), 1533 (m), 1509 (w), 1488 (m), 1449 (s), 1414 (w), 1380 (w), 1336 (m), 1312 (w), 1264 (m), 1225 (m), 1182 (m), 1160 (w), 1126 (w), 1064 (m), 1006 (w), 971 (w), 935 (m), 887 (w), 827 (s), 702 (w), 629 (w), 592 (w), 557 (w), 517 (w), 481 (w), 436 (w)
Elemental analysis	C$_{16}$H$_{16}$N$_2$O$_2$S (300.38 gmol^{-1})
Calculated (%):	C: 63.98, H: 5.37, N: 9.33, S: 10.67
Found (%):	C: 61.02, H: 5.54, N: 8.30, S: 10.03

Synthesis of 2-((2-(4-(methylamino)phenyl)benzo[*d*]thiazol-6-yl)oxy)ethyl 4-methylbenzene-sulfonate (XXIV)

XXIII (50 mg, 0.17, 1.0 eq.) was dissolved in MeCN (80 ml) and treated with NaH (60 %, 4 mg, 0.20 mmol, 1.2 eq.). The suspension was stirred for 15 min and then 4-toluenesulfonyl chloride (38 mg, 0.20 mmol, 1.2 eq.) was added. The mixture was stirred overnight at room temperature. Then the reaction was quenched by the addition of brine and the crude product was extracted with DCM. The combined organic phases were dried over Na_2SO_4 and the solvent was removed under reduced pressure. The product could be obtained as yellow solid.

Yield: 77 mg (0.17 mmol, 100 %)

Mass spectrometry ESI^+ (70 eV, MeOH)

m/z (%): 476.9 (11) $[M + Na]^+$, 455.1 (20) $[M + H]^+$, 301.1 (100) $[M - Tos]^+$, 257.0 (11) $[C_{14}H_{13}N_2OS]^+$

General Information $C_{23}H_{22}N_2O_4S_2$ (454.56 $gmol^{-1}$)

Calculated (%): C: 60.77, H: 4.88, N: 6.16, S: 14.11

Synthesis of 4-(6-(3-bromopropoxy)benzo[*d*]thiazol-2-yl)-*N*-methylaniline (XXV)

XXII (1.00 g, 0.17 mmol, 1.0 eq.) was dissolved in abs. MeCN (100 ml) and treated with NaH (60 %, 4 mg, 0.20 mmol, 1.2 eq.). The suspension was heated under reflux for 30 min at 60 °C. Then 1,3-dibromopropane (38 mg, 0.20 mmol, 1.2 eq.) was added and the mixture was stirred over night at 60 °C . The reaction was quenched by the addition of brine and the crude product was extracted with DCM. The combined organic phases were dried over Na_2SO_4 and the solvent was removed under reduced pressure. The product was purified through column chromatography on silica and could be obtained as yellow solid.

Yield:	0.56 g (3.50 mmol, 88 %)
R$_f$:	0.43 (hexane : ethyl acetate / 2 : 1)
M$_P$:	137.0 °C
^{1}H-NMR	(300 MHz, CDCl$_3$)
δ [ppm]:	7.91-7.87 (m, 3 H, C$\underline{H}^{4,\ 11,11'}$), 7.35 (s, 1 H, C$\underline{H}^7$) 7.06 (d, $^3J_{(H,H)}$ = 9 Hz, 1 H, C$\underline{H}^5$), 6.67 (d, $^3J_{(H,H)}$ = 9 Hz, 2 H, C$\underline{H}^{12,12'}$), 4.19 (t, $^3J_{(H,H)}$ = 6 Hz, 2 H, OC$\underline{H}_2$), 3.66 (t, $^3J_{(H,H)}$ = 6 Hz, 2 H, BrC$\underline{H}_2$), 2.93 (s, 3 H, NC$\underline{H}_3$), 2.38 (quint, $^3J_{(H,H)}$ = 6 Hz, 2 H, CH$_2$C$\underline{H}_2$CH$_2$)
^{13}C-NMR	(75 MHz, CDCl$_3$)
δ [ppm]:	165.65 ($\underline{C}^2$), 155.17 ($\underline{C}^6$), 150.27 ($\underline{C}^{13}$), 148.06 ($\underline{C}^9$), 134.79 ($\underline{C}^8$), 127.75 ($\underline{C}H^{11,11'}$), 121.83 ($\underline{C}H^4$), 118.98 ($\underline{C}^{10}$), 114.33 ($\underline{C}H^5$), 111.04 ($\underline{C}H^{12,12'}$), 104.31 ($\underline{C}H^7$), 65.00 (O$\underline{C}H_2$), 31.38 (CH$_2\underline{C}H_2$CH$_2$), 29.34 (Br$\underline{C}H_2$), 28.94 (N$\underline{C}H_3$)
Mass spectrometry	EI$^+$
m/z (%):	378 (12) [M + H]$^+$, 296 (7) [M - HBr]$^+$, 270 (10) [M - C$_2$H$_4$Br]$^+$, 255.0 (100) [M - C$_3$H$_6$Br]$^+$, 227.0 (10) [C$_{13}$H$_{11}$N$_3$S$_2$]$^+$
IR	KBr
$\tilde{v}$[cm^{-1}]:	3279 (w), 2925 (w), 2854 (w), 2360 (w), 1609 (s), 1561 (m), 1487 (m), 1455 (s), 1432 (m), 1416 (m), 1341 (m), 1313 (w), 1281 (m), 1263 (m), 1209 (m), 1181 (m), 1112 (w), 1063 (m), 1030 (w), 962 (w), 939 (w), 893 (w), 854 (w), 824 (m), 796 (m), 714 (w), 695 (w), 622 (w), 584 (w), 557 (w), 507 (w), 482 (w), 433 (w)
Elemental analysis	C$_{17}$H$_{17}$BrN$_2$OS (377.30 gmol^{-1})
Calculated (%):	C: 54.12, H: 4.54, N: 7.42, S: 8.50
Found (%):	C: 60.48, H: 6.01, N: 6.67, S: 8.01

Synthesis of 4-(6-(but-3-en-1-yloxy)benzo[*d*]thiazol-2-yl)-*N*-methylaniline (XXVI)

L^{3H} (453 g, 2.0 mmol, 1.0 eq.) and NaH (60 %, 80 mg, 2.2 mmol, 1.1 eq.) were dissolved in abs. THF (30 ml) and heated under reflux at 60 °C for 30 min. **XXV** (754 mg, 2.0 mmol, 1.0 eq.) was added to the formed suspension and the reaction was stirred for an additional 2 h at 60 °C. The reaction was quenched by the addition of brine, extracted with DCM and the combined organic phases were dried over Na_2SO_4. The solvent was removed under reduced pressure and the product was purified by column chromatography on silica. The product could be obtained as yellow solid. Instead of column chromatography a sauxlette with diethyl ether can also be used to extract the product.

Yield:	553 mg (1.78 mmol, 89 %)
R$_f$:	0.29 (hexane : ethyl acetate / 2 : 1)
M$_P$:	133.7 °C
^{1}H-NMR	(300 MHz, $CDCl_3$)
δ [ppm]:	7.82-7. 78 (m, 3 H, C$\underline{H}^4$, C$\underline{H}^{11,11'}$), 7.26 (d, $^4J_{(H,H)}$ = 1 Hz, 1 H, C$\underline{H}^7$), 6.98 (dd, $^3J_{(H,H)}$ = 3 Hz, $^4J_{(H,H)}$ = 1 Hz, 1 H, C$\underline{H}^5$), 6.57 (d, $^3J_{(H,H)}$ = 6 Hz, 2 H, C$\underline{H}^{12,12'}$), 6.05 (dq, $^3J_{(H,H)}$ = 6 Hz, $^4J_{(H,H)}$ = 3 Hz, 1 H, CH$_2$=C$\underline{H}$), 5.41 (d, $^3J_{(H,H)}$ = 18 Hz, 1 H, HC$\underline{H}_{trans}$=CH), 5.24 (d, $^3J_{(H,H)}$ = 18 Hz, 1 H, HC$\underline{H}_{cis}$=CH), 2.38 (d, $^3J_{(H,H)}$ = 3 Hz, 2 H, C$\underline{H}_2$O), 2.84 (s, 3 H, NC$\underline{H}_3$)
^{13}C-NMR	(75 MHz, $CDCl_3$)
δ [ppm]:	165.43 ($\underline{C}^2$), 156.21 ($\underline{C}^6$), 151.33 ($\underline{C}^{13}$), 133.14 (CH$_2$=$\underline{C}$H), 128.81 ($\underline{C}$H$^{11,11'}$), 122.79 ($\underline{C}^9$), 117.86 ($\underline{C}^{10}$), 115.58 ($\underline{C}^8$), 115.39 ($\underline{C}$H^4), 112.07 ($\underline{C}$H$^{12,12'}$), 110.86 ($\underline{C}$H$_2$=CH), 105.57 (CH^5), 105.32 ($\underline{C}$H^7), 69.50 ($\underline{C}$H$_2$O), 30.36 (N$\underline{C}$H$_3$)
Mass spectrometry	EI$^+$
m/z (%):	296 (22) [M]$^+$, 255 (100) [M - vinyl]$^+$, 227 (9) [C$_{13}$H$_9$NOS]$^+$
IR	KBr
$\tilde{V}$[cm^{-1}]:	3287 (w), 3151 (w), 3074 (w), 3038 (w), 2878 (w), 2821 (w), 1608 (s), 1561 (m), 1487 (s), 1455 (s), 1432 (m), 1417 (m), 1343 (m), 1313 (m), 1281 (m), 1265 (s), 1211 (m), 1181 (s), 1114 (w), 1061 (m), 1026 (m), 1005 (w), 965 (w), 927 (w), 894 (w), 859 (w), 826 (m), 795 (m), 766 (w), 716 (w), 697 (w), 622 (w), 586 (w), 562 (w), 509 (w), 485 (w), 434 (w)
General Information	C$_{18}$H$_{18}$N$_2$OS (310.41 gmol^{-1})
Calculated (%):	C: 69.65, H: 5.84, N: 9.02, S: 10.33

Synthesis of 4-(6-(3-azidopropoxy)benzo[*d*]thiazol-2-yl)-*N*-methylaniline (XXVII)

Sodium azide (52 mg, 0.80 mmol, 1.5 eq.) and **XXV** (200 mg, 0.53 mmol, 1.0 eq.) were dissolved in DMSO (10 ml) and stirred over night at 120 °C. The solvent was removed under reduced pressure and the crude product was suspended in water. The residue was separated by filtration and purified by column chromatography.

Yield:	152 mg (0.45 mmol, 85 %)
R$_f$:	0.30 (hexane : ethyl acetate / 2 : 1)
^{1}H-NMR	(300 MHz, CDCl$_3$)
δ [ppm]:	7.89-7.86 (m, 3 H, C$\underline{H}^{4,\ 11,11'}$), 7.33 (d, $^3J_{(H,H)}$ = 3 Hz, 1 H, C$\underline{H}^7$) 7.04 (dd, $^3J_{(H,H)}$ = 9 Hz, $^4J_{(H,H)}$ = 3 Hz, 1 H, C$\underline{H}^5$), 6.65 (d, $^3J_{(H,H)}$ = 9 Hz, 2 H, C$\underline{H}^{12,12'}$), 4.12 (t, $^3J_{(H,H)}$ = 6 Hz, 2 H, OC$\underline{H}_2$), 3.56 (t, $^3J_{(H,H)}$ = 6 Hz, 2 H, BrC$\underline{H}_2$), 2.99 (s, 3 H, NC$\underline{H}_3$), 2.10 (quint, $^3J_{(H,H)}$ = 6 Hz, 2 H, CH$_2$C$\underline{H}_2$CH$_2$)
^{13}C-NMR	(75 MHz, CDCl$_3$)
δ [ppm]:	165.63 ($\underline{C}^2$), 155.15 ($\underline{C}^6$), 150.30 ($\underline{C}^{13}$), 148.05 ($\underline{C}^9$), 134.78 ($\underline{C}^8$), 127.73 ($\underline{C}H^{11,11'}$), 121.81 ($\underline{C}H^4$), 118.99 ($\underline{C}^{10}$), 114.28 ($\underline{C}H^5$), 111.03 ($\underline{C}H^{12,12'}$), 104.25 ($\underline{C}H^7$), 64.18 (O$\underline{C}H_2$), 47.25 (CH$_2$$\underline{C}H_2CH_2$), 29.31 (N$\underline{C}H_3$), 28.34 (N$_3$$\underline{C}H_2$)
Mass spectrometry	ESI$^+$ (70 eV, MeOH)
m/z (%):	340.1 (100) [M + H]$^+$, 297.1 (86) [M - N$_3$]$^+$, 257.1 (75) [M - C$_3$H$_4$Br]$^+$, 255.1 (8) [M - C$_3$H$_6$Br]$^+$, 101.0 (42) [C$_3$H$_7$N$_3$O]$^+$
IR	KBr
$\tilde{v}$[cm^{-1}]:	3269 (m), 2926 (w), 2877 (w), 2819 (w), 2098 (s), 1608 (s), 1561 (m), 1536 (w), 1491 (m), 1455 (s), 1416 (w), 1341 (m), 1313 (m), 1283 (m), 1263 (s), 1223 (s), 1182 (s), 1112 (w), 1064 (m), 1035 (w), 963 (w), 903 (w), 821 (m), 695 (w), 629 (w), 589 (w), 557 (w), 512 (w), 434 (w)
Elemental analysis	C$_{17}$H$_{17}$N$_5$OS (339.41 gmol^{-1})
Calculated (%):	C: 60.16, H: 5.05, N: 20.63, S: 9.45
Found (%):	C: 61.77, H: 5.27, N: 17.17, S: 10.01

Synthesis of 6-bromo-*N*-ethyl-1,8-naphthalimide (XXVIII)

XXVIII was synthesised according to the literature.[290]

Yield:	76 % (Lit.: 78 %)

^{1}H-NMR (300 MHz, CDCl$_3$)

δ [ppm]: 8.79 (d, $^3J_{(H,H)}$ = 9 Hz, 1 H, C$\underline{H}^4$), 8.59 (d, $^3J_{(H,H)}$ = 9 Hz, 1 H, C$\underline{H}^2$), 8.45 (d, $^3J_{(H,H)}$ = 9 Hz, 1 H, C$\underline{H}^7$), 8.07 (d, $^3J_{(H,H)}$ = 9 Hz, 1 H, C$\underline{H}^6$), 8.87 (dd, $^3J_{(H,H)}$ = 9 Hz, $^3J_{(H,H)}$ = 9 Hz, 1 H, C$\underline{H}^3$), 4.26 (q, $^3J_{(H,H)}$ = 9 Hz, 2 H, C$\underline{H}_2$), 1.36 (t, $^3J_{(H,H)}$ = 9 Hz, 3 H, C$\underline{H}_3$)

^{13}C-NMR (75 MHz, CDCl$_3$)

δ [ppm]: 163.45 ($\underline{C}$=O), 133.23($\underline{C}$H^2), 131.98($\underline{C}$H^7), 131.17(1 C, $\underline{C}^3$), 131.09 ($\underline{C}$H^6), 130.67 ($\underline{C}^5$), 130.19 ($\underline{C}^{1,8}$), 128.07($\underline{C}^{9,10}$), 35.64 ($\underline{C}$H$_2$), 13.30 ($\underline{C}$H$_3$)

Mass spectrometry EI$^+$

m/z (%): 304.9 (93) [M(^{81}Br)]$^+$, 302.9 (91) [M(^{79}Br)]$^+$, 276.9 (98) [M(^{81}Br) - C$_2$H$_4$]$^+$, 274.9 (100) [M(^{79}Br) - C$_2$H$_4$]$^+$, 259.9 (22) [M - C$_2$H$_6$N]$^+$, 232.9 (37) [M-C$_3$H$_6$NO]$^+$

General Information C$_{14}$H$_{10}$BrNO$_2$ (304.14 gmol^{-1})

Calculated (%): C: 55.29, H: 3.31, N: 4.61

Synthesis of 2-ethyl-6-(4-(((6-(pyridin-2-yl)-1,4-dithiepan-6-yl)oxy)methyl)-1*H*-1,2,3-triazol-1-yl)-1,8-naphthalimide (NCL^3)

A solution of **XXVIII** (152 mg, 0.50 mmol, 1.00 eq.), **L^{5Ac}** (100 mg, 0.38 mmol, 0.75 eq.), CuSO$_4$ (63 mg, 0.38 mmol, 0.75 eq.) and sodium ascorbate (0.74 g, 3.75 mmol, 7.50 eq.) were suspended in DMSO (30 ml) and stirred under reflux at 110 °C. After 24 h, the reaction was allowed to cool to room temperature and a conc. solution of sodium EDTA (50 ml) was added. The mixture was stored at 4 °C and the precipitate was separated by filtration. The residue was recrystallised from methanol/diethyl ether and further purified by column chromatography on silica. The product was obtained as brown solid.

Yield: 15 mg (0.04 mmol, 8 %)

R$_f$: 0.62 (chloroform : methanol / 9 : 1)

Mass spectrometry ESI$^+$ (70 eV, MeOH)

m/z (%): 1084.7 (8) [2M + Na]$^+$, 569.8 (31) [M + K]$^+$, 553.9 (100) [M + Na]$^+$, 531.9 (23) [M + H]$^+$, 210.0 (50) [C$_{10}$H$_{12}$NS$_2$]$^+$

General Information C$_{27}$H$_{25}$N$_5$O$_3$S$_2$ (531.14 gmol^{-1})

Calculated (%): C: 61.00, H: 4.74, N: 13.17, S: 12.06

Synthesis of 2-ethyl-6-(4-(((6-(1-methyl-1*H*-imidazol-2-yl)-1,4-dithiepan-6-yl)oxy)methyl)-1*H*-1,2,3-triazol-1-yl)-1,8-naphthalimide (NCL⁵)

A solution of **XXVIII** (152 mg, 0.50 mmol, 1.00 eq.), **L**^{5Ac} (128 mg, 0.96 mmol, 0.96 eq.), CuSO$_4$ (80 mg, 0.96 mmol, 0.96 eq.) and sodium ascorbate (0.95 g, 9.60 mmol, 9.60 eq.) were suspended in DMSO (30 ml) and stirred under reflux at 110 °C. After 24 h, the reaction was allowed to cool to room temperature and a conc. solution of sodium EDTA (50 ml) was added. The mixture was stored at 4 °C and the precipitate was separated by filtration. The residue was recrystallised from methanol/diethyl ether and further purified by column chromatography on silica. The product was obtained as brown solid.

Yield: 21 mg (0.04 mmol, 8 %)

R$_f$: 0.46 (chloroform : methanol / 2 : 1)

Mass spectrometry ESI$^+$ (70 eV, MeOH)

m/z (%): 556.9 (14) [M + Na]$^+$, 535.0 (22) [M + H]$^+$, 213.0 (13) [C$_9$H$_{13}$N$_2$S$_2$]$^+$, 213.0 (100) [C$_7$H$_{10}$N$_2$]$^+$

General Information C$_{26}$H$_{26}$N$_6$O$_3$S$_2$ (534.15 gmol^{-1})

Calculated (%): C: 58.41, H: 4.90, N: 15.72, S: 11.99

Synthesis of *N*-methyl-4-(6-(3-(4-((6-(pyridin-2-yl)-1,4-dithiepan-6-yloxy)methyl)-*1H*-1,2,3-triazol-1-yl)propoxy)benzo[*d*]thiazol-2-yl)aniline (L³BTA)

Sodium L-ascorbate (590 mg, 2.50 mmol, 10 eq.) was added to a solution of copper sulphate (42 mg, 0.25 mmol, 1.0 eq.), **L³ᴴ** (67 mg, 0.25 mmol, 1.0 eq.) and **XXVII** (85 mg, 0.25 mmol, 1.0 eq.) in DMSO/water (9 : 1, 10 ml). The reaction was stirred for 24 h at room temperature before it was quenched by the addition of a conc. solution of EDTA (5 ml). The solution was poured into water (100 ml) and cooled to 10 °C. The precipitate was separated by filtration and purified by column chromatography on silica.

Yield: 53 mg (0.09 mmol, 35 %)

R$_f$: 0.77 (chloroform : methanol / 9 : 1)

^{1}H-NMR (300 MHz, DMSO-d$_6$)

δ [ppm]: 8.56 (d, $^3J_{(H,H)}$ = 6 Hz, 1 H, C$\underline{H}$$^{Py, 6}$), 8.06 (s, 1 H, C$\underline{H}$^{Triazole}), 7.75-7.80 (m, 4 H, C$\underline{H}$^{Py,3}, C$\underline{H}$$^{BTA, 11,11'}$), 7.64-7.59 (m, 2 H, C$\underline{H}$^{Py,4}, C$\underline{H}$$^{BTA, 7}$), 7.35 (t, $^3J_{(H,H)}$ = 6 Hz, 1 H C$\underline{H}$^{Py,5}), 7.05 (d, $^3J_{(H,H)}$ = 9 Hz, 1 H, C$\underline{H}$$^{BTA, 5}$), 6.62 (d, $^3J_{(H,H)}$ = 9 Hz, 2 H, C$\underline{H}$$^{BTA, 12,12'}$), 6.42 (d, $^3J_{(H,H)}$ = 6 Hz, 1 H, N$\underline{H}$), 4.53 (t, $^3J_{(H,H)}$ = 6 Hz, 2 H, OC$\underline{H}_2$CH$_2$), 4.17 (s, 2 H, OC$\underline{H}_2$C^{Triazole}), 4.04 (t, $^3J_{(H,H)}$ = 6 Hz, 2 H, N^{Triazole}C$\underline{H}_2$), 3.69 (d, $^2J_{(H,H)}$ = 12 Hz, 2 H, C$\underline{H}$H), 3.35 (d, $^2J_{(H,H)}$ = 12 Hz, 2 H, CH$\underline{H}$), 2.95 (s, 4 H, SC$\underline{H}_2$C$\underline{H}_2$S), 2.75 (s, 3 H, NC$\underline{H}_3$), 2.31 (quint, $^3J_{(H,H)}$ = 6 Hz, 2 H, CH$_2$C$\underline{H}_2$CH$_2$)

^{13}C-NMR (75 MHz, DMSO-d$_6$)

δ [ppm]: 173.87 ($\underline{C}$$^{BTA, 2}$), 160.78 ($\underline{C}H^{Py, 2}$), 155.70 ($\underline{C}$$^{BTA, 6}$), 150.35 ($\underline{C}$$^{BTA, 13}$), 148.10 ($\underline{C}$$^{Py, 6}$), 144.17 ($\underline{C}$$^{BTA, 8}$), 137.09 ($\underline{C}H^{Py, 4}$), 135.01 ($\underline{C}$^{Triazole}) 131.24 ($\underline{C}H^{BTA, 11, 11'}$), 123.81 ($\underline{C}$$^{BTA, 9}$), 123.04 ($\underline{C}H^{Py, 3}$), 122.23 ($\underline{C}H^{BTA, 4}$), 121.71 ($\underline{C}H^{Py, 5}$), 119.50 ($\underline{C}$$^{BTA, 10}$), 115.46 ($\underline{C}H^{BTA, 5}$), 111.45 ($\underline{C}H^{BTA, 12, 12'}$), 105.68 ($\underline{C}H^{BTA, 7}$), 101.71 ($\underline{C}$H^{Triazole}), 85.21 (O$\underline{C}H_2$C^{Triazole}), 65.13 (O$\underline{C}H_2CH_2$), 57.14 (N^{Triazole}$\underline{C}H_2$), 46.48 (CH$_2$$\underline{C}H_2CH_2$), 40.62 ($\underline{C}$HH), 40.40 (N^{Triazole}$\underline{C}H_2$), 38.93 (S$\underline{C}H_2CH_2$S), 29.29 (N$\underline{C}H_3$)

Mass spectrometry ESI$^+$ (70 eV, MeOH)

m/z (%): 340.1 (100) [M + H]$^+$, 297.1 (86) [M - N$_3$]$^+$, 257.1 (75) [M - C$_3$H$_4$Br]$^+$, 255.1 (8) [M - C$_3$H$_6$Br]$^+$, 101.0 (42) [C$_3$H$_7$N$_3$O]$^+$

IR KBr

$\tilde{\nu}$ [cm^{-1}]: 3368 (m), 2931 (w), 2873 (w), 1607 (s), 1561 (m), 1532 (w), 1488 (m), 1454 (s), 1431 (m), 1410 (m), 1387 (w), 1323 (w), 1263 (m), 1219 (m), 1180 (m), 1156 (w), 1110 (w), 1061 (m), 1046 (s), 1002 (w), 964 (w), 951 (w), 927 (w), 820 (s), 755 (m), 714 (w), 685 (w), 629 (w), 610 (w), 590 (w), 549 (w), 514 (w), 437 (w), 405 (w)

Elemental analysis C$_{30}$H$_{32}$N$_6$O$_2$S$_3$ (604.81 gmol^{-1})

Calculated (%):   C: 59.58, H: 5.53, N: 13.90, S: 15.91

Found (%):   C: 51.96, H: 5.25, N: 11.09, S: 13.34

Synthesis of *N*-methyl-4-(6-(3-(4-((6-(1-methyl-1*H*-imidazol-2-yl)-1,4-dithiepan-6-yloxy)methyl)-1*H*-1,2,3-triazol-1-yl)propoxy)benzo[*d*]thiazol-2-yl)aniline (L^{5}BTA)

Sodium L-ascorbate (566 mg, 2.40 mmol, 10 eq.) was added to a solution of copper sulphate (40 mg, 0.24 mmol, 1.0 eq.), **L^{5H}** (63 mg, 0.24 mmol, 1.0 eq.) and **XXVII** (81.6 mg, 0.24 mmol, 1.0 eq.) in DMSO/water (9 : 1, 10 ml). The reaction was stirred for 24 h at room temperature before it was quenched by the addition of a conc. EDTA solution (5 ml). The Solution was poured into water (100 ml) and cooled to 10 °C. The precipitate was separated by filtration and purified by column chromatography on silica.

Yield: 82 mg (0.13 mmol, 54 %)

R$_f$: 0.26 (chloroform : methanol / 1 : 20)

^{1}H-NMR (300 MHz, DMSO-d$_6$)

δ [ppm]: 8.23 (s, 1 H, C$\underline{H}^{Triazole}$), 7.92 (d, $^3J_{(H,H)}$ = 9 Hz, 2 H, C$\underline{H}^{BTA, 11,11'}$), 7.88 (d, $^3J_{(H,H)}$ = 9 Hz, 1 H, C$\underline{H}^{BTA, 5}$), 7.82 (d, $^3J_{(H,H)}$ = 1 Hz, 1 H, C$\underline{H}^{Im, 5}$), 7.82 (d, $^3J_{(H,H)}$ = 9 Hz, 1 H, C$\underline{H}^{Im, 4}$), 7.66 (d, $^4J_{(H,H)}$ = 1 Hz, 1 H, C$\underline{H}^{BTA, 7}$), 7.09 (dd, $^3J_{(H,H)}$ = 9 Hz, $^4J_{(H,H)}$ = 1 Hz, 1 H, C$\underline{H}^{BTA, 5}$), 6.97 (d, $^3J_{(H,H)}$ = 9 Hz, 2 H, C$\underline{H}^{BTA, 12,12'}$), 6. 93 (sb, $^3J_{(H,H)}$ = 6 Hz, 1 H, N$\underline{H}$), 4.55 (t, $^3J_{(H,H)}$ = 6 Hz, 2 H, OC$\underline{H_2}$CH$_2$), 4.40 (s, 2 H, OC$\underline{H_2}$C^{Triazole}), 3.56 (t, $^3J_{(H,H)}$ = 6 Hz, 2 H, N^{Triazole}C$\underline{H_2}$), 3.99 (s, 3 H, N^{Im}C$\underline{H_3}$), 3.94 (d, $^2J_{(H,H)}$ = 18 Hz, 2 H, C$\underline{H}$H), 3.60 (d, $^2J_{(H,H)}$ = 18 Hz, 2 H, CH$\underline{H}$), 3.02 (s, 4 H, SC$\underline{H_2}$C$\underline{H_2}$S), 2.81 (s, 3 H, NC$\underline{H_3}$), 2.32 (quint, $^3J_{(H,H)}$ = 6 Hz, 2 H, CH$_2$C$\underline{H_2}$CH$_2$)

^{13}C-NMR (75 MHz, DMSO-d$_6$)

δ [ppm]: 170.75 ($\underline{C}^{BTA, 2}$), 156.10 ($\underline{C}^{BTA, 6}$), 146.87 ($\underline{C}^{Im, 2}$), 143.85 ($\underline{C}^{BTA, 13}$), 142.29 ($\underline{C}^{BTA, 8}$), 134.71 ($\underline{C}^{Triazole}$), 128.55 ($\underline{C}H^{BTA, 11, 11'}$), 126.51 ($\underline{C}H^{Im, 5}$), 124.68 ($\underline{C}H^{Triazole,}$), 124.52 ($\underline{C}^{BTA, 9}$), 122.06 ($\underline{C}H^{BTA, 4}$), 119.50 ($\underline{C}^{BTA, 10}$), 118.94 ($\underline{C}H^{Im, 4}$), 116.01 ($\underline{C}H^{BTA, 5}$), 114,69 ($\underline{C}H^{BTA, 12, 12'}$), 105.68 ($\underline{C}H^{BTA, 7}$), 82.97 (O$\underline{C}H_2$C^{Triazole}), 65.20 (O$\underline{C}H_2CH_2$), 58.39 (N$^{Triazole}\underline{C}H_2$), 46.59 (CH$_2\underline{C}H_2CH_2$), 38.64 ($\underline{C}$HH), 38.10 (S$\underline{C}H_2CH_2$S), 37.52 (N$^{Triazole}\underline{C}H_2$), 30.95 (N$^{Im}\underline{C}H_3$), 29.34 (N$\underline{C}H_3$)

Mass spectrometry ESI$^+$ (70 eV, MeOH)

m/z (%): 608.1 (100) [M]$^+$, 396.1 (11) [C$_9$H$_{13}$NS$_2$]$^+$, 213.1 (60) [M - C$_9$H$_{13}$NS$_2$]$^+$

IR KBr

$\tilde{v}$[cm^{-1}]: 3416 (m), 2925 (s), 2855 (m), 1068 (s), 1592 (s), 1514 (m), 1484 (m), 1467 (m), 1416 (m), 1379 (w), 1357 (w), 1315 (w), 1267 (m), 1229 (m), 1190 (w), 1119 (w), 1057 (m), 1020 (w), 909 (w), 825 (m), 765 (w), 713 (w), 689 (w), 628 (w), 588 (w), 554 (w), 504 (w), 436 (w)

Elemental analysis C$_{29}$H$_{33}$N$_7$O$_2$S$_3$ (607.81 gmol^{-1})

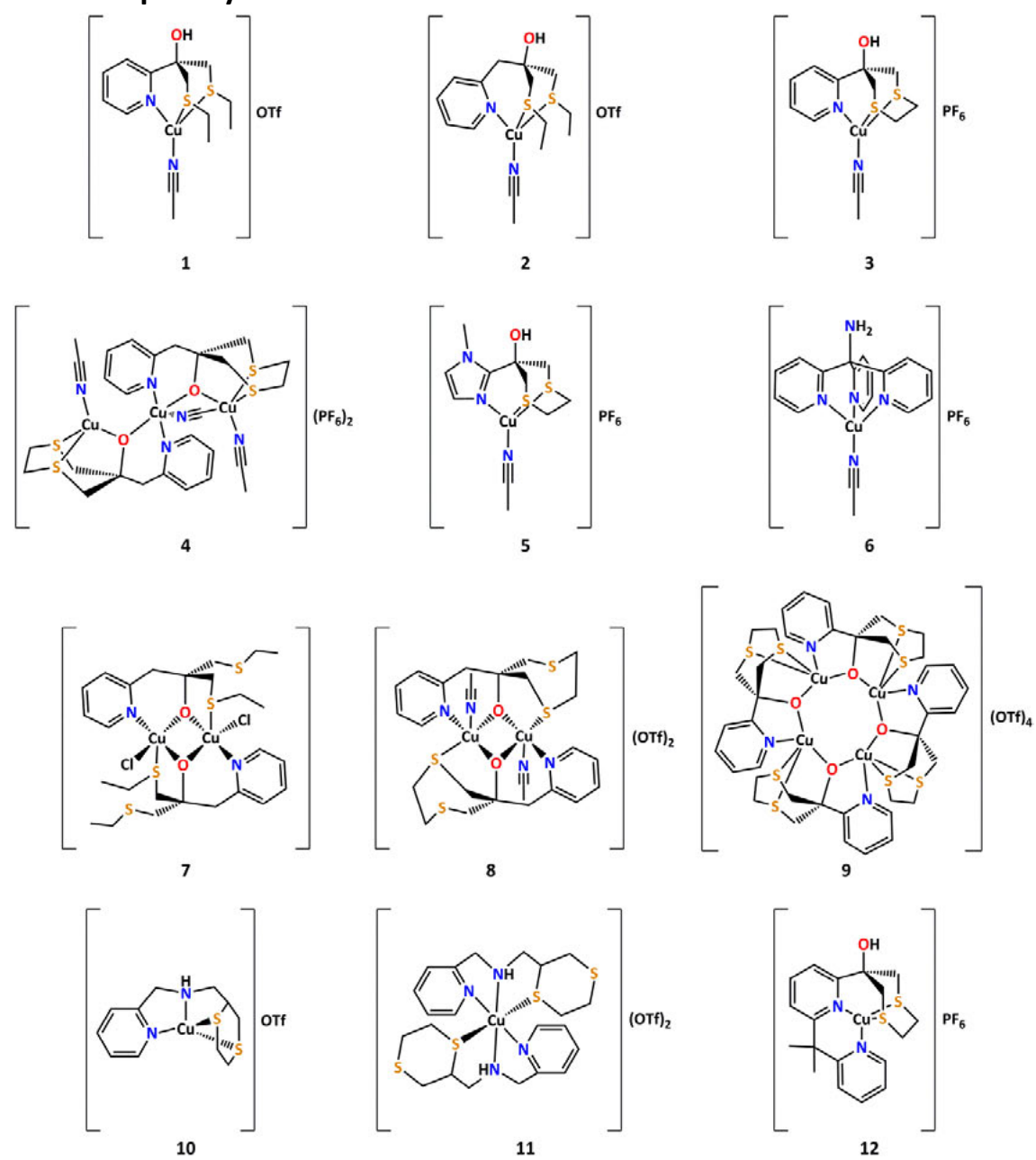Calculated (%):   C: 57.31, H: 5.47, N: 16.13, S: 15.83

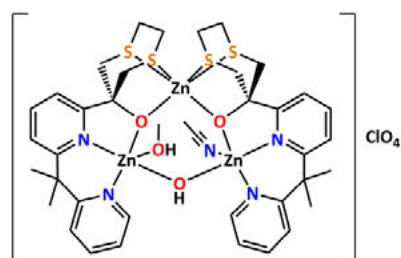Found (%):   C: 53.17, H: 5.50, N: 11.28, S: 13.34

Synthesis of *N*-methyl-4-(6-(3-(4-(((6-(6-(2-(pyridin-2-yl)propan-2-yl)pyridin-2-yl)-1,4-dithiepan-6-yl)oxy)methyl)-1H-1,2,3-triazol-1-yl)propoxy)benzo[*d*]thiazol-2-yl)aniline (L^{8}BTA)

Sodium L-ascorbate (295 mg, 1.25 mmol, 10 eq.) was added to a solution of copper sulphate (21 mg, 0.13 mmol, 1.0 eq.), **L^{8H}** (48 mg, 0.13 mmol, 1.0 eq.) and **XXVII** (43 mg, 0.13 mmol, 1.0 eq.) in DMSO/water (9 : 1, 10 ml) and stirred for 24 h at room temperature. Then the reaction was quenched by the addition of a conc. EDTA solution (5 ml). The Solution was poured into water (100 ml) and cooled to 10 °C. The precipitate was separated by filtration and purified by column chromatography on silica.
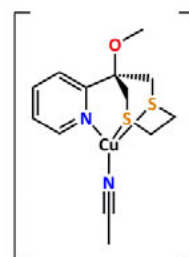
Yield:	15 mg (0.02 mmol, 16 %)
R$_f$:	0.76 (chloroform : methanol / 9 : 1)
^{1}H-NMR	(300 MHz, CDCl$_3$)

δ [ppm]: 8.45 (d, 1 H, C$\underline{H}$$^{Py, 10}$), 7.80-7.75 (m, 3 H, C$\underline{H}$$^{BTA, 4, 11,11'}$), 7.65-7.43 (m, 4 H, C$\underline{H}$$^{Py, 4, 7, 12}$, C$\underline{H}$^{Triazole}), 7.16 (m, 2 H, C$\underline{H}$$^{Py, 3, 5}$), 7.04-6.94 (m, 3 H, C$\underline{H}$$^{BTA, 5,}$ C$\underline{H}$$^{Py, 11, 13}$), 6.56 (d, $^3J_{(H,H)}$ = 6 Hz, 2 H, C$\underline{H}$$^{BTA, 4, 12,12'}$), 4.51 (t, $^3J_{(H,H)}$ = 9 Hz, 2 H, OC$\underline{H_2}$CH$_2$), 4.23 (s, 2 H, OC$\underline{H_2}$C^{Triazole}), 3.95 (t, $^3J_{(H,H)}$ = 6 Hz, 2 H, N^{Triazole}C$\underline{H_2}$), 3.65 (d, $^2J_{(H,H)}$ = 15 Hz, 2 H, C$\underline{H}$H), 3.24 (d, $^2J_{(H,H)}$ = 15 Hz, 2 H, C$\underline{H}$H), 2.88 (s, 3 H, NC$\underline{H_3}$), 2.84 (s, 4 H, SC$\underline{H_2}$C$\underline{H_2}$S), 2.35 (quint, $^3J_{(H,H)}$ = 6 Hz, 2 H, CH$_2$C$\underline{H_2}$CH$_2$), 1.74 (s, 6 H, C(C$\underline{H_3}$)$_2$)

^{13}C-NMR	(75 MHz, CDCl$_3$)

δ [ppm]: 175.67 ($\underline{C}$$^{BTA, 2}$), 167.03 ($\underline{C}$$^{Py, 6}$), 156.22 ($\underline{C}$$^{Py, 8}$), 155.48 ($\underline{C}$$^{Py, 6}$), 148.36 ($\underline{C}$$^{Py, 2}$), 146.36 ($\underline{C}H^{Py, 10}$), 144.08 ($\underline{C}$$^{BTA, 8}$), 140.98 ($\underline{C}$$^{BTA, 13}$), 137.13 ($\underline{C}H^{Py, 4}$), 136.22 ($\underline{C}H^{Py, 12}$), 138.83 ($\underline{C}$^{Triazole}), 131.10 ($\underline{C}$$^{BTA, 9}$), 128.78 ($\underline{C}H^{BTA, 11, 11'}$), 120.99 ($\underline{C}H^{Py, 5}$), 122.90 ($\underline{C}H^{BTA, 4}$), 122.76 ($\underline{C}$$^{BTA, 10}$), 121.67 ($\underline{C}H^{Py, 11}$), 120.97 ($\underline{C}H^{Py, 13}$), 118.39 ($\underline{C}H^{BTA, 5}$), 115.24 ($\underline{C}H^{Py, 3}$), 112.05 ($\underline{C}H^{BTA, 12, 12'}$), 105.25 ($\underline{C}H^{BTA, 7}$), 87.27 (O$\underline{C}H_2$C^{Triazole}), 68.16 (N^{Triazole}$\underline{C}$H$_2$), 64,69 (O$\underline{C}$H$_2$CH$_2$), 58.02 (N^{Triazole}$\underline{C}$H$_2$), 48.30 (C(C$\underline{H_3}$)$_2$), 47.00 ($\underline{C}$(CH$_3$)$_2$), 41.59 ($\underline{C}$HH), 38.97 (N$\underline{C}$H$_3$), 30.35 (S$\underline{C}$H$_2$$\underline{C}H_2$S), 29.91 (CH$_2$$\underline{C}H_2CH_2$), 28.31 (C($\underline{C}H_3$)$_2$)

Mass spectrometry	ESI$^+$ (70 eV, MeOH)

m/z (%): 745.9 (8) [M + Na]$^+$, 724.0 (100) [M + H]$^+$, 439.1 (12) [C$_{22}$H$_{25}$N$_5$OS$_2$]$^+$, 329.0 (100) [C$_{18}$H$_{21}$N$_2$S$_2$]$^+$

General Information	C$_{38}$H$_{41}$N$_7$O$_2$S$_3$ (723.97 gmol^{-1})
Calculated (%):	C: 63.04, H: 5.71, N: 13.54, S: 13.29

11.4 Complex Synthesis

13

14
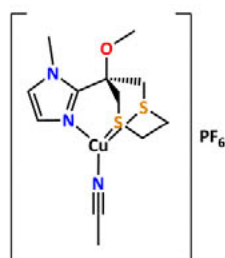
15
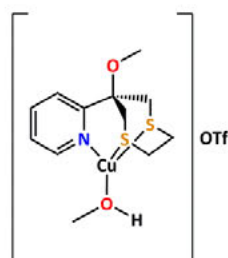
16
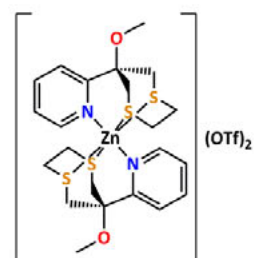
17
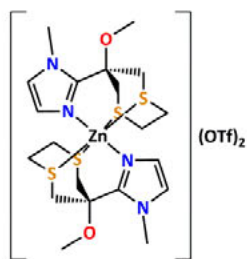
18
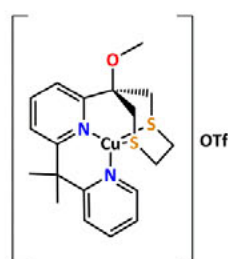
19
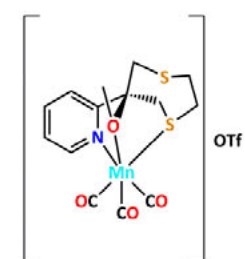
20
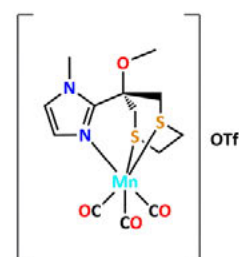
21
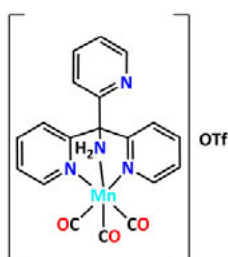
22
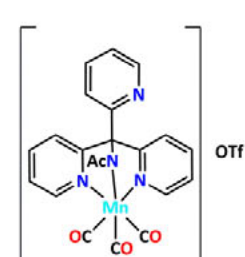
23
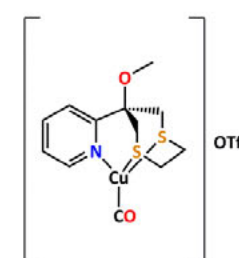
24
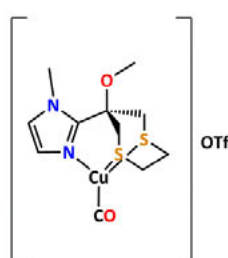
25
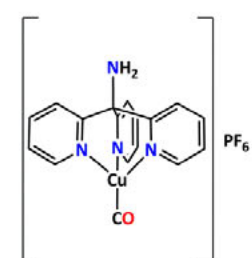
26

Synthesis of [L^{1H}Cu(MeCN)]OTf (1)

[Cu(MeCN)$_4$]OTf (188 mg, 0.5 mmol, 1.0 eq.) was added to a solution of **L^{1H}** (129 mg, 0.5 mmol, 1.0 eq.) dissolved in abs. MeCN (5 ml). The mixture was stirred over night at room temperature and then the complex was precipitated by the addition of diethyl ether (30 ml). The product was isolated by filtration and obtained as white solid.

Yield:	217 mg (0.43 mmol, 85 %)

^{1}H-NMR   (300 MHz, MeCN-d$_3$)

δ [ppm]:   8.55 (ddd, $^3J_{(H,H)}$ = 4.8 Hz, $^4J_{(H,H)}$ = 1.5 Hz, $^5J_{(H,H)}$ = 0.6 Hz 1 H, C$\underline{H}^{Py,\,6}$), 7.88 (ddd, $^3J_{(H,H)}$ = 7.8 Hz, $^3J_{(H,H)}$ = 7.8 Hz, $^4J_{(H,H)}$ = 1.5 Hz, 1 H, C$\underline{H}^{Py,\,4}$), 7.70 (ddd, $^3J_{(H,H)}$ = 7.8 Hz, $^4J_{(H,H)}$ = 1.5 Hz, $^5J_{(H,H)}$ = 0.6 Hz, 1 H, C$\underline{H}^{Py,\,3}$), 7.37 (ddd, $^3J_{(H,H)}$ = 7.8 Hz, $^3J_{(H,H)}$ = 4.8 Hz, $^4J_{(H,H)}$ = 1.5 Hz, 1 H, C$\underline{H}^{Py,\,5}$), 4.61 (s$_{br}$, 1 H, O$\underline{H}$), 3.21 (d, $^3J_{(H,H)}$ = 15.0 Hz, 2 H, C$\underline{H}$H), 3.07 (d, $^3J_{(H,H)}$ = 15.0 Hz, 2 H, CH$\underline{H}$), 2.43 (q, $^3J_{(H,H)}$ = 6 Hz, 4 H, C$\underline{H}_2$CH$_3$), 1.98 (s, 3 H, C$\underline{H}_3$CN), 1.14 (t, $^3J_{(H,H)}$ = 6 Hz, 6 H, CH$_2$C$\underline{H}_3$)

^{13}C-NMR   (75 MHz, MeCN-d$_3$)

δ [ppm]:   162.1 ($\underline{C}H^{Py,\,2}$), 147.7 ($\underline{C}H^{Py,\,6}$), 137.2 ($\underline{C}H^{Py,\,4}$), 122.6 ($\underline{C}H^{Py,\,3}$), 120.8 ($\underline{C}H^{Py,\,5}$), 75.9 ($\underline{C}$OH), 42.2 (CH$_2$), 27.9 ($\underline{C}$H$_2$CH$_3$), 13.5 (CH$_2$$\underline{C}H_3$)

Mass spectrometry   ESI$^+$ (70 eV, MeOH)

m/z (%):   639.8 (20) [HL$_2$Cu]$^+$, 319.9 (100) [M - MeCN]$^+$, 257.9 (11) [HL + H]$^+$

General Information   C$_{15}$H$_{22}$CuF$_3$N$_2$O$_4$S$_3$ (511.08 gmol^{-1})

Calculated (%):   C: 35.25, H: 4.34, N: 5.48, S: 18.82

Synthesis of [L^{2H}Cu(MeCN)]OTf (2)

[Cu(MeCN)$_4$]OTf (377 mg, 1.0 mmol, 1.0 eq.) was added to a solution of **L^{2H}** (271 mg, 1.0 mmol, 1.0 eq.) dissolved in abs. MeCN (10 ml). The reaction was stirred over night at room temperature and then the complex was precipitated by the addition of diethyl ether (30 ml). The product was isolated by filtration and obtained as white solid.

Yield:	416 mg (0.78 mmol, 78 %)
^{1}H-NMR	(300 MHz, MeCN-d$_3$)
δ [ppm]:	8.52 (dd, $^3J_{(H,H)}$ = 5.1 Hz, $^4J_{(H,H)}$ = 2.1 Hz, 1 H, C$\underline{H}^{Py, 6}$), 7.87 (ddd, $^3J_{(H,H)}$ = 7.8 Hz, $^3J_{(H,H)}$ = 7.8 Hz, $^4J_{(H,H)}$ = 2.1 Hz, 1 H, C$\underline{H}^{Py, 4}$), 7.45-7.37 (m, 2 H, C$\underline{H}^{Py, 5}$, C$\underline{H}^{Py, 3}$), 3.16 (s, 2 H, C^{Py}C$\underline{H}_2$), 2.81-2.63 (m, 8 H, C$\underline{H}_2$, C$\underline{H}_2$CH$_3$), 1.99 (s, 3 H, NCCH$_3$), 1.26 (t, $^3J_{(H,H)}$ = 9.0 Hz, 6 H, CH$_2$C$\underline{H}_3$)
^{13}C-NMR	(75 MHz, MeCN-d$_3$)
δ [ppm]:	159.0 ($\underline{C}$H$^{Py, 2}$), 148.7 ($\underline{C}$H$^{Py, 6}$), 137.7 ($\underline{C}$H$^{Py, 4}$), 126.3 ($\underline{C}$H$^{Py, 3}$), 122.6 ($\underline{C}$H$^{Py, 5}$), 74.4 ($\underline{C}$OH), 45.1 (2 C, $\underline{C}$H$_2$), 40.8 (C$^{Py}\underline{C}$H$_2$), 27.9 ($\underline{C}$H$_2$CH$_3$), 13.4 (CH$_2\underline{C}$H$_3$)
Mass spectrometry	ESI$^+$ (70 eV, MeOH)
m/z (%):	605.0 (10) [CuL$_2$ + H]$^+$, 333.9 (100) [M - H]$^+$, 241.0 (32) [L + H]$^+$
General Information	C$_{16}$H$_{24}$CuF$_3$N$_2$O4S$_3$ (525.11 gmol^{-1})
Calculated (%):	C: 36.60, H: 4.61, N: 5.33, S: 18.32

Synthesis of [L^{2H}Cu(MeCN)]OTf (2)

Synthesis of [L³Cu(MeCN)]PF₆ (3)

[Cu(MeCN)₄]PF₆ (329 mg, 0.89 mmol, 1.0 eq.) was added to a solution of **L³ᴴ** (200 mg, 0.89 mmol, 1.0 eq.) dissolved in abs. MeCN (10 ml). The reaction was stirred over night at room temperature and afterwards the complex was precipitated by the addition of diethyl ether (30 ml) and afterwards crystallised by ether diffusion in into a solution of the crude material in MeCN at 4 °C. The product could be obtained as colourless crystals.

Yield:	324 mg (0.68 mmol, 76 %)
¹H-NMR	(300 MHz, MeCN-d_3)
δ [ppm]:	8.61 (ddd, $^3J_{(H,H)}$ = 5.4 Hz, $^4J_{(H,H)}$ = 1.8 Hz, $^5J_{(H,H)}$ = 1.0 Hz, 1 H, CH$^{Py, 6}$), 8.03 (ddd, $^3J_{(H,H)}$ = 8.4 Hz, $^3J_{(H,H)}$ = 8.4 Hz, $^4J_{(H,H)}$ = 2.7 Hz, 1 H, CH$^{Py, 4}$), 7.96 (ddd, $^3J_{(H,H)}$ = 8.4 Hz, $^4J_{(H,H)}$ = 1.2 Hz, $^5J_{(H,H)}$ = 1.0 Hz 1 H, CH$^{Py, 3}$), 7.53 (t, $^3J_{(H,H)}$ = 8.4 Hz, $^3J_{(H,H)}$ = 5.4 Hz, $^4J_{(H,H)}$ = 1.2 Hz, 1 H, CH$^{Py, 5}$), 3.29-3.12 (m, 4 H, CH₂, SCH₂CH₂S)
¹³C-NMR	(75 MHz, MeCN-d_3)
δ [ppm]:	162.9 (CH$^{Py, 2}$), 148.1 (CH$^{Py, 6}$), 139.6 (CH$^{Py, 4}$), 123.7 (CH$^{Py, 3}$), 120.9 (CH$^{Py, 5}$), 43.3 (COH), 38.6 (CH₂), 37.9 (SCH₂CH₂S)
Mass spectrometry	ESI⁺ (70 eV, MeOH)
m/z (%):	607.9 (14) [HL₂Cu]⁺, 331.0 (100) [M]⁺, 290.0 (72) [CuL]⁺, 228.1 (46) [H₂L]⁺
General Information	C₁₂H₁₆CuF₆N₂OPS₂ (476.91 gmol⁻¹)
Calculated (%):	C: 30.22, H: 3.38, N: 5.87, S: 13.45

Synthesis of [L$^4_2$Cu^{2+}Cu$^+_2$(MeCN)$_3$](PF$_6$)$_2$ (4)

[Cu(MeCN)$_4$]PF$_6$ (559 mg, 1.5 mmol, 1.0 eq.) was added to a solution of **L^{4H}** (428 mg, 1.5 mmol, 1.0 eq.) dissolved in abs. MeCN (10 ml). The reaction was stirred over night at room temperature and afterwards the complex was precipitated by the addition of diethyl ether (20 ml). The product was recrystallised from MeCN/Et$_2$O at room temperature. The crude product was recrystallised from MeCN/Et$_2$O at room temperature to yield the complex as yellow crystals.

Yield:	238 mg (0.22 mmol, 44 % with respect to Cu)
Mass spectrometry	ESI$^+$ (70 eV, MeOH)
m/z (%):	304.0 (7) [CuL]$^+$, 224.1 (25) [L - OH]$^+$, 132.0 (54) [C$_5$H$_8$S$_2$]$^+$, 104.1 (72) [C$_3$H$_4$S$_2$]$^+$, 62.9 (100) [Cu]$^+$
General Information	C$_{28}$H$_{37}$Cu$_3$F$_{12}$N$_5$O$_2$P$_2$S$_4$ (1081.90 gmol^{-1})
Calculated (%):	C: 31.01, H: 3.44, N: 6.46, S: 11.83

Synthesis of [L^{5H}Cu(MeCN)]PF$_6$ (5)

[Cu(MeCN)$_4$]PF$_6$ (186 mg, 0.5 mmol, 1.0 eq.) was added to a solution of **L^{5H}** (115 mg, 0.5 mmol, 1.0 eq.) dissolved in abs. MeCN (10 ml). The reaction was stirred over night at room temperature and afterwards the complex was precipitated by the addition of diethyl ether (20 ml). The product was crystallised from MeCN/Et$_2$O at room temperature. The complex **5** could be obtained as colourless crystals.

Yield:	156 mg (0.33 mmol, 65 %)
^{1}H-NMR	(300 MHz, CDCl$_3$)
δ [ppm]:	7.0 (s, 1 H, C$\underline{H}$$^{Im, 5}$), 6.9 (s, 1 H, C$\underline{H}$$^{Im, 4}$), 4.30 (s$_{br}$, 1 H, CO$\underline{H}$), 3.86 (s, 3H, NC$\underline{H}_3$), 3.39 (d, $^2J_{(H,H)}$ = 15.0 Hz, 2 H, C$\underline{H}$H), 3.24 (d, $^2J_{(H,H)}$ = 15.0 Hz, 2 H, CH$\underline{H}$), 3.19 (s, 4 H, SC$\underline{H}_2$C$\underline{H}_2$S), 1.99 (s, 3 H, C$\underline{H}_3$CN)
^{13}C-NMR	(75 MHz, CDCl$_3$)
δ [ppm]:	148.2 ($\underline{C}$H$^{Im, 2}$) 126.2 ($\underline{C}$H$^{Im, 5}$), 123.5 ($\underline{C}$H$^{Im, 4}$), 76.9 ($\underline{C}$OH), 43.6 ($\underline{C}$H$_2$), 37.7 (S$\underline{C}$H$_2$$\underline{C}H_2$S), 36.5 (N$\underline{C}H_3$)
Mass spectrometry	ESI$^+$ (70 eV, MeOH)
m/z (%):	522.7 (11) [CuL$_2$]$^+$, 392.9 (100) [CuL]$^+$, 231.0 (15) [L]$^+$, 213.0 (12) [L - OH]$^+$, 254.1 (44) [L - OH]$^+$
Elemental Analysis	C$_{11}$H$_{17}$CuF$_6$N$_3$OPS$_2$ (479.91 gmol^{-1})
Calculated (%):	C: 22.53, H: 3.57, N: 8.76, S: 13.36
Found (%):	C: 28.19, H: 3.87, N: 8.58, S: 13.13

Synthesis of [L^{6H}Cu(MeCN)]PF$_6$ (6)

[Cu(MeCN)$_4$]PF$_6$ (186 mg, 0.5 mmol, 1.0 eq.) was added to a solution of **L^{6H}** (131 mg, 0.5 mmol, 1.0 eq.) dissolved in abs. MeCN (10 ml). The reaction was stirred over night at room temperature and afterwards the product was crystallised by slow diffusion of diethylether at room temperature. The complex **6** could be obtained as colourless crystals.

Yield:	239 mg (0,47 mmol, 93 %)
^{1}H-NMR	(300 MHz, DMSO-d$_6$)
δ [ppm]:	8.78 (d, $^3J_{(H,H)}$ = 6 Hz, 3 H, C$\underline{H}^{3,3',3''}$), 8.14 (s$_{br}$, 3 H, C$\underline{H}^{6,6',6''}$), 8.05 (dd, $^3J_{(H,H)}$ = 13 Hz, $^3J_{(H,H)}$ = 12 Hz, 3 H, C$\underline{H}^{4,4',4''}$), 7.51 (dd, $^3J_{(H,H)}$ = 8 Hz, $^3J_{(H,H)}$ = 12 Hz, 3 H, C$\underline{H}^{5,5',5''}$), 4.20 (s, 2 H, CN$\underline{H}_2$), 2.01 (s, 3 H, C$\underline{H}_3$CN)
^{13}C-NMR	(75 MHz, DMSO-d$_6$)
δ [ppm]:	158.14 ($\underline{C}^{2,2',2''}$), 149.74 ($\underline{C}H^{3,3',3''}$), 138.99 ($\underline{C}H^{4,4',4''}$), 123.43 ($\underline{C}H^{6,6',6''}$), 122.92 ($\underline{C}H^{5,5',5''}$), 118. 03 (CH$_3\underline{C}$N), 64.32 ($\underline{C}NH_2$), 1.11 (1 C, $\underline{C}$H$_3$CN)
Mass spectrometry	ESI$^+$ (70 eV, MeOH)
m/z (%):	586.0 (7) [L$_2$Cu - H]$^+$, 325.0 (100) [M - MeCN]$^+$, 246.1 (75) [L - NH$_2$]$^+$, 184.1 (34) [C$_{11}$H$_{10}$N$_3$]$^+$, 80.1 (34) [Pyridine + H]$^+$, 62.9 (69) [Cu]$^+$
IR	KBr
$\tilde{v}$ [cm^{-1}]:	3390 (m), 3321 (w), 3094 (w), 2264 (m), 1591 (s), 1463(s), 1438(s), 1367 (w), 1312 (m), 1294 (w), 1211 (w), 1164 (m), 1105 (w), 1088 (w), 1064 (m), 1015 (m), 956 (m), 833 (s), 774 (s), 754 (s), 653 (s), 635 (m), 558 (s), 511 (m), 483 (m), 447 (w), 419 (m)
General Information	C$_{18}$H$_{17}$CuF$_6$N$_5$P (511.87 gmol^{-1})
Calculated (%):	C: 42.24, H: 3.35, N: 13.68

Synthesis of [L$^2_2$Cu$_2$Cl$_2$] (7)

CuCl$_2$ (134 mg, 1.0 mmol, 0.9 eq.) was added to a solution of **L^{2H}** (298 mg, 1.1 mmol, 1.0 eq.) dissolved in MeOH (40 ml). The suspension was stirred over night at room temperature and then the solvent was removed under reduced pressure. The crude product was washed with diethyl ether. The complex **7** could be obtained as green solid.

Yield: 376 mg (0.5 mmol, 91 % with respect to **L^{2H}**)

Mass spectrometry ESI$^+$ (70 eV, MeOH)

m/z (%): 605.1 (18) [L$_2$Cu]$^+$, 334.0 (100) [LCu]$^+$, 192.2 (60) [C$_{11}$H$_{16}$NS]$^+$, 272.2 (44) [L + H]$^+$, 254.1 (44) [L - OH]$^+$

SQUID $\hat{H} = -2JS_1S_2 + g\mu_B\vec{B}(\,\vec{S}_1 + \vec{S}_2\,)$

J^{12} [cm^{-1}]: -421

General Information C$_{26}$H$_{40}$Cl$_2$Cu$_2$N$_2$O$_2$S$_4$ (738.87 gmol^{-1})

Calculated (%): C: 42.26, H: 5.46, N: 3.79, S: 17.36

Synthesis of [L$^4_2$Cu$_2$(MeCN)$_2$]OTf$_2$ (8)

[Cu(MeCN)$_4$]OTf (77 mg, 0.2 mmol, 1.0 eq.) was added to a solution of **L^{4H}** (50 mg, 0.2 mmol, 1.0 eq.) dissolved in MeCN (5 ml). The micture was stirred for 1 h under an atmosphere of dry N$_2$ and was then exposed to air over night. The complex **8** could be crystallised from MeCN/Et$_2$O as green crystals.

Yield:	97 mg (98 μmol, 98 %)
Mass spectrometry	ESI$^+$ (70 eV, MeOH)
m/z (%):	976.3 (23) [L$_3$Cu$_4$ - 3 H]$^+$, 607.6 (13) [M - 2 MeCN]$^+$, 303.9 (21) [LCu]$^+$, 264.0 (100) [L + H]$^+$, 224.0 (99) [L - OH]$^+$
SQUID	$\hat{H} = -2JS_1S_2 + g\mu_B\vec{B}(\vec{S}_1 + \vec{S}_2)$
J^{12} [cm^{-1}]:	-108
Elemental analysis	C$_{28}$H$_{34}$Cu$_2$F$_6$N$_4$O$_8$S$_6$ (988.06 gmol^{-1})
Calculated (%):	C: 34.04, H: 3.47, N: 5.67, S: 19.47
Found (%):	C: 34.19, H: 3.51, N: 5.61, S: 19.50

Synthesis of [L$^3_4$Cu$_4$]OTf$_4$ (9)

[Cu(MeCN)$_4$]OTf (377 mg, 1.0 mmol, 1.0 eq.) was added to a solution of **L^{3H}** (226 mg, 1.0 mmol, 1.0 eq.) dissolved in abs. MeCN (5 ml). The mixture was stirred for 1 h under an atmosphere of dry N$_2$ and was then exposed to air over night. The complex was precipitated through the addition of diethyl ether (10 ml) and crystallised from MeCN/Et$_2$O. The product could be obtained as green crystals.

Yield:	222 mg (0.18 mmol, 72 %)
Mass spectrometry	ESI$^+$ (70 eV, MeOH)
m/z (%):	289.9 (100) [LCu]$^+$, 228.0 (53) [L + H]$^+$, 210.0 (100) [L - OMe]$^+$, 150.1 (36) [C$_5$H$_{10}$S$_2$]$^+$

SQUID

$$\hat{H} = -2J(\,S_1 S_2 + S_2 S_3 + S_3 S_4 + S_1 S_4\,) + \sum_i g\mu_B \vec{B}\vec{S}_i$$

J$^{1\text{-}4}$ [cm^{-1}]:	-110
General Information	C$_{44}$H$_{48}$Cu$_4$F$_{12}$N$_4$O$_{16}$S$_{12}$ (1755.81 gmol^{-1})
Calculated (%):	C: 30.10, H: 2.76, N: 3.19, S: 21.91
Elemental Analysis	M + 2 MeCN
Calculated (%):	C: 31.37, H: 2.96, N: 4.57, S: 20.94
Found (%):	C: 31.55, H: 2.75, N: 4.50, S: 20.85

Synthesis of [L^{7H}Cu]OTf (10)

[Cu(MeCN)$_4$]OTf (500 mg, 1.32 mmol, 0.6 eq.) was added to a solution of **L^{7H}** (500 mg, 2.07 mmol, 1.0 eq.) dissolved in MeCN (10 ml). The reaction was stirred over night at room temperature and the complex precipitated by the addition of DCM (40 ml). The product **10** could be obtained as a colourless solid.

Yield:	438 mg (0.97 mmol, 73 %)
^{1}H-NMR	(300 MHz, DMSO-d$_6$)
δ [ppm]:	9.08 (sb, 1 H, C$\underline{H}$$^{Py, 6}$), 8.67 (d, $^3J_{(H,H)}$ = 3 Hz, 1 H, C$\underline{H}$$^{Py, 3}$), 7.92 (dd, $^3J_{(H,H)}$ = 6 Hz, $^3J_{(H,H)}$ = 6 Hz, 1 H, C$\underline{H}$$^{Py, 4}$) 7.50 (m, 1 H, C$\underline{H}$$^{Py, 5}$) 4.42 (sb, 2 H, C$\underline{H}_2$NHCH$_2$), 4.20 (sb, 2 H, CH$_2NHC\underline{H}_2$), 3.60-2.73 (m, 10 H, C$\underline{H}$^{Cyl}, C$\underline{H}_2$^{Cyl})
Mass spectrometry	ESI$^+$ (70 eV, MeOH)
m/z (%):	303 (82) [M]$^+$, 241 (58) [L + H]$^+$
IR	KBr
$\tilde{v}$[cm^{-1}]:	3051 (m), 2972 (s), 2931 (s), 2872 (m), 1586 (s), 1553 (s), 1472 (s), 1423 (s), 1396 (s), 1295 (w), 1174 (s), 1118 (s), 984 (s), 825 (s), 786 (s), 744 (s), 664 (s)
Elemental Analysis	C$_{12}$H$_{16}$CuF$_3$N$_2$O$_3$S$_3$ (453.00 gmol^{-1})
Calculated (%):	C: 31.82, H: 3.56, N: 6.18
Found (%):	C: 29.59, H: 3.85, N: 6.46

Synthesis of [$L^{7H}{}_2$Cu]OTf$_2$ (11)

[Cu(MeCN)$_4$]OTf (250 mg, 0.66 mmol, 0.6 eq.) was added to a solution of **L^{7H}** (250 mg, 1.04 mmol, 1.0 eq.) dissolved in MeCN (10 ml). The reaction was stirred for 1 h under N$_2$-atmosphere and then exposed to air over night. The product was crystallised by slow diffusion of diethylether into the mixture. The product **11** could be obtained as purple crystals.

Yield:	447 mg (0.53 mmol, 80%)
IR	KBr
$\tilde{V}$[cm^{-1}]:	3496 (m), 3219 (m), 3179 (m), 2906 (m), 1610 (s), 1573 (w), 1490 (m), 1438 (m), 1416 (m), 1282 (s), 1251 (s), 1156 (s), 1025 (s), 926 (w), 887 (w), 825 (s), 769 (s), 639 (s), 623 (s), 573 (m), 516 (m)
General Information	C$_{24}$H$_{32}$CuF$_6$N$_4$O$_5$S$_6$ (842.46 gmol^{-1})
Calculated (%):	C: 34.22, H: 3.83, N: 6.65, S: 22.84

Synthesis of [L^{8H}Cu]OTf (12)

[Cu(MeCN)$_4$]PF$_6$ (93 mg, 0.25 mmol, 1.0 eq.) was added to a solution of **L^{8H}** (87 mg, 0.25 mmol, 1.0 eq.) dissolved in MeCN (3 ml). The reaction was stirred over night at room temperature and afterwards the complex was precipitated by the addition of diethyl ether (10 ml). The crude product was purified by recrystallisation from MeCN/Et$_2$O at -23 °C. The product **12** could be obtained as colourless crystals.

Yield: 35 mg (57 µmol, 25 %)

^{1}H-NMR (500 MHz, MeCN-d$_3$)

δ [ppm]: 8.63 (dd, $^3J_{(H,H)}$ = 5 Hz, 1 H, C$\underline{H}$$^{Py, 10}$), 7.83 (dd, $^3J_{(H,H)}$ = 8 Hz, $^3J_{(H,H)}$ = 8 Hz, 2 H, C$\underline{H}$$^{Py, 4, 12}$), 7.73 (d, $^3J_{(H,H)}$ = 8 Hz, 2 H, C$\underline{H}$$^{Py, 3, 5}$), 7.33 (d, $^3J_{(H,H)}$ = 8 Hz, 1 H, C$\underline{H}$$^{Py, 13}$), 7.31 (dd, $^3J_{(H,H)}$ = 5 Hz, 1 H, C$\underline{H}$$^{Py, 11}$), 4.63 (sb, 1 H, CO$\underline{H}$), 3.31-3.21 (m, 6 H, C$\underline{H}H, SC\underline{H}_2C\underline{H}_2$S), 3.11 (d, $^2J_{(H,H)}$ = 15 Hz, 2 H, CH$\underline{H}$), 1.94 (s, 6 H, C(C$\underline{H}_3$)$_2$)

^{13}C-NMR (125 MHz, MeCN-d$_3$)

δ [ppm]: 164.71 ($\underline{C}$$^{Py, 2}$), 163.00 ($\underline{C}$$^{Py, 6}$), 151.50 ($\underline{C}$$^{Py, 8}$), 140.17 ($\underline{C}H^{Py, 10}$), 139.63 ($\underline{C}H^{Py, 4}$), 123.74 ($\underline{C}H^{Py, 12}$), 123.37 ($\underline{C}H^{Py, 11}$), 123.17 ($\underline{C}H^{Py, 13}$), 120.82 ($\underline{C}H^{Py, 5}$), 119.85 ($\underline{C}H^{Py, 3}$), 46.72 ($\underline{C}$(CH$_3$)$_2$), 44.92 ($\underline{C}$HH), 38.16 (S$\underline{C}H_2$$\underline{C}H_2$S), 28.46 (C($\underline{C}H_3$)$_2$)

Mass spectrometry ESI$^+$ (70 eV, MeOH)

m/z (%): 409.0 (100) [M]$^+$, 346.9 (11) [L+ H]$^+$

General Information C$_{18}$H$_{22}$CuF$_6$N$_2$OPS$_2$ (555.02 gmol^{-1})

Calculated (%): C: 38.95, H: 4.00, N: 5.05, S: 11.55

Synthesis of [L^8$_2$Zn$_3$(μ-OH)MeOH(MeCN)$_{0.5}$(H$_2$O)$_{0.5}$]ClO$_4$ · 1.5 MeOH (13)

Zn(ClO$_4$)$_2$ · 6 H$_2$O (54 mg, 0.14 mmol, 1.0 eq.) in MeOH (1 ml) was added to a solution of **L^{8H}** (50 mg, 0.14 mmol, 1.0 eq.) in MeOH (3 ml) and stirred over night at room temperature. The solvent was removed under reduced pressure and the product was purified by recrystallisation from MeCN/MeOH/Et$_2$O. The product **13** could be obtained as colourless crystals.

Yield:	15 mg (14 μmol, 30 % with respect to zink)
^{1}H-NMR	(300 MHz, DMSO-d$_6$)
δ [ppm]:	8.47 (d, $^3J_{(H,H)}$ = 3 Hz, 2 H, CH$^{Py, 10,10'}$), 7.71-7.65 (m, 4 H, CH$^{Py, 4,4',5,5'}$), 7.41 (d, $^3J_{(H,H)}$ = 9 Hz, 2 H, CH$^{Py, 12,12'}$), 7.28 (d, $^3J_{(H,H)}$ = 9 Hz , 2 H, CH$^{Py, 3,3'}$), 7.19 (dd, $^3J_{(H,H)}$ = 6 Hz, $^3J_{(H,H)}$ = 6 Hz, 2 H, CH$^{Py, 11,11'}$), 7.04 (d, $^3J_{(H,H)}$ = 6 Hz, 2 H, CH$^{Py, 13,13'}$), 5.59 (s, 1 H, OH), 4.11 (q, $^3J_{(H,H)}$ = 6 Hz, 1 H, CH$_3$OH), 3.42 (d, $^2J_{(H,H)}$ = 12 Hz, 4 H, CHH), 3.18 (d, $^3J_{(H,H)}$ = 6 Hz, 3 H, CH$_3$OH), 3.04 (d, $^2J_{(H,H)}$ = 12 Hz, 4 H, CHH), 2.93 (m , 8 H, SCH$_2$CH$_2$S), 2.07 (s, 1 H, CH$_3$CN), 1.76 (s, 6 H, CH$_3$)
^{13}C-NMR	(75 MHz, CDCl$_3$)
δ [ppm]:	166.00 (C$^{Py, 2}$), 163.02 (C$^{Py, 6}$), 158.94 (C$^{Py, 8}$), 148.16 (CH$^{Py, 10}$), 137.04 (CH$^{Py, 4}$), 136.22 (CH$^{Py, 12}$), 121.14 (CH$^{Py, 13}$), 121.01 (CH$^{Py, 11}$), 119.37 (CH$^{Py, 5}$), 117.57 (CH$^{Py, 3}$), 79.87 (COH), 47.76 (CC$_4$), 43.80 (CHH), 38.31 (SCH$_2$CH$_2$S), 28.13 (CH$_3$)
Mass spectrometry	ESI$^+$ (70 eV, MeOH)
m/z (%):	369.0 (22) [L + Na]$^+$, 347.0 (100) [L + H]$^+$, 329.0 (25) [L - OH]$^+$
General Information	C$_{40}$H$_{54}$ClN$_5$O$_8$S$_4$Zn$_3$ (1092.47 gmol^{-1})
Calculated (%):	C: 43.97, H: 4.98 N: 6.41, S: 11.74

Synthesis of [L^{3Me}Cu(MeCN)]OTf (14)

[Cu(MeCN)$_4$]OTf (314 mg, 0.84 mmol, 1.0 eq.) was added to a solution of **L^{3Me}** (200 mg, 0.84 mmol, 1.0 eq.) dissolved in MeCN (10 ml). The reaction was stirred over night at room temperature and afterwards the complex was precipitated by the addition of diethyl ether (30 ml). The complex was taken up in MeCN and crystallised by slow diffusion of diethylether at 4 °C. The product **14** could be obtained as colourless crystals.

Yield:	260 mg (0.52 mmol, 63 %)
^{1}H-NMR	(500 MHz, acetone-d$_6$)
δ [ppm]:	8.61 (d, $^3J_{(H,H)}$ = 5 Hz, 1 H, C$\underline{H}^{Py, 6}$), 8.07 (ddd, $^3J_{(H,H)}$ = 8 Hz, $^3J_{(H,H)}$ = 8 Hz, $^4J_{(H,H)}$ = 2 Hz, 1 H, C$\underline{H}^{Py, 4}$) 7.81 (d, $^3J_{(H,H)}$ = 8 Hz, 1 H, C$\underline{H}^{Py, 3}$), 7.49 (qd, $^3J_{(H,H)}$ = 5 Hz, $^4J_{(H,H)}$ = 2 Hz, 1 H, C$\underline{H}^{Py, 5}$), 3.66 (d, $^2J_{(H,H)}$ = 5 Hz, 2 H, C$\underline{H}$H), 3.52 (d, $^2J_{(H,H)}$ = 5 Hz, 2 H, CH$\underline{H}$), 3.42-3.36 (m, 7 H, SC$\underline{H}_2$C$\underline{H}_2$S, COC$\underline{H}_3$)
^{13}C-NMR	(125 MHz, acetone-d$_6$)
δ [ppm]:	163.47 ($\underline{C}$OCH$_3$), 151.43 ($\underline{C}^{Py, 2}$), 139.98 ($\underline{C}$H$^{Py, 6}$), 125.04 ($\underline{C}$H$^{Py, 4}$), 122.94 ($\underline{C}$H$^{Py, 3}$), 66.07 ($\underline{C}$H$^{Py, 5}$), 52.08 (CO$\underline{C}$H$_3$), 42.50 ($\underline{C}$HH), 40.08 (S$\underline{C}$H$_2\underline{C}$H$_2$S)
Mass spectrometry	ESI$^+$ (70 eV, MeOH)
m/z (%):	345.0 (21) [M]$^+$, 304.0 (100) [M - MeCN]$^+$, 226.0 (16) [L - H]$^+$, 210.1 (32) [L - OMe]$^+$, 62.9 (52) [Cu]$^+$
IR	KBr
$\tilde{v}$ [cm^{-1}]:	1262 (s), 1030 (s), 832 (s), 638 (s), 560 (s), 1595 (m), 1472 (m), 1432 (m), 1411 (m), 1167 (m), 1147 (m), 1074 (m), 755 (m), 517 (m), 483 (m), 2985 (w), 2928 (w), 2843 (w), 1371 (w), 1100 (w), 420 (w).
General Information	C$_{14}$H$_{18}$CuF$_3$N$_2$O$_4$S$_3$ (495.04 gmol^{-1})
Calculated (%):	C: 33.97, H: 3.66, N: 5.66, S: 19.43
Elemental Analysis	M + MeCN
Calculated (%):	C: 31.43, H: 4.14, N: 10.12, S: 11.99
Found (%):	C: 30.11, H: 3.54, N: 10.12, S: 10.61

Synthesis of [L^{5Me}Cu(MeCN)]PF$_6$ (15)

[Cu(MeCN)$_4$]PF$_6$ (377 mg, 1.0 mmol, 1.0 eq.) was added to a solution of **L^{5Me}** (244 mg, 1.0 mmol, 1.0 eq.) dissolved in MeCN (10 ml). The reaction was stirred over night at room temperature and afterwards the complex was precipitated by the addition of diethyl ether (30 ml). The complex was taken up in MeCN and crystallised through slow ether diffusion 4 °C. The product **15** could be obtained as colourless crystals.

Yield:	373 mg (0.76 mmol, 76 %)
^{1}H-NMR	(300 MHz, MeCN-d$_3$)
δ [ppm]:	7.04 (d, $^3J_{(H,H)}$ = 1 Hz, 1 H, C$\underline{H}^{Im, 5}$), 6.91 (d, $^3J_{(H,H)}$ = 1 Hz, 1 H, C$\underline{H}^{Im, 4}$), 3.79 (s, 3 H, NC$\underline{H}_3$), 3.50 (d, $^2J_{(H,H)}$ = 12 Hz, 2 H, C$\underline{H}$H), 3.36 (d, $^2J_{(H,H)}$ = 15 Hz, 2 H, CH$\underline{H}$), 3.19 (s, 3 H, COC$\underline{H}_3$), 3.12-3.09 (s, 4 H, SC$\underline{H}_2$C$\underline{H}_2$S)
^{13}C-NMR	(75 MHz, CDCl$_3$)
δ [ppm]:	126.36 ($\underline{C}H^{Im, 4}$), 123.76 ($\underline{C}H^{Im, 5}$), 50.91 (CO$\underline{C}H_3$), 39.85 ($\underline{C}$HH), 37.56 (S$\underline{C}H_2\underline{C}H_2$S), 34.43 (1 C, N$\underline{C}H_3$)
Mass spectrometry	ESI$^+$ (70 eV, MeOH)
m/z (%):	550.9 (17) [L$_2$Cu]$^+$, 306.9 (100) [M - MeCN]$^+$, 245.0 (3) [L + H]$^+$, 213.0 (17) [L - OH]$^+$
IR	KBr
$\tilde{V}$[cm^{-1}]:	3593 (m), 2926 (m), 2855 (w), 2116 (m), 1632 (m), 1539 (w), 1480 (m), 1411 (m), 1258 (s), 1168 (m), 1070 (m), 1033 (s), 992 (m), 849 (w), 763 (m), 693 (w), 640 (s), 576 (m), 519 (m)
Elemental Analysis	C$_{12}$H$_{19}$CuF$_6$N$_3$OPS$_2$ (493.94 gmol^{-1})
Calculated (%):	C: 29.18, H: 3.88, N: 8.51, S: 12.98
Found (%):	C: 28.74, H: 3.84, N: 8.99, S: 11.35

Synthesis of [L^{3Me}CuMeOH]OTf (16)

A complex solution of **14** (150 mg, 0.30 mmol, 1.0 eq.) in MeOH (10 ml) was stirred over night at room temperature and afterwards the complex was crystallised by slow diffusion of diethylether in the complex solution at 4 °C. The product **16** could be obtained as slightly yellow crystals.

Yield: 136 mg (0.28 mmol, 91 %)

^{1}H-NMR (300 MHz, MeOD-d$_4$)

δ [ppm]: 8.49 (d, $^3J_{(H,H)}$ = 6 Hz, 1 H, C$\underline{H}$$^{Py, 6}$), 8.07 (dd, $^3J_{(H,H)}$ = 9 Hz, $^3J_{(H,H)}$ = 6 Hz, 1 H, C$\underline{H}$$^{Py, 4}$), 7.72 (d, $^3J_{(H,H)}$ = 9 Hz, 1 H, C$\underline{H}$$^{Py, 3}$), 7.44 (dd, $^3J_{(H,H)}$ = 6 Hz, $^3J_{(H,H)}$ = 6 Hz, 1 H, C$\underline{H}$$^{Py, 5}$), 4.09 (q, $^3J_{(H,H)}$ = 3 Hz, 1 H, CH$_3$O$\underline{H}$), 3.53 (d, $^3J_{(H,H)}$ = 15 Hz, 2 H, C$\underline{H}$H), 3.36 (d, $^3J_{(H,H)}$ = 15 Hz, 2 H, CH$\underline{H}$), 3.26-3.16 (m, 10 H, C$\underline{H}_3$, C$\underline{H}_3$OH, SC$\underline{H}_2$C$\underline{H}_2$S)

^{13}C-NMR (75 MHz, MeOD-d$_4$)

δ [ppm]: 160.67 ($\underline{C}$OCH$_3$), 150.78 ($\underline{C}$$^{Py, 2}$), 140.08 ($\underline{C}H^{Py, 6}$), 125.26 ($\underline{C}H^{Py, 4}$), 123.31 ($\underline{C}H^{Py, 3}$), 122.92 ($\underline{C}H^{Py, 5}$), 52.40 (CO$\underline{C}H_3$), 44.51 ($\underline{C}$HH), 42.52 (S$\underline{C}H_2$$\underline{C}H_2$S)

Mass spectrometry ESI$^+$ (70 eV, MeOH)

m/z (%): 544.9 (17) [L$_2$Cu]$^+$, 544.9 (100) [M - MeOH]$^+$, 226.0 (13) [L - CH$_3$]$^+$

Elemental Analysis C$_{13}$H$_{19}$CuF$_3$NO$_5$S$_3$ (486.03 gmol^{-1})

Calculated (%): C: 32.13, H: 3.94, N: 2.88, S: 19.79

Found (%): C: 31.88, H: 3.73, N: 2.74, S: 19.57

Synthesis of [L$^{3Me}_2$Zn](OTf)$_2$ (17)

To a solution of **L^{3Me}** (100 mg, 0.42 mmol, 1.0 eq.) in MeCN (5 ml) was added ZnOTf$_2$ (150 mg, 0.42 mmol, 1.0 eq.). The solution was stirred for 16 h at room temperature and the product **17** precipitated through the addition of diethyl ether (10 ml).

Yield:	124 mg (0.14 mmol, 71 % with respect to **L^{3Me}**)
^{1}H-NMR	(300 MHz, MeCN-d$_3$)
δ [ppm]:	8.65 (d, $^3J_{(H,H)}$ = 3 Hz, 2 H, C$\underline{H}^{Py,\ 6,6'}$), 7.49 (s$_{br}$, 2 H, C$\underline{H}^{Py,\ 3,3'}$), 8.18 (dd, $^3J_{(H,H)}$ = 9 Hz, $^3J_{(H,H)}$ = 9 Hz, 2 H, C$\underline{H}^{Py,\ 4,4'}$) 7.67 (dd, $^3J_{(H,H)}$ = 9 Hz, $^3J_{(H,H)}$ = 9 Hz, 2 H, C$\underline{H}^{Py,\ 3,3'}$), 3.62 (d, $^2J_{(H,H)}$ = 15 Hz, 4 H, C$\underline{H}$H), 3.39 (d, $^2J_{(H,H)}$ = 15 Hz, 4 H, CH$\underline{H}$), 3.23-3.05 (m, 14 H, SC$\underline{H_2}$C$\underline{H_2}$S, COC$\underline{H_3}$)
^{13}C-NMR	(75 MHz, MeCN-d$_3$)
δ [ppm]:	169.32 ($\underline{C}^{Py,\ 2}$), 146.24 ($\underline{C}H^{Py,\ 6}$), 140.48 ($\underline{C}H^{Py,\ 4}$), 124.72 ($\underline{C}H^{Py,\ 3}$), 122.59 ($\underline{C}H^{Py,\ 5}$), 84.76 ($\underline{C}OCH_3$), 52.11 (CO$\underline{C}H_3$), 40.04 ($\underline{C}HH$), 38.72 (S$\underline{C}H_2\underline{C}H_2$S)
Mass spectrometry	ESI$^+$ (70 eV, MeOH)
m/z (%):	453.9 (48) [L + Zn + OTf]$^+$, 321.9 (24) [L + Zn + OH]$^+$, 242.0 (10) [L + H]$^+$, 210.0 (100) [L - OH]$^+$
General Information	C$_{24}$H$_{30}$F$_6$N$_2$O$_8$S$_6$Zn (846.26 gmol^{-1})
Calculated (%):	C: 34.06, H, 3.57, N: 3.31, S: 22.73

Synthesis of [L$^{5Me}_2$Zn](OTf)$_2$ (18)

ZnOTf$_2$ (149 mg, 0.41 mmol, 1.0 eq.) was added to a solution of **L^{5Me}** (100 mg, 0.41 mmol, 1.0 eq.) in MeCN (5 ml). The solution was stirred for 16 h at room temperature and the product **18** precipitated through the addition of diethyl ether (10 ml).

Yield:	130 mg (0.15 mmol, 75 % with respect to **L^{5Me}**)
^{1}H-NMR	(300 MHz, MeCN-d$_3$)
δ [ppm]:	7.36 (d, $^3J_{(H,H)}$ = 3 Hz, 2 H, C$\underline{H}^{Im,\,5,5'}$), 7.36 (d, $^3J_{(H,H)}$ = 3 Hz, 2 H, C$\underline{H}^{Im,\,4,4'}$), 4.01 (s, 3 H, NC$\underline{H}_3$), 3.56 (s, 8 H, C$\underline{H}_2$), 3.25 (s, 6 H, COC$\underline{H}_3$), 3.10 (s, 8 H, SC$\underline{H}_2C\underline{H}_2$S)
^{13}C-NMR	(75 MHz, MeCN-d$_3$)
δ [ppm]:	142.84 ($\underline{C}^{Im,\,2}$), 126.06 ($\underline{C}H^{Im,\,4}$), 118.36 ($\underline{C}H^{Im,\,5}$), 82.94 ($\underline{C}OCH_3$), 52.01 (COC$\underline{H}_3$), 38.05 ($\underline{C}H_2$), 37.56 (S$\underline{C}H_2CH_2S$), 36.33 (N$\underline{C}H_3$)
Mass spectrometry	ESI$^+$ (70 eV, MeOH)
m/z (%):	456.8 (34) [L + Zn + OTf]$^+$, 324.9 (30) [L + Zn + OH]$^+$, 245.0 (54) [L + H]$^+$, 213.1 (100) [L - OH]$^+$
General Information	C$_{22}$H$_{32}$F$_6$N$_4$O$_8$S$_6$Zn (849.97 gmol^{-1})
Calculated (%):	C: 31.00, H: 3.78, N: 6.57, S: 22.57

Synthesis of [L^{8Me}Cu]OTf (19)

[Cu(MeCN)$_4$]OTf (47 mg, 0.12 mmol, 1.0 eq.) was added to a solution of **L^{8Me}** (45 mg, 0.12 mmol, 1.0 eq.) dissolved in MeCN (5 ml). The reaction was stirred over night at room temperature. The complex was precipitated by the addition of diethyl ether (15 ml), taken up in MeCN and crystallised through slow ether diffusion 4 °C. The product **19** could be obtained as colourless crystals.

Yield:	56 mg (0.10 mmol, 81 %)

^{1}H-NMR (500 MHz, MeCN-d$_3$)

δ [ppm]: 8.58 (s, 1 H, C$\underline{H}$$^{Py, 10}$), 7.86 (dd, $^3J_{(H,H)}$ = 7 Hz, $^3J_{(H,H)}$ = 4 Hz, 2 H, C$\underline{H}$$^{Py, 4, 12}$), 7.70 (d, $^3J_{(H,H)}$ = 6 Hz, 1 H, C$\underline{H}$$^{Py, 3}$), 7.54 (d, $^3J_{(H,H)}$ = 4 Hz, 1 H, C$\underline{H}$$^{Py, 5}$), 7.47 (d, $^3J_{(H,H)}$ = 7 Hz, 1 H, C$\underline{H}$$^{Py, 13}$), 7.29 (dd, $^3J_{(H,H)}$ = 6 Hz, $^3J_{(H,H)}$ = 6 Hz, 1 H, C$\underline{H}$$^{Py, 11}$), 3.63 (d, $^2J_{(H,H)}$ = 8 Hz, 2 H, C$\underline{H}$H), 3.41-3.38 (m, 9 H, CH$\underline{H}$, SC$\underline{H}_2$C$\underline{H}_2$S, COC$\underline{H}_3$), 1.96 (s, 6 H, C(C$\underline{H}_3$)$_2$)

^{13}C-NMR (125 MHz, MeCN-d$_3$)

δ [ppm]: 165.49 ($\underline{C}$$^{Py, 2}$), 164.16 ($\underline{C}$$^{Py, 6}$), 151.40 ($\underline{C}$$^{Py, 8}$), 140.03 ($\underline{C}H^{Py, 10}$), 139.54 ($\underline{C}H^{Py, 4}$), 123.54 ($\underline{C}H^{Py, 12}$), 123.45 ($\underline{C}H^{Py, 11}$), 122.94 ($\underline{C}H^{Py, 13}$), 121.94 ($\underline{C}H^{Py, 5}$), 120.64 ($\underline{C}H^{Py, 3}$), 52.41 (CO$\underline{C}H_3$) 47.77 ($\underline{C}$(CH$_3$)$_2$), 42.24 ($\underline{C}$HH), 37.77 (S$\underline{C}H_2$$\underline{C}H_2$S), 28.37 (C($\underline{C}H_3$)$_2$)

Mass spectrometry	ESI$^+$ (70 eV, MeOH)
m/z (%):	423.0 (100) [M]$^+$
General Information	C$_{20}$H$_{24}$CuF$_3$N$_2$O$_4$S$_3$ (573.15 gmol^{-1})
Calculated (%):	C: 30.10, H: 2.76, N: 3.19, S: 21.91

Synthesis of [L^{3Me}Mn(CO)_3]OTf (20)

AgOTf (130 mg, 0.5 mmol, 1.0 eq.) was added to a solution of [Mn(CO)_4Br] (138 mg, 0.5 mmol, 1.0 eq.) in dry acetone (25 ml). The reaction was heated under reflux for 2 h. The precipitating AgBr was separated by filtration and **L^{3Me}** (120 mg, 0.5 mmol, 1.0 eq.) was added to the filtrate. The mixture was stirred under reflux at 60 °C for 1.5 h. The solvent was removed under reduced pressure and the product was further purified by re-crystallisation from DCM/Et_2O at 4 °C. The product **20** could be obtained as yellow crystals.

Yield:	250 mg (47 mmol, 97 %)
Mass spectrometry	ESI$^+$ (70 eV, MeOH)
m/z (%):	296.0 (100) [M - 3 CO]$^+$
IR	KBr
$\tilde{V}$[cm^{-1}]:	3561 (w), 3441 (w), 3151 (m), 3127 (m), 3090 (w), 2985 (m), 2940 (m), 2855 (w), 2046 (s), 1980 (s), 1954 (s), 1724 (w), 1622 (w), 1553 (w), 1492 (m), 1460 (m), 1439 (m), 1426 (m), 1258 (s), 1226 (s), 1157 (s), 1102 (s), 1580 (w), 1032 (s), 1012 (m), 984 (m), 952 (w), 862 (w), 764 (s), 723 (m), 700 (w), 674 (m), 640 (s), 573 (w), 545 (m), 517 (s), 495 (w), 474 (m), 440 (w)
General Information	C_{15}H_{15}F_3MnNO_7S_3 (529.41 gmol^{-1})
Calculated (%):	C: 34.03, H: 2.86, N: 2.65, S: 18.17

Synthesis of [L^{5Me}Mn(CO)$_3$]OTf (21)

AgOTf (130 mg, 0.5 mmol, 1.0 eq.) was added to a solution of [Mn(CO)$_4$Br] (138 mg, 0.5 mmol, 1.0 eq.) in dry acetone (25 ml). The reaction was heated under reflux for 2 h. The precipitating AgBr was separated by filtration and **L^{5Me}** (122 mg, 0.5 mmol, 1.0 eq.) was added to the filtrate. The mixture was stirred under reflux at 60 °C for 1.5 h. The solvent was removed under reduced pressure and the product was further purified by re-crystallisation from DCM/Et$_2$O at 4 °C. The product **21** could be obtained as yellow crystals.

Yield:	244 mg (0.46 mmol, 92 %)
^{1}H-NMR	(300 MHz, MeOD-d$_4$)
δ [ppm]:	7.41 (s, 1 H, CH$^{Im, 4}$), 7.27 (s, 1 H, CH$^{Im, 5}$), 3.91 (s, 3 H, COCH$_3$), 3.82 (d, $J_{(H,H)}$ = 9 Hz, 2 H, CHH), 3.55 (s, 3 H, NCH$_3$), 3.47 (d, $J_{(H,H)}$ = 9 Hz, 2 H, CHH)
Mass spectrometry	ESI$^+$ (70 eV, MeOH)
m/z (%):	298.9 (100) [M - 3 CO]$^+$
IR	KBr
$\tilde{V}$[cm^{-1}]:	3486 (w), 3093 (m), 2909 (w), 2046 (s), 1960 (s), 1940 (s), 1762 (m), 1674 (w), 1599 (m), 1531 (w), 1465 (m), 1435 (m), 1371 (w), 1283 (s), 1251 (s), 1225 (s), 1161 (s), 1062 (w), 1031 (s), 998 (w), 969 (w), 931 (w), 899 (w), 854 (w), 766 (w), 637 (s), 567 (m), 517 (m), 471 (w), 440 (w), 411 (w)
Elemental analysis	C$_{14}$H$_{16}$F$_3$MnN$_2$O$_7$S$_3$ (532.41 gmol^{-1})
Calculated (%):	C: 31.58, H: 3.03, N: 5.26, S: 18.07
Found (%):	C: 31.14, H: 3.05, N: 2.18, S: 17.85

Synthesis of [L^{6H}Mn(CO)$_3$]OTf (22)

AgOTf (130 mg, 0.5 mmol, 1.0 eq.) was added to a solution of [Mn(CO)$_4$Br] (138 mg, 0.5 mmol, 1.0 eq.) in dry acetone (25 ml). The reaction was heated under reflux for 2 h. The precipitating AgBr was separated by filtration and **L^{6H}** (131 mg, 0.5 mmol, 1.0 eq.) was added to the filtrate. The mixture was stirred under reflux at 60 °C for 1.5 h. The solvent was removed under reduced pressure and the product was further purified by re-crystallisation from DCM/Et$_2$O at 4 °C. The product **22** could be obtained as yellow crystals.

Yield:	259 mg (0.47 mmol, 95 %)
^{1}H-NMR	(300 MHz, MeOD-d$_4$)
δ [ppm]:	9.22 (d, $^3J_{(H,H)}$ = 3 Hz, 2 H, C$\underline{H}$$^{Py, 3,3'}$), 9.01 (d, $^3J_{(H,H)}$ = 3 Hz, 1 H, C$\underline{H}$$^{Py, 3''}$), 8.19 (d, $^3J_{(H,H)}$ = 6 Hz, 2 H, C$\underline{H}$$^{Py, 6,6'}$), 8.12 (d, $J_{(H,H)}$ = 6 Hz, 1 H, C$\underline{H}$$^{Py, 6''}$), 8.98 (dd, $^3J_{(H,H)}$ = 6 Hz, $^3J_{(H,H)}$ = 6 Hz, 3 H, C$\underline{H}$$^{Py, 5,5,5''}$), 7.66 (dd, $^3J_{(H,H)}$ = 3 Hz, $^3J_{(H,H)}$ = 3 Hz, 1 H, C$\underline{H}$$^{Py, 4''}$), 9.01 (d, $^3J_{(H,H)}$ = 3 Hz, 1 H, C$\underline{H}$$^{Py, 4,4'}$).
Mass spectrometry	ESI$^+$ (70 eV, MeOH)
m/z (%):	316.9 (100) [M - 3 CO]$^+$
IR	KBr
$\tilde{\nu}$[cm^{-1}]:	3003 (w), 2955 (w), 2923 (w), 2854 (w), 2043 (m), 1967 (m), 1944 (m), 1586 (w), 1464 (m), 1441 (m), 1417 (m), 1377 (w), 1273 (s), 1253 (s), 1229 (m), 1179 (m), 1157 (m), 1129 (m), 1078 (m), 1029 (s), 993 (m), 950 (m), 862 (w), 798 (m), 758 (m), 713 (m), 672 (s), 639 (s), 573 (m), 556 (w), 518 (s), 487 (m), 469 (w), 405 (w)
General Information	C$_{20}$H$_{14}$F$_3$MnN$_4$O$_6$S (550.35 gmol^{-1})
Calculated (%):	C: 43.65, H: 2.56, N: 10.18, S: 5.83

Synthesis of [L^{6Acet}Mn(CO)$_3$]OTf (23)

AgOTf (130 mg, 0.5 mmol, 1.0 eq.) was added to a solution of [Mn(CO)$_4$Br] (138 mg, 0.5 mmol, 1.0 eq.) in dry acetone (25 ml). The reaction was heated under reflux for 2 h. The precipitating AgBr was separated by filtration and **L^{6Acet}** (150 mg, 0.5 mmol, 1.0 eq.) was added to the filtrate. The mixture was stirred under reflux for 1.5 h at 60 °C. The solvent was removed under reduced pressure and the product was further purified by re-crystallisation from DCM/Et$_2$O at 4 °C. The product **23** could be obtained as yellow crystals.

Yield:	148 mg (0.25 mmol, 50 %)
^{1}H-NMR	(300 MHz, MeOD-d$_4$)
δ [ppm]:	9.23 (s, 1 H, C$\underline{H}$^{Py}), 9.03 (s, 1 H, C$\underline{H}$^{Py}), 8.73 (s, 1 H, C$\underline{H}$^{Py}), 8.41 (s, 1 H, C$\underline{H}$^{Py}), 8.15-7.96 (m, 3 H, C$\underline{H}$^{Py}), 7.68 (s, 1 H, C$\underline{H}$^{Py}), 7.45-7.42 (m, 3 H, C$\underline{H}$^{Py}), 7.22 (s, 1 H, C$\underline{H}$^{Py}), 2.40 (s, 3 H, C$\underline{H}_3$)
Mass spectrometry	EI$^+$ (70 eV)
m/z (%):	358 (86) [M - 3 CO]$^+$, 209 (100) [C$_{13}$H$_{11}$N$_3$]$^+$
IR	KBr
$\tilde{V}$[cm^{-1}]:	3475 (w), 3092 (m), 2906 (w), 2360 (w), 2045 (s), 1957 (s), 1939 (s), 1761 (m), 1674 (w), 1597 (m), 1530 (m), 1465 (m), 1435 (m), 1371 (w), 1282 (s), 1250 (s), 1225 (s), 1161 (s), 1062 (m), 1031 (s), 998 (m), 969 (w), 931 (w), 901 (w), 855 (w), 766 (m), 677 (w), 637 (s), 567 (m), 517 (m), 471 (w), 441 (w), 412 (w)
General Information	C$_{22}$H$_{15}$F$_3$MnN$_4$O$_7$S (591.38 gmol^{-1})
Calculated (%):	C: 44.68, H: 2.56, N: 9.47, S: 5.42

Synthesis of [L^{3Me}Cu(CO)]OTf (24)

CO was bubbled through a solution of **14** (120 mg, 0.35 mmol, 1.0 eq.) in acetone (10 ml) under vigorous stirring for 30 min. The product was precipitated by the addition of diethyl ether (30 ml). The product **24** could be obtained as white powder after filtration.

Yield:	72 mg (0.15 mmol, 43 %)
^{1}H-NMR	(500 MHz, acetone-d$_6$)
δ [ppm]:	8.73 (d, $^3J_{(H,H)}$ = 4 Hz, 1 H, C$\underline{H}^{Py, 6}$), 8.12 (t, $^3J_{(H,H)}$ = 8 Hz, 1 H, C$\underline{H}^{Py, 4}$), 7.85 (d, $^3J_{(H,H)}$ = 8 Hz, 1 H, C$\underline{H}^{Py, 3}$), 7.61 (t, $^3J_{(H,H)}$ = 5 Hz, 1 H, C$\underline{H}^{Py, 5}$), 3.53-3.38 (m, 11 H, C$\underline{H}_2$, SC$\underline{H}_2$C$\underline{H}_2$S, COC$\underline{H}_3$)
^{13}C-NMR	(125 MHz, acetone-d$_6$)
δ [ppm]:	163.23 ($\underline{C}$OCH$_3$), 154.16 ($\underline{C}^{Py, 2}$), 150.82 ($\underline{C}$H$^{Py, 6}$), 140.39 ($\underline{C}$H$^{Py, 4}$), 124.98 ($\underline{C}$H$^{Py, 3}$), 120.30 ($\underline{C}$H$^{Py, 5}$), 52.19 (CO$\underline{C}$H$_3$), 41.37 ($\underline{C}$HH), 38.12 (S$\underline{C}$H$_2$$\underline{C}H_2$S)
Mass spectrometry	ESI$^+$ (70 eV, MeOH)
m/z (%):	303.9 (4) [M - CO]$^+$, 264.1 (60) [L + Na]$^+$, 210.0 (100) [L - OH]$^+$
IR	KBr
$\tilde{v}$ [cm^{-1}]:	3480 (m), 2984 (m), 2928 (m), 2841 (m), 2313 (w), 2280 (w), 2255 (w), 2119 (m), 2020 (w), 1710 (w), 1597 (s), 1571 (m), 1472 (s), 1433 (s), 1414 (s), 1373 (w), 1287 (s), 1223 (s), 1165 (s), 1101 (s), 1075 (s), 1028 (s), 956 (m), 955 (m), 929 (w), 900 (w), 854 (m), 800 (m), 784 (s), 757 (m), 714 (m), 674 (w), 638 (s), 573 (m), 550 (m), 517 (s), 419 (w)
General Information	C$_{13}$H$_{15}$CuF$_3$NO$_5$S$_3$ (482.00 gmol^{-1})
Calculated (%):	C: 32.39, H: 3.14, N: 2.91, S: 19.96

Synthesis of [L^{5Me}Cu(CO)]OTf (25)

[Cu(MeCN)$_4$]OTf (187 mg, 0.5 mmol, 1.0 eq.) was added to a solution of **L^{5Me}** (122 mg, 0.5 mmol, 1.0 eq.) dissolved in acetone (10 ml). CO bubbled was through the reaction solution for 30 min. The complex was afterwards precipitated by the addition of diethyl ether (30 ml). The complex was taken up in MeCN and crystallised through slow ether diffusion 4 °C. The product could be obtained as colourless crystals.

Yield:	133 mg (0.27 mmol, 55 %)
^{1}H-NMR	(300 MHz, DMSO-d$_7$)
δ [ppm]:	7.60 (s, 1 H, CH$^{Im, 4}$), 7.27 (s, 1 H, CH$^{Im, 5}$), 4.42 (s, 3 H, COCH$_3$), 3.78-3.44 (m, 11 H, CH$_2$, NCH$_3$, SCH$_2$CH$_2$S)
^{13}C-NMR	(75 MHz, DMSO-d$_7$)
δ [ppm]:	127.34 (C$^{Im, 2}$), 124.61 (CH$^{Im, 4}$), 123.64 (CH$^{Im, 5}$), 80.58 (COCH$_3$), 51.78 (COCH$_3$), 30.52 (CH$_2$), 37.39 (SCH$_2$CH$_2$S), 35.75 (NCH$_3$)
IR	KBr
$\tilde{\nu}$[cm^{-1}]:	3495 (w), 3130 (w), 2925 (m), 2853 (w), 2281 (w), 2115 (m), 1632 (m), 1541 (m), 1481 (m), 1412 (m), 1253 (s), 1162 (s), 1070 (s), 1030 (s), 993 (m), 853 (w), 761 (m), 727 (w), 693 (w), 640 (s), 575 (m), 518 (m)
General Information	C$_{12}$H$_{16}$CuF$_3$N$_2$O$_5$S$_3$ (485.00 gmol^{-1})
Calculated (%):	C: 29.72, H: 3.33, N: 5.78, S: 19.83

Synthesis of [L^{6H}Cu(CO)]PF$_6$ (26)

CO was bubbled through a solution of **6** (235mg, 0.35 mmol, 1.0 eq.) in abs. acetone (10 ml) under strong stirring for 60 min. The formed precipitate was separated from the solvent and the product could be obtained as grey powder.

Yield:	217 mg (0.44 mmol, 87 %)
^{1}H-NMR	(500 MHz, DMF-d$_7$)
δ [ppm]:	9.08 (s, 3 H, C$\underline{H}$$^{Py, 3,3',3''}$), 8.46 (s, 3 H, C$\underline{H}$$^{Py, 4,4',4''}$), 8.19 (s, 3 H, C$\underline{H}$$^{Py, 6,6',6''}$), 7.64 (dd, $^3J_{(H,H)}$ = 6 Hz, $^3J_{(H,H)}$ = 6 Hz, 3 H, C$\underline{H}$$^{Py, 5,5',5''}$), 4.25 (s, 2 H, CN$\underline{H}_2$)
^{13}C-NMR	(125 MHz, DMF-d$_7$)
δ [ppm]:	158.34 ($\underline{C}$$^{Py, 2,2',2''}$), 151.78 ($\underline{C}H^{Py, 3,3',3''}$), 140.78 ($\underline{C}H^{Py, 4,4',4''}$), 124.59 ($\underline{C}H^{Py, 6,6',6''}$), 123.64 ($\underline{C}H^{Py, 5,5',5''}$), 64.92 ($\underline{C}NH_2$)
IR	KBr
$\tilde{V}$[cm^{-1}]:	3391 (m), 3330 (m), 3127 (w), 3109 (w), 2556 (w), 2102 (s), 2054 (m), 1996 (w), 1868 (w), 1706 (w), 1595 (s), 1465 (s), 1438 (s), 1318 (w), 1296 (w), 1216 (w), 1157 (m), 1103 (w), 1090 (m), 1065 (w), 1023 (m), 999 (w), 959 (s), 899 (w), 870 (s), 843 (s), 766 (s), 755 (s), 652 (s), 558 (s),
Elemental Analysis	C$_{17}$H$_{14}$CuF$_6$N$_4$OP (498.83 gmol^{-1})
Calculated (%):	C: 40.93, H: 2.83, N: 11.23
Found (%):	C: 40.53, H: 2.82, N: 10.98

11.5 Protocols for Solution Preparation and for the Analytic Experiments

11.5.1 Stock Solution Preparation

General Considerations

Water used for the preparation of stock solutions was either milliQ water or bidestilled water. Stock solutions of the peptides, fibrils and ThT were stored in the freezer at 4 °C and CORM stock solutions were stored under light exclusion.

Aβ$_{1-16}$ Stock Solution

Stock solutions of the Aβ$_{1-16}$ peptide (10 mM) were prepared by dissolving Aβ$_{1-16}$ · 6 TFA in D$_2$O, resulting in a pH ≈ 2. Peptide concentration was dosed by UV/Vis-spectroscopy considering the free tyrosine (ε_{276}-ε_{295} (pH < 9) = 1410 M^{-1}cm^{-1}).

Aβ$_{1-40}$ Stock Solution

Aβ$_{1-40}$ stock solution (1 mM) was prepared by dissolving Aβ$_{1-40}$ · X TFA in D$_2$O, resulting in pH ≈ 2. Peptide concentration was dosed by UV/Vis-spectroscopy considering the free tyrosine in NaOH (0.1 M) (ε_{293}-ε_{360} (pH > 9) = 2410 M^{-1}cm^{-1}).

Fibril Stock Solution of Aβ$_{1-40}$

Fibrils (500 μM) were prepared by diluting 200 μl of the Aβ$_{1-40}$ stock solution (1 mM) in 200 μl HEPES buffer (50 mM) and incubation of the resulting solution at 37 °C over 48 h. Fibril formation was tested with ThT.

Myoglobin Stock Solution

A myoglobin stock solution was prepared by dissolving myoglobin in 0.1 M phosphate buffer (7.4). The concentration was determined by UV/Vis dosing at 557 nm in the presence of dithionite. Dosing was performed three times at different myoglobin and dithionite concentrations. The stock solution was stored under light exclusion at 8 °C.

Cu^{2+} and Zn^{2+} Stock Solutions

Stock solutions of CuSO$_4$ and ZnSO$_4$ were prepared at 10 mM by dissolving the corresponding metal salts in D$_2$O.

Fz Stock Solutions

The stock solution of Fz (Fz = ferrozine, 5,6-diphenyl-3-(2-pyridyl)-1,2,4-triazine-4,4''-disulfonic acid) and ThT (Thioflavin T) was prepared at 10 mM in water.

Stock Solution of Sodium Dithionite

Stock solutions of sodium dithionite (0.1 M) were freshly prepared directly before use.

Stock Solutions of the Ligands, the Multifunctional Tools and the CORMs

The stock solutions of the synthesised compounds were prepared at 10 mM in DMSO or in DMSO-d$_6$.

Buffer Stock Solutions

HEPES buffer solutions were prepared by dissolving sodium salt of 2-(4-(2-hydroxyethyl)piperazin-1-yl)ethanesulfonic acid in water. The pH value was adjusted by adding either HCl or NaOH.

Phosphate buffer solutions were prepared by dissolving appropriate amounts of Na_2/K_2HPO4 and Na/KH_2PO4 in water. Tuning of the pH value was done by addition of HCl or NaOH. For the NMR studies D_2O were used instead of water and the pH value was adjusted with DCl and NaOD.

Tris buffer solutions were prepared by dissolving appropriate amounts of 2-amino-2-hydroxymethyl-propane-1,3-diol (Tris) in D_2O. The pH value was adjusted with DCl and NaOD.

11.5.2 Determination of Stability Constants via UV/Vis

Stability constants were determined by titration of the chromophoric $[Cu(Fz)_2]^{3-}$ complex (Fz = ferrozine, 5,6-diphenyl-3-(2-pyridyl)-1,2,4-triazine-4,4''-disulfonic acid). The $[Cu(Fz)_2]^{3-}$ complex has a characteristic UV band at 470 nm with an extinction coefficient of 4320 $M^{-1} cm^{-1}$.[145] Upon addition of ligand the UV band decreases, through metal exchange from $[Cu(Fz)_2]^{3-}$ to the ligand. Titration conditions for the experiments were 105 µM Fz, 50 µM Cu^{2+}, 100 µM $Na_2S_2O_3$ in 0.1 M HEPES buffer (pH 7.4). All stock solution were degassed and saturated with argon. A freshly prepared $Na_2S_2O_3$ solution was used to reduce Cu^{2+}. Excess of Fz was provided to compensates the partially formed $[Fe(Fz)_3]^{4-}$, visible by the shoulder at 562 nm (ε = 2600 $M^{-1} cm^{-1}$).[145] The iron trace amounts originate from the used chemicals. For the tridentate ligands L^{3H} and L^{5H} 100 µM and for the ligands L^{6H} and L^{8H} 20 µM were added stepwise. After each addition of ligand approximately two min were waited before collecting the spectra, since this time is required for equilibration and stabilisation of the UV/Vis spectra. At the end of the experiment additional $Na_2S_2O_3$ was added to reduce $[CuFz_2]^{2-}$ formed during the experiment. Only a slight increase of the absorbance corresponding to the presence of less than 5 % $[CuFz_2]^{2-}$ could be observed. Such a small value is sufficiently weak and can be neglected. Under this procedure five up to ten values were recorded and calculations of stability constants were done with equation 9, according to the literature (c_0 = $[Cu^+]_{initial}$, c_1 = $[Fz]_{initial}$, c_2 = $[L^x]$, a_{Fz} = [Fz], β_2 = 11.6).[145] The experiment was repeated at least three times to quantify the calculated values.

$$K_a^L = \beta_2 c_0 \frac{(1-a_{Fz})\frac{(\frac{c_1}{c_0}-2a_{Fz})^2}{a_{Fz}}}{(\frac{c_2}{c_0}-1+a_{Fz})} \tag{9}$$

11.5.3 Ascorbate Consumption Study

Ascorbate consumption was followed by UV/Vis spectroscopy at 265 nm (14500 $M^{-1} cm^{-1}$) over a time period of 5 min in 50 mM phosphate buffer. 100 µM sodium ascorbate, 5 µM Cu^{2+} and 7 µM of Ligand and 7 µM of $A\beta_{1-16}$ were used in the experiments. The order of addition was buffer, ascorbate, ligand/$A\beta_{1-16}$, Cu^{2+}. The ascorbate stock solutions were freshly prepared and no longer used than for 5 h. Each measurement was repeated at least three times to minimise errors and quantify the results.

11.5.4 Cell Viability Assays

Undifferentiated human neuroblastoma SH-SY5Y cells were grown under standard culture conditions in an incubator containing a humidified atmosphere with 5 % CO_2 at 37 °C. The medium used was DMEM (Dubelcoo's Modified Eagle's Medium) supplemented with 15 % foetal bovine serum (FBS). For the experiments, SH-SY5Y cells were seeded into 24-well plates at a density of 200 000 cells/well. After 24 h incubation, the medium was removed and replaced with 0.5 ml of DMEM, prior to drug exposure. Cell viability was determined by a mitochondria enzyme dependent reaction of MTT (3-(4,5-dimethylthiazol-2-yl)-2,5-diphenyltetrazolium bromide) as described elsewhere.[292] Briefly, MTT was added to SH-SY5Y cells after treatment in 24-well plates at final concentration of 5 mg/ml at 37 °C for 4 h, 24 h after testing the compound. Metabolic active cells cleaved the yellow tetrazolium salt MTT to purple formazan crystals. The reaction was terminated by removal of the supernatant and addition of 1.5 ml DMSO to dissolve the formazan product, following thorough mixing to dissolve the formazan product and the absorbance was measured by a multiplate reader at 570 nm. Results were expressed as percentage of control. Each assay was performed in triplication of at least three wells. The Cell studies as described above were performed by Isabelle Sasaki in the laboratories of the *Institut de Pharmacologie et de Biologie Structurale* (IPBS) in Toulouse, France.

11.5.5 The CO Release Experiment – Myoglobin Assay

To determine the photo active CO release of the synthesised CORMs a myoglobin assay was performed.[329,344,345] Myoglobin (Mb) can be used as CO detector, since CO has a high affinity to coordinate at the heme-iron of Mb. Upon coordination and formation of the MbCO complex changes the UV/Vis spectra. Mb has a characteristic absorption band at 555 nm (12.9 mM^{-1} cm^{-1}), whereas MbCO has two absorption bands at 540 nm (14.5 mM^{-1} cm^{-1}) and 577 nm (12.9 mM^{-1} cm^{-1}).[350] Thus, by following the absorption at three wavelengths by UV/Vis spectroscopy, the amount of released CO can be determined. Correspondingly, the band at 557 nm decreases upon formation of MbCO and the bands at 540 nm and 577 nm increase. The samples were prepared by transferring the required amount of myoglobin solution in UV/Vis cuvettes. This Mb solution was than degassed with argon and a degassed solution of dithionite and phosphate buffer were added. The CORM was added and the cuvettes shortly shaken to achieve a homogeneously sample. The final concentrations were 10 μM CORM, 10 mM dithionite, 60 μM myoglobin and 0.1 M phosphate buffer (pH 7.4). Samples were incubated in the dark between 1 h and 21 h. Stability in the dark was determined by measuring the UV/Vis spectra of the sample every 5 min for 16 h. The samples were irradiated at 365 nm to determine the number of released CO molecules. Irradiation times were at the beginning 1 min and after 1 h the irradiation time was expanded to 10 min. A spectrum was recorded after each irradiation. The measurement was repeated until no further changes could be observed. The number of released CO was calculated by using equation 10.

$$c(MbCO) = \left(\frac{A(t)}{l} - \frac{A(t=0)}{l} \right) \frac{1}{\varepsilon_{540\,nm}(MbCO) - \dfrac{A(t=0)}{c_0(Mb) \cdot l}}$$

(10)

Appendix A

Influence of CO as a Strong Donor

Introduction

The particular bonding interaction between metal atoms and carbon monoxide (CO) is well described by the bonding model according to Dewar-Chatt-Duncanson.[351–353] Metal carbonyls can be stabilised by a synergistic donor-acceptor interaction, combining the σ-donor and π-acceptor character of CO molecules (Figure 57). The 5σ-orbital, which is the highest occupied molecule orbital (HOMO) is an anti-bonding orbital predominantly comprises of C 2s, C $2p_z$ and O $2p_z$. Due to the high carbon character coordinates CO end-on *via* the carbon. Thus, formation of a σ-bond with a free, symmetrically equivalent orbital of the metal induces a slight increase of the CO bonding order (Figure 58).[354]

Figure 57 Synergistic bonding model of metal carbonyl complexes according to Dewar-Chatt-Duncanson.

The increased electron density on the metal, due to the σ-bonds, is balanced by π-backbonding in the lowest unoccupied molecular orbital (LUMO), the 2π*-orbital, of CO. The magnitude of this effect depends on the transition metal, its valency and on co-ligands. If the coordination sphere is saturated by strong σ- or π-donors, so that much electron density is pushed to the metal, then the π–backbonding becomes favoured. The opposite is present in case of other π-acceptors as co-ligands. They withdraw electron density from the metal and formation of π-backbonding to CO is disfavoured. This effect will even increase if the acceptors compete for the same d-orbitals, as seen in complexes with CO molecules in *trans* position.[355] Metal carbonyl complexes can be characterised by their specific CO stretching vibrations. The π-backbonding increases the electron density in the antibonding orbital of the CO, which therefore weakens the bond strength in CO. As a consequence lower wavenumbers ($\tilde{\nu}$) for the CO stretching vibration can be detected in metal carbonyls.[356] The value is also a sensitive indicator for the electronic situation at the metal centre. Thus, performing IR measurements, information about the electron density can be obtained. Furthermore, the stretching vibration can be used as an indirect measure of the properties of co-ligands in the complex. The tripodal ligands **L**[3Me] and **L**[5Me], which have shown the best results with respect to Cu^{+} selectivity, will be used for the synthesis of Cu^{+}-containing CO complexes. **L**[6H] was also examined in order to study the influence of stronger σ-donors.
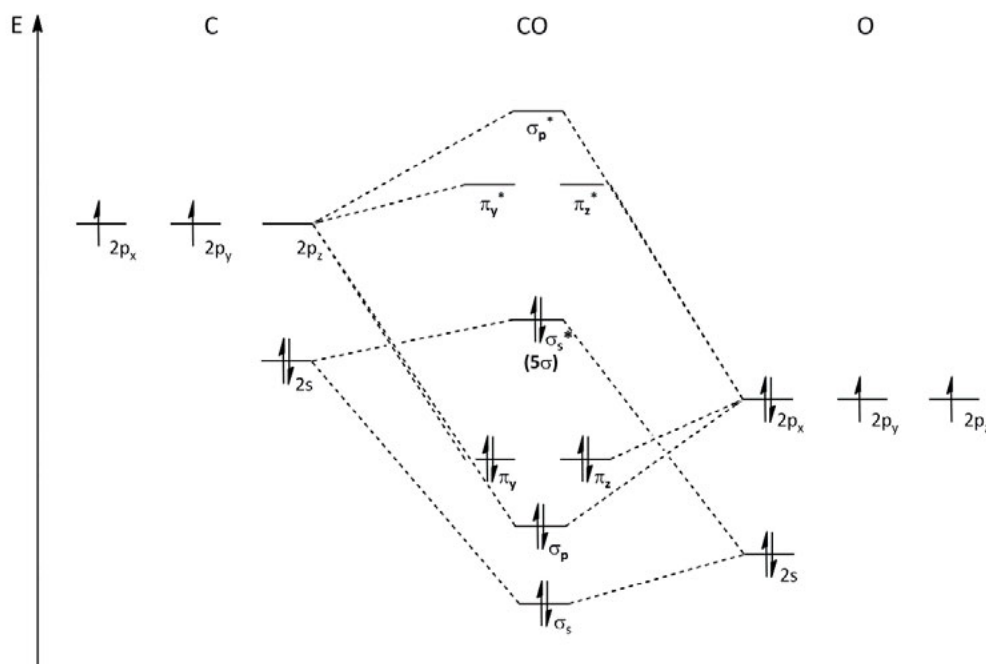
Figure 58 Molecular orbital diagram of CO. The 1s-orbitals were omitted since they are not involved in the bonding.

Synthesis and Characterisation of Cu-based CO Complexes

Precursors for the CO complexes were synthesised by dissolving equimolar amounts of ligand (L^{3Me}, L^{5Me} and L^{6H}) and [Cu(MeCN)$_4$]OTf in acetone. The solution was stirred for 30 min and afterwards CO gas was bubbled through the reaction solution. After 60 min the gas flow was stopped and CO complexes were precipitated by addition of diethyl ether. All three complexes could be synthesised in moderate to good yields (43 % - 87 %). The complexes were characterised by IR spectroscopy, NMR spectroscopy and also ESI-MS spectrometry. Unfortunately, no molecular peak could be observed in the mass spectra, since the CO molecule was obviously cleaved in the measurement. Thus, only the CO free [L^XCu]$^+$ species were recorded. Although no crystal structures could be obtained, formation of [L^{3Me}Cu(CO)]OTf (**13**), [L^{5Me}Cu(CO)]OTf (**14**) and [L^{6H}Cu(CO)]PF$_6$ (**15**) could be verified by IR spectroscopy (Figure 59). In case of **15** two different binding modes are possible: coordination by all three pyridine groups like in **6** or by two pyridine groups and the amine group. Examples for the latter one are given in the literature[250] and also by the complexes **22** and **23**. The binding mode present in **15** could be determined by its ^{1}H-NMR spectrum. The amine shows no significant high field shift and, although broadened, only one signal set could be obtained for the three pyridine groups. CO stretching vibrations and force constants of the metal carbonyl complexes are summarised in Table 28. The force constant *k* can be calculated by equation 11, with μ as reduced mass, $\tilde{V}$ as CO stretching vibration and c as velocity of light.

$$= \frac{1}{2\pi c}\sqrt{\frac{k}{\mu}} \tag{11}$$
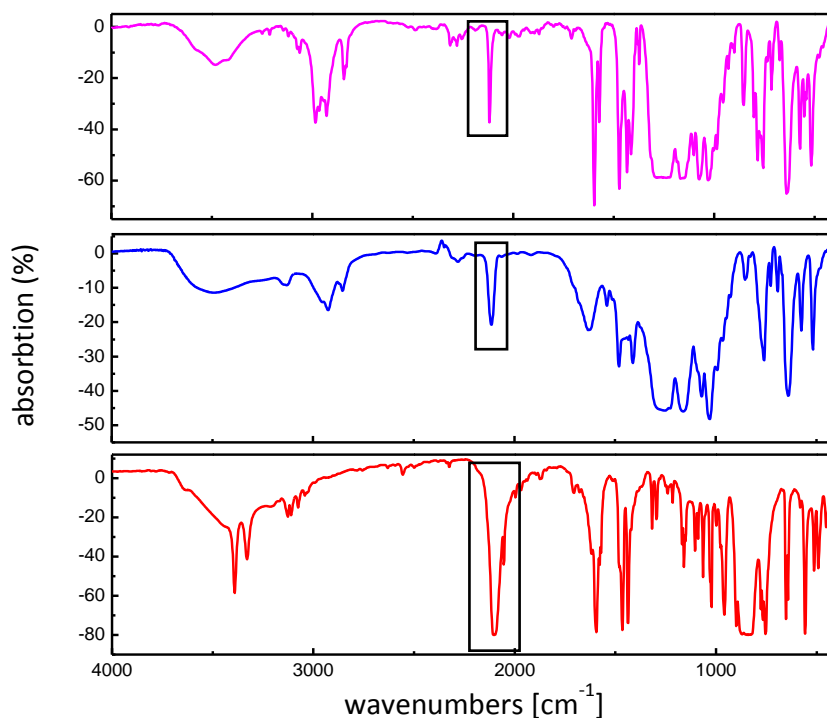
*Figure 59 IR absorption spectra for **13** (red, bottom), **14** (blue, middle) and **15** (pink, top) measured in KBr.*

The following order results for the synthesised CO complexes, according to their CO stretch frequencies: **13** ≈ **14** > **15** (Table 28). **L^{6H}** has three pyridine groups which are good σ-donors. Upon coordination electron density is pushed to the Cu$^+$ centre and thus available for π-backbonding to the CO. Thus, in complex **15**, the lowest stretching frequencies were found. The higher wavenumbers for **13** and **14** are most likely induced by the thioether sidearm. Thioether groups are rather weak donors and do not push much electron density on the metal centre.

*Table 28 CO stretching vibrations $\tilde{v}_{co}$ and force constants k of **13**, **14** and **15** and literature known complexes (tpb = tris(pyrazolyl)borate).*

	$\tilde{v}_{CO}$ [cm^{-1}]	k[N m^{-1}]
13	2118	1813
14	2114	1806
15	2102	1786
free CO[281]	2143	1856
[tpb$^{H, H}$CuCO][357]	2080	1748
[tpb$^{CF3, CF3}$CuCO][357]	2137	1846

The comparison of **13** and **14** shows, that **13** had slightly higher wavenumber for the CO stretching vibration. This difference is induced by the different nitrogen donors in the ligands. **13** has a pyridine group, whereas **14** has a *N*-methylimidazole as nitrogen donor. Pyridine is not only a good σ-donor but comprises also a π-acceptor character. Therefore, less electron density is centred on the metal and is available for the CO back-bond, resulting in a higher stretching frequency. Also *N*-methyimidazole is a π-acceptor, but not as distinct as pyridine. However, the difference is with 4 cm^{-1} only minor. As mentioned in the introduction, the CO stretching

frequency can indirectly be used to determine the binding properties of the co-ligands. Therefore, it can be assumed that both ligands **L^{3Me}** and **L^{5Me}** have approximately the same binding modes and affinities. **L^{6H}** instead seems to coordinate stronger to the Cu^{+}.

The obtained values for the tridentate ligands are rather high in comparison with literature known complexes.[358–361] Only a few Cu^{+} containing complexes are known, which reach similar or higher values. One example is the [tpb$^{CF3, CF3}$CuCO] complex, where electron density is pulled away from the metal by the electron withdrawing groups in the ligand.

Conclusion

Three mononuclear CO complexes were synthesised with **L^{3Me}**, **L^{5Me}** and **L^{6H}** and could be characterised by their specific CO vibration modes. By comparison of the CO stretching vibrations the properties of the ligands could be evaluated. For **L^{3Me}** and **L^{5Me}** only minor differences could be observed. **L^{6H}** with its three pyridine sidearms pushes more electron density towards the metal, resulting in a stronger π-backbond from the metal to the CO. Thus, it can be assumed that the strong σ-bond character of the pyridine results in stronger copper-ligand bond.

Appendix B

Attempt to Determine Metal Selectivity

Introduction

The aim of this study is the synthesis and characterisation of a multifunctional tool, which can be used to enlighten the role of Cu^+ in AD. Under consideration of inorganic and bioinorganic aspect a set of new ligands was synthesised, which should exclusively coordinate Cu^+ in aqueous solutions. The {NS_2} binding mode is a soft donor set, which should not be able to compete with the "water pressure" in the $M(H_2O)_x^{n+}$ complexes with exception of Cu^+. Cu^+ is a special case, since water is due to its rather hard character not a good donor for the soft metal ion.[232] However, it has to be proven that the theoretical concepts also apply. The ligands were coupled *via* click chemistry to a fluorescence sensor to determine their metal selectivity. As fluorescence sensor *N*-ethyl-1,8-naphtalimide was used, since related systems with the same fluorescent subunit are known in the literature (Figure 60).[289,290,362]
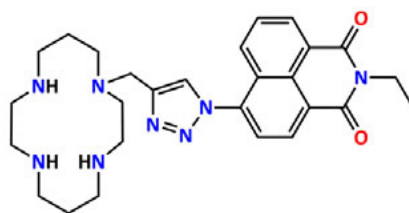
Figure 60 Cyclam-based Zn²⁺ sensor with N-ethyl-1,8-naphtalimide.[290]

Synthesis and Characterisation of Naphthalimide Coupled Ligands

Starting point for the synthesis of the naphthalimide coupled ligands (NCLs) is the commercially available 4-bromophthalic anhydride (Scheme 38). Reaction with ethyl amine in dioxane led to the fluorescent active 4-bromo-*N*-ethyl-1,8-naphtalimide (**XXVIII**).[290] The following substitution of the bromide by an azide and coupling with the alkinated ligands were done in a one pot synthesis. **XXVIII**, ligand, sodium azide, $CuSO_4 \cdot 5 H_2O$ and ascorbate were therefore suspended in DMSO and heated under reflux for 24 h. The reaction solution was poured into water and the crude product precipitated at 4 °C, which was then recrystallised from methanol/diethyl ether. The products were further purified by column chromatography on silica. The NCLs were characterised by ESI-MS and UV/Vis spectroscopy.
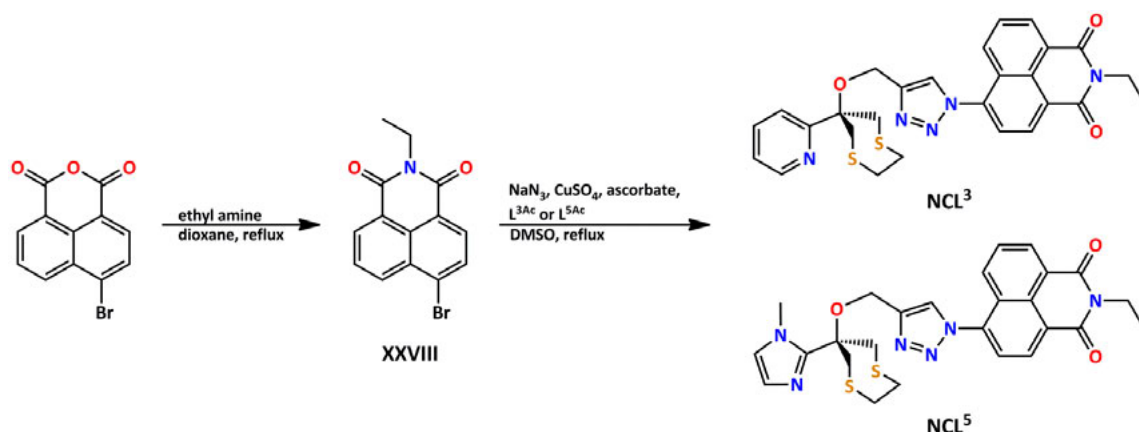
*Scheme 38 Sythesis of naphtalimide coupled ligands **NCL³** and **NCL⁵**.*

Samples were prepared with 10 μM NCL and 10 μM M^{n+} in 0.1 M HEPES buffer (pH 7.4) and measured directly after the addition of the metal and after 5 min to determine the metal selectivity of the compounds. No changes could be observed in the absorbance or in the fluorescence spectra. Thus, the concentration of metal was increased to 50 μM and the experiment repeated three times; again no spectral changes could be observed. The ferrozine and the NMR experiments presented in chapter 5 proved that the ligands are able to coordinate Cu^+ even at low concentrations. Thus, dithionite was added to the sample with Cu^{2+} to reduce it *in situ*. Again, no response could be observed in the spectra. The experiment was also carried out in water instead of HEPES to exclude any interaction of the buffer, but without any changes. Comparison with the literature known systems show that, in case of the NCLs, the linking unit between the chelator and the naphthalimide is expanded by the oxygen and to the next coordinating atom the distance is even longer.[290] Thus, it can be assumed that the chain between chelator and detector is too long to allow recognition of the metal coordination.

Appendix C

Crystallography

X–ray data for all compounds were collected on a STOE IPDS II diffractometer (graphite monochromated Mo–Kα radiation, λ = 0.71073 Å) by use of ω scans at −140 °C. The structures were solved by direct methods and refined on F^2 using all reflections with SHELX–97.[363] Most non-hydrogen atoms were refined anisotropically. Hydrogen atoms were placed in calculated positions and assigned to an isotropic displacement parameter of 1.2 / 1.5 U_{eq}(C) or to an isotropic displacement parameter of 0.08 Å^2. Atoms of the disordered part were refined isotropically. Face-indexed absorption corrections were performed numerically with the program X–RED.[364] Details of data collection and important crystal data are summarised in Table 29-Table 35.

*Table 29 Crystal data and refinement details of **2**, **3** and **4**.*

	2	3	4
empirical formula	$C_{16}H_{24}CuF_3N_2O_4S_3$	$C_{28}H_{37}Cu_2F_6N_6O_2PS_4$	$C_{34}H_{46}Cu_3F_{12}N_8O_2P_2S_4$
formula weight	525.09	889.93	1207.59
crystal size [mm³]	0.50 × 0.48 × 0.46	0.14 × 0.10 × 0.07	0.45 × 0.25 × 0.19
crystal system	Monoclinic	Monoclinic	Triclinic
space group	$P2_1/c$	$P2_1/n$	P–1
a [Å], α [°]	11.8506(5), 90	7.1846(6), 90	12.6311(4), 82.919(3)
b [Å], β [°]	9.0396(3), 105.239(3)	10.8472(6), 93.753(6)	13.5343(5), 69.541(3)
c [Å], γ [°]	21.0667(8), 90	23.4416(17), 90	16.5686(5), 62.951(2)
V [Å³]	2177.41(14)	1823.0(2)	2361.35(14)
Z	4	2	2
ρ [g/cm³]	1.602	1.621	1.698
F(000)	1080	908	1222
μ [mm^{-1}]	1.341	1.507	1.673
T_{min}/ T_{max}	0.5005 / 0.6102	0.7603 / 0.8966	0.4899 / 0.7430
θ range [°]	1.78 - 25.62	1.74 - 26.13	1.31 - 25.63
hkl range	±14, ±10, −24 - 25	±8, ±13, ±28	±15, −15 - 16, ±20
measured refl.	24864	22493	28687
unique refl. [R_{int}]	4082 [0.0497]	22493 [0]	8897 [0.0532]
observed refl. ($I > 2\sigma(I)$)	3884	17715	7804
data / restraints / param.	4082 / 0 / 268	22493 / 0 / 229	8897 / 0 / 592
goodness–of–fit (F^2)	1.059	1.087	1.040
$R1$, $wR2$ ($I > 2\sigma(I)$)	0.0268, 0.0625	0.0754, 0.2052	0.0447, 0.0991
$R1$, $wR2$ (all data)	0.0288, 0.0635	0.0949, 0.2207	0.0542, 0.1038
resid. el. dens. [e/Å^{-3}]	−0.529 / 0.589	−0.700 / 0.723	−1.872 / 1.112

*Table 30 Crystal data and refinement details of **5**, **6** and **7**.*

	5	**6**	**7**
empirical formula	$C_{11}H_{17}CuF_6N_3OPS_2$	$C_{18}H_{17}CuF_6N_5P$	$C_{26}H_{40}Cl_2Cu_2N_2O_2S_4$
formula weight	479.91	511.88	738.82
crystal size [mm³]	0.29 × 0.11 × 0.10	0.23 x 0.2 x 0.19	0.50 × 0.32 × 0.06
crystal system	Orthorhombic	Triclinic	Monoclinic
space group	*Pbca*	P -1	*P*2$_1$/*c*
a [Å], α [°]	14.7518(4), 90	8.1427(5), 102.991(5)	10.0478(4), 90
b [Å], β [°]	12.6686(4), 90	10.9121(6), 104.108(5)	16.8083(6), 114.501(3)
c [Å], γ[°]	18.8775(8), 90	12.1681(7), 99.336(5)	10.4957(5), 90
V [Å³]	3527.9(2)	994.43(10)	1612.97(12)
Z	8	2	2
ρ [g/cm³]	1.807	1.710	1.521
F(000)	1936	516	764
μ [mm^{-1}]	1.631	1.250	1.770
T_{min}/ T_{max}	0.4838 / 0.7870	0.8056 / 0.5608	0.5026 / 0.8102
θ range [°]	2.16 - 26.78	1.80 - 26.74	2.23 - 26.73
hkl range	±18, −15-16, −22 - 23	±10, ±13, ±15	±12, ±21, −10 - 13
measured refl.	32000	8954	14071
unique refl. [R_{int}]	3750 [0.0738]	4203 [0.0453]	3410 [0.0761]
observed refl. ($I > 2$ σ (I))	3120	3672	2949
data / restraints / param.	3750 / 0 / 232	4203 / 1 / 2871	3410 / 0 / 172
goodness–of–fit (F^2)	1.061	1.064	1.040
R1, wR2 ($I > 2σ(I)$)	0.0416, 0.0968	0.0342, 0.0966	0.0357, 0.0945
R1, wR2 (all data)	0.0554, 0.1028	0.0400, 0.0994	0.0426, 0.0979
resid. el. dens. [e/Å^{-3}]	−0.627 / 0.819	0.563 / -0.417	−0.870 / 0.509

*Table 31 Crystal data and refinement details of **8**, **9** and **11**.*

	8	9	11
empirical formula	$C_{28}H_{34}Cu_2F_6N_4O_8S_6$	$C_{48}H_{54}Cu_4F_{12}N_6O_{16}S_{12}$	$C_{28}H_{38}CuF_6N_6O_6S_6$
formula weight	988.03	1837.85	924.54
crystal size [mm³]	0.47 × 0.20 × 0.18	0.29 × 0.28 × 0.17	0.13 x 0.12 x 0.10
crystal system	Triclinic	Monoclinic	Monoclinic
space group	P–1	$C2/c$	P 21/c
a [Å], α [°]	7.7088(4), 71.453(4)	20.8538(6), 90	10.2109(9), 90
b [Å], β [°]	10.9316(5), 88.764(4)	15.6432(4), 99.846(2)	18.3305(10), 91.52(7)
c [Å], γ[°]	11.6881(6), 82.044(4)	20.5563(6), 90	10.2540(8), 90
V [Å³]	924.54(8)	6607.1(3)	1918.9(2)
Z	1	4	2
ρ [g/cm³]	1.775	1.848	1.600
F(000)	502	3712	950
μ [mm^{-1}]	1.573	1.752	0.973
T_{min}/ T_{max}	0.5695 / 0.7865	0.5420 / 0.7739	
θ range [°]	1.84 - 26.74	1.64 - 26.74	1.99 - 27.05
hkl range	±9, ±13, ±14	±26, ±19, ±25	−13 - 12, ±21, −13 - 12
measured refl.	12817	29051	17920
unique refl. [R_{int}]	3915 [0.0353]	7016 [0.0484]	4176 [0.1070]
observed refl. ($I > 2 \sigma$ (I))	3475	6295	2654
data / restraints / param.	3915 / 0 / 245	7016 / 0 / 443	4176 / 0 / 246
goodness–of–fit (F^2)	1.037	1.023	1.006
$R1$, $wR2$ ($I > 2\sigma(I)$)	0.0235, 0.0582	0.0259, 0.0645	0.0624, 0.0914
$R1$, $wR2$ (all data)	0.0285, 0.0594	0.0303, 0.0663	0.1153, 0.1032
resid. el. dens. [e/Å^{-3}]	−0.274 / 0.419	−0.570 / 0.393	0.510 / -0.686

*Table 32 Crystal data and refinement details of **12**, **13** and **14**.*

	12	13	14
empirical formula	$C_{20}H_{27}CuF_6N_2O_{1.50}PS_2$	$C_{79}H_{109}Cl_6N_9O_{36}S_8Zn_6$	$C_{14}H_{18}CuF_3N_2O_4S_3$
formula weight	592.07	2622.15	495.02
crystal size [mm³]	0.39 × 0.35 × 0.07	0.23 x 0.09 x 0.09	0.18 × 0.12 × 0.1
crystal system	Triclinic	Triclinic	Triclinic
space group	$P–1$	P -1	$P–1$
a [Å], α [°]	12.5659(6), 107.283(4)	11.0317(5), 81.288(4)	7.9460(16), 77.32(3)
b [Å], β [°]	13.6449(6), 97.414(4)	13.4082(7), 75.873(4)	10.147(2), 75.48(3)
c [Å], γ[°]	14.7682(6), 96.955(4)	18.6835(9), 73.220(4)	12.670(3), 71.94(3)
V [Å³]	2363.39(18)	2556.1(2	929.0(3)
Z	4	1	2
ρ [g/cm³]	1.664	1.703	1.770
$F(000)$	1212	1344	504
μ [mm⁻¹]	1.235	1.792	1.566
T_{min}/ T_{max}	0.4599 / 0.7551	0.8912 / 0.7660	0.5902 / 0.8155
θ range [°]	1.47 - 26.80	1.59 - 25.63	1.68 - 26.73
hkl range	±15, –17 - 16, ±18	±13, ±16, –22 - 19	±10, ±12, ±15
measured refl.	21059	19959	8132
unique refl. [R_{int}]	9982 [0.0537]	9582 [0.0712]	3914 [0.0387]
observed refl. ($I > 2 \sigma$ (I))	7120	5271	3297
data / restraints / param.	9982 / 21 / 638	9582 / 19 / 676	3914 / 0 / 245
goodness–of–fit (F^2)	1.004	0.924	1.029
$R1$, $wR2$ ($I > 2\sigma(I)$)	0.0402, 0.0797	0.0487, 0.0857	0.0291, 0.0685
$R1$, $wR2$ (all data)	0.0674, 0.0858	0.0953, 0.0933	0.0382, 0.0708
resid. el. dens. [e/Å⁻³]	–0.594 / 0.449	0.729 / -0.784	–0.478 / 0.418

*Table 33 Crystal data and refinement details of **15**, **16** and **20**.*

	15	16	20
empirical formula	$C_{12}H_{19}CuF_6N_3OPS_2$	$C_{13}H_{19}CuF_3NO_5S_3$	$C_{16}H_{17}Cl_2F_3MnNO_7S_3$
formula weight	493.93	486.01	614.33
crystal size [mm³]	0.22 × 0.09 × 0.07	0.48 × 0.22 × 0.21	0.41 x 0.18 x 0.06
crystal system	Monoclinic	Monoclinic	Triclinic
space group	$P2_1/c$	$P2_1/n$	P -1
a [Å], α [°]	13.323(3), 90	10.7299(3), 90	8.8842(7), 100.855(6)
b [Å], β [°]	20.232(4), 100.90(3)	9.1393(4), 104.082(3)	9.2678(19), 91.343(6)
c [Å], γ[°]	7.0048(14), 90	19.2963(6), 90	15.3671(13), 111.388(6)
V [Å³]	1854.0(6)	1835.40(11)	1151.2(3)
Z	4	4	2
ρ [g/cm³]	1.770	1.759	1.772
F(000)	1000	992	620
μ [mm^{-1}]	1.554	1.585	1.141
T_{min}/ T_{max}	0.7550 / 0.8826	0.4982 / 0.7825	0.9504 / 0.6898
θ range [°]	1.85 - 26.78	1.99 - 26.71	2.41 - 26.72°.
hkl range	±16, −24 - 25, ±8	−13 - 12, ±11, ±24	−11 - 9, ±11, ±19
measured refl.	15565	16389	10327
unique refl. [R_{int}]	3881 [0.0767]	3892 [0.0473]	4837 [0.0546]
observed refl. ($I > 2 \sigma$ (I))	2628	3587	3787
data / restraints / param.	3881 / 134 / 260	3892 / 0 / 239	4837 / 0 / 299
goodness–of–fit (F^2)	0.980	1.042	1.006
$R1$, $wR2$ ($I > 2\sigma(I)$)	0.0514, 0.0874	0.0298, 0.0765	0.0388, 0.0843
$R1$, $wR2$ (all data)	0.0912, 0.0969	0.0326, 0.0781	0.0566, 0.0887
resid. el. dens. [e/Å^{-3}]	−0.455 / 0.677	−0.680 / 0.764	0.578 / -0.764

Table 34 Crystal data and refinement details of **21**, **22** *and* **23**.

	21	**22**	**23**
empirical formula	$C_{14}H_{16}F_3MnN_2O_7S_3$	$C_{43.50}H_{36}Cl_3F_6Mn_2N_8O_{12.5}S_2$	$C_{24}H_{21}F_3MnN_4O_{7.50}$
formula weight	532.41	1265.15	629.45
crystal size [mm³]	0.38 x 0.13 x 0.03	0.37 x 0.17 x 0.07	0.4 x 0.16 x 0.12
crystal system	Monoclinic	Triclinic	Triclinic
space group	C 2/c	P -1	P -1
a [Å], α [°]	44.3894(17), 90	10.4283(9), 79.649(8)	8.7678(4), 80.831(4)
b [Å], β [°]	7.9133(2), 123.960(3)	10.4784(11), 86.381(8)	11.4794(6), 79.212(4)
c [Å], γ[°]	28.2058(11), 90	12.7220(13), 75.236(8)	13.8531(7), 87.478(4)
V [Å³]	8217.8(5)	1322.2(2)	1352.01(12)
Z	16	1	2
ρ [g/cm³]	1.721	1.589	1.546
$F(000)$	4320	640	642
μ [mm^{-1}]	1.014	0.797	0.639
T_{min}/ T_{max}	0.8884 / 0.6061	0.8881 / 0.6751	
θ range [°]	1.45 - 25.65	1.63 - 26.88	1.51 - 26.74
hkl range	±53, −9 +9, ±34	−12 +13, −13 +12, ±16	−9 -11, ±14, −16 - 17
measured refl.	31697	12696	12039
unique refl. [R_{int}]	7749 [0.1004]	5590 [0.0686]	5708 [0.0605]
observed refl. ($I > 2 \sigma (I)$)	5619	3436	4403
data / restraints / param.	7749 / 0 / 545	5590 / 4 / 365	5708 / 23 / 392
goodness–of–fit (F^2)	1.031	1.001	1.048
$R1$, $wR2$ ($I > 2\sigma(I)$)	0.0504, 0.0831	0.0631, 0.1263	0.0509, 0.1296
$R1$, $wR2$ (all data)	0.0835, 0.0910	0.1139, 0.1424	0.0690, 0.1375
resid. el. dens. [e/Å^{-3}]	0.569 / -0.318	0.782 / -1.012	0.481 / -0.632

Table 35 Crystal data and refinement details of L^{3Me}.

	L^{3Me}
empirical formula	$C_{11}H_{15}NOS_2$
formula weight	241.36
crystal size [mm³]	$0.31 \times 0.20 \times 0.17$
crystal system	Monoclinic
space group	$P2_1/c$
a [Å], α [°]	8.7459(4), 90
b [Å], β [°]	7.0971(3), 91.293(3)
c [Å], γ[°]	18.7746(8), 90
V [Å³]	1165.05(9)
Z	4
ρ [g/cm³]	1.376
$F(000)$	512
μ [mm^{-1}]	0.430
T_{min}/ T_{max}	0.7427 / 0.9065
θ range [°]	2.17 - 26.73
hkl range	±11, ±8, ±23
measured refl.	9520
unique refl. [R_{int}]	2453 [0.0482]
observed refl. ($I > 2 \sigma(I)$)	2215
data / restraints / param.	2453 / 0 / 137
goodness–of–fit (F^2)	1.059
$R1$, $wR2$ ($I > 2\sigma(I)$)	0.0279, 0.0701
$R1$, $wR2$ (all data)	0.0317, 0.0717
resid. el. dens. [e/Å^{-3}]	−0.251 / 0.258

Bibliography

[1]   M. Goedert, M. G. Spillantini, *Science* **2006**, *314*, 777–781.

[2]   *Alzheimers Dement* **2008**, *4*, 110–133.

[3]   A. Alzheimer, *Allgemeine Zeitschrift für Psychiatrie* **1907**, *64*, 146.

[4]   A. Alzheimer, *Z. Ges. Neurol. Psychiat* **1911**, 356–385.

[5]   Kraepelin, Emil, *Psychiatrie. Ein Lehrbuch Für Studierende Und Ärzte*, Barth Verlag, Leipzig, **1910**.

[6]   de Leon, M. J., *An Atlas of Alzheimer's Disease. The Encyclopedia of Visual Medicine Series*, Parthenon Publishing, Carnforth, **1999**.

[7]   J. Kang, H.-G. Lemaire, A. Unterbeck, J. M. Salbaum, C. L. Masters, K.-H. Grzeschik, G. Multhaup, K. Beyreuther, B. Muller-Hill, *Nature* **1987**, *325*, 733–736.

[8]   G. G. Glenner, C. W. Wong, *Biochem. Biophys. Res. Commun*. **1984**, *120*, 885–890.

[9]   R. D. Terry, N. K. Gonatas, M. Weiss, *Am. J. Path.* **1964**, *44*, 269–297.

[10]   E. D. EANES, G. G. GLENNER, *J. Histochem. Cytochem.* **1968**, *16*, 673 –677.

[11]   M. KIDD, *Nature* **1963**, *197*, 192–193.

[12]   G. G. Glenner, C. W. Wong, *Biochem. Biophys. Res. Commun.* **1984**, *122*, 1131–1135.

[13]   C. L. Masters, G. Simms, N. A. Weinman, G. Multhaup, B. L. McDonald, K. Beyreuther, *PNAS* **1985**, *82*, 4245 –4249.

[14]   R. Tanzi, J. Gusella, P. Watkins, G. Bruns, P. St George-Hyslop, M. Van Keuren, D. Patterson, S. Pagan, D. Kurnit, R. Neve, *Science* **1987**, *235*, 880 –884.

[15]   M. Shoji, T. Golde, J. Ghiso, T. Cheung, S. Estus, L. Shaffer, X. Cai, D. McKay, R. Tintner, B. Frangione, et al., *Science* **1992**, *258*, 126 –129.

[16]   K. Jacobsen, K. Iverfeldt, *Cell.Mol. Life Sci.* **2009**, *66*, 2299–2318.

[17]   D. J. Selkoe, *Physiol. Rev.* **2001**, *81*, 741 –766.

[18]   R. Siman, S. Mistretta, J. T. Durkin, M. J. Savage, T. Loh, S. Trusko, R. W. Scott, *JBC* **1993**, *268*, 16602 –16609.

[19]   M. S. Wolfe, W. Xia, B. L. Ostaszewski, T. S. Diehl, W. T. Kimberly, D. J. Selkoe, *Nature* **1999**, *398*, 513–517.

[20]   G. Yu, M. Nishimura, S. Arawaka, D. Levitan, L. Zhang, A. Tandon, Y.-Q. Song, E. Rogaeva, F. Chen, T. Kawarai, et al., *Nature* **2000**, *407*, 48–54.

[21]   M. Citron, T. S. Diehl, G. Gordon, A. L. Biere, P. Seubert, D. J. Selkoe, *PNAS* **1996**, *93*, 13170 –13175.

[22]   I. Hussain, D. Powell, D. R. Howlett, D. G. Tew, T. D. Meek, C. Chapman, I. S. Gloger, K. E. Murphy, C. D. Southan, D. M. Ryan, et al., *Mol. Cell. Neurosci.* **1999**, *14*, 419–427.

[23]   S. Sinha, J. P. Anderson, R. Barbour, G. S. Basi, R. Caccavello, D. Davis, M. Doan, H. F. Dovey, N. Frigon, J. Hong, et al., *Nature* **1999**, *402*, 537–540.

[24]   R. Vassar, B. D. Bennett, S. Babu-Khan, S. Kahn, E. A. Mendiaz, P. Denis, D. B. Teplow, S. Ross, P. Amarante, R. Loeloff, et al., *Science* **1999**, *286*, 735 –741.

[25]   R. Yan, M. J. Bienkowski, M. E. Shuck, H. Miao, M. C. Tory, A. M. Pauley, J. R. Brashler, N. C. Stratman, W. R. Mathews, A. E. Buhl, et al., *Nature* **1999**, *402*, 533–537.

[26]   Yong Jiao, Pin Yang, *Sci. China Ser. B* **2007**, *50*, 453–467.

[27]   A. Goate, M.-C. Chartier-Harlin, M. Mullan, J. Brown, F. Crawford, L. Fidani, L. Giuffra, A. Haynes, N. Irving, L. James, et al., *Nature* **1991**, *349*, 704–706.

[28]   A. Piccini, C. Russo, A. Gliozzi, A. Relini, A. Vitali, R. Borghi, L. Giliberto, A. Armirotti, C. D'Arrigo, A. Bachi, et al., *JBC* **2005**, *280*, 34186 –34192.

[29]   T. C. Saido, T. Iwatsubo, D. M. . Mann, H. Shimada, Y. Ihara, S. Kawashima, *Neuron* **1995**, *14*, 457–466.

[30]   M. Citron, D. Westaway, W. Xia, G. Carlson, T. Diehl, G. Levesque, K. Johnson-wood, M. Lee, P. Seubert, A. Davis, et al., *Nat. Med.* **1997**, *3*, 67–72.

[31]   D. Burdick, B. Soreghan, M. Kwon, J. Kosmoski, M. Knauer, A. Henschen, J. Yates, C. Cotman, C. Glabe, *JBC* **1992**, *267*, 546 –554.

[32]   A. Asami-Odaka, Y. Ishibashi, T. Kikuchi, C. Kitada, N. Suzuki, *Biochemistry* **1995**, *34*, 10272–10278.

[33]   J. Peisach, W. E. Blumberg, *Archives of Biochemistry and Biophysics* **1974**, *165*, 691–708.

[34]   J. S. Whitson, C. G. Glabe, E. Shintani, A. Abcar, C. W. Cotman, *Neurosci. Lett.* **1990**, *110*, 319–324.

[35]   J. Whitson, D. Selkoe, C. Cotman, *Science* **1989**, *243*, 1488 –1490.

[36]   C. S. Atwood, M. E. Obrenovich, T. Liu, H. Chan, G. Perry, M. A. Smith, R. N. Martins, *Brain Res. Rev.* **2003**, *43*, 1–16.

[37]   J. Hardy, *Science* **2002**, *297*, 353–356.

[38]   D. M. Walsh, D. M. Hartley, Y. Kusumoto, Y. Fezoui, M. M. Condron, A. Lomakin, G. B. Benedek, D. J. Selkoe, D. B. Teplow, *JBC* **1999**, *274*, 25945 –25952.

[39]   T. Oda, P. Wals, H. H. Osterburg, S. A. Johnson, G. M. Pasinetti, T. E. Morgan, I. Rozovsky, W. B. Stine, S. W. Snyder, T. F. Holzman, et al., *Exp. Neurol.* **1995**, *136*, 22–31.

[40]   W. . Klein, W. . Stine Jr., D. . Teplow, *Neurobiol. Aging* **2004**, *25*, 569–580.

[41]   T. Lührs, C. Ritter, M. Adrian, D. Riek-Loher, B. Bohrmann, H. Döbeli, D. Schubert, R. Riek, *PNAS* **2005**, *102*, 17342 –17347.

[42]   T. Miura, K. Suzuki, N. Kohata, H. Takeuchi, *Biochemistry* **2000**, *39*, 7024–7031.

[43]   D. Han, H. Wang, P. Yang, *BioMetals* **2008**, *21*, 189–196.

[44]   C. Talmard, L. Guilloreau, Y. Coppel, H. Mazarguil, P. Faller, *ChemBioChem* **2007**, *8*, 163–165.

[45]   F. Chiti, C. M. Dobson, *Annu. Rev. Biochem.* **2006**, *75*, 333–366.

[46]   H. Kozlowski, M. Luczkowski, M. Remelli, D. Valensin, *Coordin. Chem. Rev.* **2012**, *256*, 2129–2141.

[47]   D. B. Teplow, N. D. Lazo, G. Bitan, S. Bernstein, T. Wyttenbach, M. T. Bowers, A. Baumketner, J.-E. Shea, B. Urbanc, L. Cruz, et al., *Acc. Chem. Res.* **2006**, *39*, 635–645.

[48]   P. T. Lansbury, H. A. Lashuel, *Nature* **2006**, *443*, 774–779.

[49]   J. Schnabel, *Nature* **2011**, *475*, S12–S14.

[50]   C. Haass, D. J. Selkoe, *Nat. Rev. Mol. Cell. Biol.* **2007**, *8*, 101–112.

[51]   M. Higuchi, N. Iwata, Y. Matsuba, K. Sato, K. Sasamoto, T. C. Saido, *Nat. Neurosci.* **2005**, *8*, 527–533.

[52]   H. Benveniste, G. Einstein, K. R. Kim, C. Hulette, G. A. Johnson, *PNAS* **1999**, *96*, 14079–14084.

[53]   C. R. Jack, *Magnet. Reson. In Med.* **2004**, *52*, 1263–1271.

[54]   Y. Z. Wadghiri, *Magnet. Reson. Med.* **2003**, *50*, 293–302.

[55]   J. Zhang, *Magnet. Reson. Med.* **2004**, *51*, 452–457.

[56]   C. A. Mathis, *Bioorg. Med. Chem.* **2002**, *12*, 295–298.

[57]   W. E. Klunk, *Ann. Neurol.* **2004**, *55*, 306–319.

[58]   R. F. Rosen, B. J. Ciliax, T. S. Wingo, M. Gearing, J. Dooyema, J. J. Lah, J. A. Ghiso, H. LeVine, L. C. Walker, *Acta Neuropathol.* **2009**, *119*, 221–233.

[59]   M.-P. Kung, *Brain Res.* **2002**, *956*, 202–210.

[60]   H. Bennhold, *Dtsch. Arch. Klin. Med.* **1923**, *142*, 32–46.

[61]   P. Divry, *J. de Neur.* **1927**, *27*, 643–657.

[62]   P. S. Vassar, C. F. A. Culling, *Arch. Pathol.* **1959**, *68*, 487–98.

[63]   G. Kelenyi, *J. Histochem. Cytochem.* **1967**, *15*, 172 –180.

[64]   A. Nordberg, *Lancet Neurol.* **2004**, *3*, 519–527.

[65]   D. M. Skovronsky, *PNAS* **2000**, *97*, 7609–7614.

[66]   Y. Wang, C. A. Mathis, G. F. Huang, M. L. Debnath, D. P. Holt, L. Shao, W. E. Klunk, *J. Mol.Neurosci.* **2003**, *20*, 255–260.

[67]   B. J. Bacskai, *PNAS* **2003**, *100*, 12462–12467.

[68]   B. J. Bacskai, *Nat. Med.* **2001**, *7*, 369–372.

[69]   N. Tolboom, M. Yaqub, W. M. van der Flier, R. Boellaard, G. Luurtsema, A. D. Windhorst, F. Barkhof, P. Scheltens, A. A. Lammertsma, B. N. M. van Berckel, *J. Nucl.Med.* **2009**, *50*, 191 –197.

[70]   Y. Hung, A. Bush, R. Cherny, *J. Biol. Inorg. Chem.* **2010**, *15*, 61–76.

[71]   Atwood C. S., Huang X., Moir R. D., Tanzi R. E., Bush A. I., *Met. Ions Biol. Syst.* **1999**, *36*, 309–364.

[72]   S. Magaki, R. Raghavan, C. Mueller, K. C. Oberg, H. V. Vinters, W. M. Kirsch, *Neurosci. Lett.* **2007**, *418*, 72–76.

[73]   D. L. Samudralwar, C. C. Diprete, B.-F. Ni, W. D. Ehmann, W. R. Markesbery, *J. Neurol. Sci.* **1995**, *130*, 139–145.

[74]   M. . Lovell, J. . Robertson, W. . Teesdale, J. . Campbell, W. . Markesbery, *J. Neurol. Sci.* **1998**, *158*, 47–52.

[75]   M. A. Smith, P. L. R. Harris, L. M. Sayre, G. Perry, *PNAS* **1997**, *94*, 9866 –9868.

[76]   G. Liu, W. Huang, R. D. Moir, C. R. Vanderburg, B. Lai, Z. Peng, R. E. Tanzi, J. T. Rogers, X. Huang, *J. Struct. Biol.* **2006**, *155*, 45–51.

[77]   S. W. Suh, K. B. Jensen, M. S. Jensen, D. S. Silva, P. J. Kesslak, G. Danscher, C. J. Frederickson, *Brain Res.* **2000**, *852*, 274–278.

[78]   L. M. Sayre, G. Perry, M. A. Smith, *Curr. Opin. Chem. Biol.* **1999**, *3*, 220–225.

[79]   Multhaup G., Masters C.L., *Met. Ions Biol.Syst.***1999**, 365–387.

[80]   S. P. Gabbita, M. A. Lovell, W. R. Markesbery, *J. Neurochem.* **1998**, *71*, 2034–2040.

[81]   W. Kaim, B. Schwederski, *Bioanorganische Chemie*, Vieweg & Teubner Verlag, **2005**.

[82]   E. Gaggelli, H. Kozlowski, D. Valensin, G. Valensin, *Chem. Rev.* **2006**, *106*, 1995–2044.

[83]   A. I. Bush, R. E. Tanzi, *Neurotherapeutics* **2008**, 421–432.

[84]   R. A. Floyd, *P. Sco. Exp. Biol. Med.* **1999**, *222*, 236–245.

[85]   J. Dong, C. S. Atwood, V. E. Anderson, S. L. Siedlak, M. A. Smith, G. Perry, P. R. Carey, *Biochemistry* **2003**, *42*, 2768–2773.

[86]   L. M. Miller, Q. Wang, T. P. Telivala, R. J. Smith, A. Lanzirotti, J. Miklossy, *J. Struct. Biol.* **2006**, *155*, 30–37.

[87]   A. C. Leskovjan, A. Lanzirotti, L. M. Miller, *NeuroImage* **2009**, *47*, 1215–1220.

[88]   C. D. Syme, R. C. Nadal, S. E. J. Rigby, J. H. Viles, *JBC* **2004**, *279*, 18169 –18177.

[89]   González, Martín, Cacho, Breñas, Arroyo, García-Berrocal, Navajo, González-Buitrago, *Eur. J. Clin. Invest.* **1999**, *29*, 637–642.

[90]   R. Squitti, P. Pasqualetti, G. Dal Forno, F. Moffa, E. Cassetta, D. Lupoi, F. Vernieri, L. Rossi, M. Baldassini, P. M. Rossini, *Neurology* **2005**, *64*, 1040 –1046.

[91]   R. Squitti, G. Barbati, L. Rossi, M. Ventriglia, G. Dal Forno, S. Cesaretti, F. Moffa, I. Caridi, E. Cassetta, P. Pasqualetti, et al., *Neurology* **2006**, *67*, 76 –82.

[92]   R. Squitti, D. Lupoi, P. Pasqualetti, G. Dal Forno, F. Vernieri, P. Chiovenda, L. Rossi, M. Cortesi, E. Cassetta, P. M. Rossini, *Neurology* **2002**, *59*, 1153 –1161.

[93]   R. Squitti, P. Pasqualetti, E. Cassetta, G. Dal Forno, S. Cesaretti, F. Pedace, A. Finazzi-Agrò, P. M. Rossini, *Neurology* **2003**, *60*, 2013 –2014.

[94]   H. Kessler, F.-G. Pajonk, P. Meisser, T. Schneider-Axmann, K.-H. Hoffmann, T. Supprian, W. Herrmann, R. Obeid, G. Multhaup, P. Falkai, et al., *J. Neur. Transm.* **2006**, *113*, 1763–1769.

[95]   Frank-Gerald Pajonk, Holger Kessler, Tillmann Supprian, Pegah Hamzei, Daniela Bach, Janina Schweickhardt, Wolfgang Herrmann, Rima Obeid, Andreas Simons, Peter Falkai, et al., *Journal of Alzheimer's Disease* **2005**, 23–27.

[96]   H. Kessler, F.-G. Pajonk, D. Bach, T. Schneider-Axmann, P. Falkai, W. Herrmann, G. Multhaup, J. Wiltfang, S. Schäfer, O. Wirths, et al., *J. Neur. Transm.* **2008**, *115*, 1651–1659.

[97]   M. . Deibel, W. . Ehmann, W. . Markesbery, *J. Neurol. Sci.* **1996**, *143*, 137–142.

[98]   S. A. James, I. Volitakis, P. A. Adlard, J. A. Duce, C. L. Masters, R. A. Cherny, A. I. Bush, *Free Rad. Biol. Med.* **2012**, *52*, 298–302.

[99]   P. Faller, *Free Rad. Biol. Med.* **2012**, *52*, 747–748.

[100] C. S. Atwood, R. D. Moir, X. Huang, R. C. Scarpa, N. M. E. Bacarra, D. M. Romano, M. A. Hartshorn, R. E. Tanzi, A. I. Bush, *JBC* **1998**, *273*, 12817 –12826.

[101] A. I. Bush, R. D. Moir, K. M. Rosenkranz, R. E. Tanzi, *Science* **1995**, *268*, 1921 –1923.

[102] C. S. Atwood, R. C. Scarpa, X. Huang, R. D. Moir, W. D. Jones, D. P. Fairlie, R. E. Tanzi, A. I. Bush, *J. Neurochem.* **2000**, *75*, 1219–1233.

[103] P. Faller, *ChemBioChem* **2009**, *10*, 2837–2845.

[104] X. Huang, C. S. Atwood, M. A. Hartshorn, G. Multhaup, L. E. Goldstein, R. C. Scarpa, M. P. Cuajungco, D. N. Gray, J. Lim, R. D. Moir, et al., *Biochemistry* **1999**, *38*, 7609–7616.

[105] C. Opazo, X. Huang, R. A. Cherny, R. D. Moir, A. E. Roher, A. R. White, R. Cappai, C. L. Masters, R. E. Tanzi, N. C. Inestrosa, et al., *JBC* **2002**, *277*, 40302 –40308.

[106] A. R. White, T. Du, K. M. Laughton, I. Volitakis, R. A. Sharples, M. E. Xilinas, D. E. Hoke, R. M. D. Holsinger, G. Evin, R. A. Cherny, et al., *JBC* **2006**, *281*, 17670 –17680.

[107] T. Borchardt, J. Camakaris, R. Cappai, C. L. Masters, K. Beyreuther, G. Multhaup, *Biochem. J.* **1999**, *344*, 461–467.

[108] M. A. Cater, K. T. McInnes, Q.-X. Li, I. Volitakis, La fontaine Sharon, J. F. B. Mercer, A. I. Bush, *Biochem J* **2008**, *412*, 141–152.

[109] P. S. Donnelly, A. Caragounis, T. Du, K. M. Laughton, I. Volitakis, R. A. Cherny, R. A. Sharples, A. F. Hill, Q.-X. Li, C. L. Masters, et al., *JBC* **2008**, *283*, 4568 –4577.

[110] T. A. Bayer, S. Schäfer, A. Simons, A. Kemmling, T. Kamer, R. Tepests, A. Eckert, K. Schüssel, O. Eikenberg, C. Sturchler-Pierrat, et al., *PNAS* **2003**, *100*, 14187 –14192.

[111] A. L. Phinney, B. Drisaldi, S. D. Schmidt, S. Lugowski, V. Coronado, Y. Liang, P. Horne, J. Yang, J. Sekoulidis, J. Coomaraswamy, et al., *PNAS* **2003**, *100*, 14193 –14198.

[112] Y. H. Hung, E. L. Robb, I. Volitakis, M. Ho, G. Evin, Q.-X. Li, J. G. Culvenor, C. L. Masters, R. A. Cherny, A. I. Bush, *JBC* **2009**, *284*, 21899 –21907.

[113] G. Kong, L. Miles, G. Crespi, C. Morton, H. Ng, K. Barnham, W. McKinstry, R. Cappai, M. Parker, *Eur. Biophys. J.* **2008**, *37*, 269–279.

[114] K. J. Barnham, W. J. McKinstry, G. Multhaup, D. Galatis, C. J. Morton, C. C. Curtain, N. A. Williamson, A. R. White, M. G. Hinds, R. S. Norton, et al., *JBC* **2003**, *278*, 17401 –17407.

[115] J. W. Karr, V. A. Szalai, *Biochemistry* **2008**, *47*, 5006–5016.

[116] L. Guilloreau, L. Damian, Y. Coppel, H. Mazarguil, M. Winterhalter, P. Faller, *J. Biol. Inorg. Chem.* **2006**, *11*, 1024–1038.

[117] P. Faller, C. Hureau, *Dalton Trans.* **2009**, 1080–1094.

[118] T. Kowalik-Jankowska, M. Ruta, K. Wiśniewska, L. Łankiewicz, *J. Inorg. Biochem.* **2003**, *95*, 270–282.

[119] W. Garzon-Rodriguez, A. K. Yatsimirsky, C. G. Glabe, *Bioorg. Med. Chem. Lett.* **1999**, *9*, 2243–2248.

[120] J. W. Karr, H. Akintoye, L. J. Kaupp, V. A. Szalai, *Biochemistry* **2005**, *44*, 5478–5487.

[121] B. Raman, T. Ban, K. Yamaguchi, M. Sakai, T. Kawai, H. Naiki, Y. Goto, *JBC* **2005**, *280*, 16157 –16162.

[122] J. Danielsson, R. Pierattelli, L. Banci, A. Gräslund, *FEBS Journal* **2007**, *274*, 46–59.

[123] V. Tõugu, A. Karafin, P. Palumaa, *J. Neurochem.* **2008**, *104*, 1249–1259.

[124] L. Hou, M. G. Zagorski, *J. Am. Chem. Soc.* **2006**, *128*, 9260–9261.

[125] L. Q. Hatcher, L. Hong, W. D. Bush, T. Carducci, J. D. Simon, *J. Phys. Chem. B* **2008**, *112*, 8160–8164.

[126] A. Bush, W. Pettingell, G. Multhaup, M. d Paradis, J. Vonsattel, J. Gusella, K. Beyreuther, C. Masters, R. Tanzi, *Science* **1994**, *265*, 1464 –1467.

[127] C. C. Curtain, F. E. Ali, D. G. Smith, A. I. Bush, C. L. Masters, K. J. Barnham, *JBC* **2003**, *278*, 2977 –2982.

[128] J. W. Karr, V. A. Szalai, *J. Am. Chem. Soc.* **2007**, *129*, 3796–3797.

[129] C. Hureau, Y. Coppel, P. Dorlet, P. L. Solari, S. Sayen, E. Guillon, L. Sabater, P. Faller, *Angew. Chem.* **2009**, *121*, 9686–9689.

[130] J. W. Karr, L. J. Kaupp, V. A. Szalai, *J. Am. Chem. Soc.* **2004**, *126*, 13534–13538.

[131] V. Minicozzi, F. Stellato, M. Comai, M. D. Serra, C. Potrich, W. Meyer-Klaucke, S. Morante, *JBC* **2008**, *283*, 10784 –10792.

[132] X. Huang, M. P. Cuajungco, C. S. Atwood, M. A. Hartshorn, J. D. A. Tyndall, G. R. Hanson, K. C. Stokes, M. Leopold, G. Multhaup, L. E. Goldstein, et al., *JBC* **1999**, *274*, 37111 – 37116.

[133] F. Stellato, G. Menestrina, M. Serra, C. Potrich, R. Tomazzolli, W. Meyer-Klaucke, S. Morante, *Eur. Biophys. J.* **2006**, *35*, 340–351.

[134] C. Hureau, L. Charlet, P. Dorlet, F. Gonnet, L. Spadini, E. Anxolabéhère-Mallart, J.-J. Girerd, *J. Biol. Inorg. Chem.* **2006**, *11*, 735–744.

[135] K. J. Barnham, F. Haeffner, G. Ciccotosto, C. C. Curtain, D. Tew, C. Mavros, K. Beyreuther, D. Carrington, C. L. Masters, R. A. Cherny, et al., *The FASEB Journal* **2004**, *18*, 1427 –1429.

[136] M. E. Rice, *Trends in Neurosciences* **2000**, *23*, 209–216.

[137] A. Voronova, W. Meyer-klaucke, T. Meyer, A. Rompel, B. Krebs, J. Kazantseva, R. Sillard, P. Palumaa, *Biochem. J.* **2007**, *408*, 139–148.

[138] J. Shearer, V. A. Szalai, *J. Am. Chem. Soc.* **2008**, *130*, 17826–17835.

[139] C. Hureau, V. Balland, Y. Coppel, P. Solari, E. Fonda, P. Faller, *J. Biol. Inorg. Chem.* **2009**, *14*, 995–1000.

[140] R. A. Himes, G. Y. Park, G. S. Siluvai, N. J. Blackburn, K. D. Karlin, *Angew. Chem. Int. Edit.* **2008**, *47*, 9084–9087.

[141] T. N. Sorrell, D. L. Jameson, *J. Am. Chem. Soc.* **1983**, *105*, 6013–6018.

[142] I. Sanyal, K. D. Karlin, R. W. Strange, N. J. Blackburn, *J. Am. Chem. Soc.* **1993**, *115*, 11259–11270.

[143] R. A. Himes, G. Y. Park, A. N. Barry, N. J. Blackburn, K. D. Karlin, *J. Am. Chem. Soc.* **2007**, *129*, 5352–5353.

[144] J. Shearer, P. E. Callan, T. Tran, V. A. Szalai, *Chem. Commun.* **2010**, *46*, 9137–9139.

[145] B. Alies, B. Badei, P. Faller, C. Hureau, *Chem. Eur. J.* **2012**, *18*, 1161–1167.

[146] H. A. Feaga, R. C. Maduka, M. N. Foster, V. A. Szalai, *Inorg. Chem.* **2011**, *50*, 1614–1618.

[147] V. Balland, C. Hureau, J.-M. Savéant, *PNAS* **2010**, *107*, 17113 –17118.

[148] P. V. Robandt, R. R. Schroeder, D. B. Rorabacher, *Inorg. Chem.* **1993**, *32*, 3957–3963.

[149] D. B. Rorabacher, *Chem. Rev.* **2004**, *104*, 651–698.

[150] N. Le Poul, M. Campion, G. Izzet, B. Douziech, O. Reinaud, Y. Le Mest, *J. Am. Chem. Soc.* **2005**, *127*, 5280–5281.

[151] N. Le Poul, M. Campion, B. Douziech, Y. Rondelez, L. Le Clainche, O. Reinaud, Y. Le Mest, *J. Am. Chem. Soc.* **2007**, *129*, 8801–8810.

[152] S. Tubek, *Biol. Trace Elem. Res.* **2007**, *119*, 1–9.

[153] N. M. Lowe, A. Green, J. M. Rhodes, M. Lombard, R. Jalan, M. J. Jackson, *Clin. Sci.* **1993**, *84*, 113–117.

[154] C. J. Frederickson, S. W. Suh, D. Silva, C. J. Frederickson, R. B. Thompson, *J. Nutr.* **2000**, *130*, 1471S –1483S.

[155] Y. Mekmouche, Y. Coppel, K. Hochgräfe, L. Guilloreau, C. Talmard, H. Mazarguil, P. Faller, *ChemBioChem* **2005**, *6*, 1663–1671.

[156] V. Streltsov, *Eur. Biophys. J.* **2008**, *37*, 257–263.

[157] S. Zirah, S. A. Kozin, A. K. Mazur, A. Blond, M. Cheminant, I. Ségalas-Milazzo, P. Debey, S. Rebuffat, *JBC* **2006**, *281*, 2151 –2161.

[158] T. M. J. Allinson, E. T. Parkin, A. J. Turner, N. M. Hooper, *J. Neurosci. Res.* **2003**, *74*, 342–352.

[159]   D. E. Hoke, J.-L. Tan, N. T. Ilaya, J. G. Culvenor, S. J. Smith, A. R. White, C. L. Masters, G. M. Evin, *FEBS Journal* **2005**, *272*, 5544–5557.

[160]   S. Matsuzaki, T. Manabe, T. Katayama, A. Nishikawa, T. Yanagita, H. Okuda, Y. Yasuda, S. Miyata, S. Meshitsuka, M. Tohyama, *J. Neurochem.* **2004**, *88*, 1345–1351.

[161]   C. Talmard, A. Bouzan, P. Faller, *Biochemistry* **2007**, *46*, 13658–13666.

[162]   A. Clements, D. Allsop, D. M. Walsh, C. H. Williams, *J. Neurochem.* **1996**, *66*, 740–747.

[163]   A. I. Bush, W. H. Pettingell, M. D. Paradis, R. E. Tanzi, *JBC* **1994**, *269*, 12152 –12158.

[164]   F. Ricchelli, D. Drago, B. Filippi, G. Tognon, P. Zatta, *Cell. Mol. Life Sci.* **2005**, *62*, 1724–1733.

[165]   O. Kakhlon, Z. I. Cabantchik, *Free Rad. Biol. Med.* **2002**, *33*, 1037–1046.

[166]   F. Bousejra-ElGarah, C. Bijani, Y. Coppel, P. Faller, C. Hureau, *Inorg. Chem.* **2011**, *50*, 9024–9030.

[167]   J. Hu, J. R. Connor, *J. Neurochem.* **1996**, *67*, 838–844.

[168]   D. A. Loeffler, J. R. Connor, P. L. Juneau, B. S. Snyder, L. Kanaley, A. J. DeMaggio, H. Nguyen, C. M. Brickman, P. A. LeWitt, *J. Neurochem.* **1995**, *65*, 710–716.

[169]   J. R. Connor, S. L. Menzies, S. M. St. Martin, E. J. Mufson, *J. Neurosci. Res.* **1992**, *31*, 75–83.

[170]   M. J. House, T. G. St. Pierre, C. McLean, *Magn. Reson. Med.* **2008**, *60*, 41–52.

[171]   R. Leite, W. Jacob-Filho, M. Saiki, L. Grinberg, R. Ferretti, *J. Radioanal. Nucl. Chem.* **2008**, *278*, 581–584.

[172]   Andrási E., Farkas É., Gawlik D., Rösick U., Brätter P., *Journal of Alzheimer's Disease* **2000**, *2*, 17–26.

[173]   D. G. Smith, R. Cappai, K. J. Barnham, *Biochim. Biophys. Acta - Biomembranes* **2007**, *1768*, 1976–1990.

[174]   I. Grundke-Iqbal, J. Fleming, Y.-C. Tung, H. Lassmann, K. Iqbal, J. G. Joshi, *Acta Neuropathologica* **1990**, *81*, 105–110.

[175]   K. Jellinger, W. Paulus, I. Grundke-Iqbal, P. Riederer, M. Youdim, *J. Neur. Transm.* **1990**, *2*, 327–340.

[176]   M. A. Smith, K. Wehr, P. L. R. Harris, S. L. Siedlak, J. R. Connor, G. Perry, *Brain Res.* **1998**, *788*, 232–236.

[177]   C. Hureau, P. Faller, *Biochimie* **2009**, *91*, 1212–1217.

[178]   A. Andorn, R. Britton, B. Bacon, R. Kalaria, *Mol. Chem. Neuropathol.* **1998**, *33*, 15–26.

[179]   C. A. Rottkamp, A. K. Raina, X. Zhu, E. Gaier, A. I. Bush, C. S. Atwood, M. Chevion, G. Perry, M. A. Smith, *Free Rad. Biol. Med.* **2001**, *30*, 447–450.

[180]   X. Huang, C. S. Atwood, R. D. Moir, M. A. Hartshorn, R. E. Tanzi, A. I. Bush, *J. Biol. Inorg. Chem.* **2004**, *9*, 954–960.

[181]   D. Valensin, C. Migliorini, G. Valensin, E. Gaggelli, G. La Penna, H. Kozlowski, C. Gabbiani, L. Messori, *Inorg. Chem.* **2011**, *50*, 6865–6867.

[182]   B. Halliwell, *Biochem. J.* **2007**, *401*, 1–11.

[183]   N. Singh, A. K. Dhalla, C. Seneviratne, P. K. Singal, *Mol. Cell. Biochem.* **1995**, *147*, 77–81.

[184]   A. Ramond, D. Godin-Ribuot, C. Ribuot, P. Totoson, I. Koritchneva, S. Cachot, P. Levy, M. Joyeux-Faure, *Fundam. Clinic. Pharm.* **2011**.

[185]   O. M. Dean, M. van den Buuse, M. Berk, D. L. Copolov, C. Mavros, A. I. Bush, *Neurosci. Lett.* **2011**, *499*, 149–153.

[186]   Y. de Diego-Otero, Y. Romero-Zerbo, R. el Bekay, J. Decara, L. Sanchez, F. R. Fonseca, I. del Arco-Herrera, *Neuropsychopharmacol.* **2008**, *34*, 1011–1026.

[187]   J. Amer, H. Ghoti, E. Rachmilewitz, A. Koren, C. Levin, E. Fibach, *Brit. J. Haematol.* **2006**, *132*, 108–113.

[188]   G. Kennedy, V. A. Spence, M. McLaren, A. Hill, C. Underwood, J. J. F. Belch, *Free Rad. Biol. Med.* **2005**, *39*, 584–589.

[189]   P. Mitchel, J. Moyle, *Nature* **1967**, *213*, 137–139.

[190]   I. Hajimohammadreza, M. Brammer, *Neurosci. Lett.* **1990**, *112*, 333–337.

[191]   M. A. Lovell, W. D. Ehmann, S. M. Butler, W. R. Markesbery, *Neurology* **1995**, *45*, 1594 – 1601.

[192]   D. L. Marcus, C. Thomas, C. Rodriguez, K. Simberkoff, J. S. Tsai, J. A. Strafaci, M. L. Freedman, *Exp. Neurol.* **1998**, *150*, 40–44.

[193]   K. Hensley, N. Hall, R. Subramaniam, P. Cole, M. Harris, M. Aksenov, M. Aksenova, S. P. Gabbita, J. F. Wu, J. M. Carney, et al., *J. Neurochem.* **1995**, *65*, 2146–2156.

[194]   M. Aksenov, M. Aksenova, D. A. Butterfield, W. R. Markesbery, *J. Neurochem.* **2000**, *74*, 2520–2527.

[195]   M. Y. Aksenov, M. V. Aksenova, D. A. Butterfield, J. W. Geddes, W. R. Markesbery, *Neuroscience* **2001**, *103*, 373–383.

[196]   C. D. Smith, J. M. Carney, P. E. Starke-Reed, C. N. Oliver, E. R. Stadtman, R. A. Floyd, W. R. Markesbery, *PNAS* **1991**, *88*, 10540 –10543.

[197]   M. A. Smith, L. M. Sayre, V. E. Anderson, P. L. R. Harris, M. F. Beal, N. Kowall, G. Perry, *J. Histochem. Cytochem.* **1998**, *46*, 731 –735.

[198]   L. Lyras, N. J. Cairns, A. Jenner, P. Jenner, B. Halliwell, *J. Neurochem.* **1997**, *68*, 2061–2069.

[199]   P. Mecocci, U. MacGarvey, M. F. Beal, *Ann Neurol.* **1994**, *36*, 747–751.

[200]   P. Mecocci, U. MacGarvey, A. E. Kaufman, D. Koontz, J. M. Shoffner, D. C. Wallace, M. F. Beal, *Ann Neurol.* **1993**, *34*, 609–616.

[201]   D. A. Butterfield, J. Drake, C. Pocernich, A. Castegna, *Trends in Molecular Medicine* **2001**, *7*, 548–554.

[202]   D. A. Butterfield, C. M. Lauderback, *Free Rad. Biol. Med.* **2002**, *32*, 1050–1060.

[203]   M. A. Lovell, W. D. Ehmann, M. P. Mattson, W. R. Markesbery, *Neurobiol. Aging* **1997**, *18*, 457–461.

[204]   W. . Markesbery, M. . Lovell, *Neurobiol. Aging* **1998**, *19*, 33–36.

[205]   K. S. MONTINE, P. J. KIM, S. J. OLSON, W. R. MARKESBERY, T. J. MONTINE, *J. Neuropath. Exp. Neur.* **1997**, *56*.

[206]   R. Subramaniam, F. Roediger, B. Jordan, M. P. Mattson, J. N. Keller, G. Waeg, D. A. Butterfield, *J. Neurochem.* **1997**, *69*, 1161–1169.

[207]   H. Esterbauer, R. J. Schaur, H. Zollner, *Free Rad. Biol. Med.* **1991**, *11*, 81–128.

[208]   X. Huang, M. P. Cuajungco, C. S. Atwood, M. A. Hartshorn, J. D. A. Tyndall, G. R. Hanson, K. C. Stokes, M. Leopold, G. Multhaup, L. E. Goldstein, et al., *JBC* **1999**, *274*, 37111 – 37116.

[209]   D. A. Butterfield, J. Kanski, *Peptides* **2002**, *23*, 1299–1309.

[210]   V. S. Sharov, D. A. Ferrington, T. C. Squier, C. Schöneich, *FEBS Lett* **1999**, *455*, 247–250.

[211]   D. A. Butterfield, A. I. Bush, *Neurobiol. Aging* **2004**, *25*, 563–568.

[212]   F. E. Ali, F. Separovic, C. J. Barrow, R. A. Cherny, F. Fraser, A. I. Bush, C. L. Masters, K. J. Barnham, *J. Peptide Sci.* **2005**, *11*, 353–360.

[213]   A. Schiewe, L. Margol, B. Soreghan, S. Thomas, A. Yang, *Pharmaceut. Res.* **2004**, *21*, 1094–1102.

[214]   Edward M. Arnett, *Prog. Phys. Org. Chem.* **1963**, *1*, 223–403.

[215]   S. Varadarajan, S. Yatin, J. Kanski, F. Jahanshahi, D. A. Butterfield, *Brain Res. Bulletin* **1999**, *50*, 133–141.

[216]   S. Varadarajan, J. Kanski, M. Aksenova, C. Lauderback, D. A. Butterfield, *J. Am. Chem. Soc.* **2001**, *123*, 5625–5631.

[217]   E. D. Roberson, L. Mucke, *Science* **2006**, *314*, 781 –784.

[218]   F. Bard, C. Cannon, R. Barbour, R.-L. Burke, D. Games, H. Grajeda, T. Guido, K. Hu, J. Huang, K. Johnson-Wood, et al., *Nat. Med.* **2000**, *6*, 916–919.

[219]   R. B. DeMattos, K. R. Bales, D. J. Cummins, J.-C. Dodart, S. M. Paul, D. M. Holtzman, *PNAS* **2001**, *98*, 8850 –8855.

[220]   F. Gervais, J. Paquette, C. Morissette, P. Krzywkowski, M. Yu, M. Azzi, D. Lacombe, X. Kong, A. Aman, J. Laurin, et al., *Neurobiol. Aging* **2007**, *28*, 537–547.

[221]   J. L. Eriksen, S. A. Sagi, T. E. Smith, S. Weggen, P. Das, D. C. McLendon, V. V. Ozols, K. W. Jessing, K. H. Zavitz, E. H. Koo, et al., *J. Clin. Invest.* **2003**, *112*, 440–449.

[222]   B. Regland, W. Lehmann, I. Abedini, K. Blennow, M. Jonsson, I. Karlsson, M. Sjögren, A. Wallin, M. Xilinas, C. G. Gottfries, *Dementia and Geriatric Cognitive Disorders* **2001**, *12*, 408–414.

[223]   S. Macfarlane, B. Maree Mastwyk, L. MacGregor, L. Kiers, R. Cherny, Q. X. Li, A. Tammer, D. Carrington, C. Mavros, I. Volitakis, *Arch. Neurol.* **2003**, *60*, 1685–1691.

[224]   B. A. Ritchie CW, *Arch. Neurol.* **2003**, *60*, 1685–1691.

[225]   P. A. Adlard, R. A. Cherny, D. I. Finkelstein, E. Gautier, E. Robb, M. Cortes, I. Volitakis, X. Liu, J. P. Smith, K. Perez, et al., *Neuron* **2008**, *59*, 43–55.

[226]   L. Lannfelt, K. Blennow, H. Zetterberg, S. Batsman, D. Ames, J. Harrison, C. L. Masters, S. Targum, A. I. Bush, R. Murdoch, et al., *Lancet Neurol.* **2008**, *7*, 779–786.

[227]   N. G. Faux, C. W. Ritchie, A. Gunn, A. Rembach, A. Tsatsanis, J. Bedo, J. Harrison, L. Lannfelt, K. Blennow, H. Zetterberg, et al., *Journal of Alzheimer's Disease* **2010**, *20*, 509–516.

[228]   L. Bica, P. J. Crouch, R. Cappai, A. R. White, *Mol. BioSyst.* **2009**, *5*, 134–142.

[229]   S. K. Balani, G. T. Miwa, L.-S. Gan, J.-T. Wu, F. W. Lee, *Curr. Top. Med. Chem.* **2005**, *5*, 1033–1038.

[230]   Edward H. Kerns, Li Di, *Drug-like Properties: Concepts, Structure Design and Methods: From ADME to Toxicity Optimization*, Elsevier Inc., Oxford, **2008**.

[231]   C. A. Lipinski, F. Lombardo, B. W. Dominy, P. J. Feeney, *Adv. Drug Deliver Rev.* **2001**, *46*, 3–26.

[232]   R. G. Pearson, *J. Am. Chem. Soc.* **1963**, *85*, 3533–3539.

[233]   H. Irving, R. J. P. Williams, *J. Chem. Soc.* **1953**, 3192–3210.

[234]   P. J. Blower, J. R. Dilworth, *Coordin. Chem. Rev.* **1987**, *76*, 121–185.

[235]   T. Konno, *B. Chem. Soc. Jpn.* **2004**, *77*, 627–649.

[236]   M. Hidai, Y. Mizobe, H. Matsuzaka, *J. Organomet. Chem.* **1994**, *473*, 1–14.

[237]   J. E. Biaglow, R. W. Issels, L. E. Gerweck, M. E. Varnes, B. Jacobson, J. B. Mitchell, A. Russo, *Rad. Res.* **1984**, *100*, 298–312.

[238]   K. D. Held, J. E. Biaglow, *Rad. Res.* **1994**, *139*, 15–23.

[239]   G. Capozzi, G. Modena, in *The Thiol Group (1974)*, John Wiley & Sons, Ltd., **1974**, pp. 785–839.

[240]   T. Meier, R. D. Issels, *Biochem. Pharmacol.* **1995**, *50*, 489–496.

[241]   T. M. Jeitner, D. A. Lawrence, *Toxicological Sciences* **2001**, *63*, 57 –64.

[242]   A. Saeed, H. Rafique, A. Hameed, S. Rasheed, *Pharm. Chem. J.* **2008**, *42*, 191–195.

[243]   C. A. Mathis, Y. Wang, D. P. Holt, G.-F. Huang, M. L. Debnath, W. E. Klunk, *J. Med. Chem.* **2003**, *46*, 2740–2754.

[244]   P. C. Kunz, W. Huber, A. Rojas, U. Schatzschneider, B. Spingler, *Eur. J. Inorg. Chem.* **2009**, *2009*, 5358–5366.

[245]   H. Pfeiffer, A. Rojas, J. Niesel, U. Schatzschneider, *Dalton Trans.* **2009**, 4292–4298.

[246]   K. Meister, J. Niesel, U. Schatzschneider, N. Metzler-Nolte, D. A. Schmidt, M. Havenith, *Angew. Chem. Int. Edit.* **2010**, *49*, 3310–3312.

[247]   S. Cooper, S. Rawle, Springer Berlin / Heidelberg, **1990**, pp. 1–72.

[248]   S. G. Murray, F. R. Hartley, *Chem. Rev.* **1981**, *81*, 365–414.

[249]   N. J. Curtis, R. S. Brown, *Can. J. Chem.* **1981**, *59*, 65–75.

[250]   P. J. Arnold, S. C. Davies, J. R. Dilworth, M. C. Durrant, D. V. Griffiths, D. L. Hughes, R. L. Richards, P. C. Sharpe, *J. Chem. Soc., Dalton Trans.* **2001**, 736–746.

[251]   J. G. Woollard-Shore, J. P. Holland, M. W. Jones, J. R. Dilworth, *Dalton Trans.* **2010**, *39*, 1576–1585.

[252]   A. Vaskevich, I. Rubinstein, *J. Electroanal. Chem.* **2000**, *491*, 87–94.

[253]   D. G. Humphrey, G. D. Fallon, K. S. Murray, *J. Chem. Soc., Chem. Commun.* **1988**, 1356–1358.

[254]   R. R. Conry, W. S. Striejewske, A. A. Tipton, *Inorg. Chem.* **1999**, *38*, 2833–2843.

[255]   R. R. Conry, A. A. Tipton, W. S. Striejewske, E. Erkizia, M. A. Malwitz, A. Caffaratti, J. A. Natkin, *Organometallics* **2004**, *23*, 5210–5218.

[256]   R. R. Conry, *Chem. Commun.* **1998**, 555–556.

[257]   A. W. Addison, T. N. Rao, J. Reedijk, J. van Rijn, G. C. Verschoor, *J. Chem. Soc., Dalton Trans.* **1984**, 1349–1356.

[258]   M. Mikuriya, K. Toriumi, T. Ito, S. Kida, *Inorg. Chem.* **1985**, *24*, 629–631.

[259]   M. Mikuriya, M. Nakamura, H. Ōkawa, S. Kida, *Inorganica Chimica Acta* **1983**, *68*, 111–117.

[260]   S. Roy, P. Mitra, A. K. Patra, *Inorg. Chim. Acta* **2011**, *370*, 247–253.

[261]   K. J. Tubbs, A. L. Fuller, B. Bennett, A. M. Arif, L. M. Berreau, *Inorg. Chem.* **2003**, *42*, 4790–4791.

[262]   Eckhard Bill, *julX*, Max-Planck Institute For Chemical Energy Conversion, Mühlheim/Ruhr, **n.d.**

[263]   L. Merz, W. Haase, *J. Chem. Soc., Dalton Trans.* **1980**, *0*, 875–879.

[264]   M. Handa, N. Koga, S. Kida, *B. Chem. Soc. Jpn.* **1988**, *61*, 3853–3857.

[265]   V. M. Miskowski, J. A. Thich, R. Solomon, H. J. Schugar, *J. Am. Chem. Soc.* **1976**, *98*, 8344–8350.

[266]   M. Selva, P. Tundo, C. A. Marques, *Synthetic Comm.* **1995**, *25*, 369–378.

[267]   M. E. G. Skinner, T. Toupance, D. A. Cowhig, B. R. Tyrrell, P. Mountford, *Organometallics* **2005**, *24*, 5586–5603.

[268]   S. Bhattacharyya, K. A. Neidigh, M. A. Avery, J. S. Williamson, *Synlett* **31**, *1999*, 1781–1783.

[269]   V.P. Arya, S.P. Ghate, *Indian J. Chem* **1971**, *904*, 14514.

[270]   B. Unterhalt, M. Möllers, *Arch. Pharm. Pharm. Med. Chem.* **1990**, *323*, 317–318.

[271]   J. Ipaktschi, *Chem. Ber.* **1984**, *117*, 856–858.

[272]   R. C. Fuson, A. J. Speziale, *J. Am. Chem. Soc.* **1949**, *71*, 1582–1584.

[273]   C. A. Sprecher, A. D. Zuberbühler, *Angew. Chem.* **1977**, *89*, 185–186.

[274]   D.-H. Lee, N. N. Murthy, K. D. Karlin, *B. Chem. Soc. Jpn.* **2007**, *80*, 732–742.

[275]   D.-H. Lee, N. N. Murthy, K. D. Karlin, *Inorg. Chem.* **1996**, *35*, 804–805.

[276]   F. L. Urbach, U. Knopp, A. D. Zuberbühler, *HCA* **1978**, *61*, 1097–1106.

[277]   G. Guillot, E. Mulliez, P. Leduc, J. C. Chottard, *Inorg. Chem.* **1990**, *29*, 577–579.

[278]   T. Kauffmann, J. König, A. Woltermann, *Chem. Ber.* **1976**, *109*, 3864–3868.

[279]   G. R. Newkome, W. E. Puckett, G. E. Kiefer, V. D. Gupta, Y. Xia, M. Coreil, M. A. Hackney, *J. Org. Chem.* **1982**, *47*, 4116–4120.

[280]   R. Ziessel, J.-M. Lehn, *HCA* **1990**, *73*, 1149–1162.

[281]   E. Riedel, *Anorganische Chemie*, Walter De Gruyter GmbH & Co.KG, Berlin, **2004**.

[282]   Z. Zhang, J. Gao, D. Wang, T. Xu, *Acta Cryst. E* **2006**, *62*, m3412–m3413.

[283]   A. L. Johnson, N. Hollingsworth, G. Kociok-Köhn, K. C. Molloy, *Inorg. Chem.* **2008**, *47*, 12040–12048.

[284]   G.-F. Zhang, M.-H. Yin, Y.-L. Dou, Q.-P. Zhou, J.-B. She, *J. Coord. Chem.* **2008**, *61*, 1272–1282.

[285]   Eastburn SD, Tao BY, *Biotechnol. Adv.* **1994**, *12*, 325–339.

[286]   E. M. M. Del Valle, *Proc. Biochem.* **2004**, *39*, 1033–1046.

[287]   R. Arun, K. C. K. Ashok, V. V. N. S. S. Sravanthi, *ChemInform* **2009**, *40*, no–no.

[288]   L. E. Scott, M. Telpoukhovskaia, C. Rodriguez-Rodriguez, M. Merkel, M. L. Bowen, B. D. G. Page, D. E. Green, T. Storr, F. Thomas, D. D. Allen, et al., *Chem. Sci.* **2011**, *2*, 642–648.

[289]   F. M. Pfeffer, A. M. Buschgens, N. W. Barnett, T. Gunnlaugsson, P. E. Kruger, *Tetrahedron Letters* **2005**, *46*, 6579–6584.

[290]   E. Tamanini, A. Katewa, L. M. Sedger, M. H. Todd, M. Watkinson, *Inorg. Chem.* **2008**, *48*, 319–324.

[291]   Lisa Minor, *Handbook of Assay Development in Drug Discovery*, Taylor & Francis Group, Boca Raton, **2006**.

[292]   O. Cuvillier, T. Levade, *Blood* **2001**, *98*, 2828–2836.

[293]   C. I. Stains, K. Mondal, I. Ghosh, *ChemMedChem* **2007**, *2*, 1674–1692.

[294]   H. LeVine III, in *Amyloid, Prions, and Other Protein Aggregates*, Academic Press, **1999**, pp. 274–284.

[295]   C. Rodríguez-Rodríguez, M. Telpoukhovskaia, C. Orvig, *Coordin. Chem. Rev.* **2012**, *256*, 2308–2332.

[296]   Y. Heo, Y. S. Song, B. T. Kim, J.-N. Heo, *Tetrahedron Letters* **2006**, *47*, 3091–3094.

[297]   V. J. Majo, J. Prabhakaran, J. J. Mann, J. Dileep Kumar, *Tetrahedron Letters* **2003**, *44*, 8535–8537.

[298]   C. G. Stuckwisch, *J. Am. Chem. Soc.* **1949**, *71*, 3417–3417.

[299]   N. Suzuki, T. Nomoto, Y. Toya, N. Kanamori, B. Yoda, A. Saeki, *Biosci. Biotech. Biochem.* **1993**, *57*, 1561–1562.

[300]   P. D. Bartlett, E. S. Lewis, *J. Am. Chem. Soc.* **1950**, *72*, 405–407.

[301]   H. Finkelstein, *Ber. Dtsch. Chem. Ges.* **1910**, *43*, 1528–1532.

[302]   N. Hirota-Nakaoka, K. Hasegawa, H. Naiki, Y. Goto, *JBC* **2003**, *134*, 159–164.

[303]   A. Loksztejn, W. Dzwolak, *Biochemistry* **2009**, *48*, 4846–4851.

[304]   W. E. Klunk, H. Engler, A. Nordberg, Y. Wang, G. Blomqvist, D. P. Holt, M. Bergström, I. Savitcheva, G.-F. Huang, S. Estrada, et al., *Ann Neurol.* **2004**, *55*, 306–319.

[305]   A. Albert, R. Goldacre, J. Phillips, *J. Chem. Soc.* **1948**, 2240–2249.

[306]   R. Linnell, *J. Org. Chem.* **1960**, *25*, 290–290.

[307]   H. Walba, R. W. Isensee, *J. Org. Chem.* **1961**, *26*, 2789–2791.

[308]   W. E. Klunk, Y. Wang, G. Huang, M. L. Debnath, D. P. Holt, C. A. Mathis, *Life Sciences* **2001**, *69*, 1471–1484.

[309]   S. Pietri, J. R. Séguin, P. D'Arbigny, M. Culcasi, *Free Rad. Biol. Med.* **1994**, *16*, 523–528.

[310]   A. J. Tortolani, S. R. Powell, V. Mišik, W. B. Weglicki, G. J. Pogo, J. H. Kramer, *Free Rad. Biol. Med.* **1993**, *14*, 421–426.

[311]   R. V. Panganamala, H. M. Sharma, R. E. Heikkila, J. C. Geer, D. G. Cornwell, *Prostaglandins* **1976**, *11*, 599–607.

[312]   J. . Phillis, A. . Estevez, M. . O'Regan, *Neurosci. Lett.* **1998**, *244*, 109–111.

[313]   C.-D. Badrakhan, F. Petrat, M. Holzhauser, A. Fuchs, E. E. Lomonosova, H. de Groot, M. Kirsch, *J. Biochem. Bioph. Meth.* **2004**, *58*, 207–218.

[314]   L. Ackermann, H. K. Potukuchi, D. Landsberg, R. Vicente, *Org. Lett.* **2008**, *10*, 3081–3084.

[315]   M. Desmard, R. Foresti, D. Morin, M. Dagouassat, A. Berdeaux, E. Denamur, S. H. Crook, B. E. Mann, D. Scapens, P. Montravers, et al., *Antioxidants & Redox Signaling* **2011**, *16*, 153–163.

[316]   J. E. Clark, C. J. Green, R. Motterlini, *Biochem. Biophys. Res. Comm.* **1997**, *241*, 215–220.

[317]   K. S. Davidge, R. Motterlini, B. E. Mann, J. L. Wilson, R. K. Poole, in *Adv. Microb. Physiol.* **2009**, pp. 85–167.

[318]   P. R. Ortiz de Montellano, *Curr. Opin. Chem. Biol.* **2000**, *4*, 221–227.

[319]   P. G. Wang, M. Xian, X. Tang, X. Wu, Z. Wen, T. Cai, A. J. Janczuk, *Chem. Rev.* **2002**, *102*, 1091–1134.

[320]   C. Szabo, *Nat Rev Drug Discov* **2007**, *6*, 917–935.

[321]   J. Boczkowski, J. J. Poderoso, R. Motterlini, *Trends Biochem. Sci.* **2006**, *31*, 614–621.

[322]   R. Motterlini, L. E. Otterbein, *Nat. Rev. Drug Discov.* **2010**, *9*, 728–743.

[323]   S. W. Ryter, J. Alam, A. M. K. Choi, *Physiol. Rev.* **2006**, *86*, 583 –650.

[324]   J. E. Clark, P. Naughton, S. Shurey, C. J. Green, T. R. Johnson, B. E. Mann, R. Foresti, R. Motterlini, *Circ. Res.* **2003**, *93*, e2 –e8.

[325]   R. Motterlini, J. E. Clark, R. Foresti, P. Sarathchandra, B. E. Mann, C. J. Green, *Circ. Res.* **2002**, *90*, e17 –e24.

[326]   Motterlini R., Sawle P., Bains S., Hammad J., Alberto R., Foresti R., Green C.J., *FASEB J* **2005**, *19*, 284–286.

[327]   R. Alberto, R. Motterlini, *Dalton Trans.* **2007**, 1651–1660.

[328]   T. S. Pitchumony, B. Spingler, R. Motterlini, R. Alberto, *Org. Biomol. Chem.* **2010**, *8*, 4849–4854.

[329]   Motterlini R., *Biochem. Soc. Trans.* **2007**, *35*, 1142–1146.

[330]   U. Schatzschneider, *Inorg. Chim. Acta* **2011**, *374*, 19–23.

[331]   C. R. Child, S. Kealey, H. Jones, P. W. Miller, A. J. P. White, A. D. Gee, N. J. Long, *Dalton Trans.* **2011**, *40*, 6210–6215.

[332]   R. D. Rimmer, H. Richter, P. C. Ford, *Inorg. Chem.* **2009**, *49*, 1180–1185.

[333]   C. S. Jackson, S. Schmitt, Q. P. Dou, J. J. Kodanko, *Inorg. Chem.* **2011**, *50*, 5336–5338.

[334]   K. Splith, I. Neundorf, W. Hu, H. W. P. N'Dongo, V. Vasylyeva, K. Merz, U. Schatzschneider, *Dalton Trans.* **2010**, *39*, 2536–2545.

[335]   I. Neundorf, J. Hoyer, K. Splith, R. Rennert, H. W. Peindy N'Dongo, U. Schatzschneider, *Chem. Commun.* **2008**, 5604–5606.

[336]   W. Huber, R. Linder, J. Niesel, U. Schatzschneider, B. Spingler, P. C. Kunz, *Eur. J. Inorg. Chem.* **2012**, *2012*, 3140–3146.

[337]   E. W. Abel, G. Wilkinson, *J. Chem. Soc.* **1959**, 1501–1505.

[338]   J. C. Anderson, D. S. James, J. P. Mathias, *Tetrahedron: Asymmetry* **1998**, *9*, 753–756.

[339]   D. V. Griffiths, M. J. Al-Jeboori, P. J. Arnold, Y.-K. Cheong, P. Duncanson, M. Motevalli, *Inorg. Chim. Acta* **2010**, *363*, 1186–1194.

[340]   C. R. Martinez, B. L. Iverson, *Chem. Sci.* **2012**, *3*, 2191–2201.

[341]   C. Janiak, *J. Chem. Soc., Dalton Trans.* **2000**, *0*, 3885–3896.

[342]   H.-M. Berends, P. Kurz, *Inorg. Chim. Acta* **2012**, *380*, 141–147.

[343]   F. Mohr, J. Niesel, U. Schatzschneider, C. W. Lehmann, *Z. anorg. allg. Chem.* **2012**, *638*, 543–546.

[344]   A. J. Atkin, J. M. Lynam, B. E. Moulton, P. Sawle, R. Motterlini, N. M. Boyle, M. T. Pryce, I. J. S. Fairlamb, *Dalton Trans.* **2011**, *40*, 5755–5761.

[345]   S. McLean, B. E. Mann, R. K. Poole, *Anal. Biochem.* **2012**, *427*, 36–40.

[346]   G. J. Kubas, B. Monzyk, A. L. Crumbliss, in *Inorganic Syntheses*, John Wiley & Sons, Inc., **1979**, pp. 90–92.

[347]   F. Neese, *WIREs Comput Mol Sci* **2012**, *2*, 73–78.

[348]   A. Schafer, H. Horn, R. Ahlrichs, *J. Chem. Phys.* **1992**, *97*, 2571–2577.

[349]   F. Weigend, R. Ahlrichs, *Phys. Chem. Chem. Phys.* **2005**, *7*, 3297–3305.

[350]   W. J. Bowen, *JBC* **1949**, *179*, 235–245.

[351]   M.J.S. Dewar, *Bull. Soc. Chim. Fr.* **1951**, *18*, C71–79.

[352]   J. Chatt, L. A. Duncanson, *J. Chem. Soc.* **1953**, 2939–2947.

[353]   J. Chatt, L. A. Duncanson, L. M. Venanzi, *J. Chem. Soc.* **1955**, 4456–4460.

[354]   Christoph Elschenbroich, *Organometallchemie*, Teubner B.G. GmbH, Stuttgart, **1993**.

[355]   B. J. Coe, S. J. Glenwright, *Coordin. Chem. Rev.* **2000**, *203*, 5–80.

[356]   E. R. Davidson, K. L. Kunze, F. B. C. Machado, S. J. Chakravorty, *Acc. Chem. Res.* **1993**, *26*, 628–635.

[357]   S. Imai, K. Fujisawa, T. Kobayashi, N. Shirasawa, H. Fujii, T. Yoshimura, N. Kitajima, Y. Moro-oka, *Inorg. Chem.* **1998**, *37*, 3066–3070.

[358]   N. Kitajima, K. Fujisawa, C. Fujimoto, Y. Morooka, S. Hashimoto, T. Kitagawa, K. Toriumi, K. Tatsumi, A. Nakamura, *J. Am. Chem. Soc.* **1992**, *114*, 1277–1291.

[359]   H. V. Rasika Dias, T. K. H. H. Goh, *Polyhedron* **2004**, *23*, 273–282.

[360]   K. Fujisawa, T. Ono, Y. Ishikawa, N. Amir, Y. Miyashita, K. Okamoto, N. Lehnert, *Inorg. Chem.* **2006**, *45*, 1698–1713.

[361]   Y. Kajita, H. Arii, T. Saito, Y. Saito, S. Nagatomo, T. Kitagawa, Y. Funahashi, T. Ozawa, H. Masuda, *Inorg. Chem.* **2007**, *46*, 3322–3335.

[362]   M. Sawa, T. L. Hsu, T. Itoh, M. Sugiyama, S. R. Hanson, P. K. Vogt, C. H. Wong, *PNAS* **2006**, *103*, 12371.

[363]   G. Sheldrick, *Acta Cryst. A* **2008**, *64*, 112–122.

[364]   STOE & CIE GmbH, *X-RED*, STOE & CIE GmbH, Darmstadt (Germany), **2002**.

List of Abbreviations

AD	Alzheimer's Disease
APP	amyloid precursor protein
Asp	asparagine
Aβ	β-amyloid
CORM	CO releasing molecule
CPP	cell penetrating peptide
d	douplet
DFT	density functional theory
DMEM	Dubelcoo's Modified Eagle's Medium
EI	electron ionisation (MS-technique)
ESI	electrospray ionisation (MS-technique)
FBS	foetal bovine serum
Glu	glutamine
His	histidine
IR	infrared spectroscopy
J	magnet coupling (SQUID) / NMR coupling constant
LFSE	ligand field stabilising energy
m	multiplet (NMR) / medium (IR)
M	molar
Mb	myoglobin
MbCO	carboxymyoglobin
Met	methionine
MS	mass spectroscopy
NFT's	neurofibrillary tangles
NMR	nuclear magnetic resonance
ROS	reactive oxygen species
RT	room temperature
s	singlet (NMR) / strong (IR)
SQUID	superconducting quantum interference device
t	triplet
THF	tetrahydrofuran
tpb	tris(pyrazol)borate
tpm	tris(pyrazolyl)methane
tpp	tris(pyridine-2yl)-phosphane
Tyr	tyrosine
UV-Vis	ultraviolet-visible
Val	valine
w	weak (IR)
δ	NMR shift
ε	extinction coefficient
μ_{eff}	effective magnetic moment
$\tilde{\nu}$	stretch frequency

List of Scientific Contributions

Publications

M. Rittmeier, S. Dechert, S. Demeshko and F. Meyer, „New Tripodal Tridentate Ligands with {NS$_2$} Donor Set and a Backbone Hydroxo Anchor, and Their Copper(I) and Copper(II) Complexes", *ZAAC*, **2013**, *639*, 1445-1454.

Oral Presentations at Workshops

M. Rittmeier, F. Meyer, "*Synthesis of Multifunctional Chelating Agents Targeting Copper(I) in Alzheimer´s Disease*", Workshop of the International Research Training Group GRK 1422 "*Metal Sites in Biomolecules: Structures, Regulation and Mechanism*", Lund, Sweden, February **2011**.

M. Rittmeier, F. Meyer, "*Copper(I)-specific Chelators for the Treatment of Alzheimer's Disease*", Workshop of the International Research Training Group GRK 1422 "*Metal Sites in Biomolecules: Structures, Regulation and Mechanism*", Hofgeismar, Germany, April **2012**.

Posters Presented at Conferences and International Workshops

M. Rittmeier, M. Sietzen, S. Fakih, F. Meyer, "Design and Characterisation of Copper(I) Selective Ligands targeting Alzheimer's Disease ", *Workshop of the International Research Training Group GRK 1422 "Metal Sites in Biomolecules: Structures, Regulation and Mechanism"*, Goslar, Germany, February **2010**.

M. Rittmeier, M. Sietzen, S. Fakih, F. Meyer, "Research of the Role of Copper(I)-Ions in the Formation of fibrillar amyloid plaques in Alzheimer's Disease", *Jungchemiker Forum (JCF)*, Göttingen, Germany, March **2010**.

M. Rittmeier, S. Dechert, P. Faller, F. Meyer, "Synthesis of Copper(I) Selective Ligands for Biomedical Application", *10th European Biological Inorganic Chemistry Conference (EuroBIC 10)*, Thessaloniki, Greece, June **2010**.

M. Rittmeier, P. Faller, F. Meyer, "Copper(I)-specific Chelators for the Treatment of Alzheimer's Disease", *11th European Biological Inorganic Chemistry Conference (EuroBIC 11)*, Granada, Spain, September **2012**.

M. Rittmeier, S. Dechert, P. Faller, F. Meyer, "Multifunctional Tools Targeting Cu(I) In Alzheimer's Disease", 16. Vortragstagung der Wöhler-Vereinigung (GDCh), Göttingen, Germany, September **2012**.

Acknowledgements

Curriculum Vitae

Personal

Name: Markus Rittmeier
Date of Birth: September 19th 1984
Place of Birth: Köln
Nationality: German
Marital Status: single

Education

09/1991 - 07/1995	Grundschule / St. Georg Schule	Nesselröden
09/1991 - 07/1995	OS / St. Ursula Schule	Duderstadt
09/1997 - 07/2001	Heinz Sielmann Realschule	Duderstadt
09/2001 - 07/2004	Arnoldi – Fachgymnasium Wirtschaft	Göttingen

Academic Career

10/2004 - 05/2009	Georg-August Universität Göttingen
	Undergraduate student at the Institute of Inorganic Chemistry
05/2009	Diplomprüfung (Grade: 1.3)
06/2009 - 03/2013	Ph.D. Student at the Institute of Inorganic Chemistry (Göttingen) under the supervision of Prof. Dr. Franc Meyer
	Ph.D. Thesis: "Design and Characterisation of Multifunctional Tools for the Elucidation of Cu^{+} Chemistry in Alzheimer`s Disease"